MECHANISM AND MITIGATION OF CLOGGING IN CONTINUOUS CASTING NOZZLES

BY

KEITH GERARD RACKERS

B.S., University of Missouri - Rolla, 1989

THESIS

Submitted in partial fulfillment of the requirements
for the degree of Master of Science in Mechanical Engineering
in the Graduate College of the
University of Illinois at Urbana-Champaign, 1995

Urbana, Illinois

ABSTRACT

Clogging of the nozzles used for the continuous casting of steel results in decreased caster efficiency and decreased product quality. A literature review has revealed that nozzle clogs are generally composed of solid steel, deoxidation products, complex oxides, reaction products, or a combination of these constituents. Prior work suggests that the clogging is worsened by the presence of turbulent recirculation zones, rough nozzle walls, poor steel cleanliness, and air aspiration. Experimental observations of tundish nozzle samples indicate a large variability in the extent of clogging and the amount of void space and solid steel within the clog. Several different one dimensional heat and mass transfer models of the nozzle were developed to investigate the effect of heat transfer on the clogging process. The results suggest that skulling alone is not a likely cause for clogging during normal casting conditions. However, skulling is predicted to occur within a clog buildup and is hypothesized to increase the clogging rate by supporting the thin clog filaments from breaking off in the fast-moving steel. A new nozzle design is proposed which employs an electric heater and facilitates determination of the relationship between heat transfer and nozzle clogging. Other modeling efforts illustrate specific conclusions regarding the potential for air aspiration, suggest requirements for effective argon distribution, and discuss the impact of air aspiration and steel cleanliness on nozzle clogging.

TABLE OF CONTENTS

LIST OF TABLES

PAGE

LIST OF FIGURES

PAGE

NOMENCLATURE

A_{sg}	Slide gate opening area
g	Gravitational acceleration
h	Height of steel above slide gate
$\dot{m}$	Mass flow rate of steel
m_γ	Surface tension gradient
R	Particle radius
Re	Reynold's number
V	Particle Velocity
γ	Nozzle flow characteristic factor
ρ_{Fe}	Density of steel
ε	Emissivity
μ	Viscosity of steel
σ	Stefan-Boltzmann constant, $\frac{W}{m^2K^4}$
C_p	Heat capacity, $\frac{J}{kgK}$

CHAPTER 1 - INTRODUCTION

1.1 BACKGROUND

Continuous casting of steel is one of the most important material processing operations employed today. Approximately 70% of the steel produced in the world and 84.5% of the steel produced in the United States is continuously cast [1-3]. These continuous cast products are chiefly in the forms of slabs, blooms, and billets.

Although continuous casting has been in industrial use for over thirty years [4], many problems associated with this process have not been resolved. These problems include product defects (e.g., cracks, inclusions, porosity, and segregation) and operational problems (e.g., breakouts and nozzle clogging).

1.2 PROCESS OVERVIEW

The typical slab-casting process is illustrated in Figure 1.1. Steel from the basic oxygen furnace is poured into the ladle (a refractory lined vessel with has a typical capacity of 250 tons). While in the ladle, various alloying and treatment processes are performed to adjust the chemistry to the desired level. The steel contained within one ladle is defined as a heat. Since no intentional modifications are generally made to the steel subsequent to the ladle metallurgy operations, the steel composition in a given heat is effectively fixed.

The steel is subsequently poured into a tundish (a refractory lined vessel which has a typical capacity of 40 tons). In addition to directing the steel to the mold, the tundish serves two basic functions. First it enables uninterrupted casting while empty ladles are being exchanged for full ones. Second it allows additional inclusion removal (primarily by flotation which results because inclusions are less dense than steel).

Molten steel is introduced into the mold cavity through a submerged entry nozzle. The liquid steel solidifies along the four walls of the water-cooled, copper mold. This solidified steel shell acts as a container for the molten steel as it is being withdrawn from the mold and grows in thickness as it travels down the mold.

To aid in the withdrawal process, the mold oscillates at approximately 1 Hz while the strand is slowly withdrawn out from the mold. Mold powder is added to the free surface of the liquid steel and forms flux which flows between the mold wall and the solidified shell, acting as a lubricant. At the exit of the mold, rollers pull the partially solidified steel strand and is continuously withdrawn from the mold. Water sprays cool the strand as it is being pulled by the rollers. The completely solidified slab is then cut into desired lengths by torches.

The flow of steel from the tundish to the mold for a typical caster is further illustrated in Figure 1.2. The liquid steel flows through a tundish nozzle, past a slide gate, through a submerged entry nozzle, and out the nozzle ports. The primary purposes of this flow passage are to prevent exposure to air and consequent oxidation of the steel stream and to regulate the flow of steel into the mold. The nozzles and slide gate are constructed from refractory materials to enable their extended service at high temperatures. The flow is regulated by adjusting the position of the slide gate.

Another frequently employed tundish-to-mold flow control system is shown in Figure 1.3. In this system, the vertical position of the stopper rod is adjusted to regulate the flow.

During the casting process, a buildup (clog) containing steel impurities may form on the nozzle wall. This clog adversely affects product quality by changing the flow pattern and by degrading the internal quality of the final product when large chunks of it break off and enter the flow stream. Also, as the buildup progresses, the flow control device (e.g., slide gate or stopper rod) must be opened to maintain the desired flow rate. Once the flow control device reaches its maximum position, production must stop and the nozzle must be replaced. The significance, mechanism, and mitigation of nozzle clogging will be discussed in more detail in this study.

1.3 OBJECTIVE OF STUDY

The objective of this study is to improve understanding of the mechanisms involved in continuous casting nozzle clogging and to suggest countermeasures to reduce clogging. To achieve this, this work will review the proposed mechanisms for nozzle clogging, discuss metallographic examinations of nozzle clogs, and present results of mathematical models of the nozzle and clog.

1.4 METHODOLOGY

First, the literature is reviewed to understand the significance of nozzle clogging and previously-proposed theories for clogging. Then metallographic examinations of clogged nozzles and the associated casting conditions will be discussed to illustrate one particular type of clog. Next, the results of one-dimensional heat and mass transfer analyses and fluid flow analyses of clogged nozzles will be presented to determine the relative importance of several clogging mechanisms.

1.5 REFERENCES

1. Iron and Steel Institute. *Percentage of crude steel continuously cast, 1981-1990*. Iron and Steelmaker. 17: 16, 1991.

2. Iron and Steel Institute. *Percentage of crude steel continuously cast in the U.S.A., 1992-1993*. Iron and Steelmaker. 20: 14, 1993.

3. McAloon, T.: Iron & Steel Society, Warrendale, PA, private communication, 1994.

4. United States Steel: "Continuous Casting of Semi-Finished Steel Products" in *The Making, Shaping, and Treating of Steel*, W.T. Lankford Jr., N.L. Samways, R.F. Craven and H.E. McGannon, eds., Herbick & Held, Pittsburgh, PA, 1985, pp. 741-771.

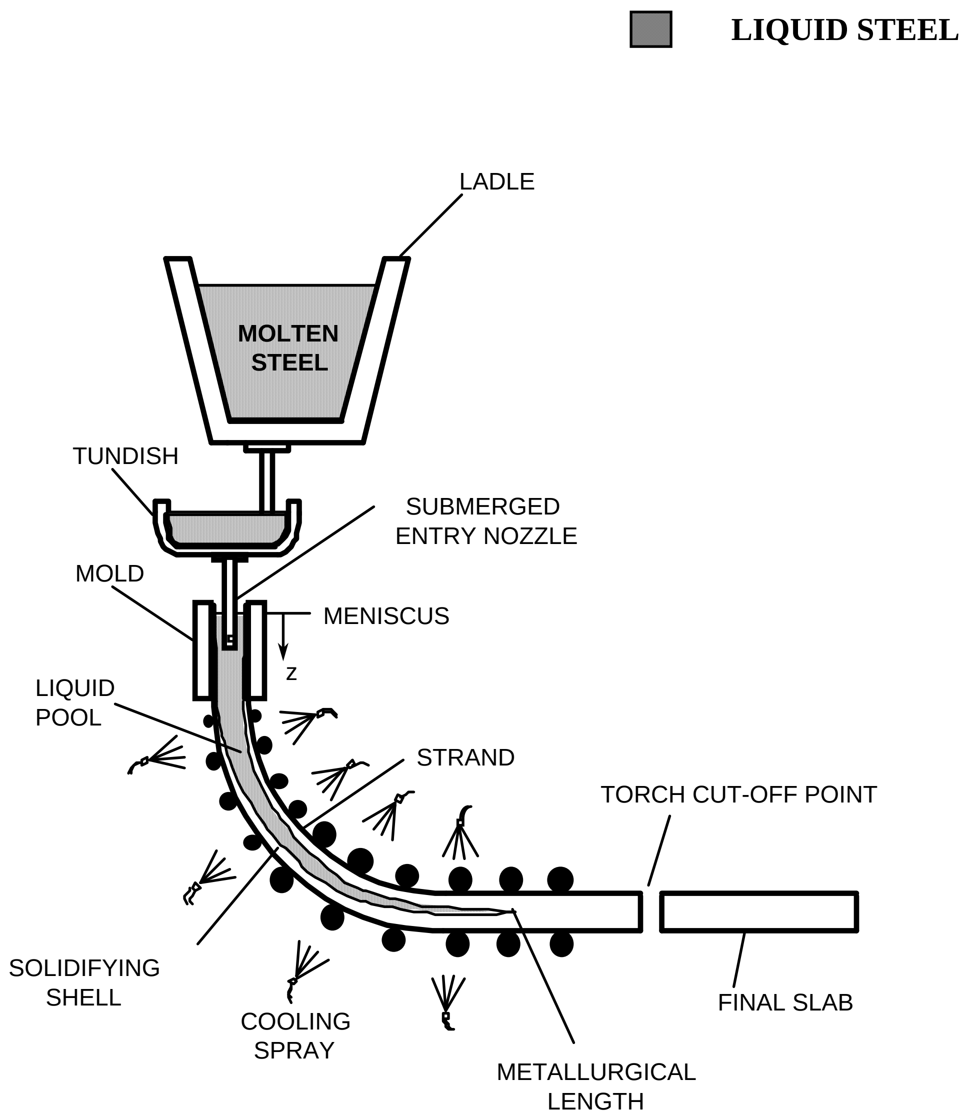

FIGURE 1.1 - Schematic Overview of the Continuous Casting Process

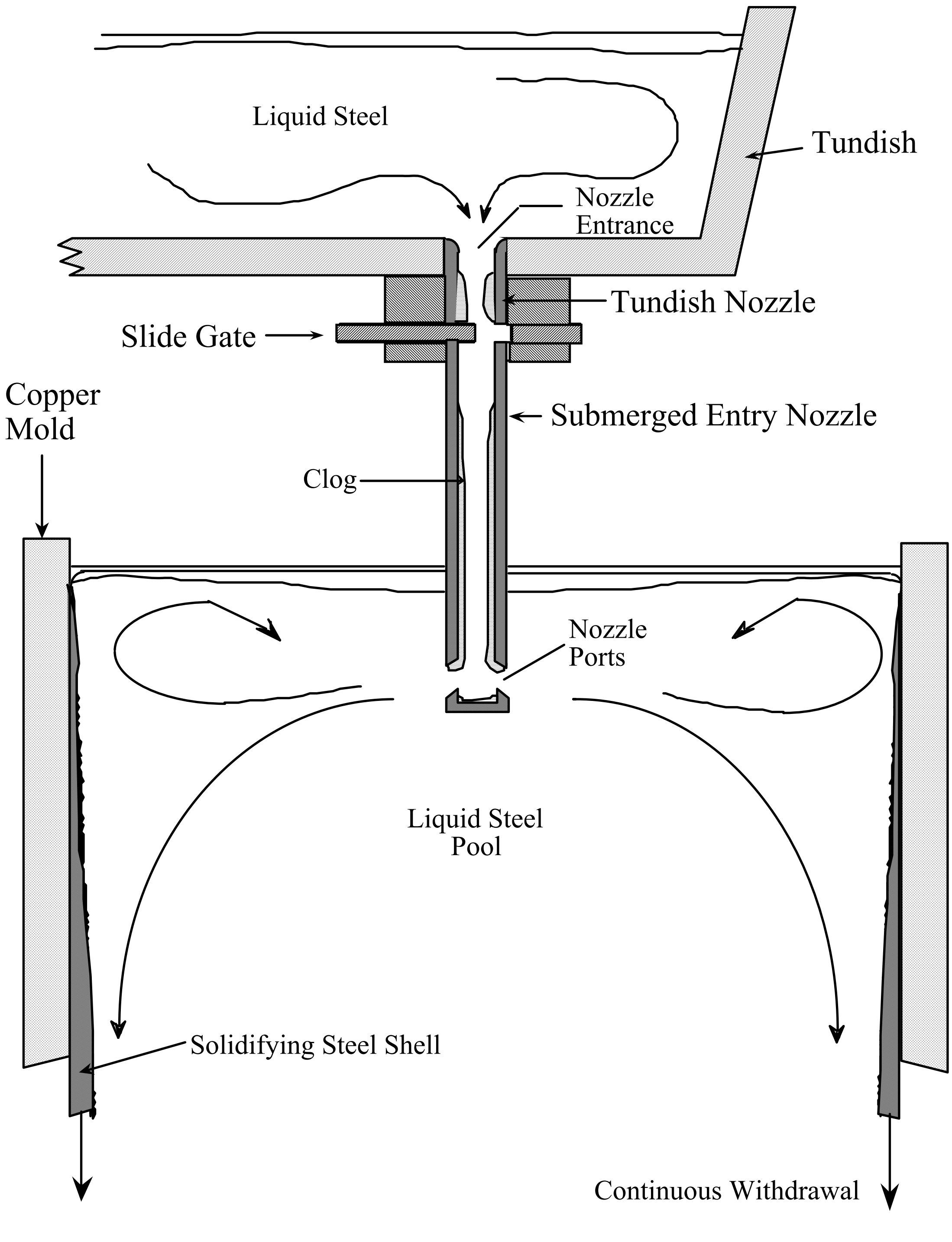

FIGURE 1.2 - Schematic of Continuous Caster Tundish Slide Gate System

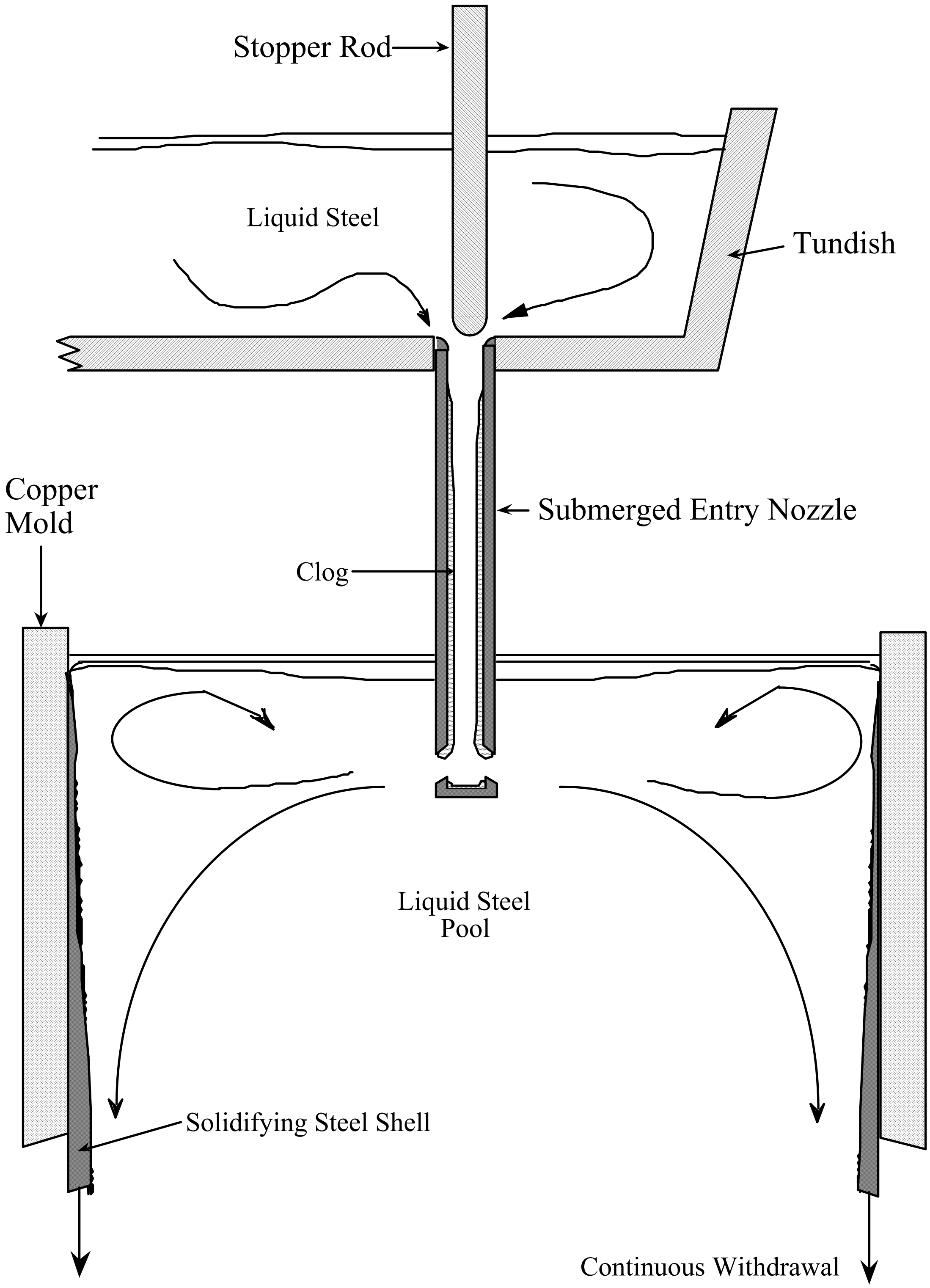

FIGURE 1.3 - Schematic of Continuous Caster Stopper Rod System

CHAPTER 2 - LITERATURE SURVEY

2.1 IMPORTANCE OF CLOGGING

Clogging in continuous casting nozzles is defined as the buildup of material in the flow passage between the tundish and mold (see Figure 1.1). The consequences of clogging include:

- Decreased productivity. To compensate for clogging, the flow control device (e.g., slide gate) must be further opened. If the clogging becomes sufficiently severe, the flow control device will no longer be able to compensate and then either a decrease in casting speed or replacement of the nozzle must result. These events reduce the net casting throughput and thereby reduce productivity.
- Increased cost. Depending on the casting shop, some portions of the clogged nozzles (e.g. submerged entry nozzle) can be independently replaced during casting. Other clogged portions (e.g., tundish nozzle) can only be replaced by changing tundishes. Several authors report that nozzle clogging (not tundish lining lifetime) limits the allowable tundish lifetime[1, 2]. For example, Haers et al. reported that clogging reduced the number of heats (290 tons) cast from twelve to six[3]. Therefore nozzle clogging results in additional costs for tundish refurbishment as well as for nozzle replacement.
- Decreased quality. Nonmetallic particles can become dislodged from the clog buildup and result in unacceptable cleanliness defects in the product, especially in deep drawn applications requiring that oxides be smaller than fifty microns in diameter[4-11]. The restriction of the flow passage may also cause undesirable flow patterns in the mold. This may lead to problems such as mold flux ingestion, shell thinning, and mold level fluctuations[6, 12-14]. In addition, level transients occurring when a tundish is replaced due to tundish nozzle clogging, can also reduce quality[3].

2.2 TYPES OF CLOGS

There are four general types of clogging, each from a different origin. In practice, clogging within a single nozzle could be due to a combination of two or more types. The classification chosen here distinguishes between clogs consisting of deoxidation products, solidified steel, complex oxides, and reaction products.

2.2.1 AGGLOMERATION OF DEOXIDATION PRODUCTS

Buildups consisting of deoxidation products from the earlier steelmaking process and reoxidation products formed prior to entering the nozzle (e.g., alumina, titania, zirconia) have been observed in the nozzles. These products, referred together as “deoxidation products”, are of the same composition and size (typically 1 - 20 micron[10, 15-17]) as is found in the mold[10, 16]. The deoxidation products sinter together to form a network[16, 18-20].

This sintered matrix may or may not encompass steel. Steel has been found within the matrix for heats with low residual deoxidation product content, as might be found when using vacuum degassing treatment (e.g. Dortmund Hoerder (DH) degassing) or for high carbon concentrations[10, 14]. No steel is found within the matrix when the deoxidation product concentration is high, as might be found when using argon bubbling during secondary refining and low carbon concentrations (e.g. less than 0.10% C)[10, 14]. The solidification of steel within the nozzle (either with or without an inclusion network) is referred to as "skulling".

2.2.2 SOLID STEEL BUILDUP

If the superheat is low, and the heat transfer from the stream is high, the steel may simply freeze within the nozzle, leading to a solid steel clog. This is especially likely at the start of cast if nozzle preheat is inadequate[21].

2.2.3 AGGLOMERATION OF COMPLEX OXIDES

Clogs containing nonmetallic materials not resulting from deoxidation have also been observed. Clogs have been observed in the submerged entry nozzle port area which have a chemistry indicative of a combination of mold flux and deoxidation particles. Here it is believed that the mold flux is drawn into the top of the ports due to the recirculation flow pattern in the upper part of the mold combined with the tendency of the flux to coat the nozzle[14, 22]. Once inside the nozzle, the flux assimilates deoxidation particles, thereby increasing the clog volume[6].

Clogs containing calcium aluminates or calcium sulfides have also been observed on calcium treated heats[6, 11, 15, 23-25]. Calcium is added to help alleviate clogging as discussed later in further detail.

2.2.4 REACTION PRODUCT BUILDUP

Clogging with the composition of deoxidation products but deposited in a film instead of a sintered network of particles has been observed. The source for these buildups has been attributed to reactions between the deoxidant and 1) air drawn into the nozzle due to the negative gauge pressure and the porosity of the nozzle[19, 26], 2) oxygen evolved from the steel due to the lower steel temperature adjacent to the nozzle[27], and 3) oxygen generated by silica refractory decomposition[18, 19, 26, 28, 29]. These mechanisms are consistent with the reported observations of increased clogging as soluble aluminum concentration is increased[4, 30].

2.3 CAUSES OF CLOGGING

For those clogs consisting of solidified steel or reaction products, the transport and attachment mechanism are straightforward because the clogging phenomenon takes place at the nozzle wall. For clogs containing inclusions, the processes of inclusion transport and attachment is more complicated. These processes are discussed below:

2.3.1 TRANSPORT OF INCLUSIONS

In general, the flow in continuous casting nozzles is turbulent ($Re \approx 10^5$). Inclusions, consisting primarily of deoxidation products, are easily transported throughout the bulk flow because of turbulent mixing. However, inclusion transport to the nozzle wall is hindered by the presence of a viscous sub-layer near the wall. Since flow in this layer is predominantly parallel to the wall, little driving force is present to promote inclusion deposition. It has been estimated that in order for an inclusion to be propelled from the bulk flow to the nozzle wall it would need an initial velocity in the direction of the wall which is two orders of magnitude greater than the bulk velocity[31]. To account for sufficient transport of inclusions across this viscous sub-layer to cause clogging, several theories have been proposed:

- Turbulent Recirculation Zones. Within a recirculation zone, the viscous sub-layer is essentially absent and turbulent velocity fluctuations exist in the near wall region. Those fluctuations oriented toward the wall will enable deposition, particularly at the separation point[31].
- Turbulent Flow. Other authors maintain that turbulent eddies, even in the absence of a recirculation zone, will transport a significant quantity of inclusions across the sub-layer to the nozzle wall[17].
- Rough Nozzle Walls. As the roughness of the nozzle wall is increased (e.g., due to irregular buildup or erosion) the probability of interception of entrained inclusion particles increases[11, 31, 32].
- Convex Surfaces. Since the density of alumina is less than steel, alumina will tend to be driven toward the wall for flow over a convex surface (e.g., tundish nozzle entry). This driving force is expected to be significant only for large alumina particles (e.g., >36 micron[17]).

2.3.2 ATTACHMENT OF INCLUSIONS

Inclusions are attached to the nozzle wall by surface tension and, after sufficient time, by sintered bonds. The surface tension of the steel creates a void and, consequently, an attractive force between the inclusion and the wall (or another inclusion)[10, 33]. The magnitude of this force for the case of a 2.5 micron deoxidation product attaching to a ceramic filter has been calculated to be approximately an order of magnitude greater than the drag and buoyant forces on the particle[20].

The sintered bond between the particle and wall (or another particle) forms relatively rapidly at these temperatures (e.g., only 0.03 seconds is required for two ten micron particles to develop a sufficient neck between them to withstand drag and buoyant forces[20]).

2.4 WAYS TO AVOID CLOGGING

The most obvious means to reduce clogging is to decrease the concentration of deoxidation products and the formation of reoxidation products[4, 10, 14, 24, 34, 35]. Means to achieve this increase in steel cleanliness have been reviewed by Byrne et al. and Szekeres[6, 14]. The important aspects of clean steelmaking include:

- Ladle Refining Practice. A vacuum degassing treatment yields better cleanliness than does argon bubbling[36].
- Reoxidation Prevention. Submerged ladle-to-tundish pouring, shielded tundish surface, and crack-free, non-porous refractories with leak-tight joints will reduce exposure of the steel to oxygen and thereby improve cleanliness[14].
- Inclusion Removal. Optimal tundish flow patterns[37] as well as filtration[20, 33, 38] and electromagnetic techniques[39] can remove inclusions from the melt.
- Flux Entrainment Prevention. Submerged ladle-to-tundish pouring and avoidance of ladle slag carryover will reduce the amount of exogenous inclusions in the melt[6, 14].

It is unlikely that steel cleanliness improvements will completely eliminate nozzle clogging. Dawson calculated that for typical casting conditions, nozzle blockage could occur if as little as one in every 1500 nonmetallic inclusions were deposited on the nozzle[31]. To reduce the deposition of the entrained inclusions, several techniques have been utilized as discussed below.

2.4.1 ARGON INJECTION

Argon injected through the nozzle wall or stopper rod into the steel stream is widely employed to reduce nozzle clogging. A typical injection rate is 5 five liter/minute (STP)[27, 40]. Several reasons have been suggested for the improved clogging resistance:

- A film of argon is formed on the nozzle wall which prevents the inclusion from contacting the wall[41-43].
- The argon bubbles flush the inclusions off the nozzle[42].
- The argon bubbles promote the flotation of inclusions[19].

- Argon injection increases the turbulence and thereby causes the deposit to be flushed off[34]. It is noted that this mechanism contradicts a previously mentioned hypothesis which states that turbulence enhances deposition.
- The partial vacuum inside the nozzle is decreased which thereby reduces air aspiration through the nozzle[14, 42]. In the absence of argon injection, negative gauge pressure has been measured in water models near the slide gate and the stopper rod seating surface[42]. In addition to increasing the nozzle pressure, the argon may replace air as the aspirated gas and thereby reduce clogging.
- The argon prevents chemical reactions between the steel and the refractory[19].

The argon can be injected through the pores in the refractory material[1, 2, 18, 41, 43, 44] or via machined or laser cut holes in the refractory[7, 18, 19]. Tailoring the argon flow to be greater in areas of high deposition[18, 44] and to be locally uniform[2, 44] has been shown to reduce clogging.

Disadvantages of argon injection include increased quality defects and nozzle slag line erosion due to increased mold level fluctuations[14, 27], bubble entrapment by the solidifying steel shell[8, 14, 44], and nozzle cracking due to high back pressure or decreased nozzle thermal shock resistance[1, 18, 44]. It is also suspected that argon injection tends to move a given clogging problem to a different location[32].

2.4.2 CALCIUM TREATMENT

Alumina clogging can be reduced by adding calcium to the steel to prevent the formation of solid alumina[25, 30, 45, 46]. As shown in Figure 2.1, for a typical melt temperature of 1550° C, liquid is the equilibrium phase for calcia-alumina mixtures containing 40 - 60% alumina. Furthermore, it is believed that under steelmaking conditions, mixtures containing a higher fraction of alumina will also be liquid. This is based on the observation that when $CaO{\cdot}2Al_2O_3$ inclusions (79% alumina) are found in the final cast product, these inclusions take a spherical form and the nozzle experiences much less clogging[23].

The disadvantages of calcium treatment include:

- Increased clogging relative to the non-treated condition if insufficient calcium is added, due to the formation of solid $CaO{\cdot}6Al_2O_3$[17, 23, 25].
- Erosion of refractories[5, 14, 27].
- Cost of calcium treatment.
- A possibly undesirable change in steel composition.

Also, calcium treatment will not work for high sulfur steels because calcium will react with sulfur to form solid calcium sulfide instead of liquefying the alumina[11] (e.g., sulfur must be less than 0.007% for a typical total aluminum concentration of 0.04%[47]). However, it has been proposed that calcium treatment might still be successful if the sulfur is added after calcium treatment[32].

2.4.3 NOZZLE MATERIAL MODIFICATIONS

A variety of nozzle compositions have been investigated. Calcia additions to the nozzle[10, 48-50] can decrease clogging by liquefying the inclusions, as discussed above. The effectiveness of this method is limited by the diffusion of the calcia to the refractory surface[50].

Other compositions and coatings have also been attempted[1, 3, 29, 32, 40, 51-53], but the cause for the decreased clogging is uncertain. For example, the addition of boron nitride has been shown to markedly reduce clogging[29, 32, 40]. However, it is not known whether the beneficial effect of boron nitride is due to the formation of a liquid boron oxide film[29], decreased surface roughness[31], or another cause. Other possible explanations for the observed clogging reduction of the various materials investigated are decreased thermal conductivity[51-53], decreased contact angle with steel[29, 51, 52], reduced reactivity with steel[26], and decreased air aspiration[3].

2.4.4 NOZZLE GEOMETRY MODIFICATIONS

In an effort to reduce the effect of clogging, oversized nozzle bores[3, 54] and replaceable submerged entry nozzles[3] are widely employed. To reduce the degree of clogging, the following have been investigated:

- Improved joint sealing. Strengthening the steelwork that holds the nozzle in place was found to reduce air aspiration and thereby reduce clogging[18].
- Rounded nozzle entrance. Incorporating a rounded entrance (in lieu of a sharp corner) to the tundish nozzle and ensuring proper vertical alignment can reduce clogging at the nozzle entrance by eliminating separated flow[31].
- Internal step. A five millimeter annular step incorporated at the mid-height of the submerged entry nozzle has been found to decrease alumina buildup in the lower part of the nozzle as well as decreasing flow impingement on the mold wide face[55].
- Varying nozzle internal diameter. Increasing the nozzle internal diameter just below the stopper rod seating surface has reduced clogging[14, 56].
- Flat bottomed nozzle. Decreased port clogging was observed when the elevation of the nozzle internal bottom and port bottom were coincident (i.e., no nozzle well)[55].
- Insulation around nozzle. Insulation, as well as preheat and heating, around the clogging location was observed to reduce clogging[14].

2.5 SUMMARY

Clogging in continuous casting nozzles results in decreased productivity, increased maintenance expense, and decreased product quality. Clogging results from deposition of deoxidation products, solidification on the nozzle wall, formation of complex oxides, or chemical reactions at the nozzle wall. These mechanisms may work together in practice. Effective clogging countermeasures include improving steel cleanliness, adding calcium, injecting argon, and eliminating flow recirculation zones.

It is clear from this review of nozzle clogging that the mechanisms for clogging are varied and the importance of the various phenomena at play are not well understood. The remainder of this thesis will present experimental investigations and mathematical models of nozzle clogging.

2.6 REFERENCES

1. L.T. Hamilton: "Technical Note - The Introduction of "Slit" Submerged Entry Nozzles to No. 1 Slab Caster, BHP International Group Pt. Kembla, NSW", *Bull. Proc. Austras. Inst. Min Metall.,* 1985, vol. 290 (No. 8), pp. 75-78.

2. M. Schmidt, T.J. Russo and D.J. Bederka: "Steel Shrouding and Tundish Flow Control to Improve Cleanliness and Reduce Plugging", *73rd ISS Steelmaking Conference*, ISS, Detroit, MI, 1990, Vol. 73, pp. 451-460.

3. F. Haers et. al.: " First Experience in Using the Caster Tube Change Device (TCD90)", *Fourth International Conference on Continuous Casting*, 1988.

4. G.C. Duderstadt, R.K. Iyengar and J.M. Matesa: "Tundish Nozzle Blockage in Continuous Casting", *Journal of Metals,* 1968, (April), pp. 89-94.

5. B. Hoh et. al.: "Improvement of Cleanliness in Continuous Casting", *Fourth International Conference on Continuous Casting*, 1988, pp. 211-222.

6. M. Byrne, T.W. Fenicle and A.W. Cramb: "The Sources of Exogenous Inclusions in Continuous Cast, Aluminum-Killed Steels", *ISS Transactions,* 1989, vol. 10, pp. 51-60.

7. H.T. Tsai, W.J. Sammon and D.E. Hazelton: "Characterization and Countermeasures for Sliver Defects in Cold Rolled Products", *73rd ISS Steelmaking Conference*, Detroit, MI, 1990, Vol. 73, pp. 49-59.

8. N. Bessho et. al. *Numerical Analysis of Fluid Flow in the Continuous Casting Mold by a Bubble Dispersion Model*. Iron and Steelmaker. 39-44, 1991.

9. K. Tanizawa et. al.: "Influence of the Steelmaking Conditions on Nonmetallic Inclusions and Product Defects", *1st European Conference on Continuous Casting*, Florence, Italy, 1991, pp. 1.491-1.550.

10. S. Ogibayashi et. al.: "Mechanism and Countermeasure of Alumina Buildup on Submerged Nozzle in Continuous Casting", *75th ISS Steelmaking Conference*, ISS, Toronto, Canada, 1992, Vol. 75, pp. 337-344.

11. W. Fix, H. Jacobi and K. Wünnenberg: "Collision-controlled Growth of Composites in Casting Nozzles", *Steel Research,* 1993, vol. 64 (1), pp. 71-76.

12. M.C.M. Cornelissen et. al.: "The Restless Mold, Incidental Disturbances Result in Localized Product Defects", *1st European Conference on Continuous Casting*, Florence, Italy, 1991, pp. 1.215-1.224.

13. J. Herbertson et. al.: "Modeling of Metal Delivery to Continuous Casting Molds", *74th ISS Steelmaking Conference*, ISS, Washington, D.C., 1991, Vol. 74, pp. 171-185.

14. E.S. Szekeres: "Review of Strand Casting Factors Affecting Steel Product Cleanliness", *Fourth International Conference on Clean Steel*, Balatonszéplak, Hungary, 1992.

15. Y.K. Shin et. al.: "Construction and Start-up of a Billet Caster at Pohang Works", *Ironmaking and Steelmaking,* 1988, vol. 15 (3), pp. 143-149.

16. S.N. Singh: "Mechanism of Alumina Buildup in Tundish Nozzles During Continuous Casting of Aluminum-Killed Steels", *Metallurgical Transactions,* 1974, vol. 5, pp. 2165-2178.

17. F.G. Wilson et. al.: "Effect of Fluid Flow Characteristics on Nozzle Blockage in Aluminum-Killed Steels", *Ironmaking and Steelmaking,* 1987, vol. 14 (6), pp. 296-309.

18. S.R. Cameron: "The Reduction of Tundish Nozzle Clogging During Continuous Casting at Dofasco", *75th ISS Steelmaking Conference*, ISS, Toronto, Canada, 1992, Vol. 75, pp. 327-332.

19. M.C. Tai, C.H. Chen and C.L. Chou: "Development and Benefits of Four-Port Submerged Nozzle for Bloom Continuous Casting", *Continuous Casting '85*, London, England, 1985, pp. 19.1-19.6.

20. K. Uemura et. al.: "Filtration Mechanism of Non-metallic Inclusions in Steel by Ceramic Loop Filter", *ISIJ International,* 1992, vol. 32 (1), pp. 150-156.

21. J. Szekely and S.T. DiNovo: "Thermal Criteria for Tundish Nozzle or Taphole Blockage", *Metallurgical Transactions,* 1974, vol. 5 (March), pp. 747-754.

22. B.G. Thomas and X. Huang: "Effect of Argon Gas on Fluid Flow in a Continuous Slab Casting Mold", *76th ISS Ironmaking and Steelmaking Conference*, ISS, Dallas, Texas, 1993, Vol. 76, pp. 273-289.

23. G.M. Faulring, J.W. Farrell and D.C. Hilty: "Steel Flow Through Nozzles: Influence of Calcium", in *Continuous Casting, Volume One, Chemical and Physical Interactions During Transfer Operations*, Iron and Steel Society, Warrendale, PA, 1985, pp. 57-66.

24. G.A. Demasi and R.F. Hartmann: "Development of the Ladle Shroud Mechanism and its Metallurgical Benefits", in *The Shrouding of Steel Flow for Casting and Teeming*, Iron and Steel Society, Warrendale, PA, 1986, pp. 3-11.

25. B. Bergmann, N. Bannenberg and R. Piepenbrock: "Castability Assurance of Al-Killed Si-Free Steel by Calcium Cored Wire Treatment", *1st European Conference on Continuous Casting*, Florence, Italy, 1991, pp. 1.501-1.508.

26. Y. Fukuda, Y. Ueshima and S. Mizoguchi: "Mechanism of Alumina Deposition on Alumina Graphite Immersion Nozzle in Continuous Caster", 1992, vol. 32, pp. 164-168.

27. H.F. Schrewe: "Metallurgy and Cleanness", in *Continuous Casting of Steel - Fundamental Principles and Practice*, Stahl Elsen Co., 1987, pp. 100-103.

28. S.K. Saxena et. al.: "Mechanism of Clogging of Tundish Nozzle during Continuous Casting of Aluminum-Killed Steel", *Scandinavian Journal of Metallurgy,* 1978, (7), pp. 126-133.

29. E. Lührsen et. al.: "Boron Nitride Enrichment of the Submerged Entry Nozzles: A Solution to Avoid Clogging", *1st European Conference on Continuous Casting*, Florence, Italy, 1991, pp. 1.37-1.57.

30. K.H. Bauer: "Influence of Deoxidation on the Castability of Steel", *Continuous Casting of Steel*, Biarritz, France, 1976.

31. S. Dawson. *Tundish Nozzle Blockage During the Continuous Casting of Aluminum-Killed Steel*. Iron and Steelmaker. 33-42, 1990.

32. N.A. McPherson and A. McLean: *Continuous Casting - Volume Six - Tundish to Mold Transfer Operations*, Iron and Steel Society, Warrendale, PA, 1992, pp. 11-15.

33. P.F. Wieser: "Filtration of Irons and Steels", in *Foundry Processes, Their Chemistry and Physics*, S. Katz and C.F. Landefeld, eds., Plenum Press, New York, 1988, pp. 495-512.

34. A.W. Cramb and I. Jimbo: "Interfacial Considerations in Continuous Casting", *ISS Transactions,* 1990, vol. 11, pp. 67-79.

35. C.H. Bode, J.D. Duke and F.J. Dewez: "Design of Slab-Casting Facilities to Maximize Machine Availability", *Continuous Casting of Steel*, Biarritz, France, 1976.

36. United States Steel: "Secondary Steelmaking or Ladle Metallurgy", in *The Making, Shaping, and Treating of Steel*, W.T. Lankford Jr. et. al., eds., Herbick & Held, Pittsburgh, PA, 1985, pp. 671-690.

37. A.K. Sinha and Y. Sahai: "Mathematical Modeling of Inclusion Transport and Removal in Continuous Casting Tundishes", *ISIJ International,* 1993, vol. 33 (5), pp. 556-566.

38. D. Apelian and K.K. Choi: "Metal Refining by Filtration", in *Foundry Processes, Their Chemistry and Physics*, S. Katz and C.F. Landefeld, eds., Plenum Press, New York, 1988, pp. 467-493.

39. S. Taniguchi and ". J. K. Brimacombe Vol. , No. , , pp..: "Application of Pinch Force to the Separation of Inclusion Particles from Liquid Steel", *ISIJ International,* 1994, vol. 34 (9), pp. 722-731.

40. E. Höffken, H. Lax and G. Pietzko: "Development of Improved Immersion Nozzles for Continuos Slab Casting", *Fourth International Conference on Continuous Casting*, 1988.

41. H. Buhr and J. Pirdzun: "Development of Refractories for Continuous Casting", *Continuous Casting of Steel*, Biarritz, France, 1976.

42. L.J. Heaslip et. al. *Model Study of Fluid Flow and Pressure Distribution During SEN Injection - Potential for Reactive Metal Additions During Continuous Casting*. Iron and Steelmaker. 49-64, 1987.

43. T.R. Meadowcroft and R.J. Milbourne: "A New Process for Continuously Casting Aluminum Killed Steel", *Journal of Metals,* 1971, (June), pp. 11-17.

44. I. Sasaka et. al.: "Improvement of Porous Plug and Bubbling Upper Nozzle For Continuous Casting", *74th ISS Steelmaking Conference*, ISS, Washington, D.C., 1991, Vol. 74, pp. 349-356.

45. J.R. Bourguignon, J.M. Dixmier and J.M. Henry: "Different Types of Calcium Treatment as Contribution to Development of Continuous Casting Process", *Continuous Casting '85*, London, England, 1985, pp. 7.1-7.9.

46. D. Bolger: "Stopper Rod and Submerged Nozzle Design and Operation in Continuous Casting", *77th ISS Steelmaking Conference*, ISS, Chicago, IL, 1994, Vol. 77, pp. 531-537.

47. K. Larsen and R.J. Fruehan: "Calcium Modification of Oxide Inclusions", *ISS Transactions,* 1991, vol. 12, pp. 125-132.

48. E. Marino: "Use of Calcium Oxide as Refractory Material in Steel Making Processes", in *Refractories for the Steel Industry*, R. Amavis, eds., Elsevier Applied Science, New York, 1990, pp. 59-68.

49. T. Aoki et. al.: "Alumina Clogging Resistant Materials for Tundish Shrouds", *74th ISS Steelmaking Conference*, ISS, Washington, D.C., 1991, Vol. 74, pp. 357-360.

50. P.M. Benson, Q.K. Robinson and H.K. Park: "Evaluation of Lime-Containing Sub-Entry Shroud Liners to Prevent Alumina Clogging", *76th ISS Ironmaking and Steelmaking Conference*, ISS, Dallas, Texas, 1993, Vol. 76, pp. 533-539.

51. L.I. Evich et. al.: "Experience in the Use of Chamotte Nozzles in Slide Gates in Teeming of Stainless Steel", *Ogneupory,* 1985, (11), pp. 44-46.

52. K.K. Strelov: “Clogging of the Channel of a Fosterite Nozzle in Teeming of Aluminum-Deoxidized Steel”, *Ogneupory,* 1985, (8), pp. 46-49.

53. R. Szezesny, C. Naturel and J. Schoennahl: “Tundish Nozzles with a Double Layer Conception Used at Vallourec Saint-Saulve Plant”, *Fourth International Conference on Continuous Casting*, 1988, pp. 495-502.

54. A. Jaffuel and J.P. Robyns: “FLO CON Slide Nozzles”, *Continuous Casting of Steel*, Biarritz, France, 1976.

55. N. Tsukamoto et. al.: “Improvement of Submerged Nozzle Design Based on Water Model Examination of Tundish Slide Gate”, *74th ISS Steelmaking Conference*, ISS, Washington, D.C., 1991, Vol. 74, pp. 803-808.

56. United States Steel: “The Physical Chemistry of Iron and Steelmaking”, in *The Making, Shaping, and Treating of Steel*, W.T. Lankford Jr. et. al., eds., Herbick & Held, Pittsburgh, PA, 1985, pp. 367-502.

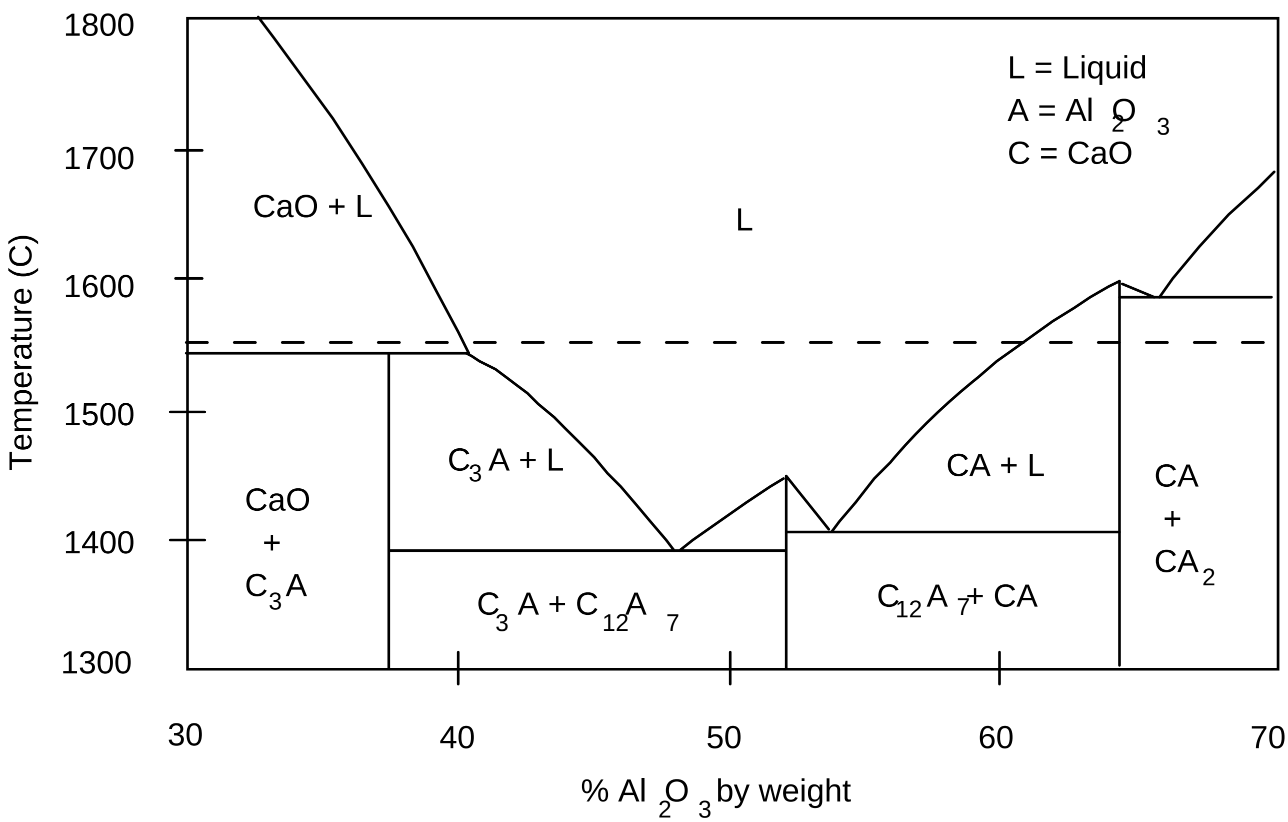

FIGURE 2.1 - Calcia-Alumina Phase Diagram

CHAPTER 3 - EXPERIMENTS

3.1 OVERVIEW

The aim of this experimental study is to characterize and quantify the clogging found in tundish nozzles from Inland Steel and to correlate this with the available casting data. This work will be used to determine clogging mechanisms that warrant further study. In addition, it will illustrate the large cast-to-cast variation in clogging behavior.

3.2 TUNDISH NOZZLE CLOGGING CHARACTERIZATION

Inland Steel provided a total of 15 tundish nozzle samples for evaluation. Inland utilizes a slide gate system to control the flow of steel from the tundish to the mold (see Figure 1.2). Each of their tundishes is equipped with two tundish nozzles (see Figure 3.1) and can thereby feed two strands. When a tundish is replaced (e.g. due to excessive tundish nozzle clogging), the slide gate is closed and the steel above the slide gate and in the tundish is allowed to freeze. While the steel is cooling, the tundish is moved off of the casting floor to the tundish refurbishment area. Here the tundish is turned upside down and the chunk of solid steel in the tundish and tundish nozzles falls out with the tundish nozzles attached. The tundish nozzles are then broken off and samples are obtained by cutting the pieces of solid steel which were previously in the tundish nozzles, off of the remainder of the chunk of solid steel. Often, the non-metallic deposit on the tundish nozzle inner diameter is captured by this steel “plug” and is therefore available for examination. The plugs from various tundish nozzles were halved longitudinally with a band saw and provided to the University for this investigation.

3.2.1 MACROETCHING INVESTIGATION

Visual examination of the as-provided samples revealed a clog buildup near the nozzle inner diameter surrounding a solid steel core as expected (e.g., see Figure 3.2). To determine the full extent of the clog buildup and to reveal variations in the structure of the clog, several samples were exposed to an elevated temperature hydrochloric acid macro-etch[1].

The macro-etch was accomplished within an exhaust hood and utilized an electric skillet to heat the diluted hydrochloric acid bath to an aim temperature of 70˚ - 80˚ C. The procedure used for the etch is as follows:

1) Install a handle on the sample. Holes were drilled and tapped on the surface opposite the sectioned surface and a handle was attached.

2) Mill the sectioned surface. This step was skipped for some samples as it was found that an adequate etch could be obtained without milling.

3) Preheat the sample. The sample was placed, with the sectioned surface down, onto glass stirring rods in a Pyrex dish. This dish was then placed onto wooden spacers in an electric skillet. The skillet and the dish were then filled with water. The sample was then heated till the water in the Pyrex dish reached the aim temperature. It was found that covering the electric skillet greatly reduced the preheat time (e.g., 20 min. vs. 45 min.). The temperature of the electric skillet was adjusted so as to avoid excessive boiling.

4) Etch the sample. The Pyrex dish was then drained and refilled with a mixture containing 50% deionized water and 50% concentrated hydrochloric acid (37% hydrochloric acid by weight). This bath was heated to the aim temperature for approximately one hour.

5) Preserve the sample. After etching, the sample was rinsed with water. This caused a film of rust to quickly form on the sectioned surface. This rust was then removed by scrubbing with cotton balls soaked with a 50% deionized water - 50% phosphoric acid mixture[1]. The surface was then dried, coated with a clear oil, and wrapped with Seran Wrap, to reduce rust formation.

A total of four samples were etched in this fashion. A discussion of the etched samples as well as the other samples is given below.

3.2.2 DISCUSSION OF TUNDISH NOZZLE EXAMINATIONS

• *Cast 9267, Strand 2:*

First consider Figure 3.2. The direction of steel flow during casting was from the wide end to the narrow end. The flat surface at the base of the narrow end was formed when the slide gate closed at the end of cast. The shiny area in the core of the sample corresponds to steel that was trapped and frozen when the slide gate closed.

The clog surrounding the core appears as gray because the alumina inclusions in that region effectively increase the surface roughness and thereby diffuse the incident light. Therefore the shade of grade is a measure of the amount of steel entrapped within the clog. The dark regions within the clog correspond to shadows created by relatively deep depressions. These depressions were likely regions of pure alumina buildup from which the alumina fell out during machining. Alternately, these regions may have been the paths by which the injected argon gas reached the steel stream.

In general, it appears that the clogged thickness increases rapidly with distance down from the nozzle entrance (defined in Figure 1.2), then reaches a relatively constant thickness, and finally decreases at the nozzle exit. However, it is unclear whether this final profile is indicative of the natural growth pattern of the clog or instead the effectiveness of the rodding procedure (the procedure whereby a bundle of steel rods is manually jabbed in and out of the tundish nozzle from the top side). The reason for the greater buildup in the tundish nozzle mid-section may be due to the higher heat transfer in that region and/or the inability of the rodding to remove a buildup containing solid steel.

Figure 3.3 shows the macro-etched version of the sample shown in Figure 3.2. The boundary between the clog and the steel core can now be seen more clearly. The grain structure of the steel core is now visible due to the preferential dissolution of the relatively high energy grain boundaries. It is seen that the grains are oriented vertically, indicating that the heat loss after cast termination was mainly through the bottom of the nozzle.

The clog region in Figure 3.3 now appears darker due to pits generated when the steel surrounding the alumina inclusions was dissolved thereby allowing the inclusions to subsequently fall out. This statement is corroborated by the observation of a significant quantity of inclusions in the used etchant. The white areas within the clog are artifacts of the macro-etching procedure (i.e., lint from the cotton swabs used to preserve the sample).

As shown in Figure 3.4, the extent of clogging can be observed accurately in the saw cut surface without etching. In Figure 3.4, a transparency showing the clog profile as traced from the pre-etched sample, is placed onto the etched sample. The good agreement in clog profiles is clear.

- *Cast 9361, Strands 1&2:*

Figure 3.5 shows the clog resulting from casting with a different type of nozzle under different casting conditions. As indicated in Table 3.1, the nozzle corresponding to this sample delivered argon to the nozzle inner diameter via “pierced” holes (see Figure 3.1), unlike the sample shown in Figure 3.2 in which a porous sleeve was used to distribute the argon to the inner diameter. Also, the heats corresponding to this sample had approximately fourteen times the carbon concentration of the heats corresponding to the prior sample. Therefore, assuming all other things equal, the cleanliness of this steel should have been much better (because less aluminum deoxidation was required). Finally, this sample came from a single strand cast (the other nozzle became clogged with frozen steel at the start of cast).

The clogging pictured in Figure 3.5 is generally less severe than that seen in Figure 3.2. The abrupt increase in clog thickness near the bottom of the sample likely corresponds to the distance which the rods were jabbed into the nozzle.

The sample corresponding to the other strand for this cast is shown in Figure 3.6. From the macro-etch, it appears that the freezing which occurred at the start of cast was greatest in the nozzle mid-section. A distinct line (marked by small bubbles) appears to distinguish the skull that formed at the start of cast from the later freezing that occurred after the slide gate was closed. This provides evidence that even partial clogging is sufficient to stop casting. The thinner layer of initially frozen steel near the bottom of the nozzle was likely due to the higher mixing of the flow near the slide gate in this region, which prevents the stagnant flow regions conducive to skull formation.

- *Cast 9369, Strand 1:*

The last macro-etched sample is shown in Figure 3.7. (The distorted shape of this sample is an artifact resulting from the process of removing the sample from the tundish.) This again corresponds to a pierced hole nozzle. The average carbon concentration for the heats corresponding to this sample is roughly equal to that for the first sample discussed (Figure 3.2) so the steel should have approximately the same cleanliness. The final extent of clogging in this sample is roughly the same as in the first sample discussed. However, the surface of this sample contains more voids. This suggests that the concentration of alumina in the clog in this sample was higher, possibly due to the better insulating characteristics of this nozzle. Alternately, the increased void fraction may indicate that a larger volume of argon was entrapped within the alumina clog due to the relative improvement in argon injection for this nozzle (as indicated by the back-pressure in Table 3.1).

- *Remaining Samples:*

The remaining samples show the same types of clogging discussed above, differing only in the extent of clogging and the amount of void spaces on the sectioned surface. In general, the degree of void space within the clog was greater for the samples from lower carbon concentrations heats. This observation is consistent with the observations of prior authors as discussed in chapter 2.

3.3 CASTING DATA EVALUATION

In addition to the above samples, Inland Steel also provided data describing several of the process parameters during the casting of these samples. Two types of data were provided: 1) detailed measurements corresponding to every 100 mm of slab cast and 2) summary measurements which provide average values for an entire slab. Also, Inland Steel provided a strip chart recording of the temperature at the inlet to a tundish nozzle during a typical cast sequence. This data is discussed below.

3.3.1 DETAILED DATA

The measurements taken at 100 mm intervals were: strand speed, slide gate position (fraction open), strand width, and tundish melt weight. Also, a calculated ‘nozzle clogging factor’ was included with the data. The nozzle clogging factor is the ratio of the actual-to-predicted steel flow rate through the nozzle. The predicted flow rate is calculated assuming inviscid, irrotational flow modified by a correction factor (γ) (usually about 1.0 to 1.4):

$$\dot{m} = \gamma \, \rho_{Fe} \, A_{sg} \sqrt{2 \, g \, h}$$

(See Nomenclature page for symbol descriptions.) This data was provided for four casts and is shown in Figures 3.8 - 3.14.

As expected the clogging, as indicated by slide gate position for relatively constant casting conditions, increases with time. It is seen that rodding events and submerged entry nozzle replacements during the cast can greatly decrease the clogging (see Figure 3.8, position 1500). It is also noted that the slide gate position varies more greatly with time as the clogging increases. This may be due to two causes. First, as the flow passage is constricted by the clog buildup, the shear stress on the surface of the clog will increase, thereby promoting clog removal. Second, as will be discussed in the next chapter, the increment of slide gate travel needed to compensate for an increment of additional clog buildup increases as the clog thickness increases.

The detailed data presented here will be utilized in the next chapter to calibrate a flow model of the tundish/tundish nozzle/slide gate/submerged entry nozzle.

3.3.2 SUMMARY DATA

The summary data for each slab contained averaged values of: slide gate position, nozzle clogging factor, argon flow rates and back pressures in the tundish nozzle and slide gate top plate, casting speed, tundish melt weight, # of rodding events, # of slow downs to prevent breakout, tundish melt temperature, and mold width; as well as other slab identification and specification information. The data also indicated when a submerged entry nozzle replacement occurred.

Figures 3.15 - 3.27 display the clogging factor evolution for the nozzle samples considered. The figures also display the corresponding superheat, measured in the bulk tundish, as well as indicate when ladle change, submergence entry nozzle (SEN) replacements, and rodding events took place. The average levels of argon flow and back-pressure are given for each sample in Table 3.1.

The figures indicate that nozzle clogging is a complex process which depends on many process variables. For example, consider Cast 9361, Strand 2 (Figure 3.17). For this cast, the clogging factor indicates that a significant amount of clogging occurs at the onset of cast. The clogging worsens from slab 13 to slab 19 of the cast. At this time, the submerged entry nozzle was replaced and the tundish nozzle was rodded. This results in a substantial reduction in clogging. It is speculated that the initial clogging in this nozzle is due to skulling (recall that the other strand for this cast froze at the start of cast). As casting progressed, the skull gradually melted and was replaced by a deoxidation product buildup. Then the clogging in the submerged entry nozzle was eliminated by nozzle replacement and the deoxidation product buildup in the tundish nozzle was reduced by rodding to a level not detectable by slide gate position. It is speculated that this clog network must have contained only liquid steel, possibly due to the higher superheat at that time.

The effectiveness of submerged entry nozzle replacement and rodding varies considerably. For example, during Cast 9267, Strand 1, (Figure 3.15) replacement of the submerged entry nozzles and rodding did little to reduce clogging. It is speculated that the tundish nozzle clogging contained a significant amount of skulling and thereby reduced the effectiveness of rodding.

In addition to the argon back-pressure and flowrate summary data, Inland provided additional plots of argon back-pressure for Cast 9030. An excerpt from these plots is shown in Figure 3.28. The significance of back-pressure will be further discussed in Chapter 4.

3.3.3 NOZZLE INLET TEMPERATURE DATA

Inland Steel performed thermocouple measurements in September 1994 to determine the variation of temperature at the tundish nozzle entrance during casting. A section of the strip chart recording for this test is shown in Figure 3.29. Each block in the direction of the strip chart travel represents 3 minutes. Each block in the direction perpendicular to the strip chart travel represents 5.5˚ C. It is seen from this figure that large changes in melt temperature can occur in the nozzle well during ladle changes. For example, the temperature dropped approximately 14˚ C from 9:20 to the ladle change at 9:45. The temperature then quickly increased approximately 20˚ C during the following 9 minutes. The strip chart data is compared with the bulk tundish temperature data in Figure 3.30 for a time span corresponding to three heats. It is seen that the variation in the bulk tundish temperature (as was presented above) is not nearly as large (i.e., the tundish temperature dropped 3˚ C and then increased 6˚ C over the same time span).

The cause for the difference in temperature trends for the bulk tundish region and the tundish nozzle entrance is likely due to the tundish flow patterns. It has been suggested that the flow may "short circuit" during the ladle change and thereby cause the large variations in the temperature of steel passing through the nozzle[2]. In this theory, the new, hot steel would bypass the old steel in the tundish in the time following the ladle change. This would allow the old steel additional time to cool. Then later during that heat, the flow pattern would again change and the old, cool steel would enter the nozzle.

This test indicates that the tundish nozzle sees a significant range of casting temperature during a normal cast. The next chapter presents a model which assesses the importance of this temperature variation on nozzle clogging.

3.4 SUMMARY

The experimental investigations presented here suggest that heat transfer may play an important role in the clogging process. It is also clear that other process variables also have a significant role to play. For example, the degree of clogging removed by rodding, the amount of clogging in the submerged entry nozzles, the integrity of the argon distribution system (i.e., did nozzle cracks develop), the temperature distribution in the preheated nozzle prior to cast, the cleanliness of the steel, and the temperature of the steel entering the nozzle should all play a crucial role in determining the clogging.

Since it is impractical or impossible to obtain this type of data from an operating caster, mathematical models are developed in the next chapter and applied to estimate the importance of various phenomena to the nozzle clogging process.

3.5 REFERENCES

1. A.O. Benscoter: "Metallographic Techniques and Microstructures: Carbon and Alloy Steels", in *Metals Handbook*, Vol. 9, K. Mills et. al., eds., American Society for Metals, Metals Park, Ohio, 1985, pp. 165-196.

2. R. Gass: private communication, 1995.

TABLE 3.1 - Casting Conditions for Nozzle Samples

Cast	Nozzle Type	% C [1]	% Al [1,2]	Argon Back-Pressure (kPa) [3]	Argon Flowrate (L/min) [4]	# of Rodding Events [5]	# of Heats Cast [6]
9267	porous [7]	.00226	.03876	14/17	6.5/5.1	8/2	5
9361	pierced [8]	.03217	.04407	0/78	0/4.2	0/1	3 [9]
9369	pierced	.00183	.04094	68/43	4.0/5.5	1/3	7
9374	pierced	.00173	.04409	70/77	5.5/4.2	1/1	8
9380	pierced	.01124	.06276	81/83	5.4/4.1	0/0	5
24486 [10]	pierced	.09164	.04810				10
9388	pierced	.00271	.25302	88/84	5.1/4.2	2/0	10
9030	pierced			39/?[11]	4.8/?[11]	1/2	6

[1] Average for all heats.
[2] Soluble aluminum concentration.
[3] Gauge pressure in the argon line feeding the tundish nozzle.
[4] Argon flowrate to the tundish nozzle.
[5] Rodding is the process of jabbing a bundle of steel rods into the tundish nozzle during casting to remove clog buildup. The number of rodding events on each of the two strands is indicated in the table by x/y.
[6] A heat is defined as the contents of one ladle and consists of about 250×10^3 kg of steel.
[7] An alumina-graphite nozzle with sufficient porosity to pass argon.
[8] A dense alumina-graphite nozzle with 0.4 mm drilled holes for passing argon.
[9] Single strand cast (tundish nozzle for strand 1 became blocked with frozen steel at the start of the cast).
[10] Cast on #2 slab caster (all other data from #1 slab caster).
[11] Two sources of data conflict for this sample.

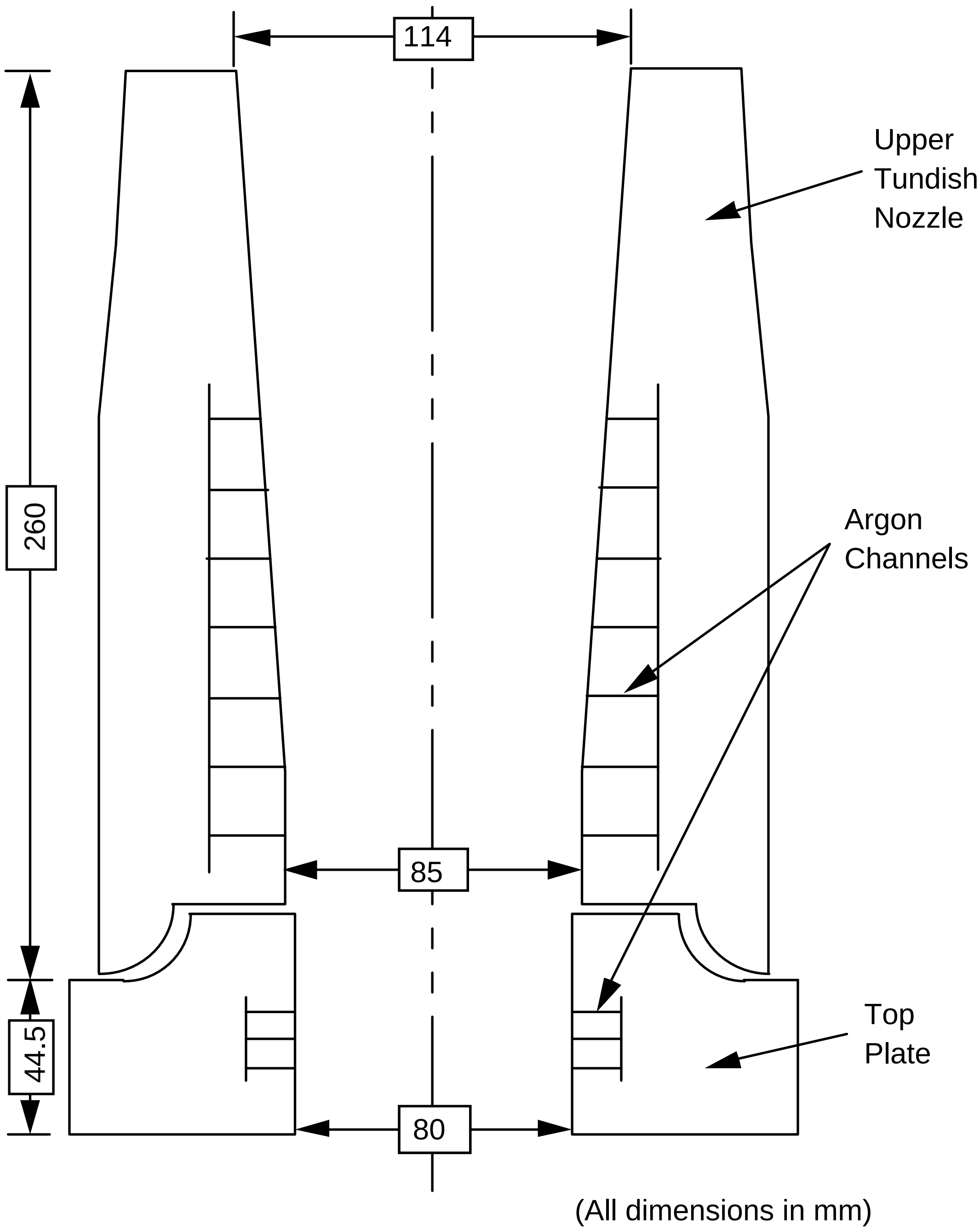

FIGURE 3.1 - Upper Tundish Nozzle and Slide Gate Top Plate

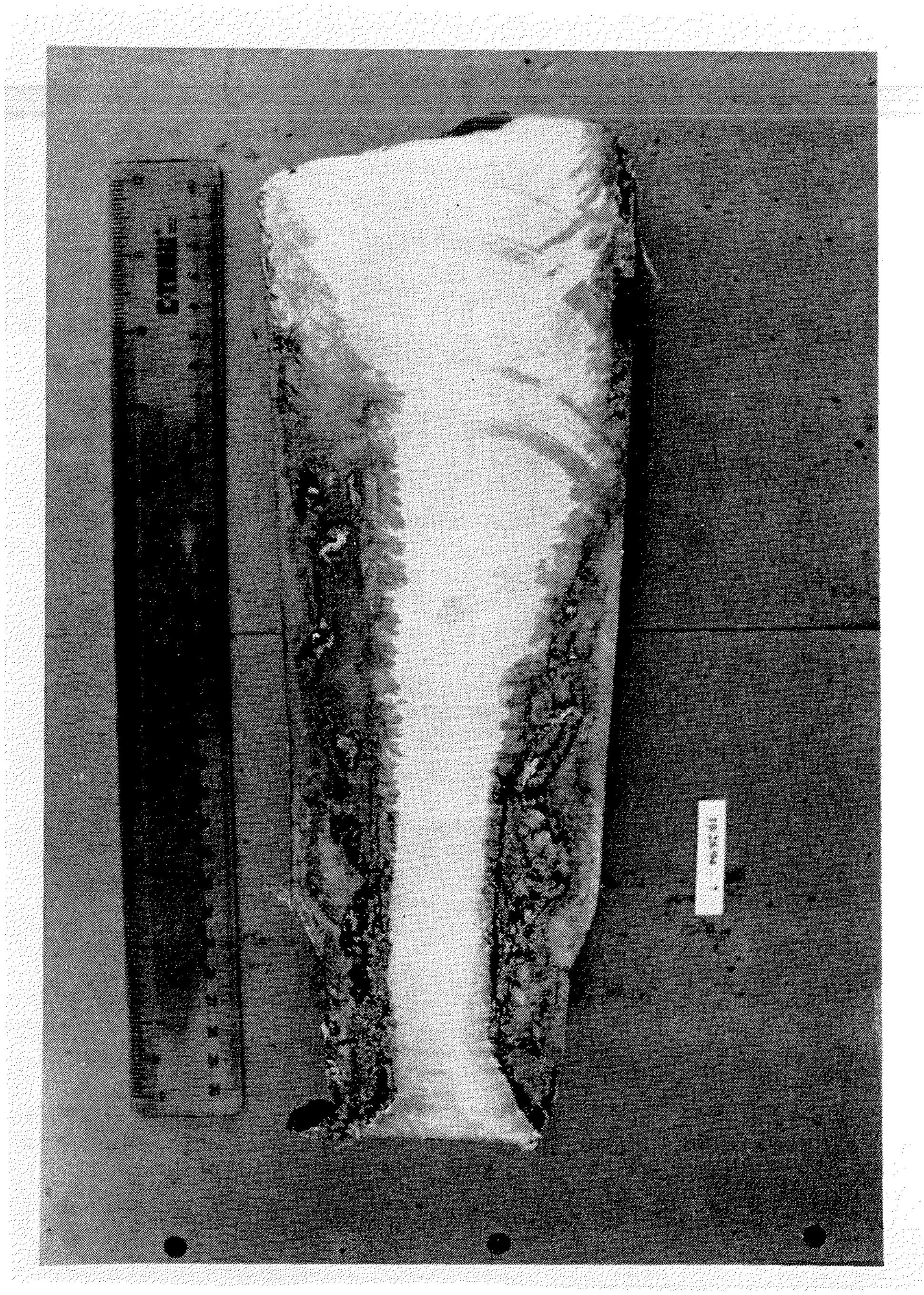

FIGURE 3.2 - Milled Tundish Nozzle Sample (Cast 9267, Strand 2)

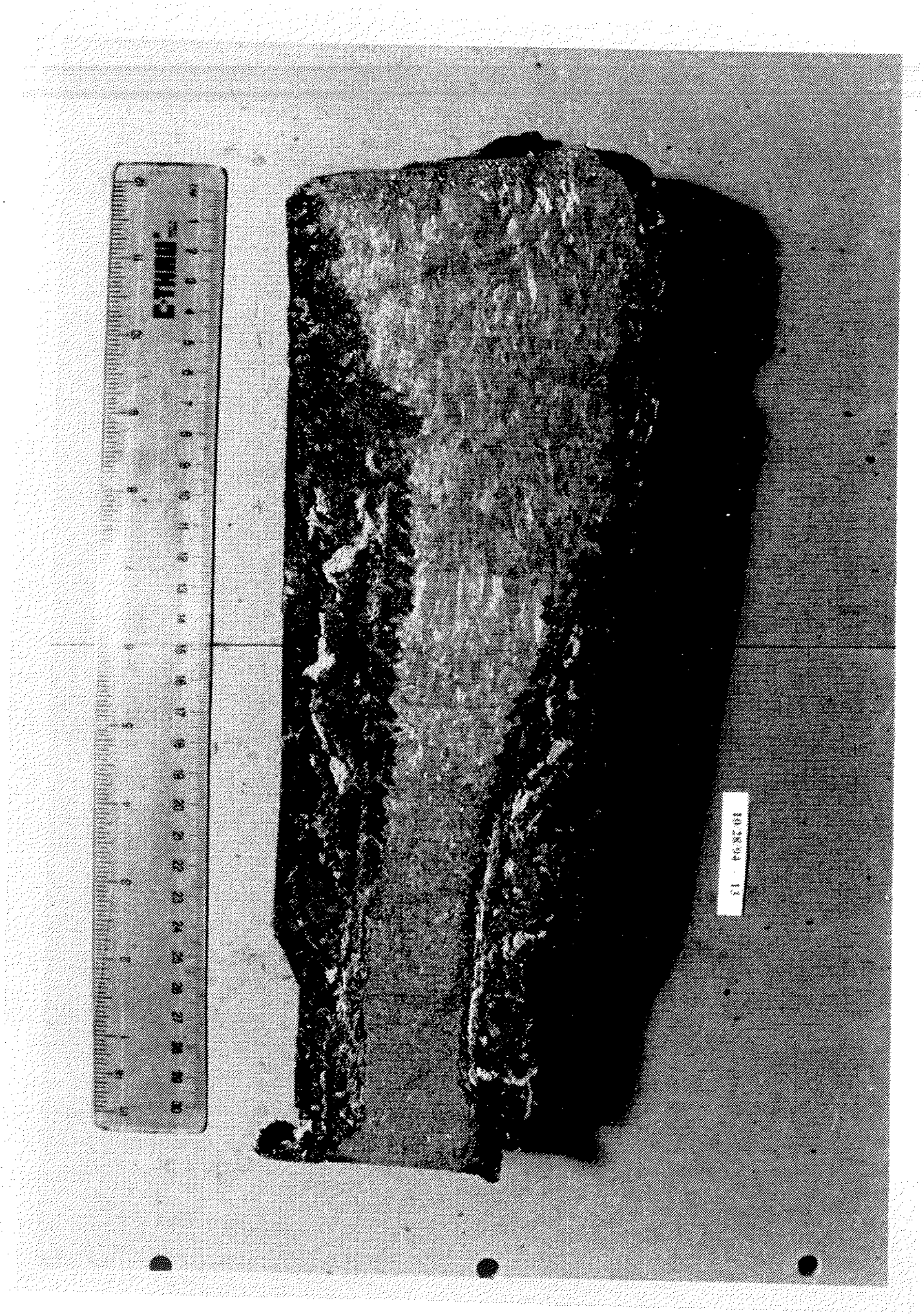

FIGURE 3.3 - Macro-Etched Tundish Nozzle Sample (Cast 9267, Strand 2)

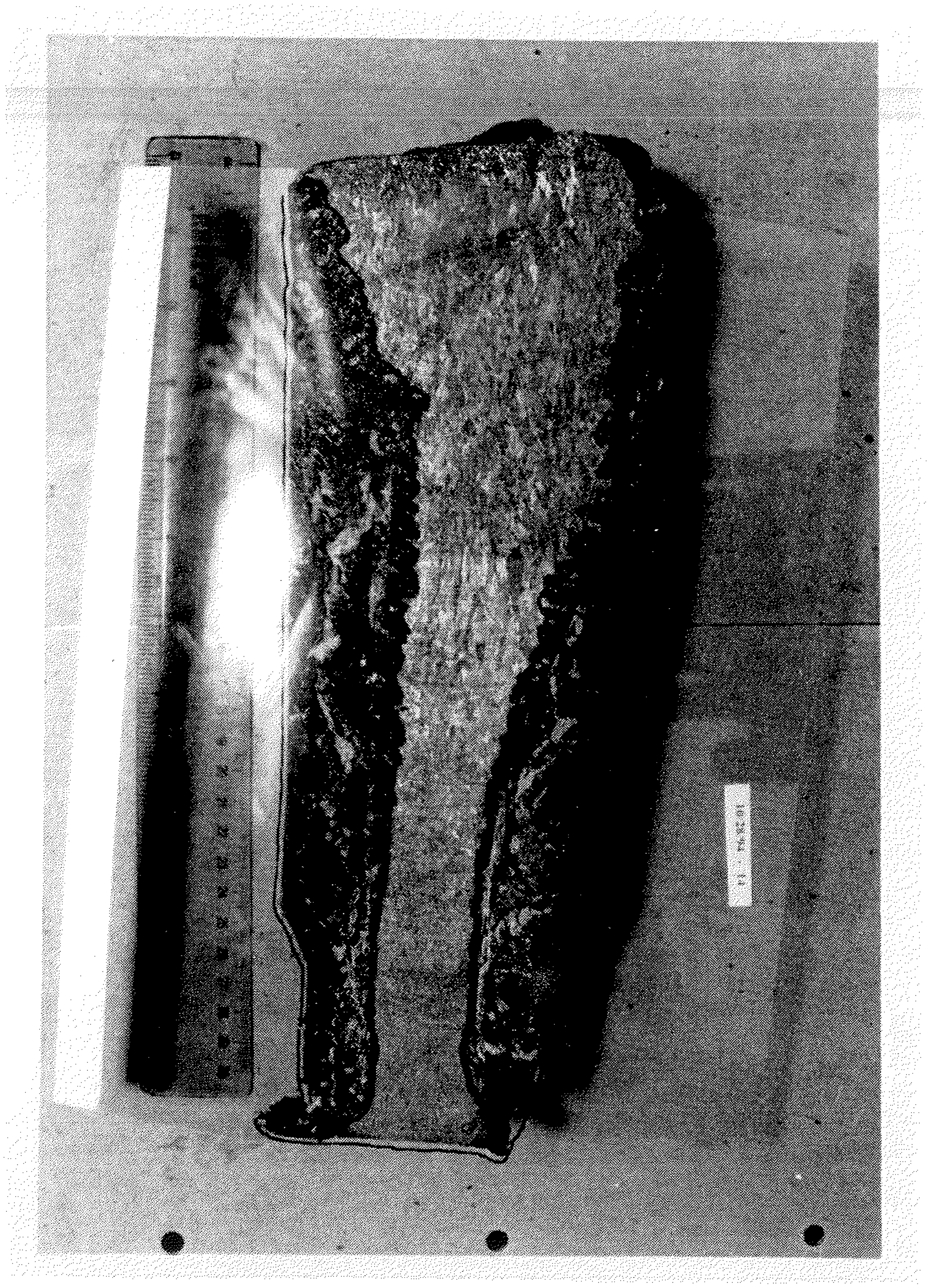

FIGURE 3.4 - Validation of Visual Observations of Unetched Samples

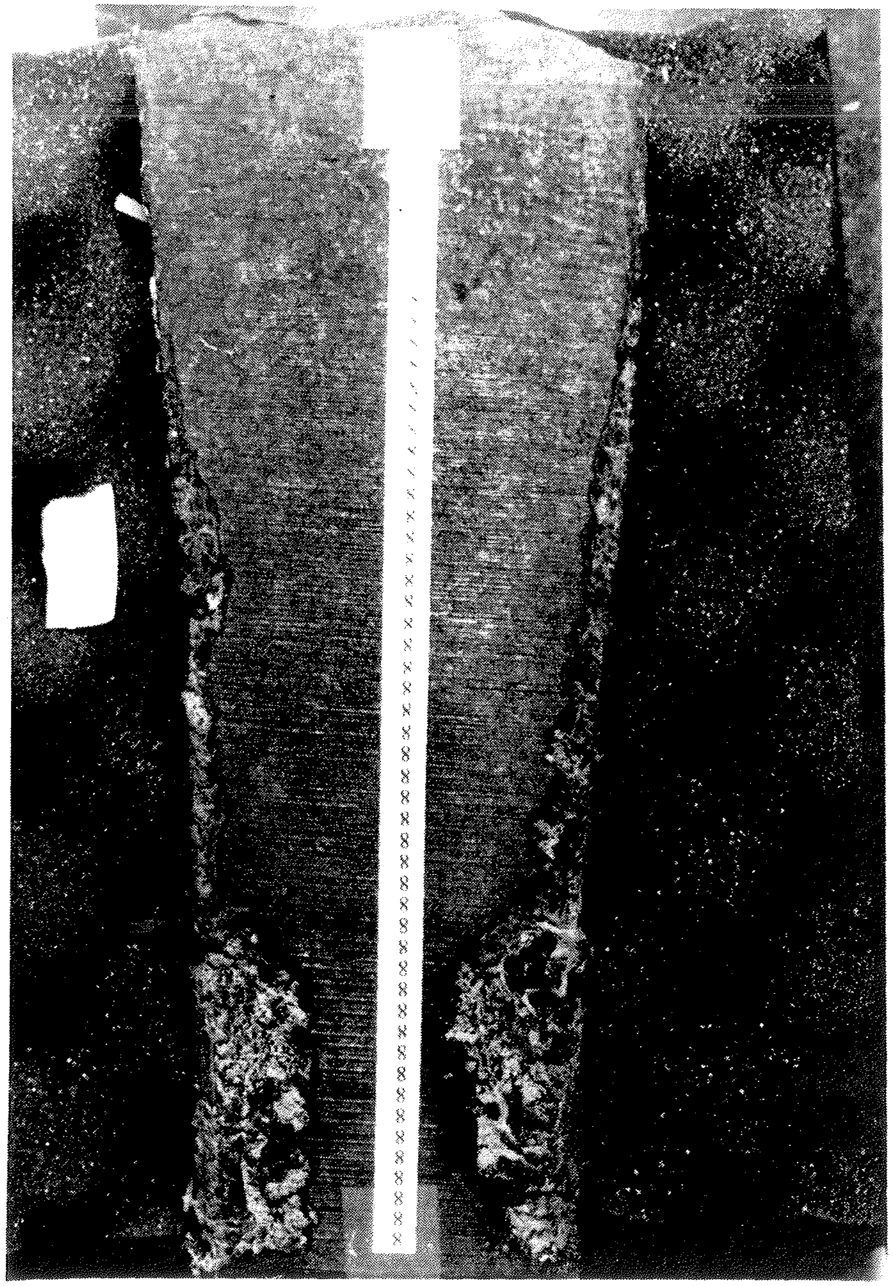

FIGURE 3.5 - Macro-Etched Tundish Nozzle Sample (Cast 9361, Strand 2)

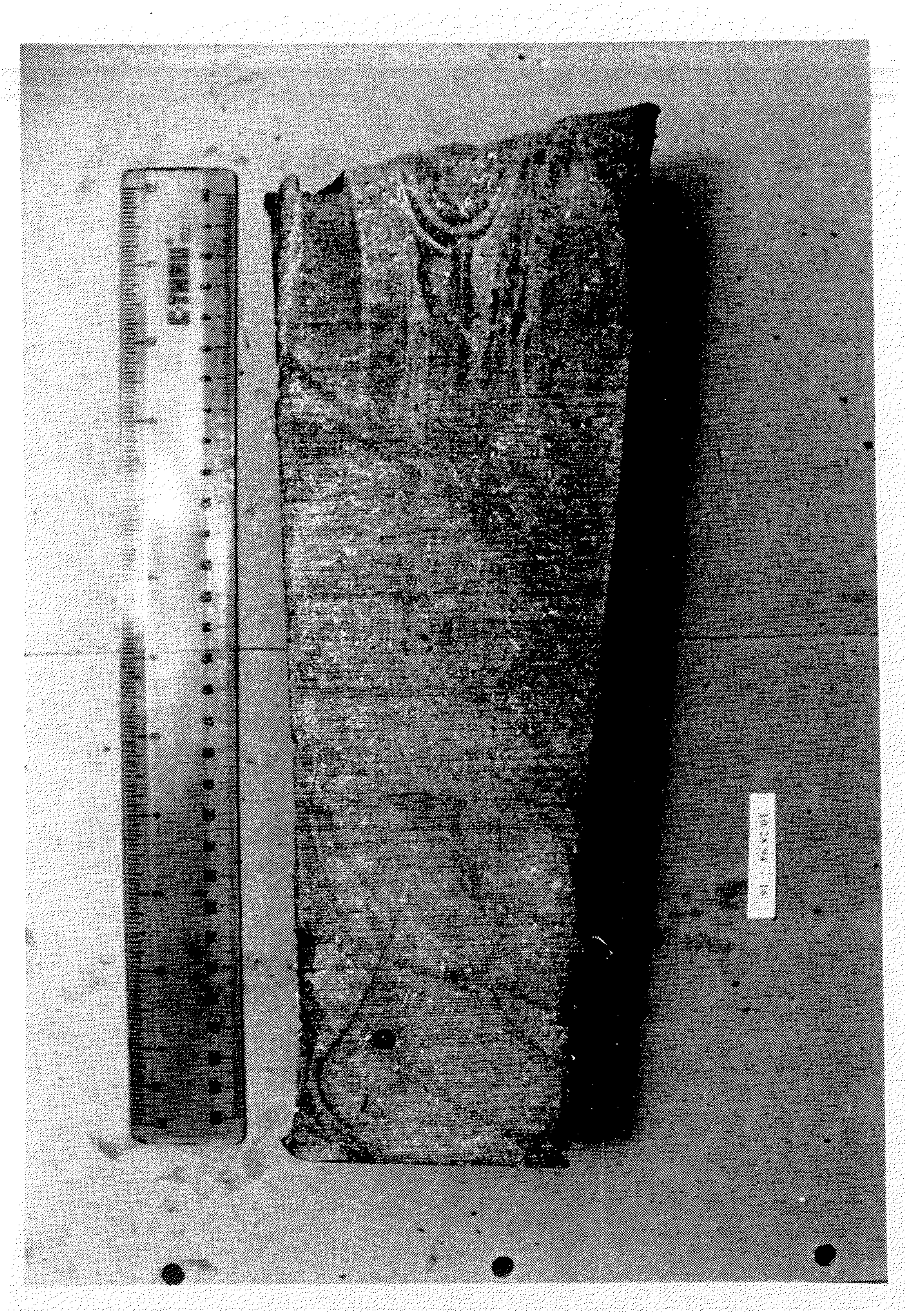

FIGURE 3.6 - Macro-Etched Tundish Nozzle Sample (Cast 9361, Strand 1)

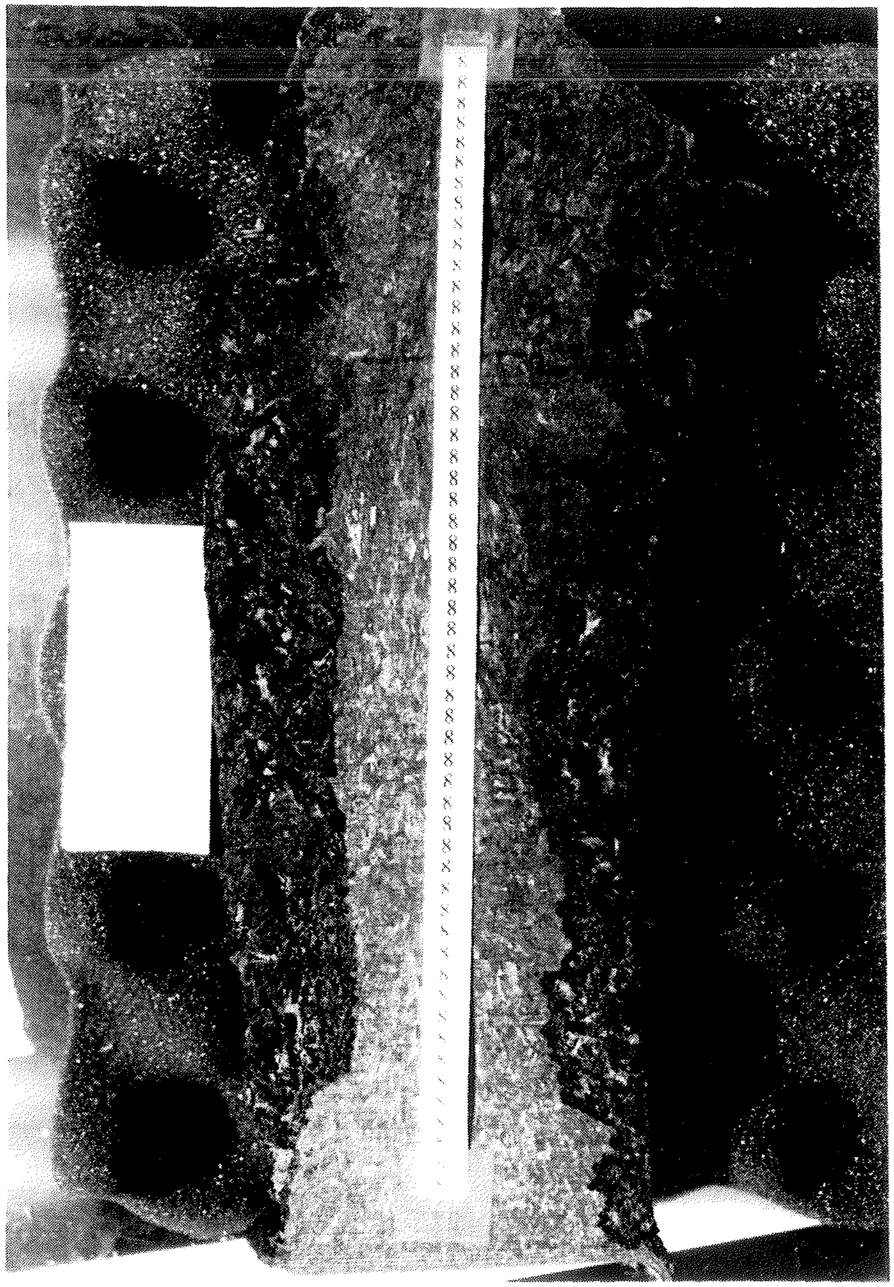

FIGURE 3.7 - Macro-Etched Tundish Nozzle Sample (Cast 9369, Strand 1)

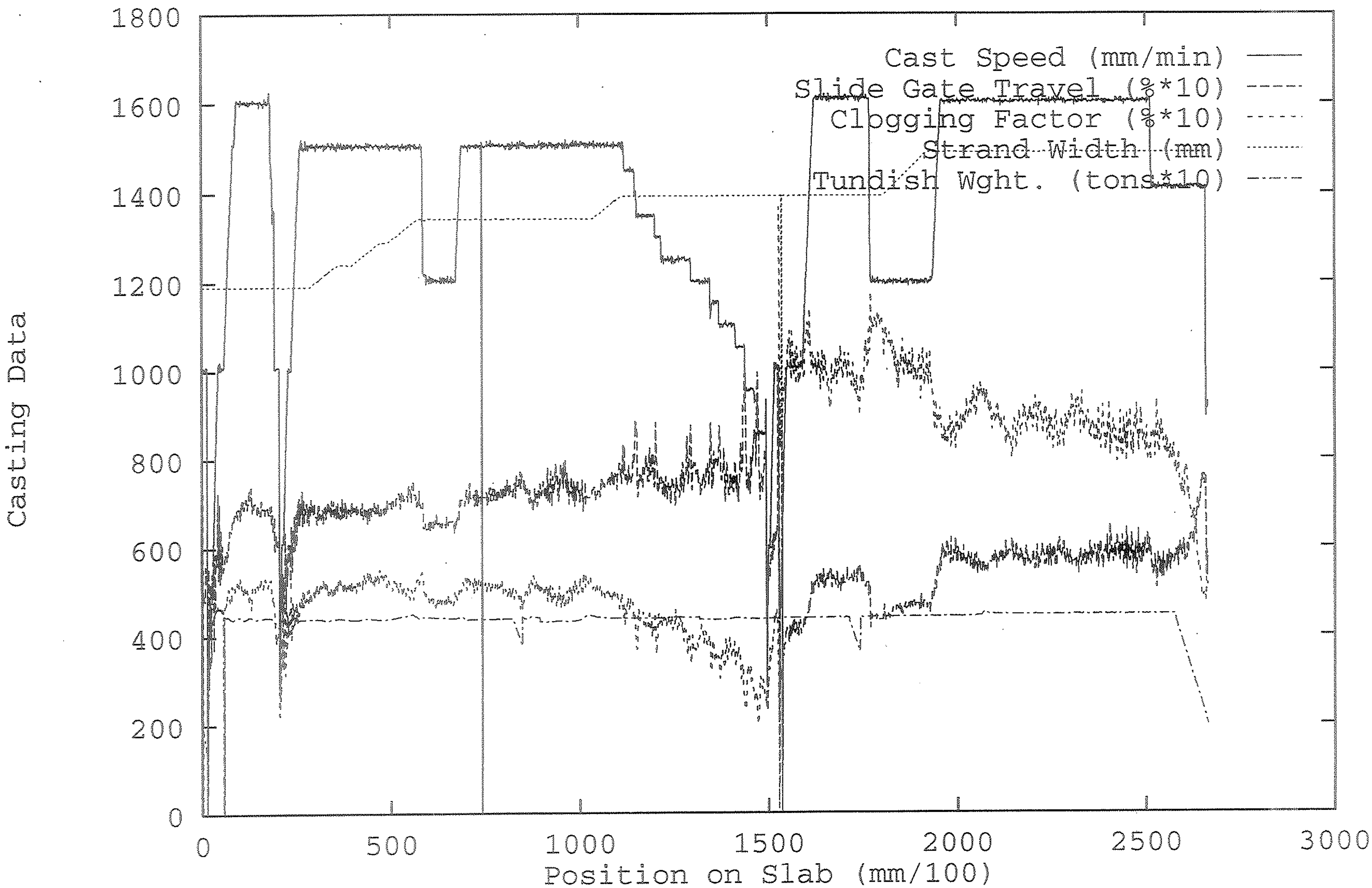

FIGURE 3.8 - Casting Data vs. Strand Position (Cast 9361, Strand 2)

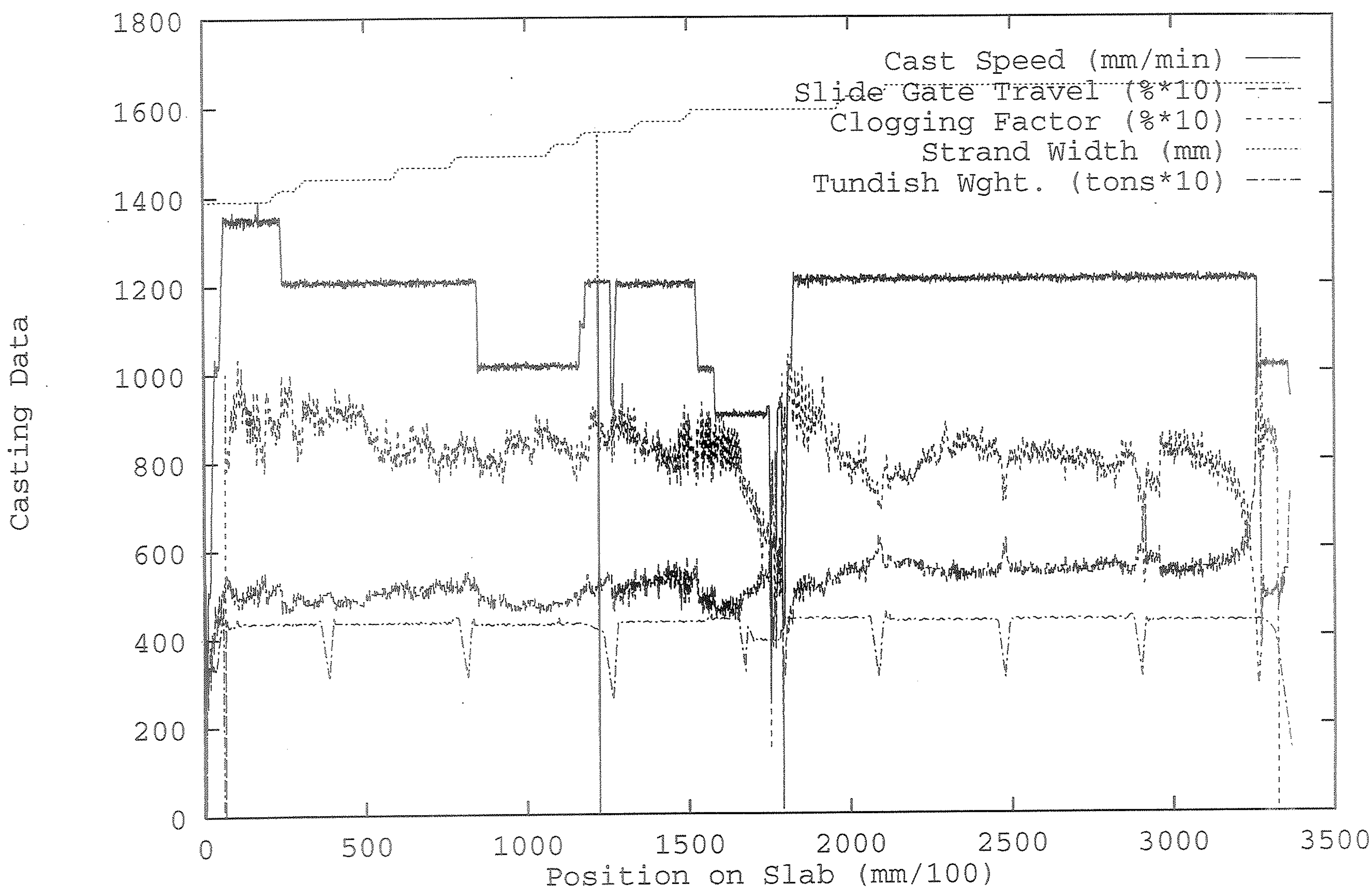

FIGURE 3.9 - Casting Data vs. Strand Position (Cast 9374, Strand 1)

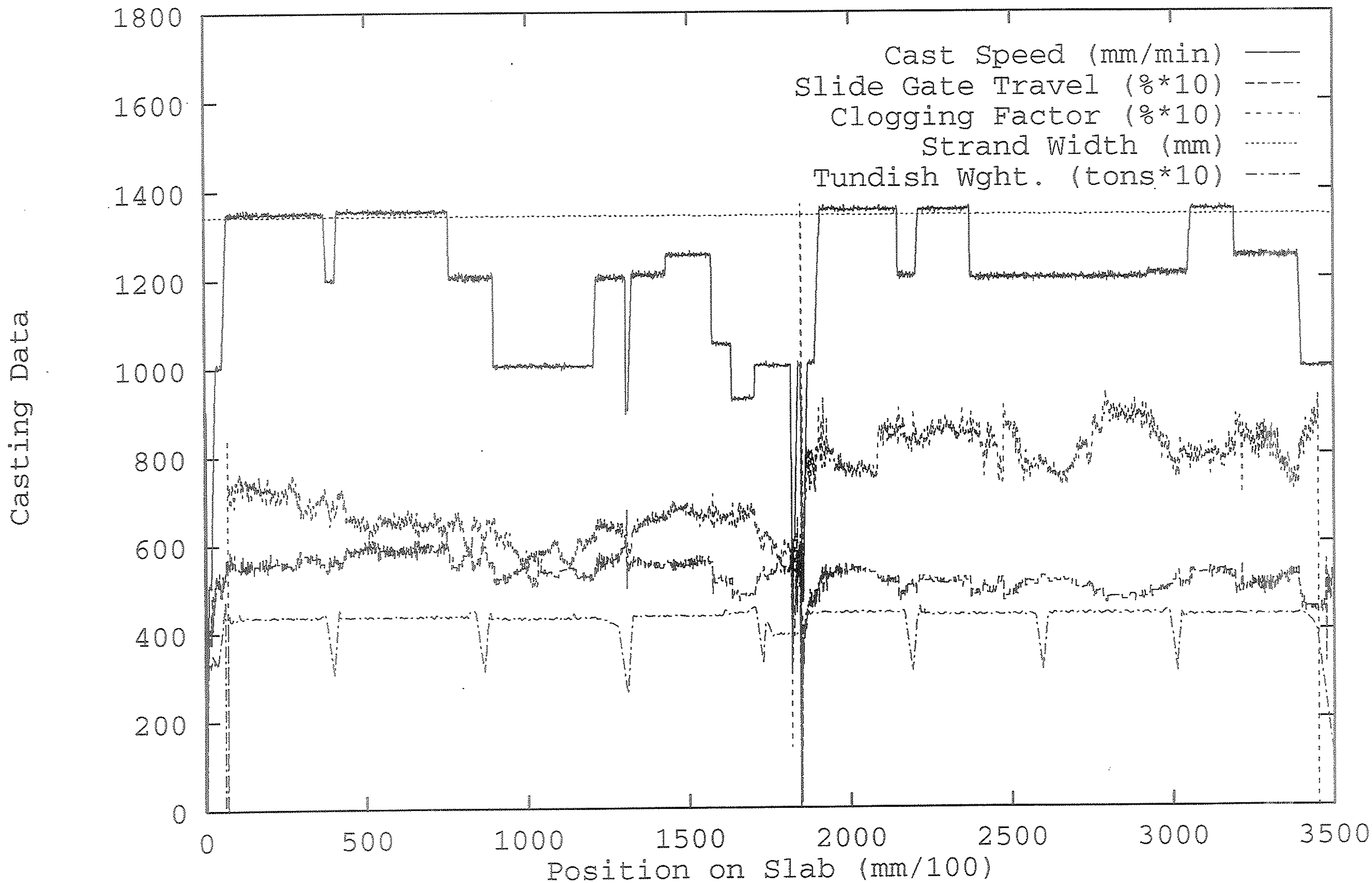

FIGURE 3.10 - Casting Data vs. Strand Position (Cast 9374, Strand 2)

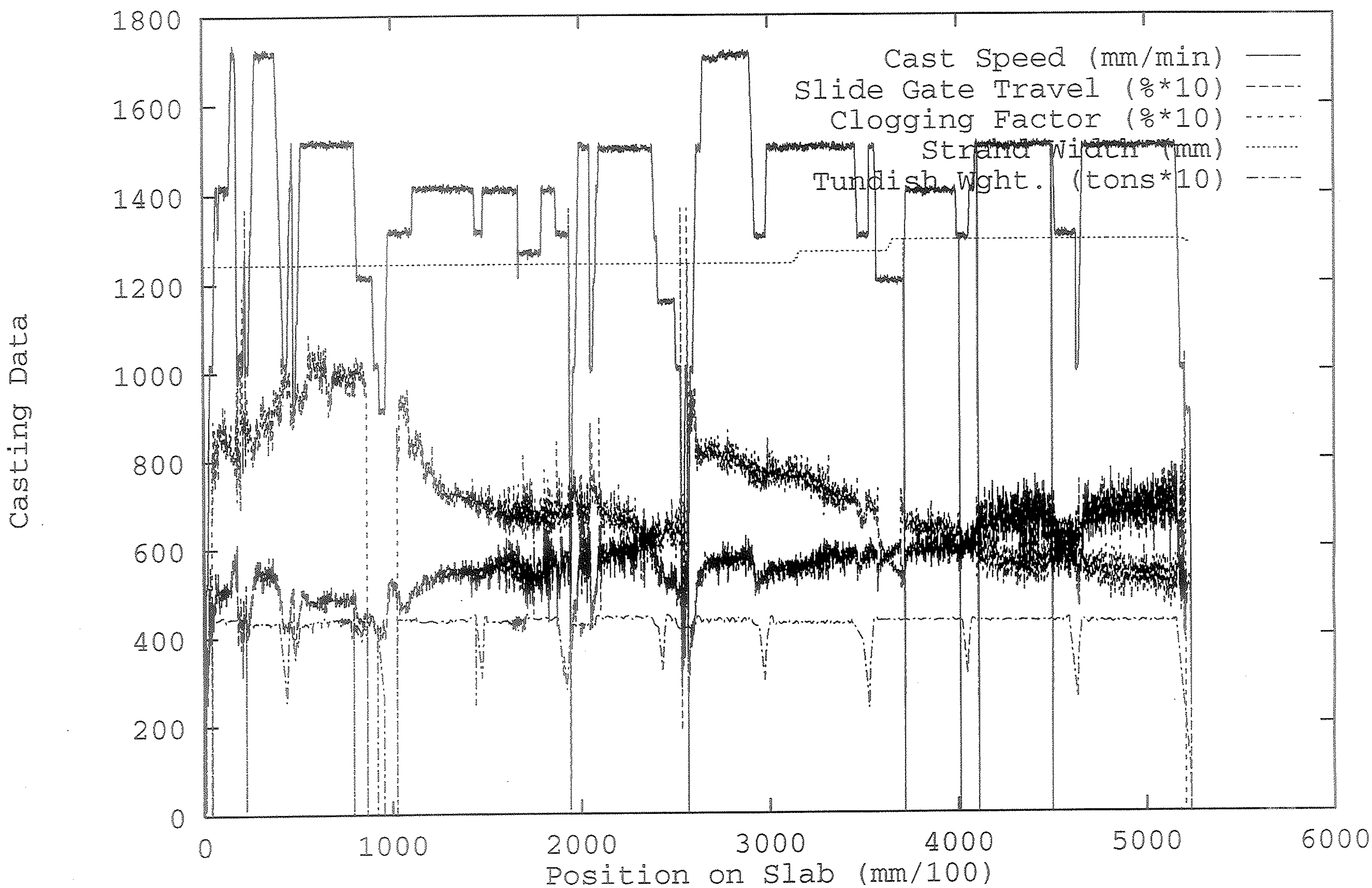

FIGURE 3.11 - Casting Data vs. Strand Position (Cast 9388, Strand 1)

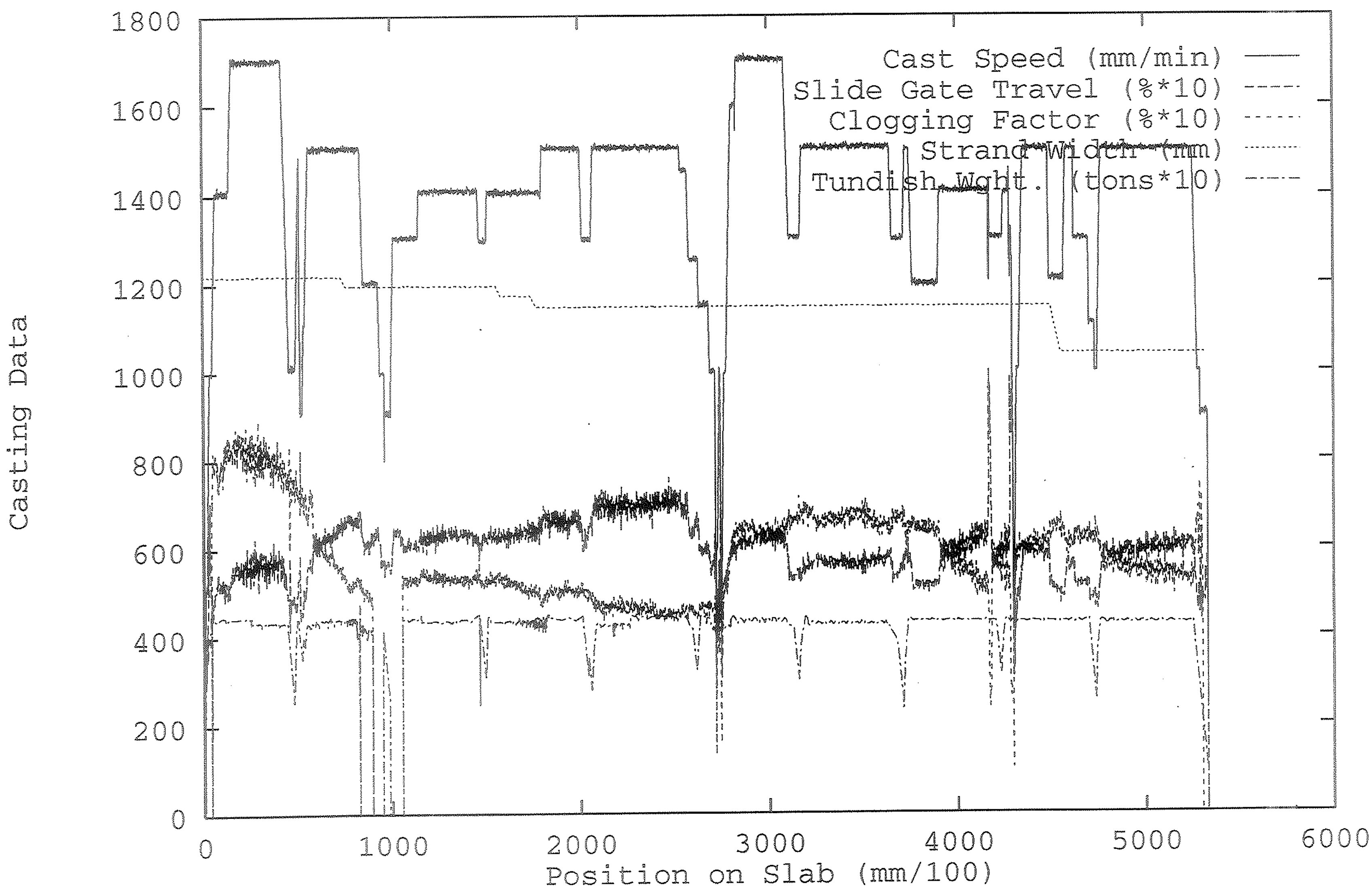

FIGURE 3.12 - Casting Data vs. Strand Position (Cast 9388, Strand 2)

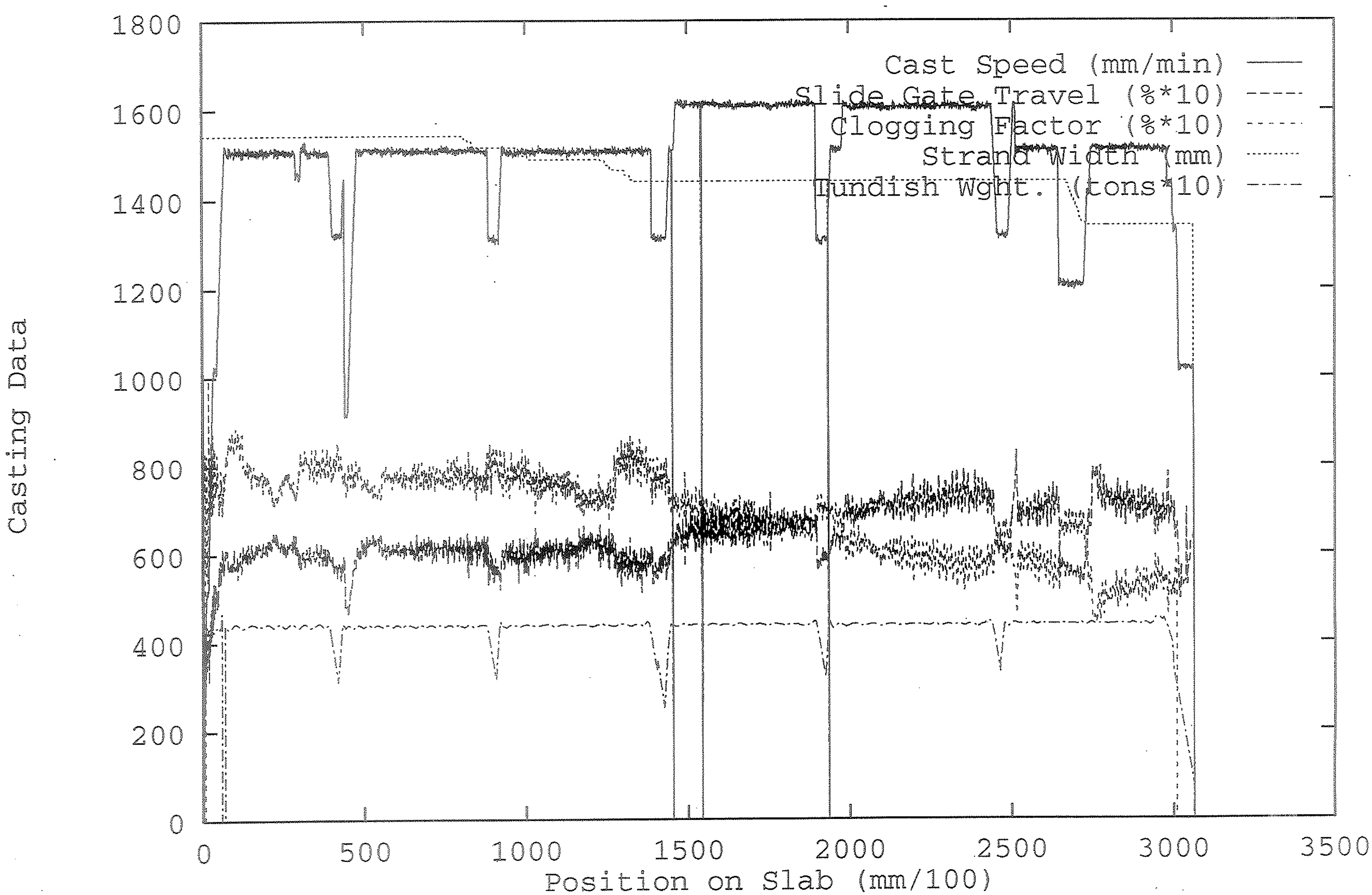

FIGURE 3.13 - Casting Data vs. Strand Position (Cast 9030, Strand 1)

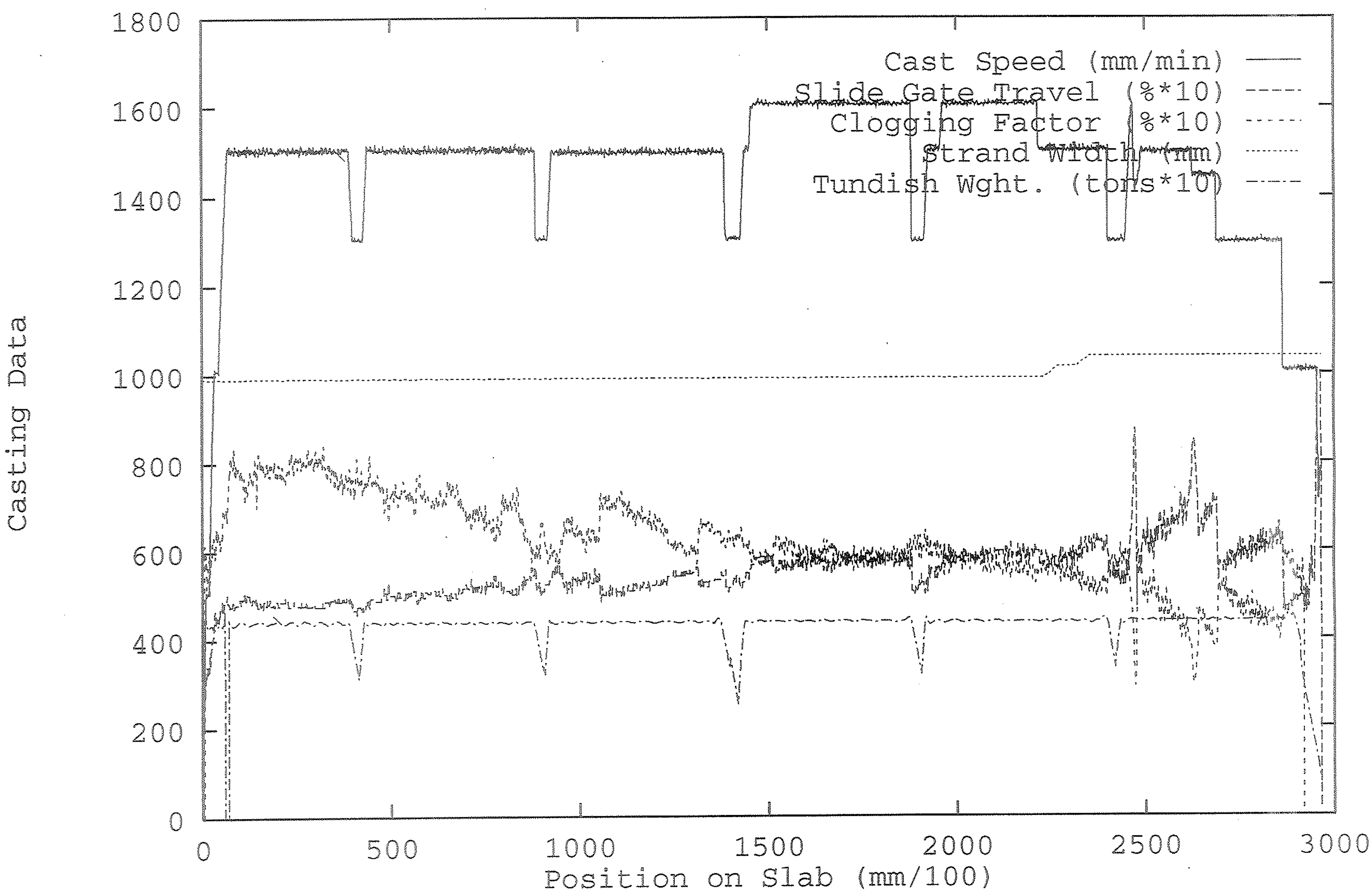

FIGURE 3.14 - Casting Data vs. Strand Position (Cast 9030, Strand 2)

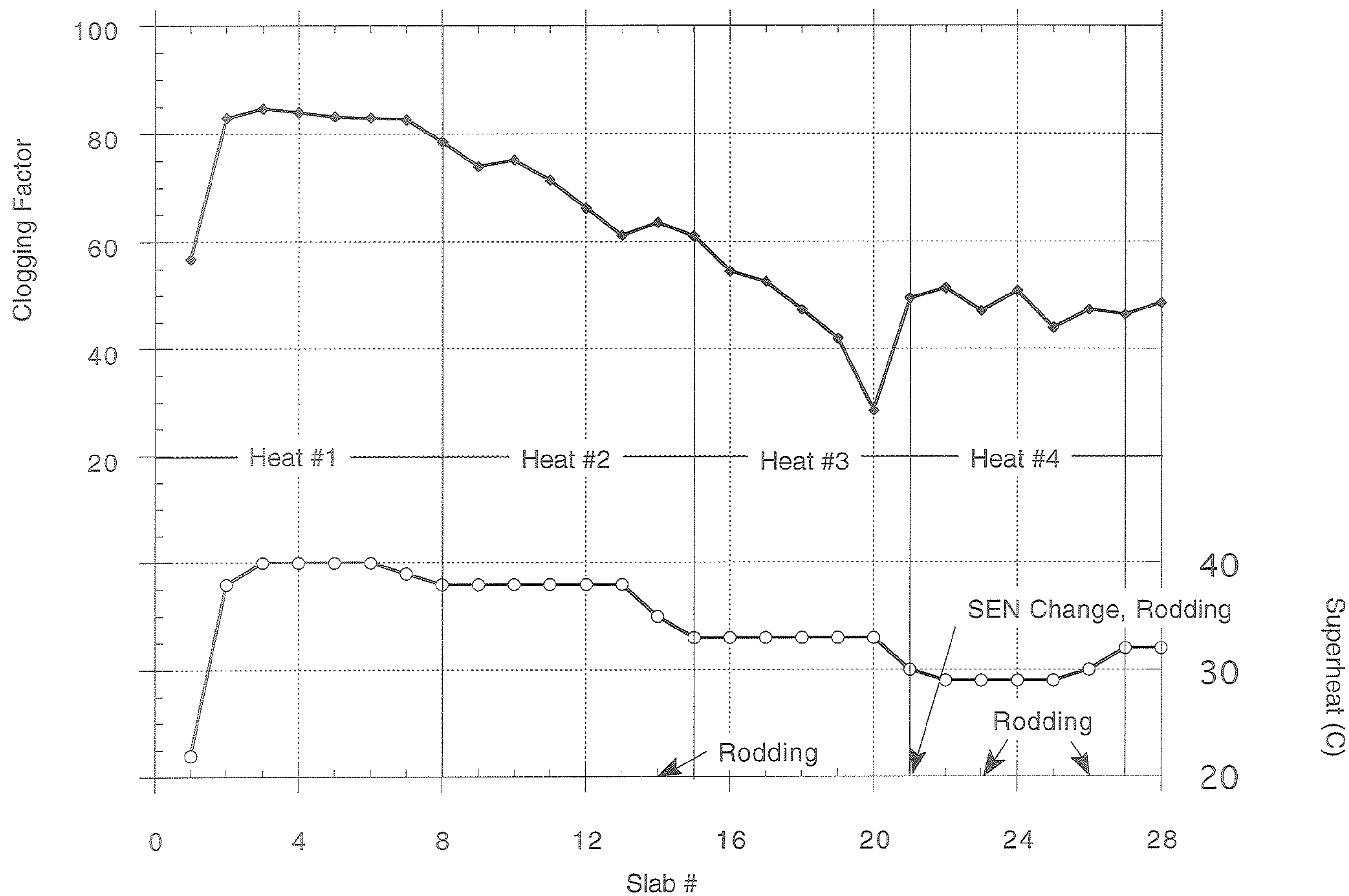

FIGURE 3.15 - Summary Data (Cast 9267, Strand 1)

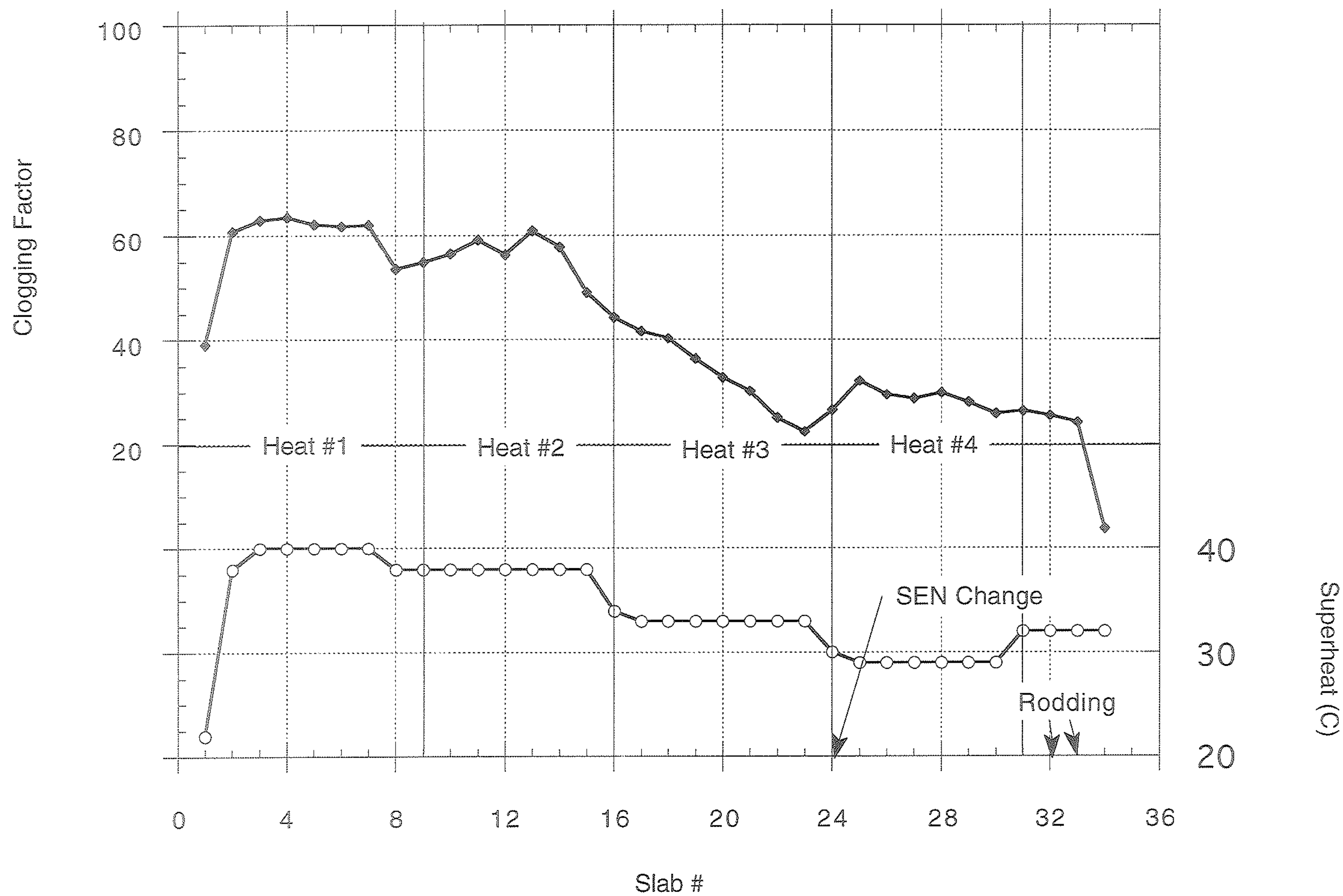

FIGURE 3.16 - Summary Data (Cast 9267, Strand 2)

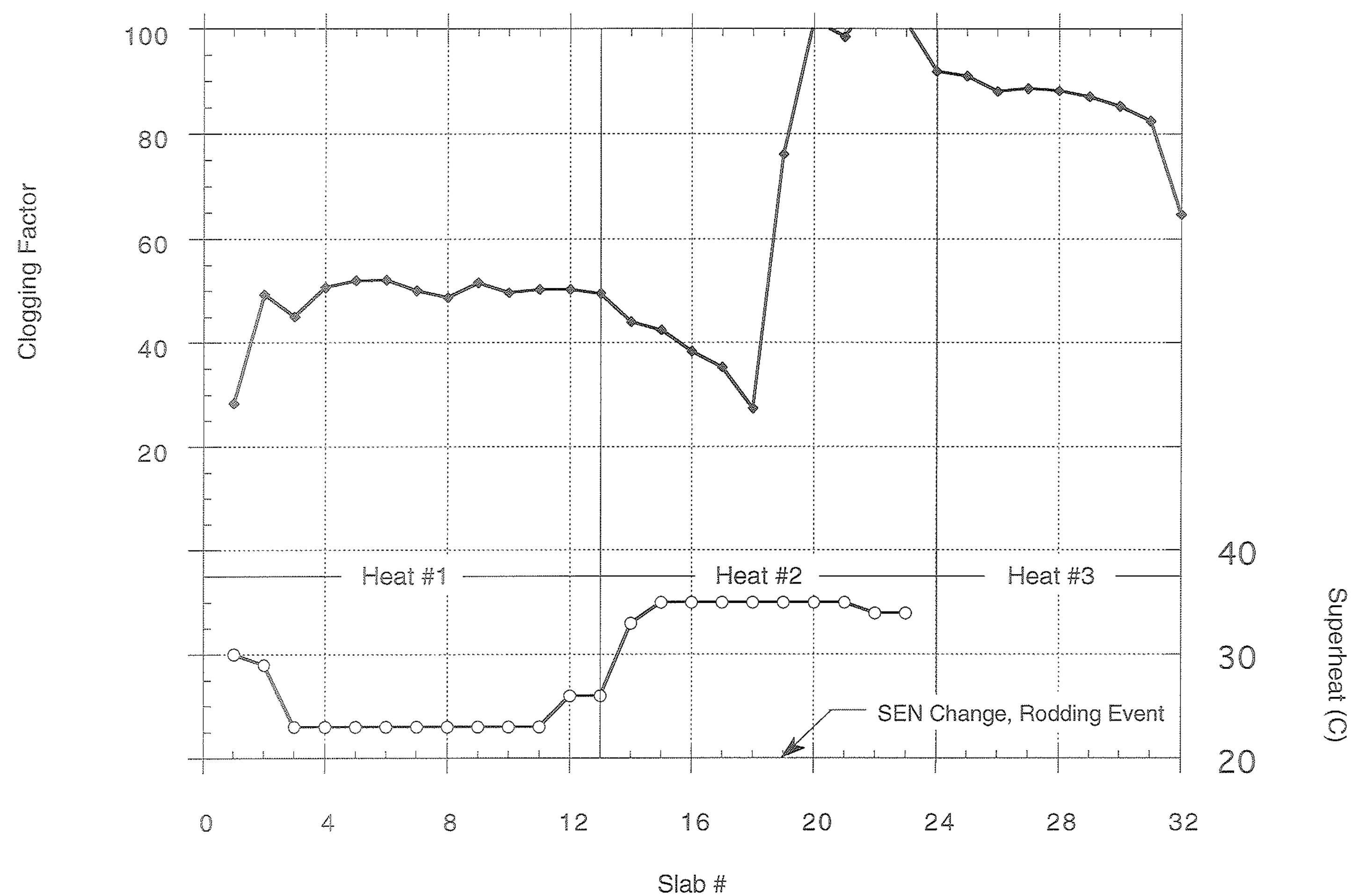

FIGURE 3.17 - Summary Data (Cast 9361, Strand 2)

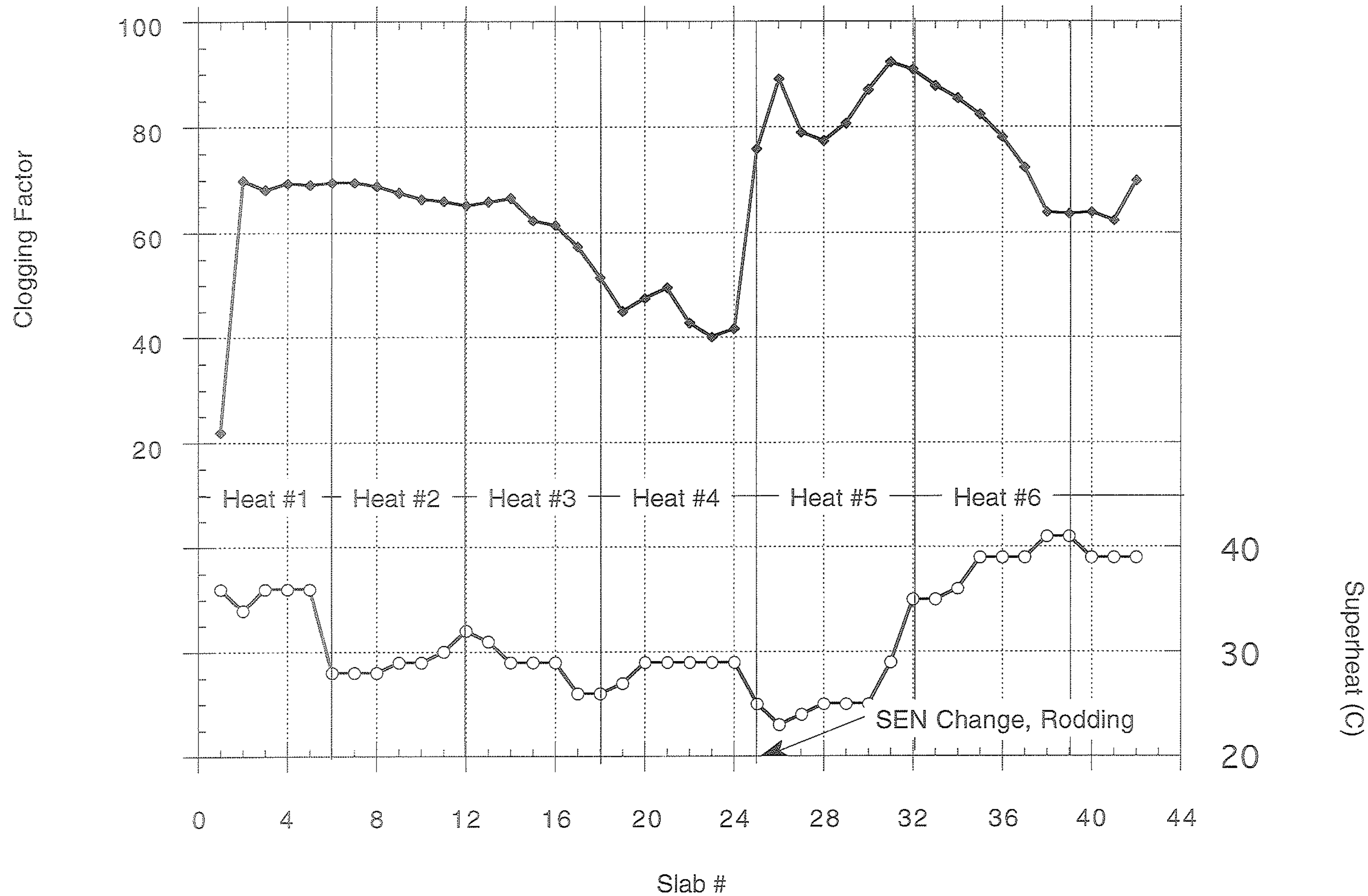

FIGURE 3.18 - Summary Data (Cast 9369, Strand 1)

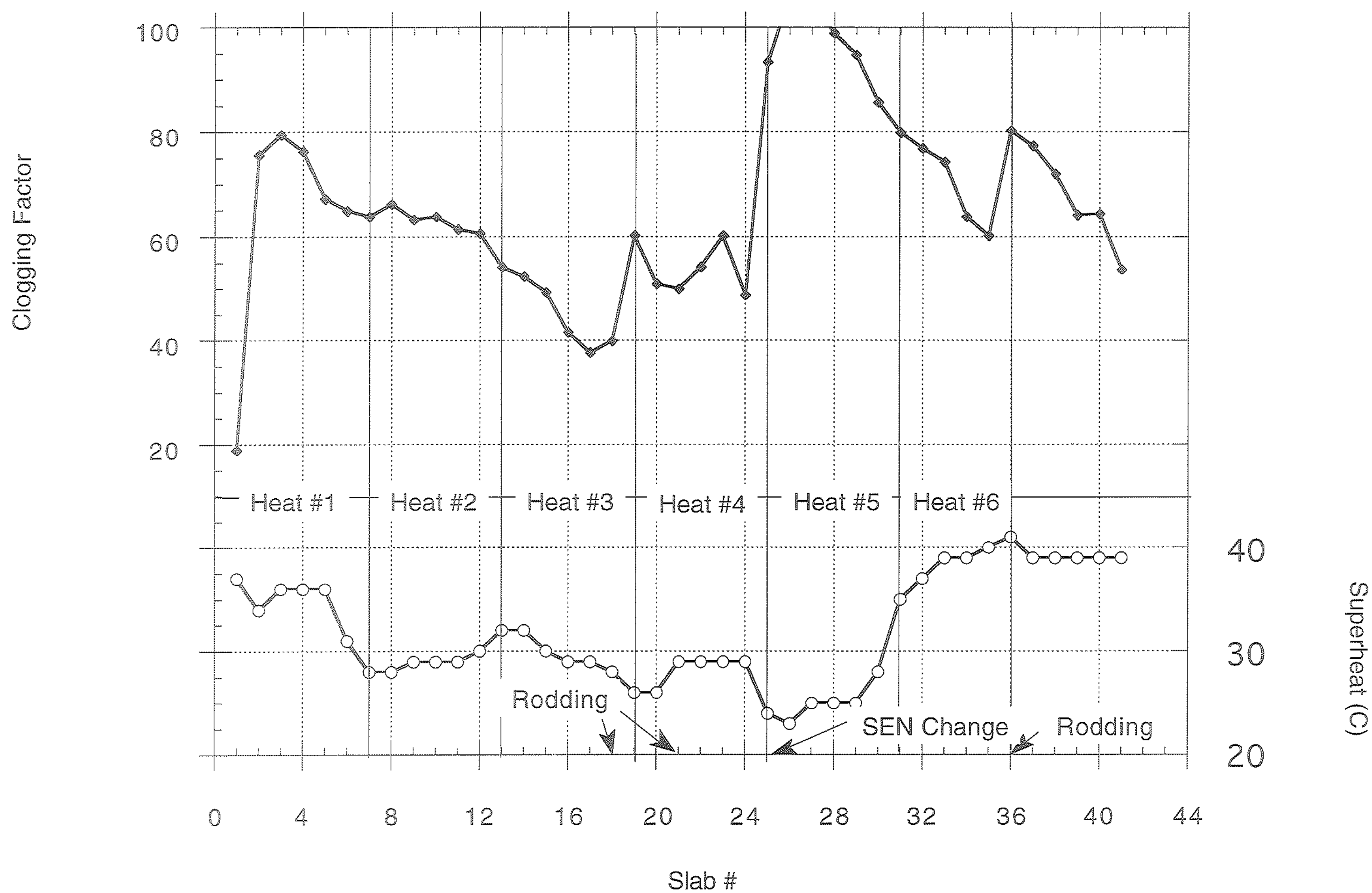

FIGURE 3.19 - Summary Data (Cast 9369, Strand 2)

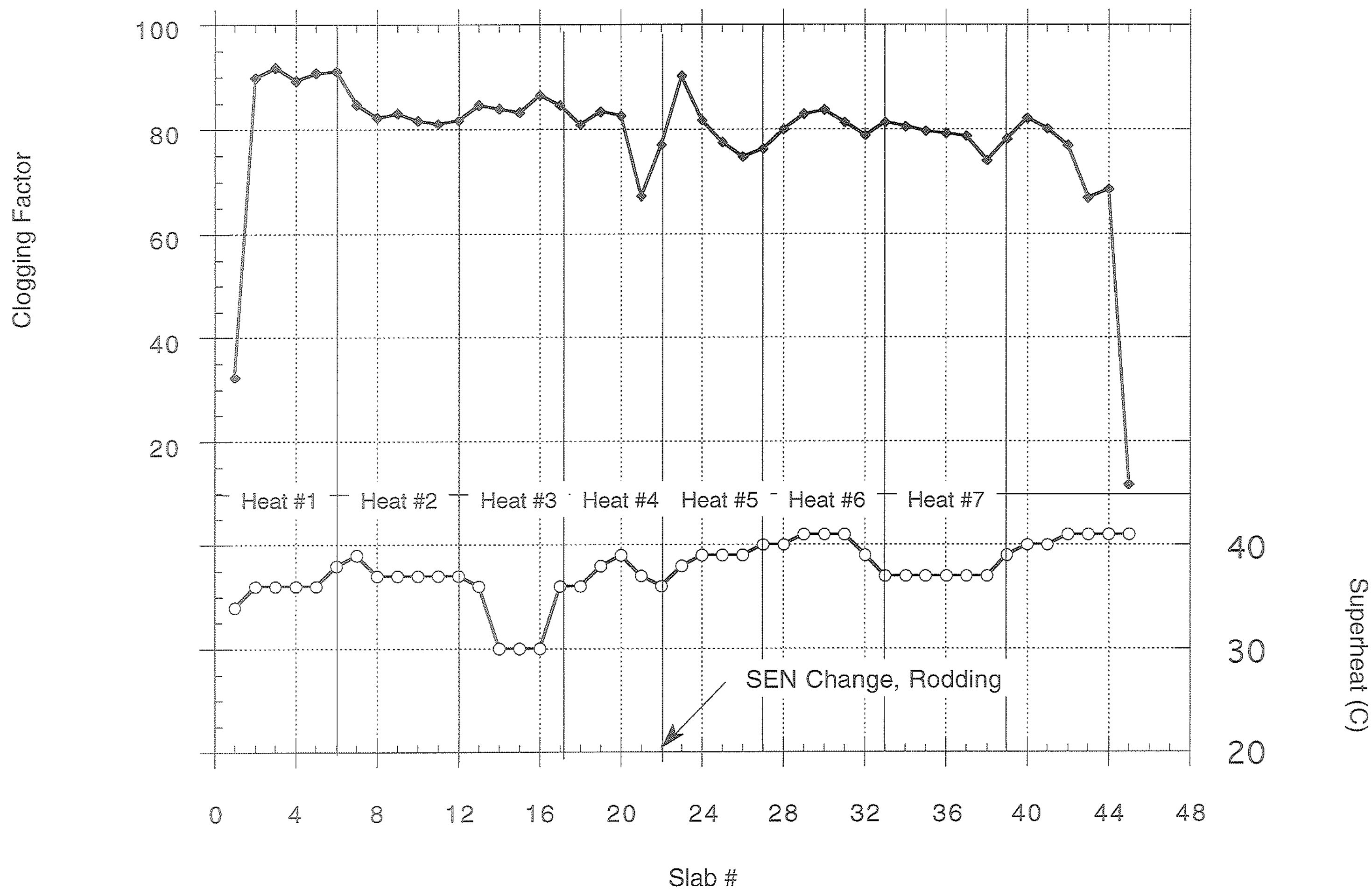

FIGURE 3.20 - Summary Data (Cast 9374, Strand 1)

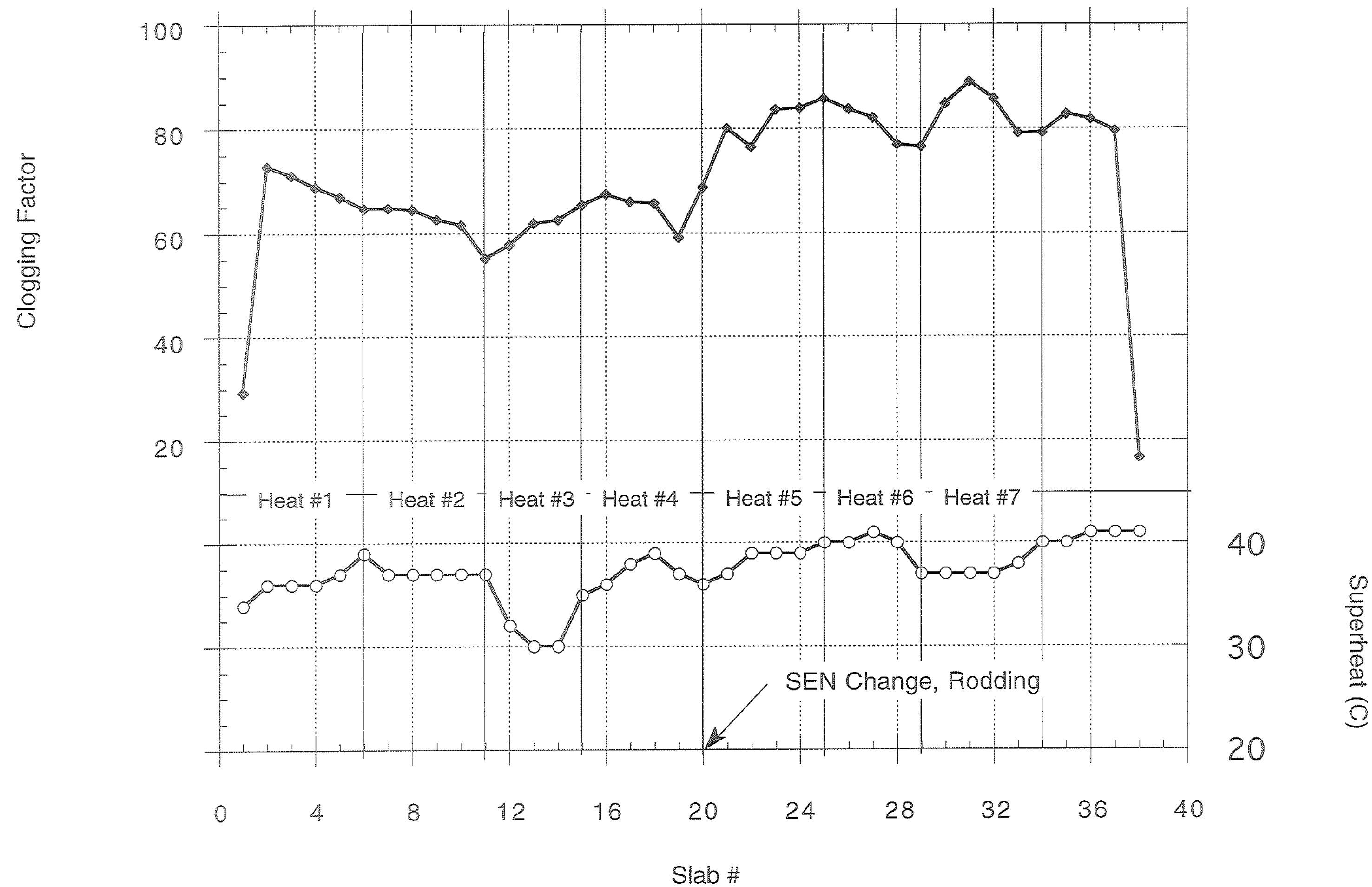

FIGURE 3.21 - Summary Data (Cast 9374, Strand 2)

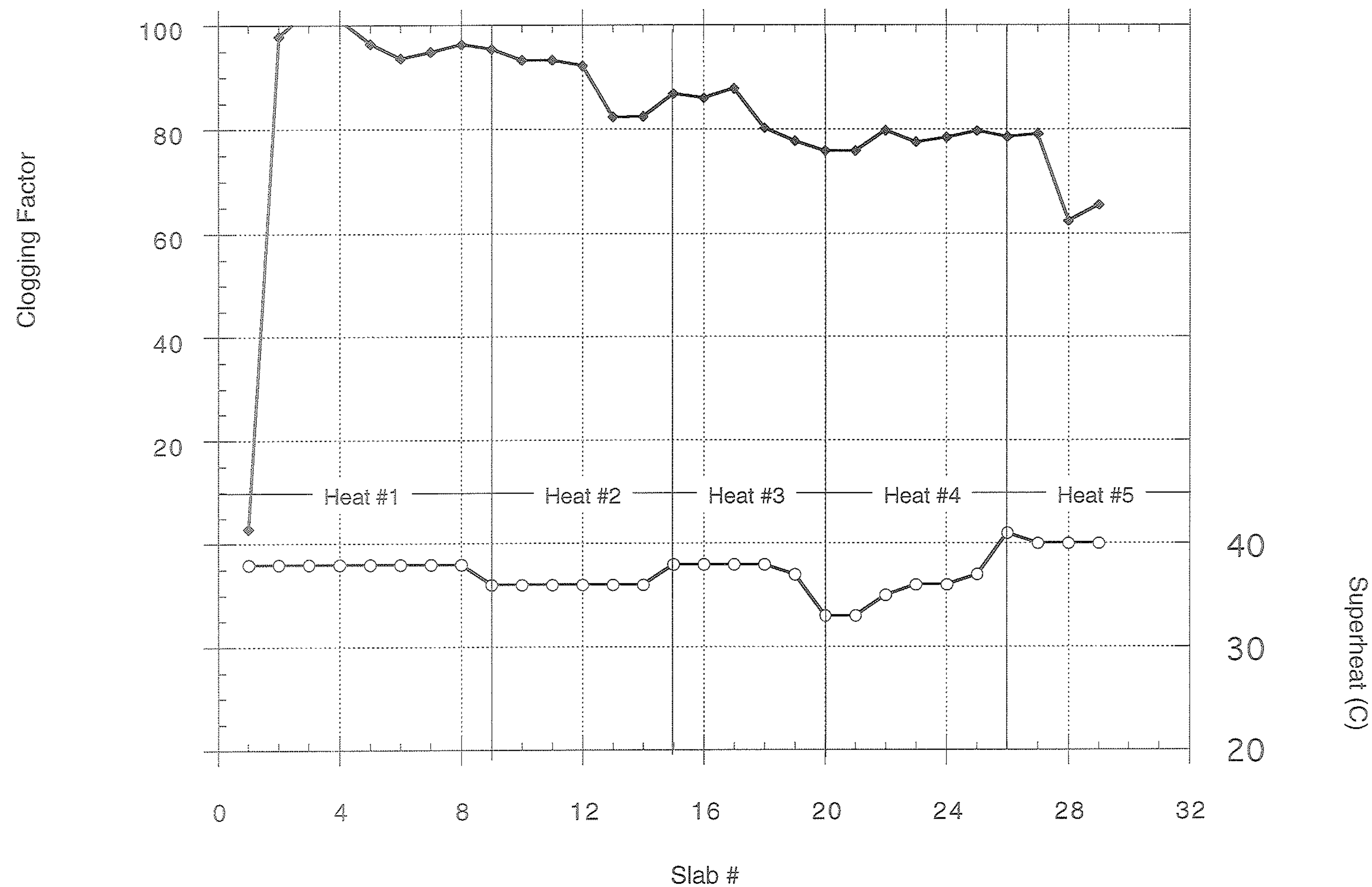

FIGURE 3.22 - Summary Data (Cast 9380, Strand 1)

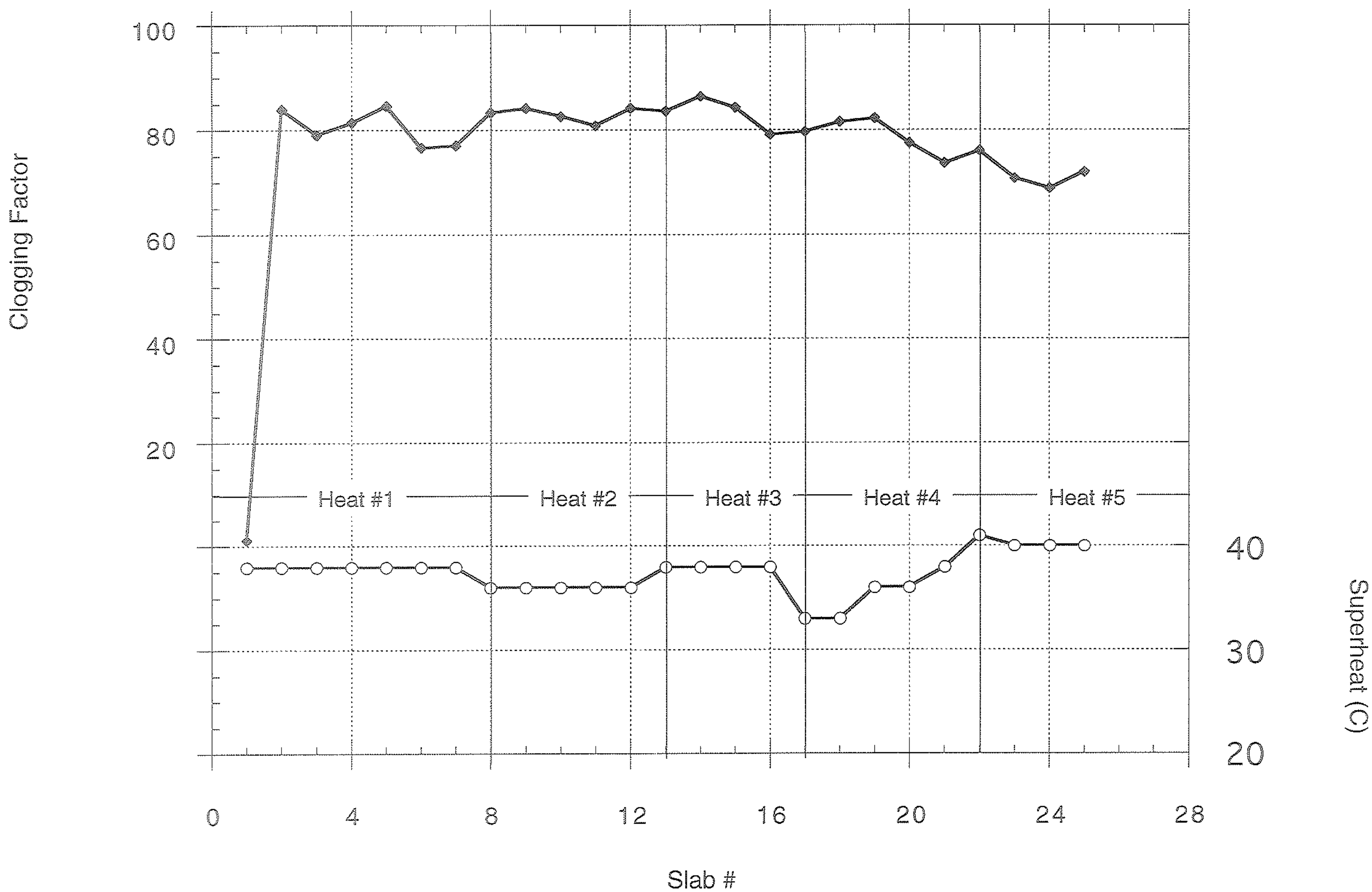

FIGURE 3.23 - Summary Data (Cast 9380, Strand 2)

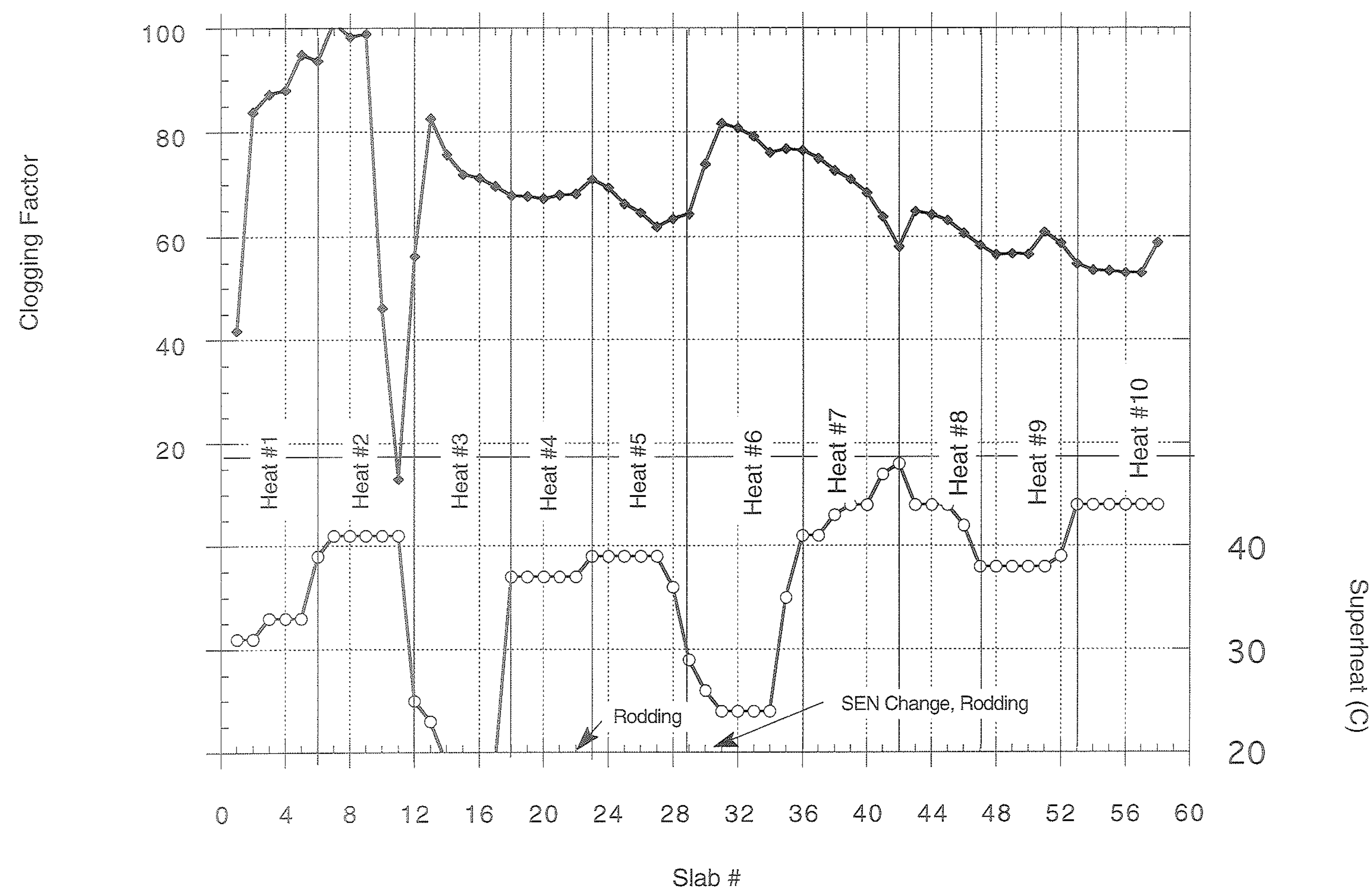

FIGURE 3.24 - Summary Data (Cast 9388, Strand 1)

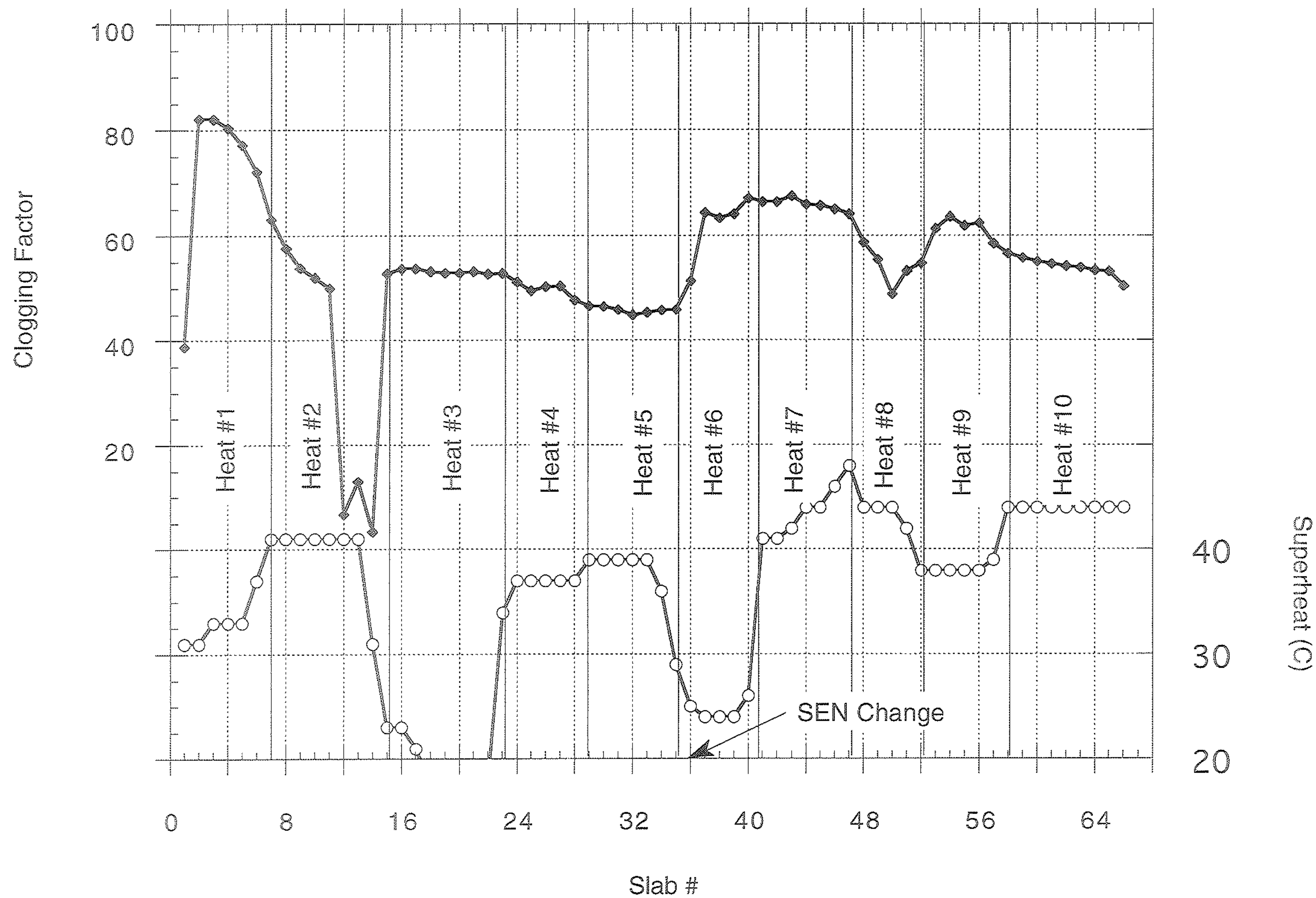

FIGURE 3.25 - Summary Data (Cast 9388, Strand 2)

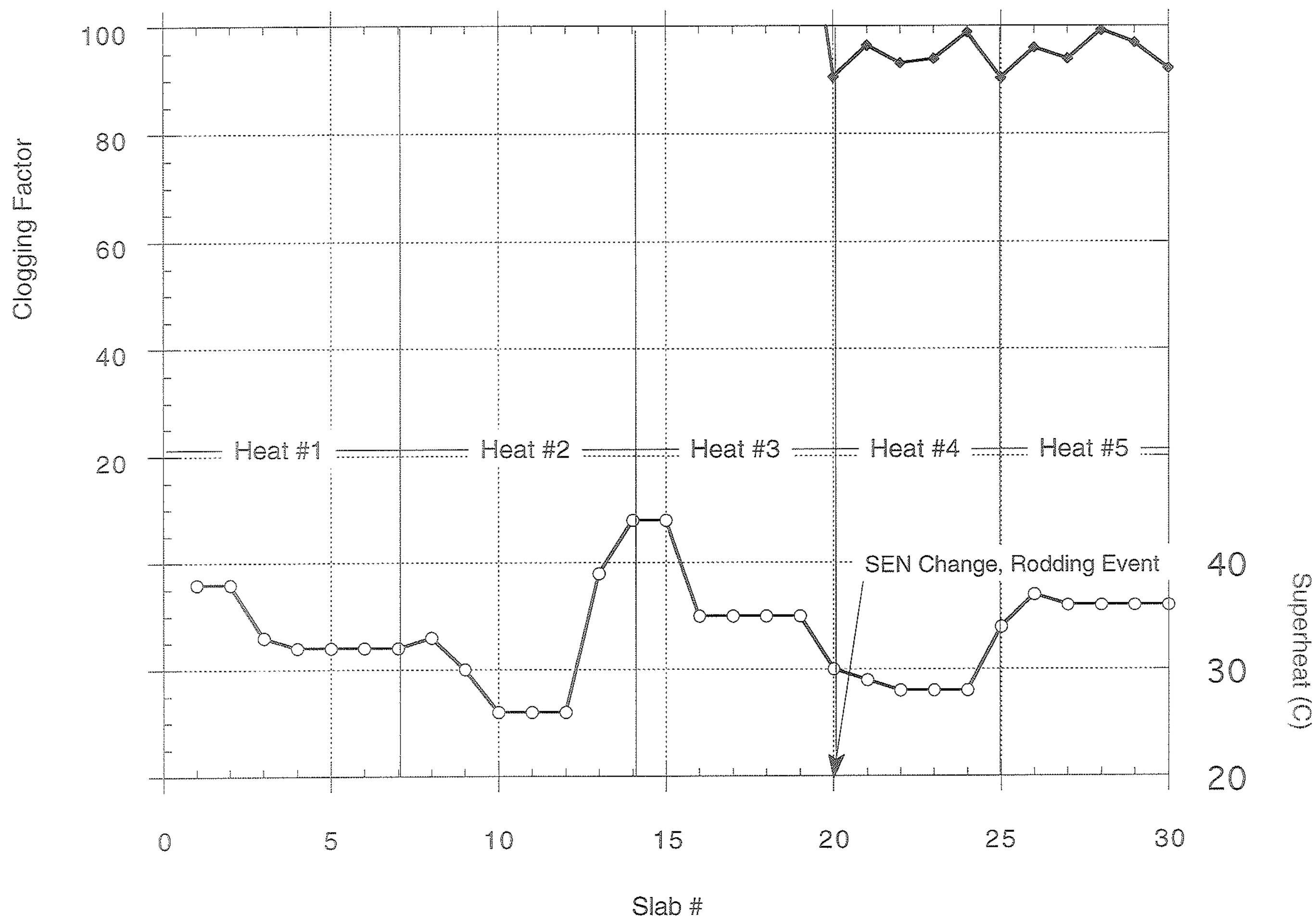

FIGURE 3.26 - Summary Data (Cast 9030, Strand 1)

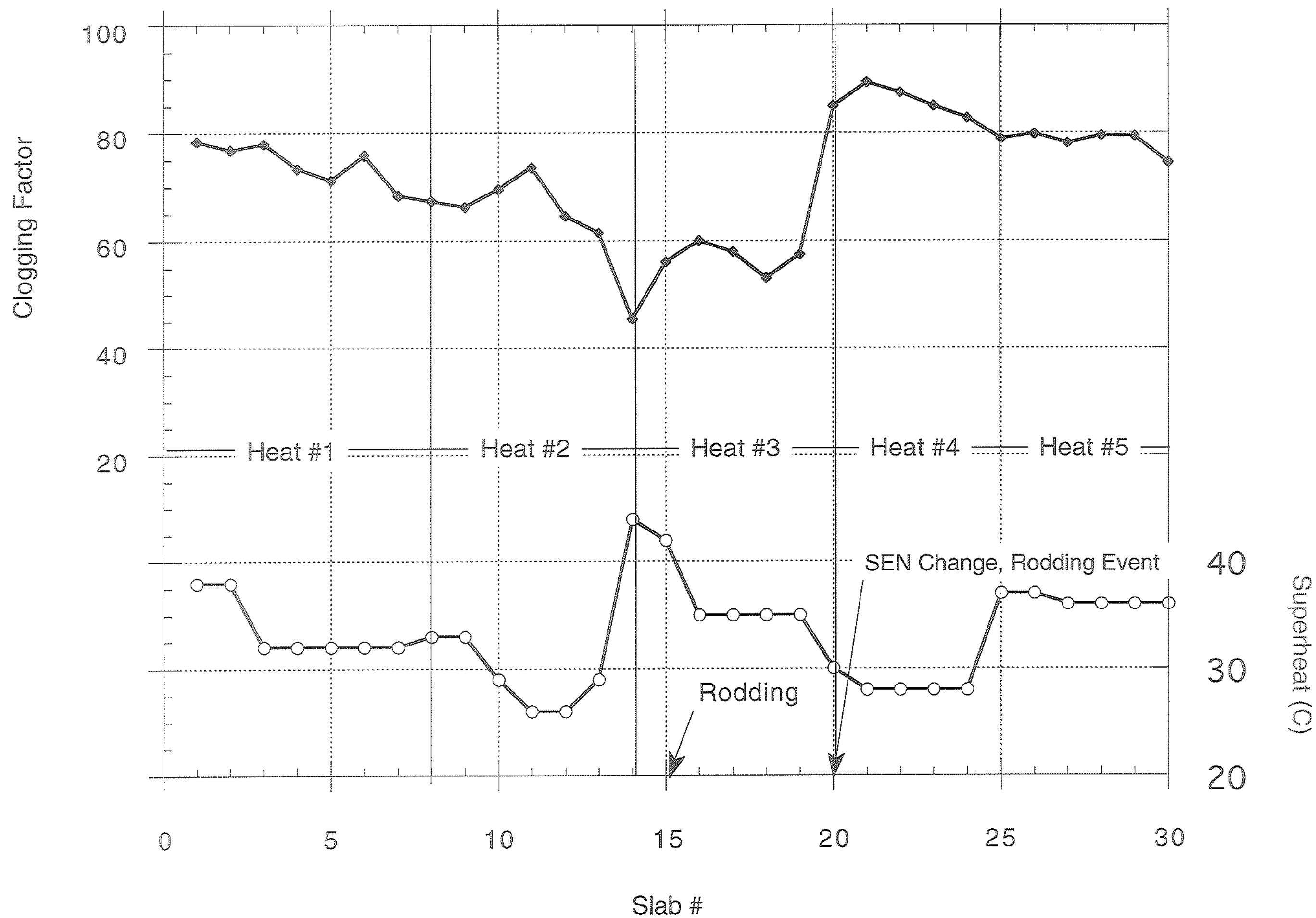

FIGURE 3.27 - Summary Data (Cast 9030, Strand 2)

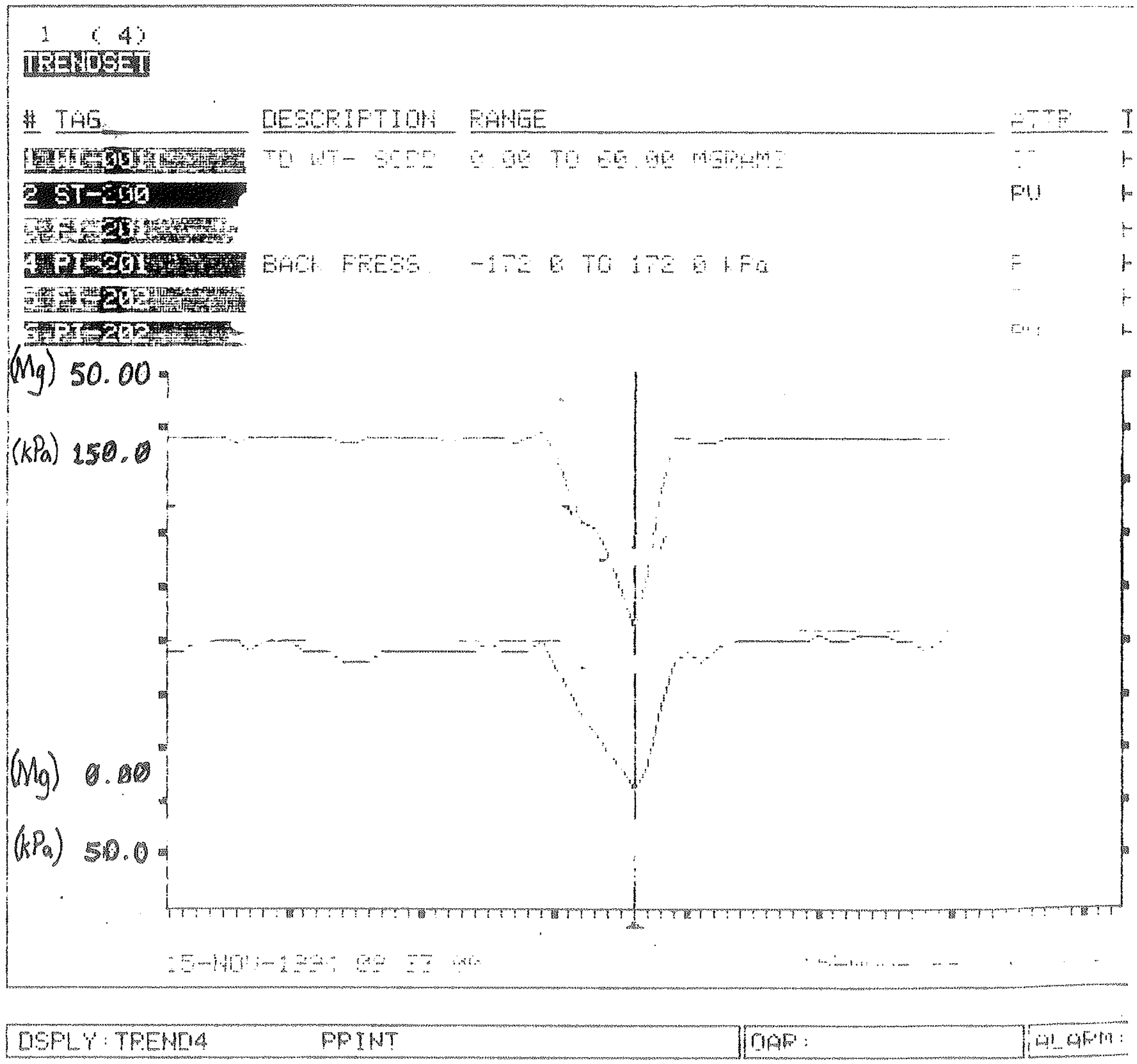

FIGURE 3.28 - Variation of Argon Back-Pressure During Ladle Change

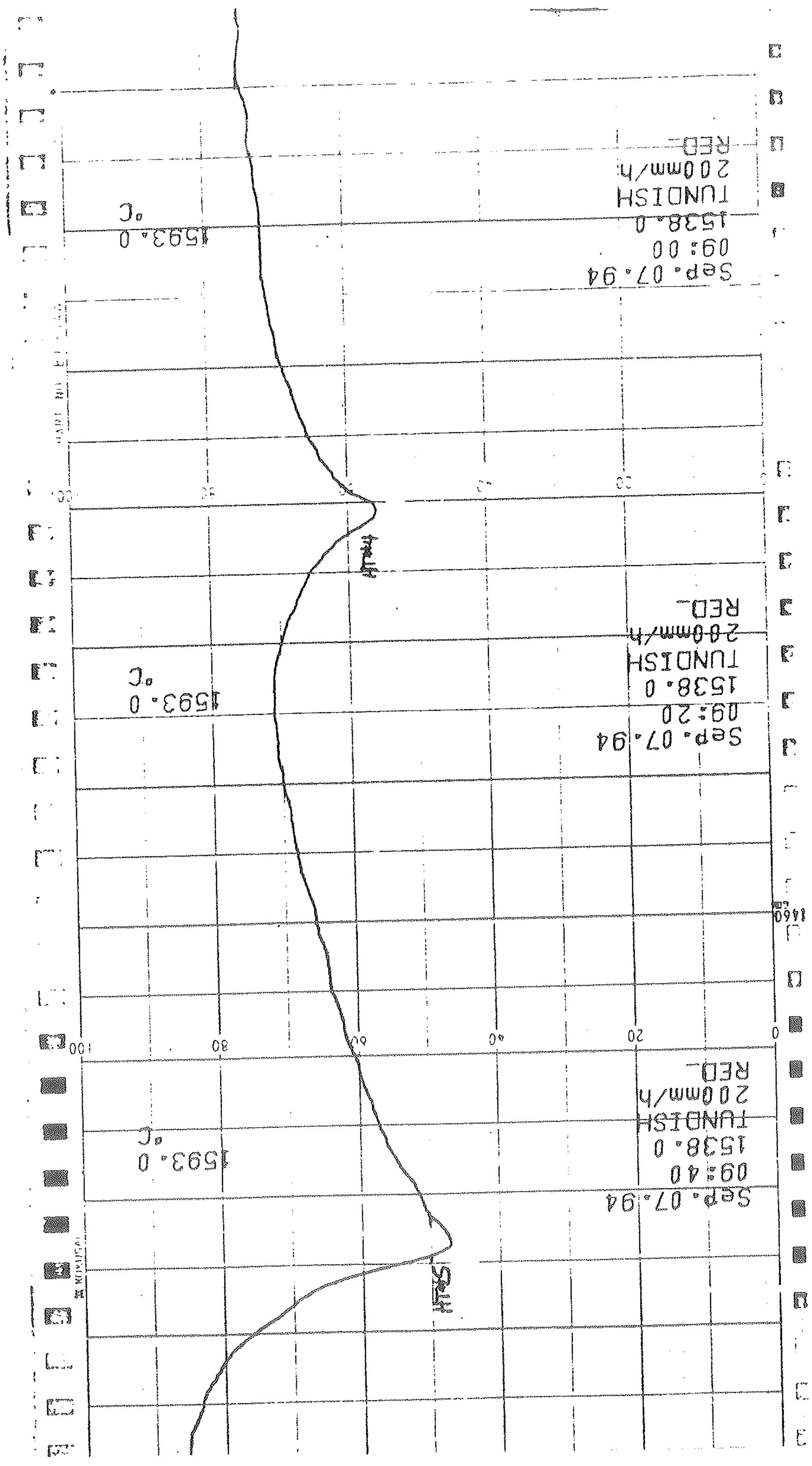

FIGURE 3.29 - Strip Chart Recording of Temperature in the Tundish Well

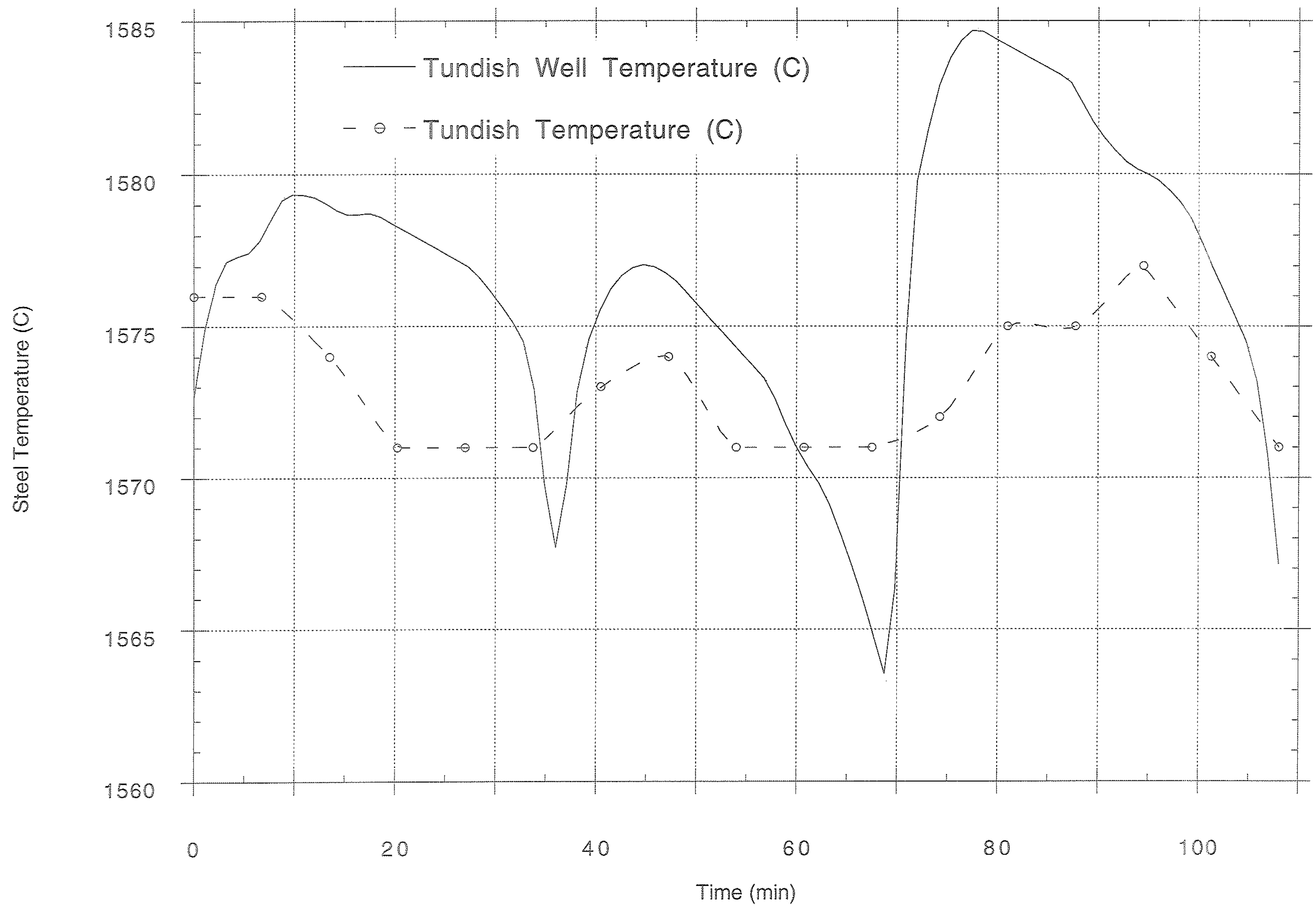

Figure 3.30 - Comparison of Tundish Well Temperature and Bulk Tundish Temperature

CHAPTER 4 - MATHEMATICAL MODELS

4.1 OVERVIEW

This chapter presents the formulation and results of several different mathematical models of various aspects of clogging. These models include structural models of the clog buildup, steady state heat transfer models of the clog and nozzle, a transient heat transfer model of cast-initiation skulling, a transient heat and mass transfer model of skull growth within a clog, fluid flow model of the tundish-to-mold flow, mass balance models for inclusion deposition and reoxidation product formation, surface tension model for inclusion transport. These models were solved using Mathematica and FORTRAN programs and are given in Appendix A and B. Conclusions regarding clog formation and prevention will be drawn from the model results and interpreted with experimental data in Chapter 3. Finally, a new nozzle design will be presented which addresses concerns highlighted by these models.

4.2 STRUCTURAL MODEL

The clog matrix has been described as a friable powdery buildup that could be easily removed by the touch of a finger[1] To explain the ability of this buildup to withstand erosion by the turbulent, fast-flowing molten steel, Duderstadt[2] proposed that the clog was strengthened by solid steel dendrites which grew radially inward due to heat loss through the nozzle wall. However, essentially pure alumina buildups have also been observed in practice[2, 3]. Furthermore, Ogibayashi et al.[3] claimed that the steel within the clog matrix is liquid during casting as evidenced by the observation of pure alumina clogging and alumina clogging with entrapped steel both appearing in the same region. As mentioned in Chapter 2, Ogibayashi et al. concluded that the presence of pure alumina or alumina embedded in steel will be determined by the steel cleanliness (i.e., concentration of alumina in the steel).

Several questions are prompted by the above observations:

1) How dense must a clog matrix be to withstand erosion?

2) Under what conditions is the clog pure and when is it embedded in steel?

3) Is the embedded steel in the clog solid or liquid?

4) How can steel cleanliness affect the clog morphology? In other words, if clog growth is envisioned as the entrapment of entrained inclusions by the clog matrix, then how does the rate at which the inclusions are entrapped (which will clearly be a function of concentration) affect where the inclusions are entrapped? In fact, since the ejection of the steel from between the deposited inclusions[3] requires finite time, the amount of steel within the clog should increase as the steel cleanliness decreases if no other mechanisms are acting. Since in practice,

the amount of steel instead decreases as cleanliness decreases, another mechanism must be acting.

Simplified models to address these issues were developed. Models addressing the first two questions are addressed in this section. Models addressing the last two questions are presented in Sections 4.3 and 4.4 respectively.

The model developed for the structural analysis of the clog considered a single “finger” of alumina protruding radially into the bulk flow as a cantilever beam. If attention is restricted to areas with a uniform mean flow (e.g., ignore boundary layers and separation zones), the clog can be approximated by an alumina rod subjected to a distributed load resulting from the drag force imposed by the molten steel flow (Figure 4.1). The equations, material properties, and solution procedure are shown in Appendix A.1.

Assuming a bulk flow of 1.6 m/s (corresponds to 3 ton/min. through a 76 mm diameter nozzle bore), alumina failure stress of 300 MPa[4], and drag corresponding to flow past a cylinder; the maximum length of a 10 micron diameter rod would be 0.5 mm (i.e. at this length the outer fiber bending stress would exceed the failure stress). Clearly, even if the inclusions were completely sintered together, the buildup must be greater than one inclusion in diameter to reach the extent of clogs observed in practice. For the buildup to extend 20 mm radially into the bore, the alumina rod must be 0.26 mm in diameter.

The “pure” alumina clogs observed in practice will still have significant spacing between the deposited particles. Therefore, the buildup must be thicker than the value predicted above to offset the reduction in effective strength. The density of the pure alumina clog will depend on the packing efficiency of the inclusions.

As shown in Appendix A.2, if the clog is modeled as a group of 10 micron diameter finger-like structures (see Figure 4.2) and the critical distance between the fingers for ejection of molten steel is calculated[3], the volume fraction of alumina in a “pure alumina” clog is 17%. This value ranges from 9% to 28% for rod diameters from 5 to 20 micron.

The structural model above was modified to account for a porous clog buildup containing a volume fraction of 17% alumina rods by reducing the failure stress by 83%. For this porous buildup with 83% void fraction to extend 20 mm radially into the bore, its diameter must be 0.62 mm.

Note that in both cases, buildups of significant length can survive if the buildup is only a fraction of a millimeter wide. Solid alumina rods are very strong for their size, being able to support a length at least fifty times its diameter. Even so, if the deposition process progresses by the addition of inclusion particles to random locations on a clog matrix, then it can be concluded that only a fraction of the buildup fingers are likely to have sufficient cross-sectional area to continue growing. It also follows that the fraction of the buildup fingers that continue to grow will be greater if their unsupported length is decreased by steel solidifying in the previously-deposited inclusion network.

4.3 HEAT TRANSFER MODELS

This section formulates and presents the results of steady state and transient heat transfer analyses of the tundish and submerged entry nozzles.

4.3.1 STEADY STATE ANALYSES

To determine whether the steel within the matrix solidifies during casting, a one dimensional, steady state heat transfer model of the submerged entry nozzle was developed (Figure 4.3). The Sleicher and Rouse correlation[5] was used to predict the heat loss from the molten steel stream to the clog front (ahead of the solid steel interface). The liquid steel within the clog was assumed to be stagnant and the heat transfer in this region was therefore by conduction only. Similarly, the heat transfer through the region of the clog containing solid steel and through the nozzle was by conduction. The material properties of the clog in this and subsequent analyses were approximated by using the properties for steel (a reasonable assumption considering the large fraction of steel entrapped). Heat was lost to ambient by radiation. The velocity of the steel stream increases as the clog grows in order to maintain a constant casting rate. The dimensions, material properties, and casting conditions considered are shown in Table 4.1. The solution procedure is shown in Appendix A.3.

For a sufficiently thick clog, the entrapped steel adjacent to the wall will freeze. The effect of clog thickness on the frozen steel (i.e., skull) thickness is shown in Figure 4.4. It is seen that for clog thicknesses greater than 3.5 mm, skulling will occur. A consequence of increased skulling that the unsupported length of the clog matrix will decrease. The effect of varying the assumed parameters (see Table 4.1) on the skulling behavior can be seen in Figure 4.5. It is seen that increasing the conductivity of the refractory and/or lowering the freezing temperature will substantially increase skulling and decrease stagnant liquid layer thickness.

A similar model was developed for the tundish nozzle (see Figure 4.6 and Table 4.1). As shown in Appendix A.4, the resulting skulling behavior is similar. The calculations show that the large mounting block, which surrounds the tundish nozzle, has a small effect on heat transfer. It was found that increasing the mounting block diameter up to 250 mm slightly increases heat loss because the mounting block behaves as a radiator instead of an insulator in this range.

4.3.2 TRANSIENT ANALYSIS

At the initiation of cast, the nozzle will not have a steady state temperature distribution as assumed in the prior section. A one dimensional, explicit, finite difference code was developed to determine the importance of this initial transient (see Appendix B.1 and B.2) for the tundish nozzle. Preheating was simulated by imposing a fixed temperature on the nozzle inner diameter. Heat transfer during casting was calculated using the Sleicher and Rouse correlation as in the previous method. Sensible heat loss of the skull was neglected. The solidification front was assumed to be at the liquidus temperature (see section 4.4). Table 4.1 lists the material properties utilized. Table 4.2 lists the conditions studied with this model. The code was validated by inputting the steady state temperature distribution as the initial condition and verifying that the temperature remained the same at future time steps (see Figure 4.7).

As seen in Figure 4.8 and 4.9 for a superheat of 25˚ C, a skull forms at the initiation of casting for the range of preheat temperatures and times considered. However the skull generally persists for only a relatively short time and has a small thickness (i.e. maximum of 3 minutes and 9 mm for the cases considered). As shown in Figure 4.10 and 4.11, skulling will persist a long time if the superheat is sufficiently low (e.g., the skull takes about 1/2 hr to remelt if the superheat is at 12˚ C). In addition, the thickness of the mounting block has little effect on this initial transient as shown in Figure 4.12. In contrast with the previous section, these results illustrate that permanent skull formation is very difficult with a clog matrix.

The initial transient discussed above may have a significant impact on the clogging process. This transient will prevent argon injection into the nozzle until the skull remelts. In addition, if a sufficient thickness of inclusions deposit on the skull, they may prevent the skull from remelting and thereby permanently prevent argon injection in that region. Finally, the large temperature gradients occurring within the nozzle at the start of cast may cause nozzle cracking and thereby allow air aspiration or leakage of argon out of the system.

4.4 HEAT AND MASS TRANSFER MODEL

In the prior section it was observed that the degree of skulling occurring within a clog was closely related to the difference between the bulk steel temperature and the temperature of the solid-liquid interface. Thus, the temperature of the interface relative to the solidus and liquidus temperatures is important. This temperature is determined by the concentration of solute at the interface.

freezing temperature of the steel (and similarly on the superheat). To determine the temperature of the solid/liquid interface, the concentration of the solute at the interface is required. This section formulates and presents the results of a solidification model which accounts for solute rejection at the liquid-solid interface and investigates the effects of solute rejection on the interface temperature, steel stream temperature variations on clogging, and clogging rates on stagnant layer thicknesses.

Figure 4.13 presents a schematic describing the transient algorithm utilized to model this solidification problem. The algorithm can be divided into roughly six steps. Starting at the beginning of time level n, the first step is to take the velocity of the clog and solidification front (V_7 and V_6) and calculate the new position of the clog and solidification front (x_6 and x_7). In the second step, the amount of solute rejected from the solid during the time step and the amount of solute diffused out of the clog is calculated. In the third step, a mass balance on the solute and the assumption of a "steady state" planar solidification concentration profile is utilized to predict the concentration of solute in the liquid at the interface (Cl_6). Planar solidification is a valid assumption (see Appendix A.5) because of the slow growth rate. In the fourth step, the equilibrium phase diagram is used to calculate the concentration of the solid and the temperature of the interface (Cs_6 and T_6) corresponding to the liquid concentration found in step three. In the fifth step, the temperature profiles radially inward and outward from the interface are calculated independently given the interface temperature. Finally, the heat flux imbalance resulting from the temperature profiles calculated in the prior step is used to calculate the velocity of the solidification front. In addition, the velocity of the clog front is calculated by an assumed relationship between the clog front velocity and the stagnant liquid layer thickness. The details of this formulation are presented in Appendix A.5. This algorithm has been implemented in a FORTRAN code (see Appendix B.3 and B.4).

The relationship assumed between the stagnant liquid layer thickness and the clogging velocity accounts for the hypothesized increase in clogging rate if the unsupported length of the clog is decreased. To illustrate the reasonability of the assumed relationship between stagnant liquid layer thickness and clogging rate, I have run the model for the standard conditions shown in Table 4.1 while varying the superheat. The results are shown in Figure 4.14. It is seen that as the superheat is varied from 10˚ C to 50 ˚ C the time required for the clog to reach a radial position of 20 mm (i.e. 20 mm radius casting channel - a typical final clog value) varies from 1.3 to 2.4 hours. This is typical of the time between start of cast and rodding/submerged entry nozzle replacement. Therefore the predicted clogging behavior is reasonable.

Figure 4.15 - 4.17 show the results of the model for a cast having a carbon concentration of 0.095%, a constant superheat of 32˚ C, and a constant flow rate of 0.008664 m^3/s (typical values from the data provided). Figure 4.15 shows the evolution of the excess solute concentration in the liquid at the interface (i.e. the amount over the free stream concentration). After the solid begins to form (about 1000 sec.), the concentration begins to increase. It is noted that the concentration profile reaches a plateau well below the theoretical excess concentration for steady state planar growth (about 0.46 %C). This is expected because solute is rapidly swept away by the fast-moving bulk flow. The final excess concentration lies closely to zero (with the consequence that freezing occurs near the liquidus temperature) rather than at the theoretical value for stagnant solidification (corresponding to freezing at the solidus temperature). The resulting growth in the solidified layer and clog is shown in Figure 4.16 and 4.17. Here again it

is seen that the assumption of freezing at the liquidus vice solidus temperature better approximates the results of the model which includes solute rejection.

This model was also used to determine the effect of melt temperature variations on the clogging process. From the temperature strip chart data and detailed casting data provided, the melt temperature and flowrate histories shown in Figure 4.18 were obtained. These histories represent one heat of steel and are considered a reasonable upper bound on the actual temperature and flow variations expected. The model repeated these histories until the unclogged radius reached 20 mm (a typical limiting clog as discussed below). Melt chemistries of 0.02% C and 0.06% C were considered.

Figures 4.19 and 4.20 show the results of this transient run. The solidification rate is shown in Figure 4.19 and is compared with the solidification rate that would have occurred for a constant superheat of 32˚ C (i.e., the average of the high and low temperatures). It is seen that the skulling accelerates prior to the ladle change but then recedes after introduction of the new heat. The net effect of this transient is shown in Figure 4.20. It is observed that neither the temperature transient nor the carbon concentrations considered have any appreciable effect on the resulting clogging behavior (i.e., the difference between final clogging times was less than ten minutes for the four cases). It is therefore expected that the average superheat plays a large role in the clog process than does the variation in temperature.

Finally, this model was used to test a mechanism proposed in response to the question posed in section 4.2 regarding the relationship between steel cleanliness and clog morphology. The mechanism proposed is that cleaner steels cause clogs containing a greater amount of entrapped steel because the clogging rate is slower which causes the stagnant layer to be smaller (because of increased interface temperature) which therefore allows the matrix less time to assimilate inclusions (and thereby decreases the volume fraction of inclusions in the final clog).

To test this hypothesis, I examined the stagnant layer thickness that would evolve if clogging preceded at the fixed rates of 5 mm/hr (representative of a clean steel with a slow growing clog) and 20 mm/hr (representative of a dirty steel with rapid clogging rate). The resulting stagnant layer thicknesses are plotted versus position in Figure 4.21. It is observed that the difference in stagnant layer thickness predicted is less than 0.3 mm throughout the simulated cast. It is therefore unlikely that this skulling mechanism is responsible for the variation in clog morphology.

4.5 FLUID FLOW MODELS

This section will formulate and present the results of fluid flow and related models. The first model will estimate the operating characteristics of the slide gate system for varying degrees of clogging.

4.5.1 SLIDE GATE SYSTEM MODEL

In order to assess the significance of the casting data provided, it is necessary to first understand the degree of clogging indicated by a certain slide gate position for a known casting rate and tundish level. A model was developed of this flow configuration which divides the system into separate simple components for which analytic or empirical relations are available. The tundish nozzle and submerged entry nozzle were modeled as a rough pipe whose radius was decreased by an amount equal to the clog thickness. The nozzle ports were modeled as a tee. The slide gate was modeled as an orifice of equivalent cross section and subsequently adjusted to better match caster data. The pressure drop due to flow acceleration at the tundish nozzle entrance was determined using Bernoulli's equation. The casting conditions considered are given in Table 4.3. A complete description of the model can be fond in Appendix A.6.

To validate the model, the detailed casting data provided was utilized to calculate the actual flow resistance of the system (i.e. the pressure drop divided by the volume flow rate squared). This data is shown in Figures 4.22 - 4.28. Since the flow resistances calculated include the effects of clogging, the flow resistance of a clog-free nozzle should lie below this data. Therefore a set of lower bound curves was generated for the flow resistances shown in Figure 4.22 and these lower bounds were compared to the model.

It was found that the model over predicts the actual flow resistance for a slide gate travel of 50% or less. However, the absolute position of the slide gate recorded is not always exact. Therefore, the model was calibrated by adjusting the slide gate position used by the model to a value approximately 20% further open than the actual value. Using this adjustment, the model was able to provide a good match to the lower bound curves. It is noted that a portion of the difference between the uncalibrated model and the measurements may be due to uncertainties in the measured position of the slide gate. Although the relative motion of the slide gate is known accurately, its absolute position must be calibrated each time a tundish is replaced. This may also explain why the lower bound curves from Figure 4.22 do not provide a lower bound for some of the other casts (e.g., see Figures 4.20 and 4.21).

The relationship between degree of clogging and the slide gate position required to maintain the casting rate is shown in Figure 4.29. It is seen that very little slide gate travel is required until the clog reaches a critical thickness. After reaching the critical thickness, a small increase in clog thickness necessitates a large change in slide gate position. The underlying reason for this behavior is that for a fixed casting rate, the turbulent pressure drop through a rough pipe is inversely proportional to the fifth power of the pipe radius. This result indicates that slide gate position is generally a poor indicator of the extent of initial clogging.

This analysis was also utilized to estimate the pressure distribution in the nozzle and to predict conditions and regions at which air aspiration were most likely to occur. Figure 4.30

shows the gauge pressure within the tundish and submerged entry nozzles for a casting speed of 4 ton/min. and three different clogging conditions.

The first condition represents casting through a nozzle with no clogging. As expected, the majority of the pressure drop for this case is due to the slide gate. The largest magnitude of negative gauge pressure occurs just below the slide gate. Note that the pressure in the upper half of the submerged entry nozzle is predicted to be below atmospheric pressure, making this region susceptible to aspiration. These results are in good qualitative agreement with the measurements of Heaslip et. al.[6] who performed a series of water modeling experiments which quantified the effect of gas injection on the pressure distribution.

The second condition considered represents a tundish and submerged entry nozzle with a limiting amount of clogging (i.e., the required slide gate position to maintain cast speed is 100%). It is noted here that the pressure everywhere remains above atmospheric. The final case considered represents limiting clogging in the tundish nozzle and no clogging in the submerged entry nozzle. This would be a conservative estimate for the situation occurring after submerged entry nozzle replacement. For this case the entire tundish nozzle is below atmospheric pressure. This suggests that severe clogging in the tundish nozzle might accelerate clogging by encouraging aspiration (particularly in a cracked or porous nozzle or near nozzle joints).

The results presented here might help explain the variation in clogging observed in the samples provided. For example, the average back-pressure for cast 9267 was 14 and 17 kPa for strands one and two respectively (see Table 3.1). The clogging for this particular tundish nozzle was severe (only five heats were cast and ten rodding evolutions were required). By comparing these back-pressures with the predicted pressure within the nozzle, it is seen that the argon was not under sufficient pressure to enter the stream (e.g., for a clean nozzle, Figure 4.30 indicates that the steel pressure is about 80 kPa). Therefore the beneficial effect of argon injection was absent during this cast. To obtain any benefit from argon, it is obvious that the argon back-pressure must exceed the ferrostatic pressure shown in these figures.

Furthermore, it is noted that the tundish nozzle design depicted in Figure 3.1 will not likely result in an even distribution of argon flow over the nozzle inner diameter. This is because the pressure generally increases with distance into the nozzle and the argon flow resistance of the nozzle wall also increases with distance into the nozzle (because the length of the pierced holes is greater near the bottom than near the top of the nozzle). This will result in decreased argon flow with distance into the nozzle. To increase the uniformity of argon distribution, the flow resistance of each vertical level of holes could be tailored to account for the ferrostatic pressure at that level. Also, if the flow resistance between the argon slit and the nozzle internal diameter is increased and the back pressure increased correspondingly, then the argon distribution will be more uniform (the calculated pressure drop through the nozzle for the current design is only 0.5

kPa). This uniformity in argon distribution results from the smaller percentage difference between the pressure drop across the nozzle wall at the top and bottom of the nozzle (even though the actual change in pressure drop would remain the same). Increasing the flow resistance of the nozzle wall would also reduce argon pressure variation in the slit.

4.5.2 FRACTION OF ALUMINA CAPTURED BY CLOG

When no clogging countermeasures are employed, nozzle clogging has been observed to limit sequence casting to 1-3 heats[7, 8]. Assuming 250 ton heats and a 30 ppm combined oxygen concentration in the tundish, 32 kg of alumina will pass through the nozzles in two heats.

The mass of alumina in the clog will depend upon the amount of entrapped steel is within the clog. If a “pure alumina” clog is assumed, the clog will contain approximately 17% volume fraction of alumina (see section 4.2). Considering a two strand caster[7] having 1 m long nozzles with 20 mm thick clogs, the amount of alumina within the clogs is calculated to be 5.1 kg (see Appendix A.7.1).

Taking the ratio of the deposited alumina to the alumina throughput, it is seen that in these severe clogging situations about 16% of the alumina passing through the nozzle is deposited (assuming the clog is composed of deoxidation products). This indicates that in the absence of clogging countermeasures (e.g., argon injection), transport of the inclusions to the nozzle wall is fairly efficient. This also emphasizes that measures to produce cleaner steel should be effective in reducing clogging rate for these conditions. In addition, measures to reduce transport are likewise seen to be very important.

4.5.3 SIGNIFICANCE OF REOXIDATION

Nitrogen pickup between the tundish and mold can be used to quantify the reoxidation occurring in the nozzle[9]. Prior to efforts to improve nozzle air-tightness, McPherson[9] measured nitrogen pickup values of 5 ppm. Considering 250 ton heats and assuming all the aspirated oxygen forms alumina, this reoxidation source would generate 1.4 kg of alumina in two heats, as shown in Appendix A.7.2. This is a substantial fraction of the typical clog mass calculated above (i.e., 5.1 kg).

The aspirated oxygen also accelerates the deposition of inclusions by creating a surface tension gradient around the inclusion which in turn causes a net force on the particle in the direction of the wall. This is shown schematically in Figure 4.31. Considering a linear variation in surface tension with position, and assuming Stokes drag on the particle, it is shown in Appendix A.7.3 that the surface tension induced particle velocity is:

$$V = \frac{-2\, m_\gamma\, R}{9\, \mu}$$

Consider aspiration occurring evenly over the length of a 1 m long, 80 mm diameter nozzle which results in a nitrogen pickup of 0.3 ppm (a relatively air-tight system)[10]. Assume that the oxygen does not react with the steel or deoxidants in the vicinity of the wall. The concentration gradient needed to diffuse the oxygen through the near-wall region to the bulk flow (D_O=2.5 cm^2/s[11]) will in turn generate a surface tension gradient due to the effect of oxygen concentration on steel surface tension (≈ -5 (N/m) / (atom% O)[11]). This surface tension gradient results in a surprisingly high particle velocity of 0.9 m/s for a 10 micron diameter particle.

In light of this analysis and prior publications discussing inclusion transport[12], it is concluded that in some regions (e.g., in the vicinity of the aspiration and outside of flow recirculation zones), this surface tension-induced transport mechanism may be the dominant mode for transporting inclusions to the wall. Thus it is critical to avoid aspiration in order to reduce both the formation of clog product and transport of inclusions across the viscous sub-layer.

4.6 PROPOSED NOZZLE DESIGN

The heat transfer calculations above indicated that a layer of solidified steel may exist within a clog buildup. It is hypothesized that this skull will increase the clogging rate by reducing clog reentrainment. Also it was experimentally observed that nozzles having low argon back-pressure have increased clogging. The low back-pressure was likely due to nozzle cracking, which may have resulted from thermal shock at cast initiation.

To address these concerns, the tundish nozzle schematically portrayed in Figures 4.32 and 4.33 is proposed. This nozzle is electrically heated with a ceramic element (e.g., molybdenum disilicide). The element will be wound into a groove on the outer diameter of an alumina graphite tube to give the winding pattern shown in Figure 4.32. This ceramic tube would then be placed inside a larger diameter silica tube to give the assembled view shown in Figure 4.33.

Alumina graphite was chosen for the inner tube because of its good wear properties and for consistency with the existing design. Silica was chosen for the outer tube because it is a relatively good insulator and will thereby reduce the required output of the heating element. The desired temperature distribution for this nozzle is to have the entire inner cylinder at the casting temperature as shown in Figure 4.34. This would ensure that no heat was lost from the stream.

The dimensions of the inner and outer cylinders were chosen to ensure that: 1) the diameter of the outer cylinder was less than nine inches[13] and 2) the temperature of the steel can surrounding the nozzle remains below 1300° F[13]. These limits are due to tundish configuration and steel can oxidation limits respectively. The power output required of the heating element was calculated to be 11.2 kW.

4.7 REFERENCES

1. S.N. Singh: "Mechanism of Alumina Buildup in Tundish Nozzles During Continuous Casting of Aluminum-Killed Steels", 1974, vol. 5, pp. 2165-2178.

2. G.C. Duderstadt, R.K. Iyengar and J.M. Matesa: "Tundish Nozzle Blockage in Continuous Casting", 1968, (April), pp. 89-94.

3. S. Ogibayashi et. al.: "Mechanism and Countermeasure of Alumina Buildup on Submerged Nozzle in Continuous Casting", *75th ISS Steelmaking Conference*, ISS, Toronto, Canada, 1992, Vol. 75, pp. 337-344.

4. K. Uemura et. al.: "Filtration Mechanism of Non-metallic Inclusions in Steel by Ceramic Loop Filter", 1992, vol. 32 (1), pp. 150-156.

5. L.C. Burmeister: "Turbulent Flow in Ducts", in *Convective Heat Transfer*, John Wiley & Sons, New York, NY, 1993, pp. 342-344.

6. L.J. Heaslip et. al. *Model Study of Fluid Flow and Pressure Distribution During SEN Injection - Potential for Reactive Metal Additions During Continuous Casting.* Iron and Steelmaker. 49-64, 1987.

7. L.T. Hamilton: "Technical Note - The Introduction of "Slit" Submerged Entry Nozzles to No. 1 Slab Caster, BHP International Group Pt. Kembla, NSW", 1985, vol. 290 (No. 8), pp. 75-78.

8. J.R. Bourguignon, J.M. Dixmier and J.M. Henry: "Different Types of Calcium Treatment as Contribution to Development of Continuous Casting Process", *Continuous Casting '85*, London, England, 1985, pp. 7.1-7.9.

9. N.A. McPherson: "Continuously Cast Clean Steel", *68th ISS Steelmaking Conference*, ISS, Detroit, MI, 1985, Vol. 68, pp. 13-25.

10. S.R. Cameron: "The Reduction of Tundish Nozzle Clogging During Continuous Casting at Dofasco", *75th ISS Steelmaking Conference*, ISS, Toronto, Canada, 1992, Vol. 75, pp. 327-332.

11. United States Steel: "The Physical Chemistry of Iron and Steelmaking", in *The Making, Shaping, and Treating of Steel*, W.T. Lankford Jr. et. al., eds., Herbick & Held, Pittsburgh, PA, 1985, pp. 367-502.

12. S. Dawson. *Tundish Nozzle Blockage During the Continuous Casting of Aluminum-Killed Steel*. Iron and Steelmaker. 33-42, 1990.

13. D. Janssen: private communication, 1995.

14. G.B. Shaw: "Property Requirements for Submerged Entry Nozzles", *Continuous Casting of Steel*, Biarritz, France, 1976.

15. M.N. Özisik: "Appendix B- Physical Properties, Appendix C - Radiation Properties", in *Heat Transfer - A Basic Approach*, McGraw-Hill, New York, NY, 1985, pp. 736-762.

16. W. Kurz and D.J. Fisher: "Appendix 14 - Relevant Physical Properties for Solidification", in *Fundamentals of Solidification*, Trans Tech Publications, Switzerland, 1992, pp. 293-294.

17. C.J. Smithells: "The Physical Properties of Liquid Metals", in *Smithells Metals Reference Book*, Butterworth & Co Ltd, England, 1983, pp. 14.6-14.7.

18. United States Steel: "Refractories for Iron and Steelmaking, Steel Plant Fuel and Economy", in *The Making, Shaping, and Treating of Steel*, W.T. Lankford Jr. et. al., eds., Herbick & Held, Pittsburgh, PA, 1985, pp. 49, 108.

19. F.M. White: "Viscous Flow in Ducts", in *Fluid Mechanics*, McGraw-Hill, New York, NY, 1986, pp. 334.

TABLE 4.1 - Heat Transfer Analysis Parameters

Case	Parameter	Value	Source
Submerged Entry Nozzle Steady State Analysis	Refractory:		alumina-graphite
	Conductivity	9.0 W/(m °C)	[14]
	Emissivity	0.5	[15]
1. Standard Conditions	Steel:		0.16 % C
	Flowrate	4 ton/min.	
	Bulk Flow Temperature	1550 °C	
	Freezing Temperature	1525 °C	liquidus[16]
	Conductivity -		
	Liquid	33 W/(m °C)	[16]
	Solid	35 W/(m °C)	[16]
	Density	7015 kg/m^3	[17]
	Viscosity	0.0055 kg/(m s)	[17]
	Thermal Diffusivity	$6.1*10^{-6}$ m^2 / s	[16]
	Ambient:		
	Temperature	27 °C	
	Geometry:		
	Nozzle Inner Diameter	76 mm	
	Nozzle Outer Diameter	135 mm	
2. Low Flow Rate	Steel Flowrate	3 ton/min.	
3. High Emissivity	Refractory Emissivity	0.96	oxidized steel coating[18]
4. Low Conductivity	Refractory Conductivity	1.5 W/(m °C)	[18]
5. Low Freezing Temperature	Steel Freezing Temperature	1493 °C	solidus[16]
Tundish Nozzle Transient Analysis (standard conditions unless otherwise indicated)	Steel:		
	Latent Heat of Fusion	$1.93*10^9$ J/m^3	[16]
	Specific Heat	$5.74*10^6$ J/m^3	[16]
	Liquidus Slope	-81 °C/(%C)	[16]
	Partition Coefficient	0.17	[16]
	Diffusion Coefficient	$2*10^8$ m^2/s	[16]
Tundish Nozzle Steady State Analysis (standard conditions unless otherwise indicated)	Steel Hardware:		
	Emissivity	0.96	oxidized steel[18]
	Air:		
	Conductivity	0.0891 W/(m °C)	[15]
	Geometry:		
	Nozzle Inner Diameter	85 mm	
	Nozzle Outer Diameter	193 mm	
	Mounting Outer Diameter	250 mm	

TABLE 4.2 - Parameters Varied in the Tundish Nozzle Initial Transient Analysis

Case:	Preheat Temperature	Preheat Time	Superheat	Mounting Block Outer Radius
1.	1000 °K	1 hour	25° C	25 cm
2.	1200 °K	1 hour	25° C	25 cm
3.	1400 °K	1 hour	25° C	25 cm
4.	1600 °K	1 hour	25° C	25 cm
5.	1000 °K	1/2 hour	25° C	25 cm
6.	1000 °K	1 minute	25° C	25 cm
7.		none	25° C	25 cm
8.	1000 °K	1 hour	25° C	50 cm
9.	1000 °K	1 hour	30° C	25 cm
10.	1000 °K	1 hour	20° C	25 cm
11.	1000 °K	1 hour	15° C	25 cm
12.	1000 °K	1 hour	12° C	25 cm
13.	1000 °K	1 hour	10° C	50 cm

TABLE 4.3 - Fluid Flow Analysis Parameters

Parameter	Value	Source
Density	7015 kg/m^3	[17]
Tundish Melt Height	1203 mm	
Nozzle Submergence Depth	203 mm	
Tundish Nozzle Length	343 mm	
Submerged Entry Nozzle Length	840 mm	
Nozzle Inner Diameter	80 mm	
Nozzle Surface Roughness	0.5 mm	
Port Resistance Coefficient	0.8	50 mm Dia. Tee[19]

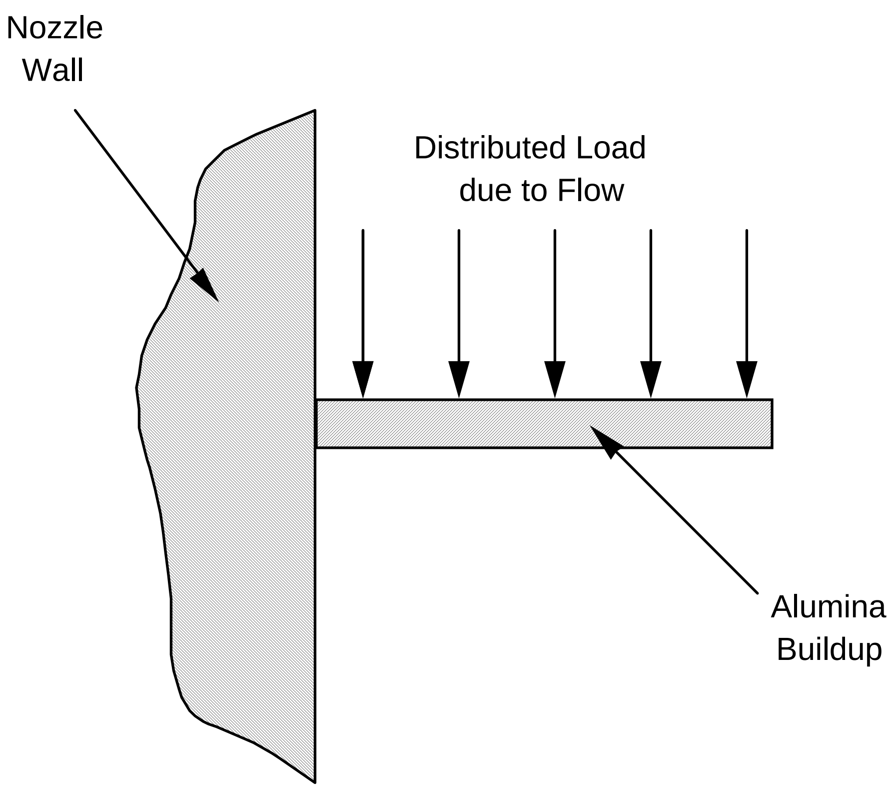

FIGURE 4.1 - Clog Structural Analysis Model

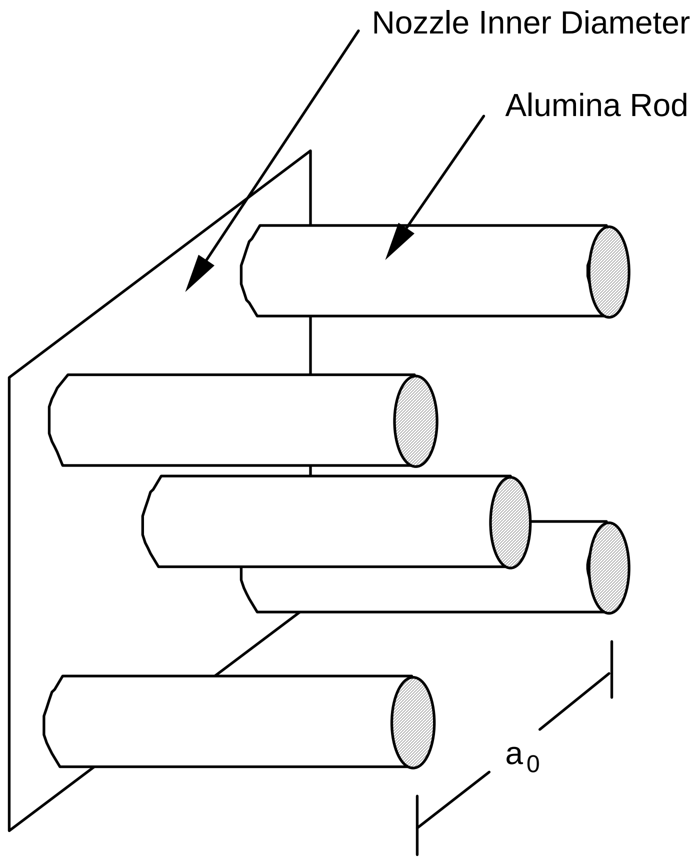

a_0 - Horizontal/Vertical Spacing Between Rods

FIGURE 4.2 - Clog Porosity Analysis Model

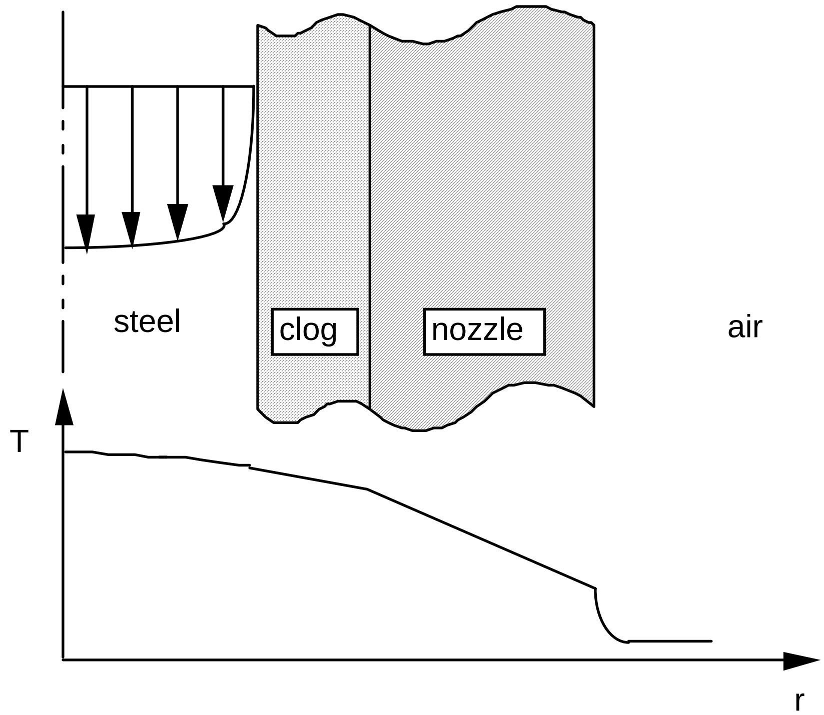

FIGURE 4.3 - Submerged Entry Nozzle Heat Transfer Model

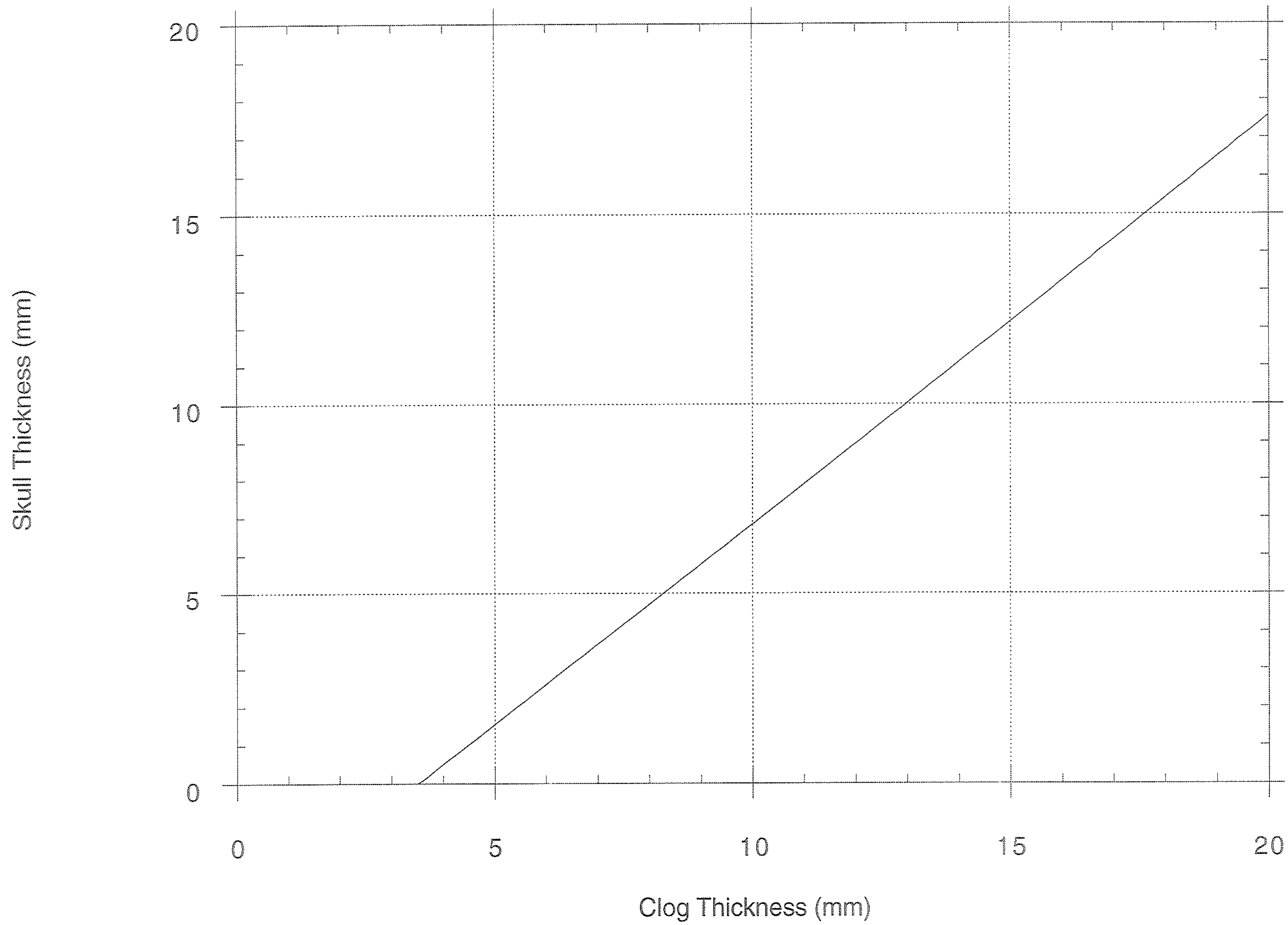

FIGURE 4.4 - Effect of Clog Thickness on Skull Thickness

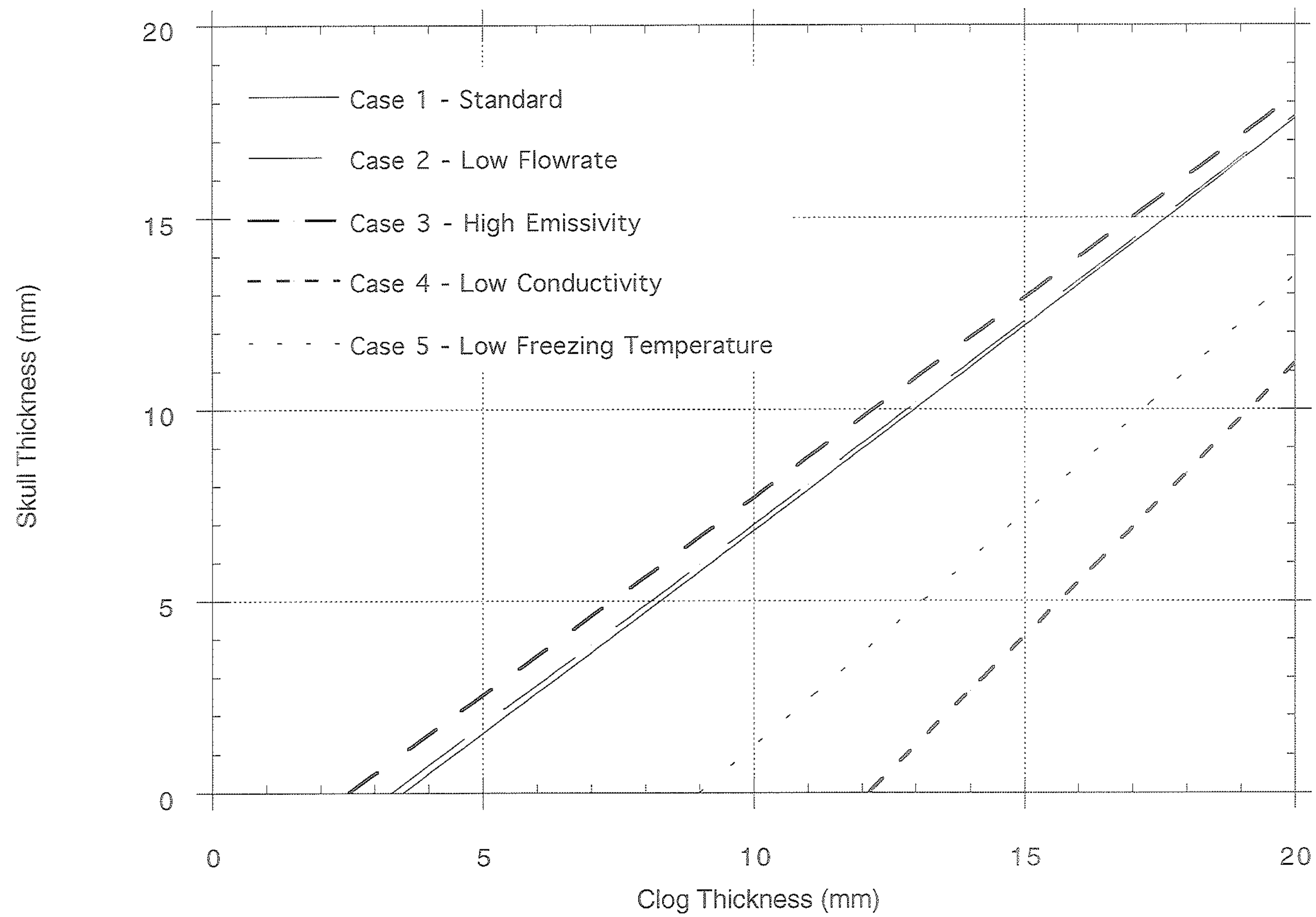

FIGURE 4.5 - Effect of Casting Conditions on Skull Thickness

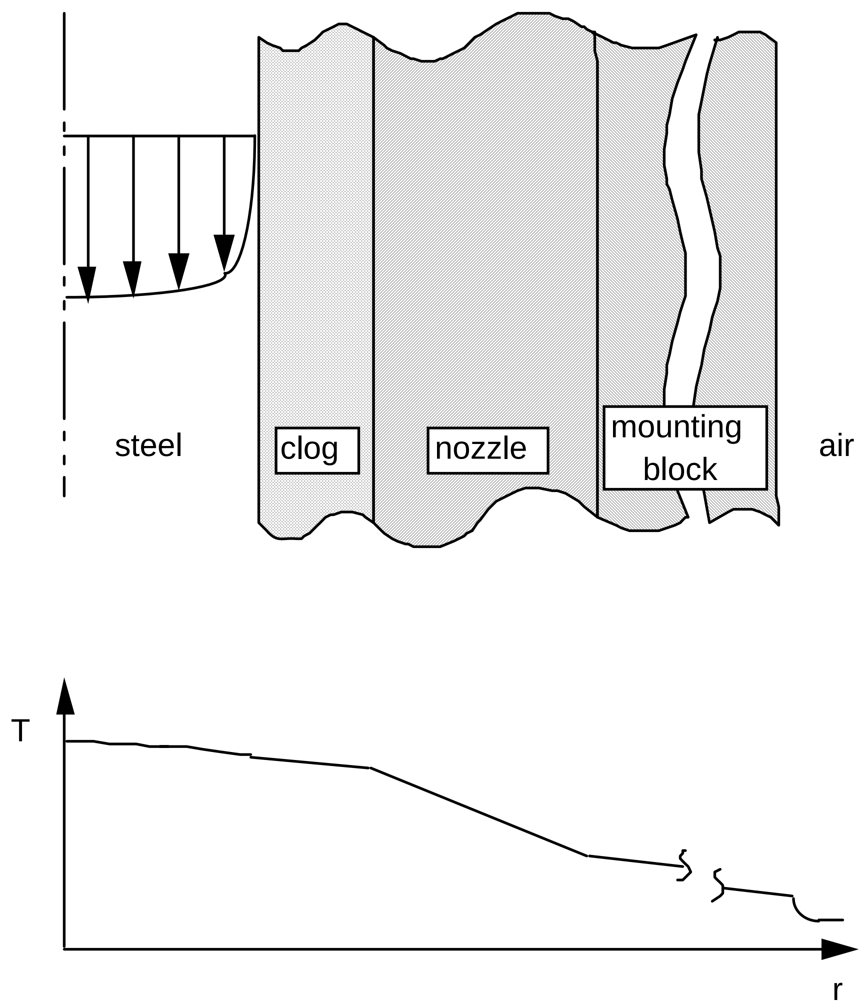

FIGURE 4.6 - Tundish Nozzle Heat Transfer Model

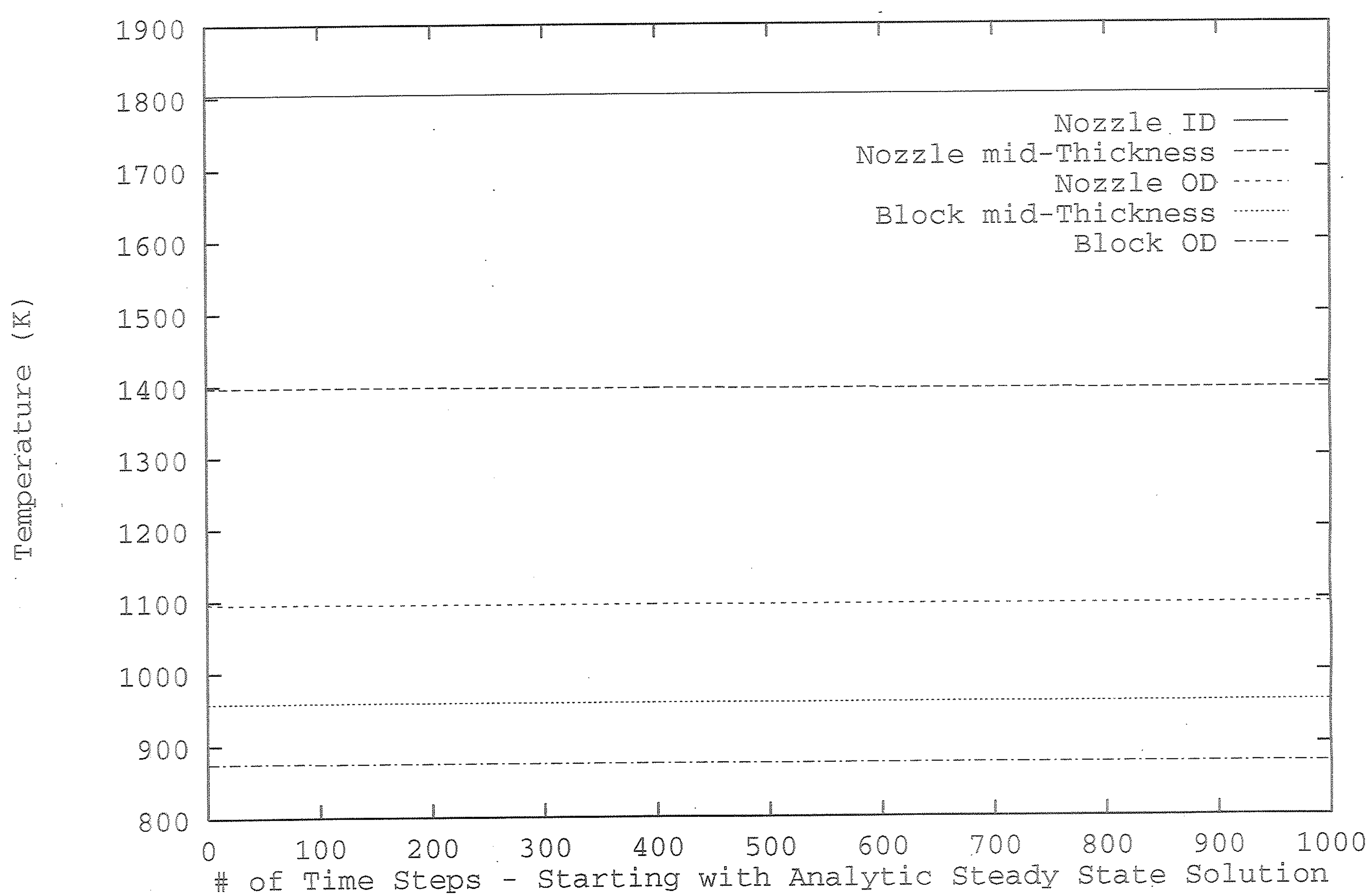

FIGURE 4.7 - Validation of Tundish Nozzle Initial Transient Model

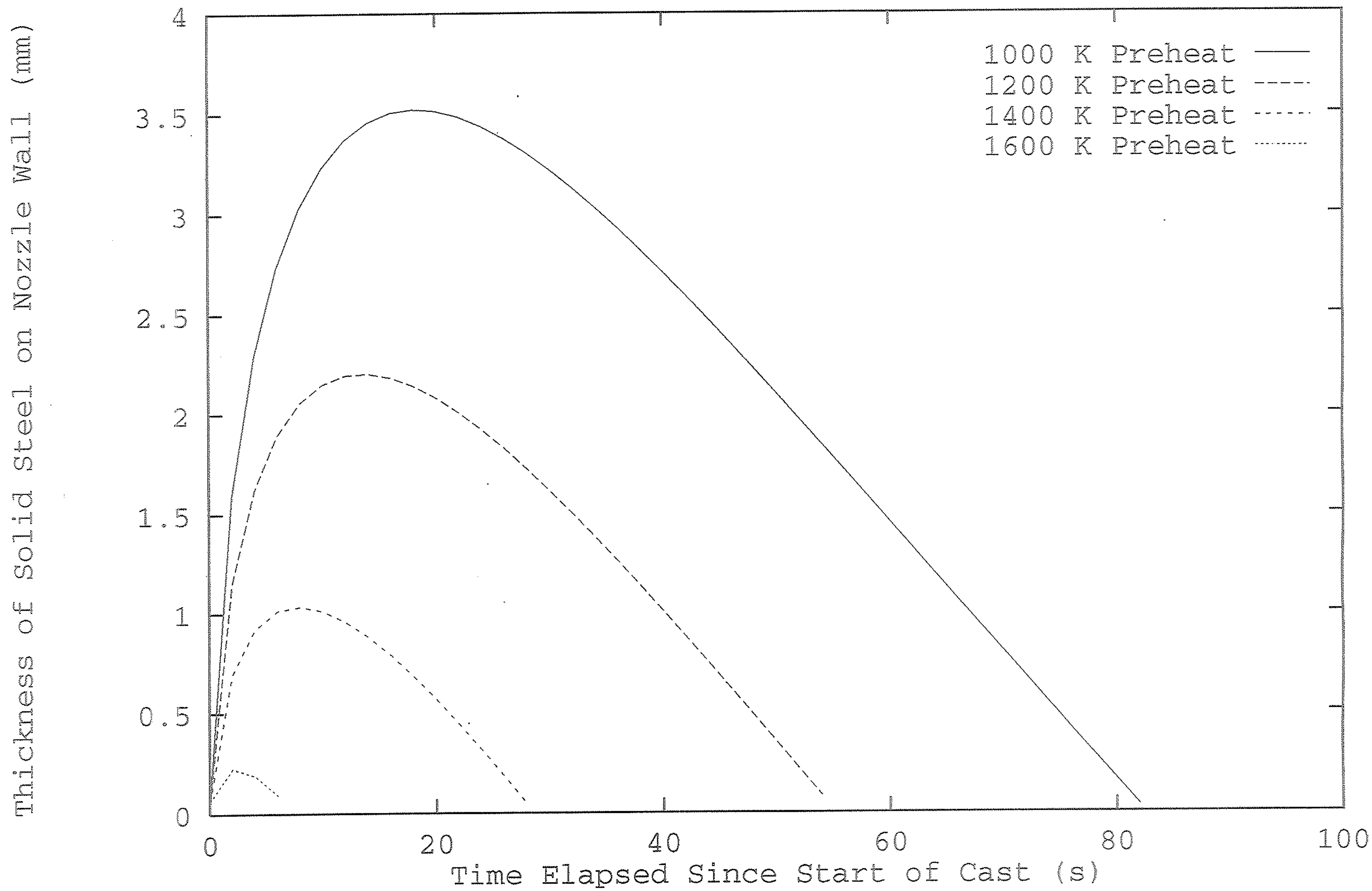

FIGURE 4.8 - Effect of Nozzle Preheat Temperature on Initial Skulling

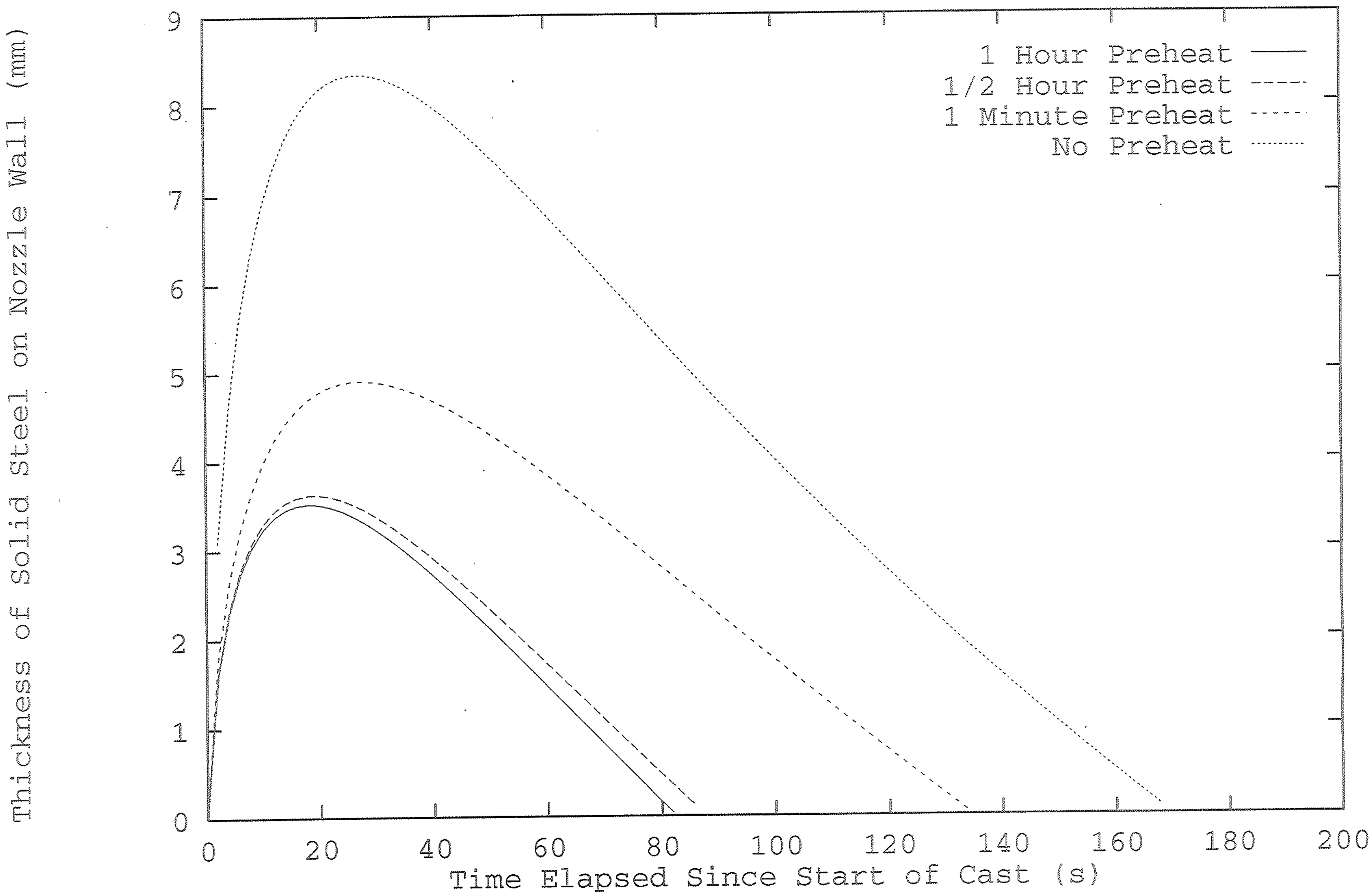

FIGURE 4.9 - Effect of Nozzle Preheat Time on Initial Skulling

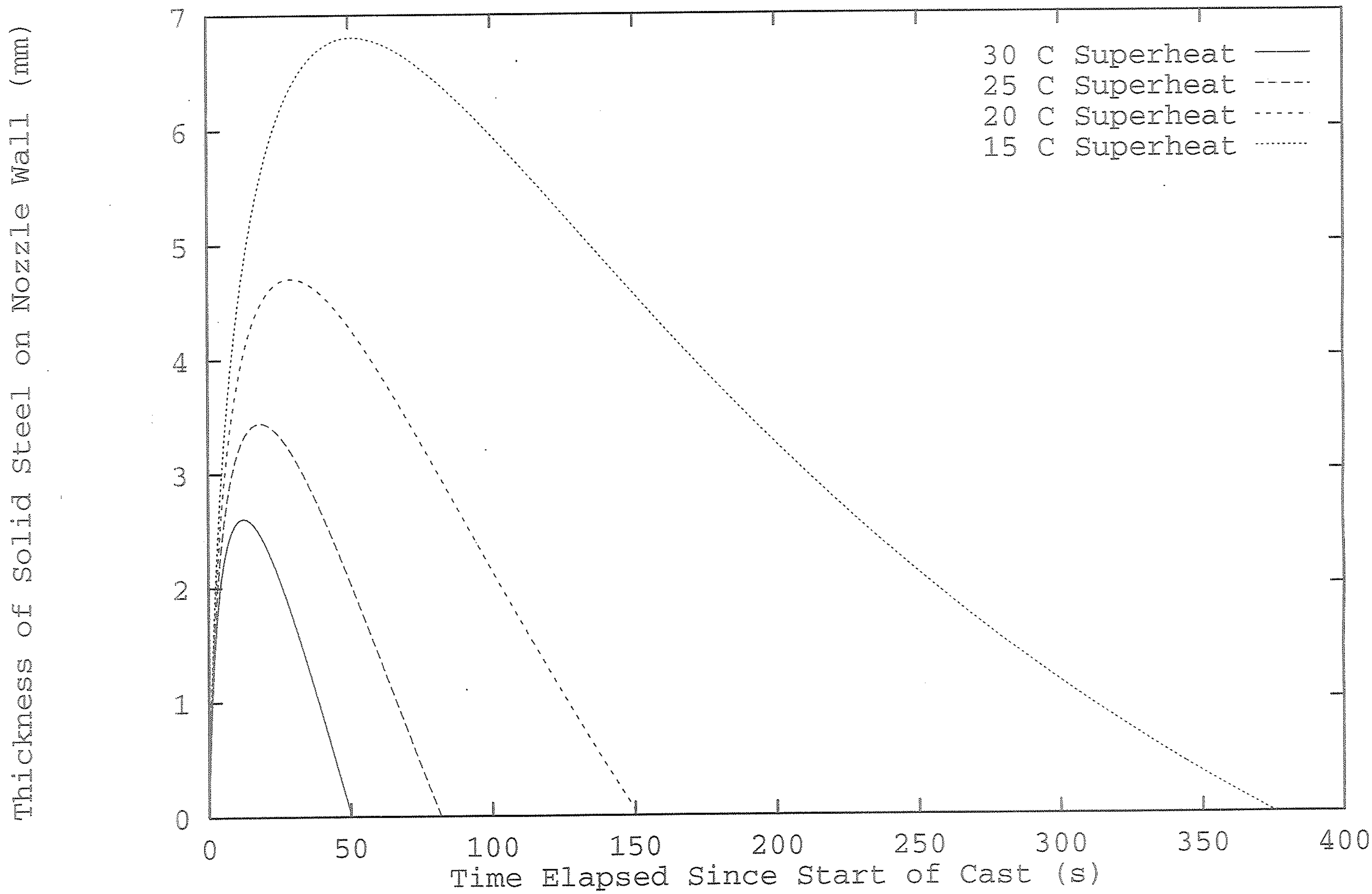

FIGURE 4.10 - Effect of Superheat on Initial Skulling

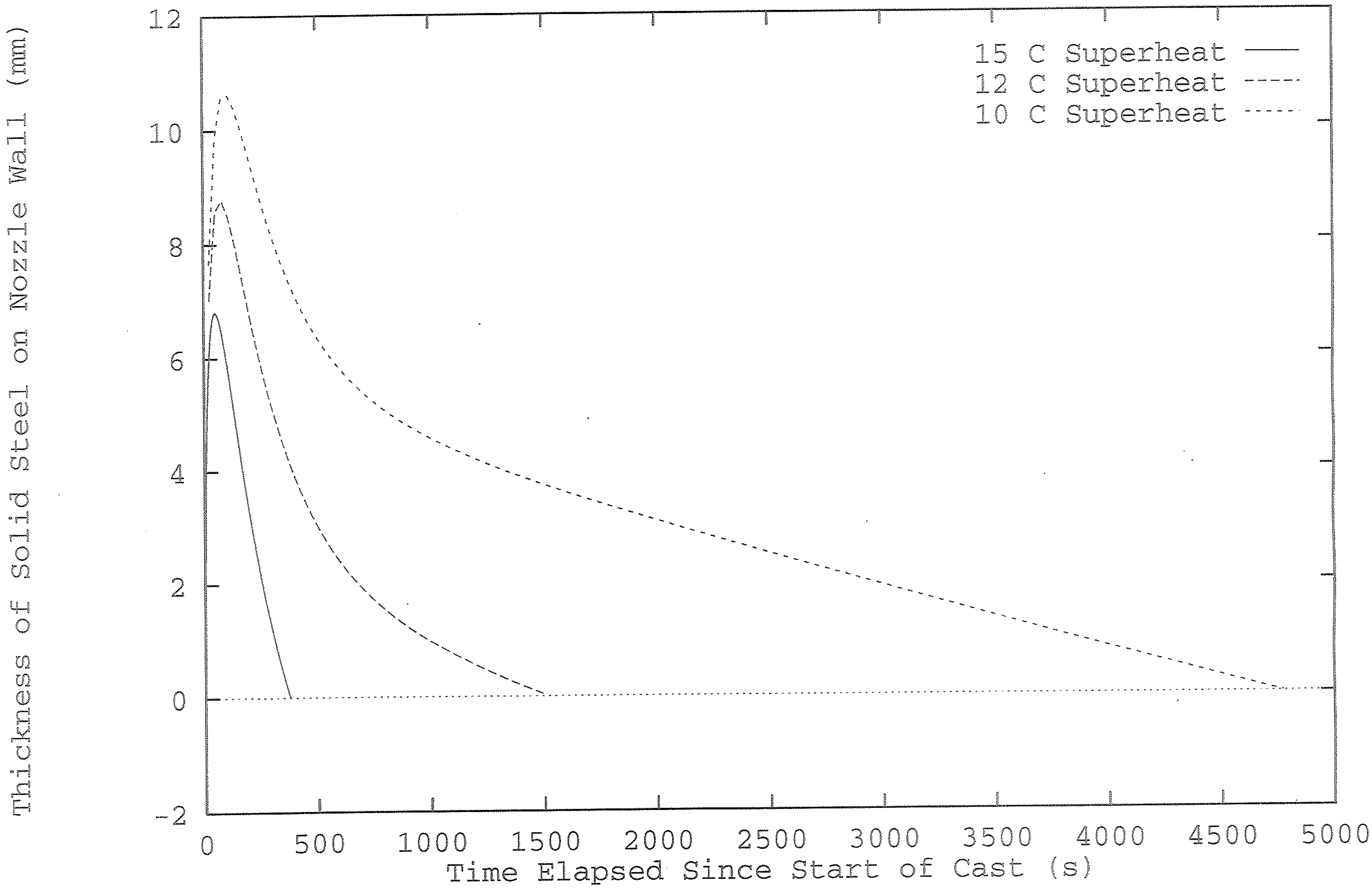

FIGURE 4.11 - Effect of Low Superheat on Initial Skulling

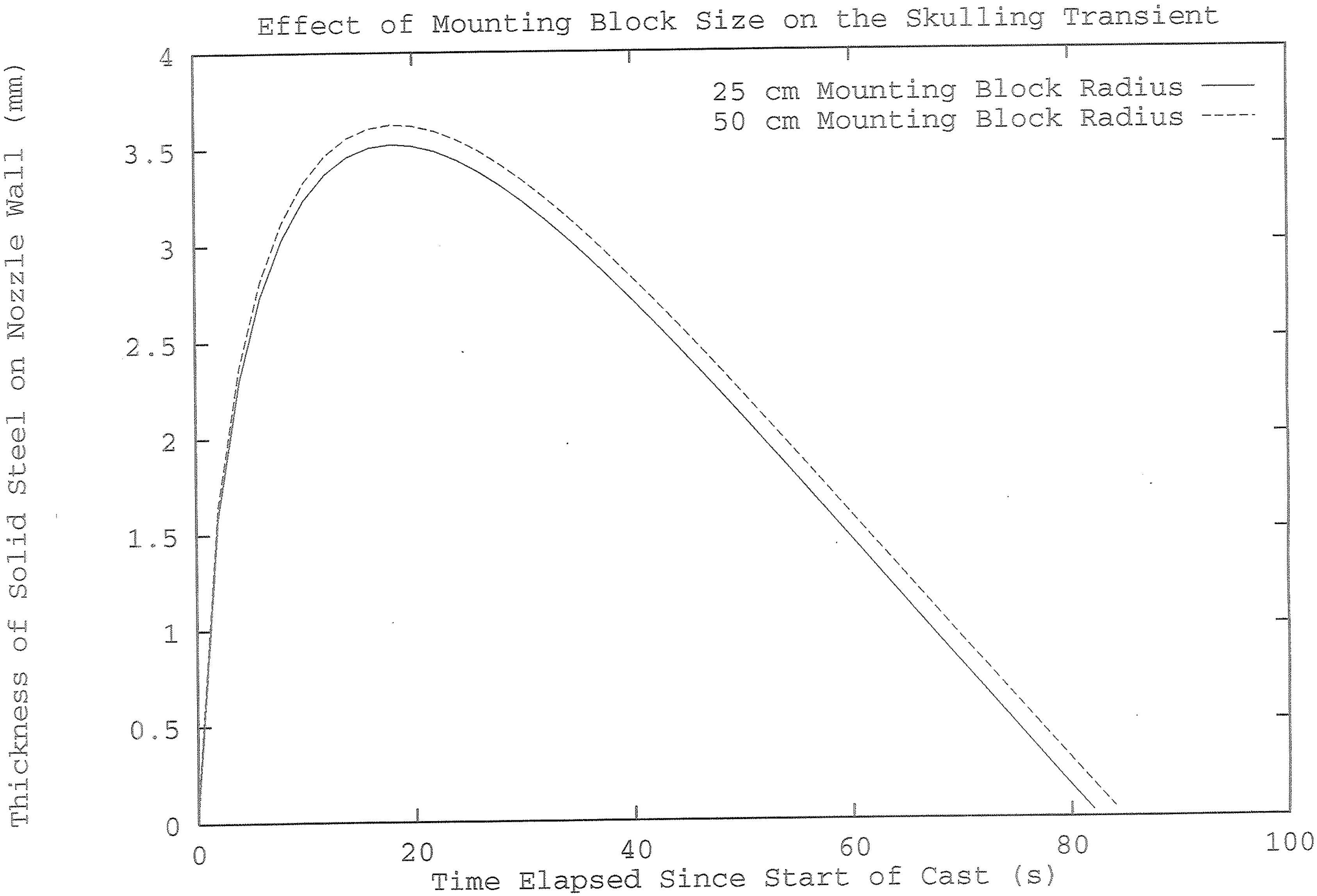

FIGURE 4.12 - Effect of Mounting Block Size on Initial Skulling

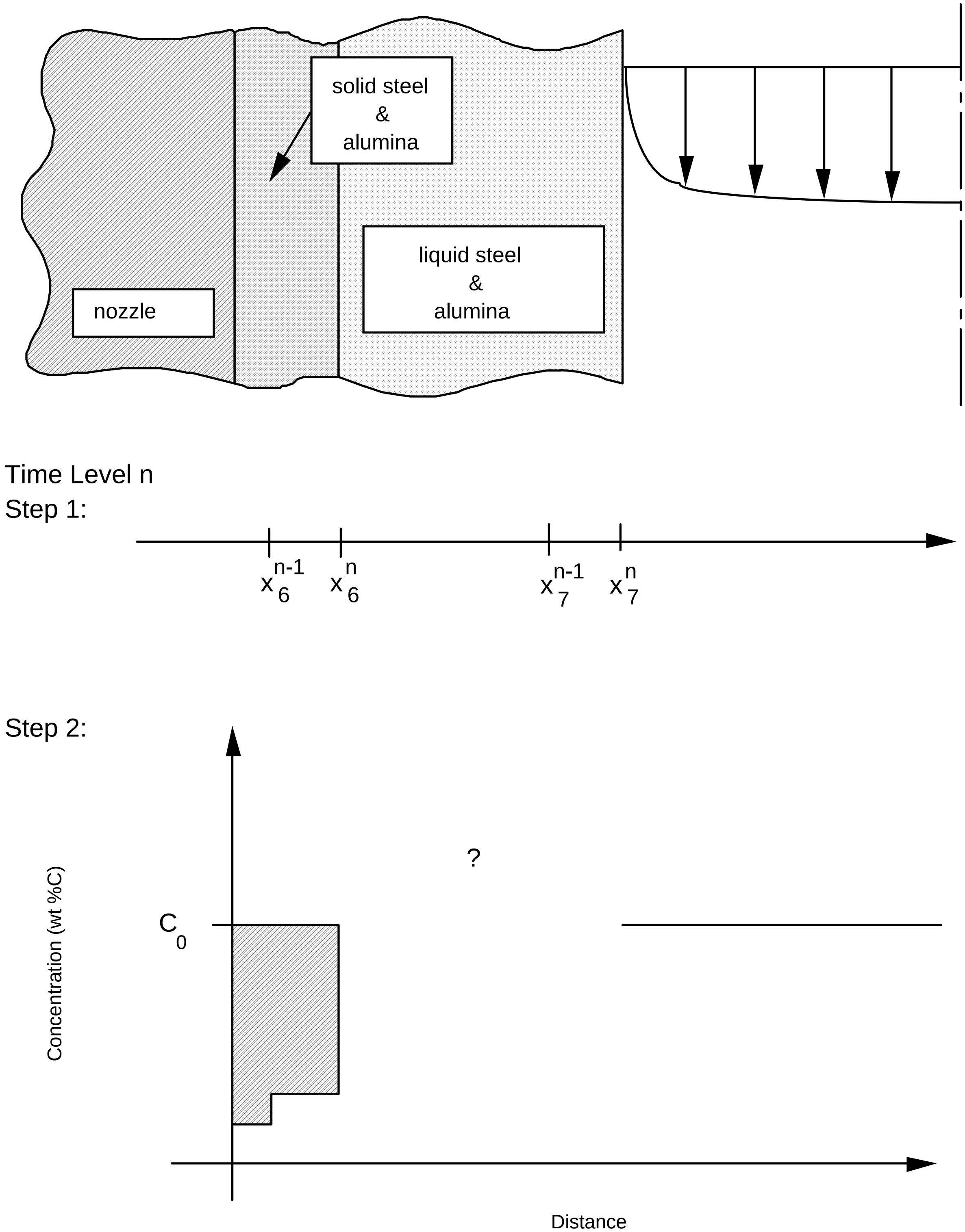

FIGURE 4.13 - Solidification Analysis Algorithm, Part 1

Step 3:

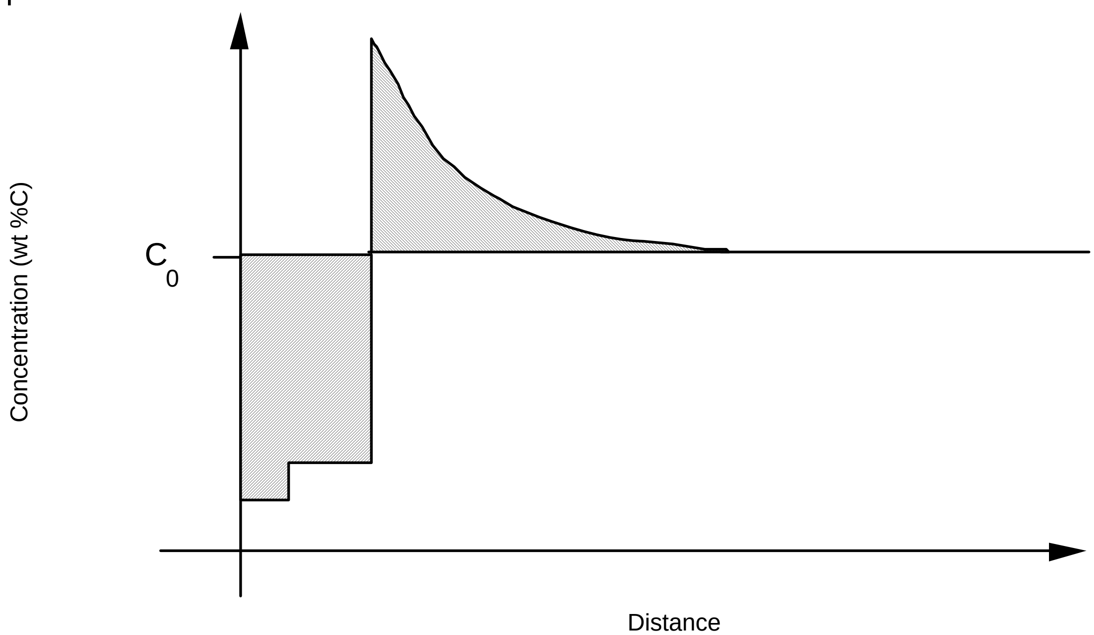

Step 4:

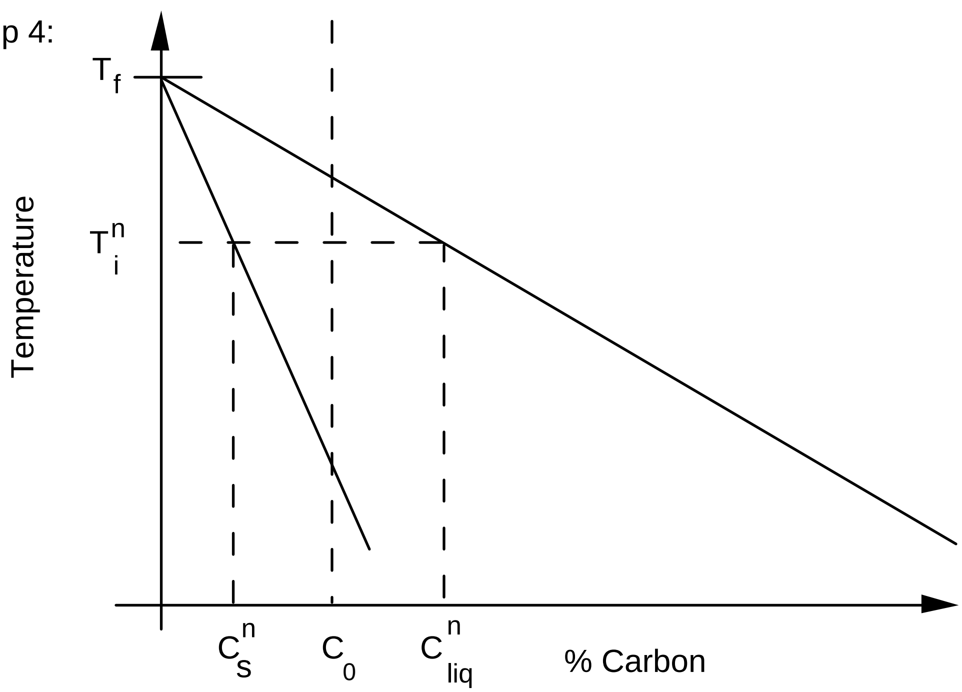

FIGURE 4.13 - Solidification Analysis Algorithm, Part 2

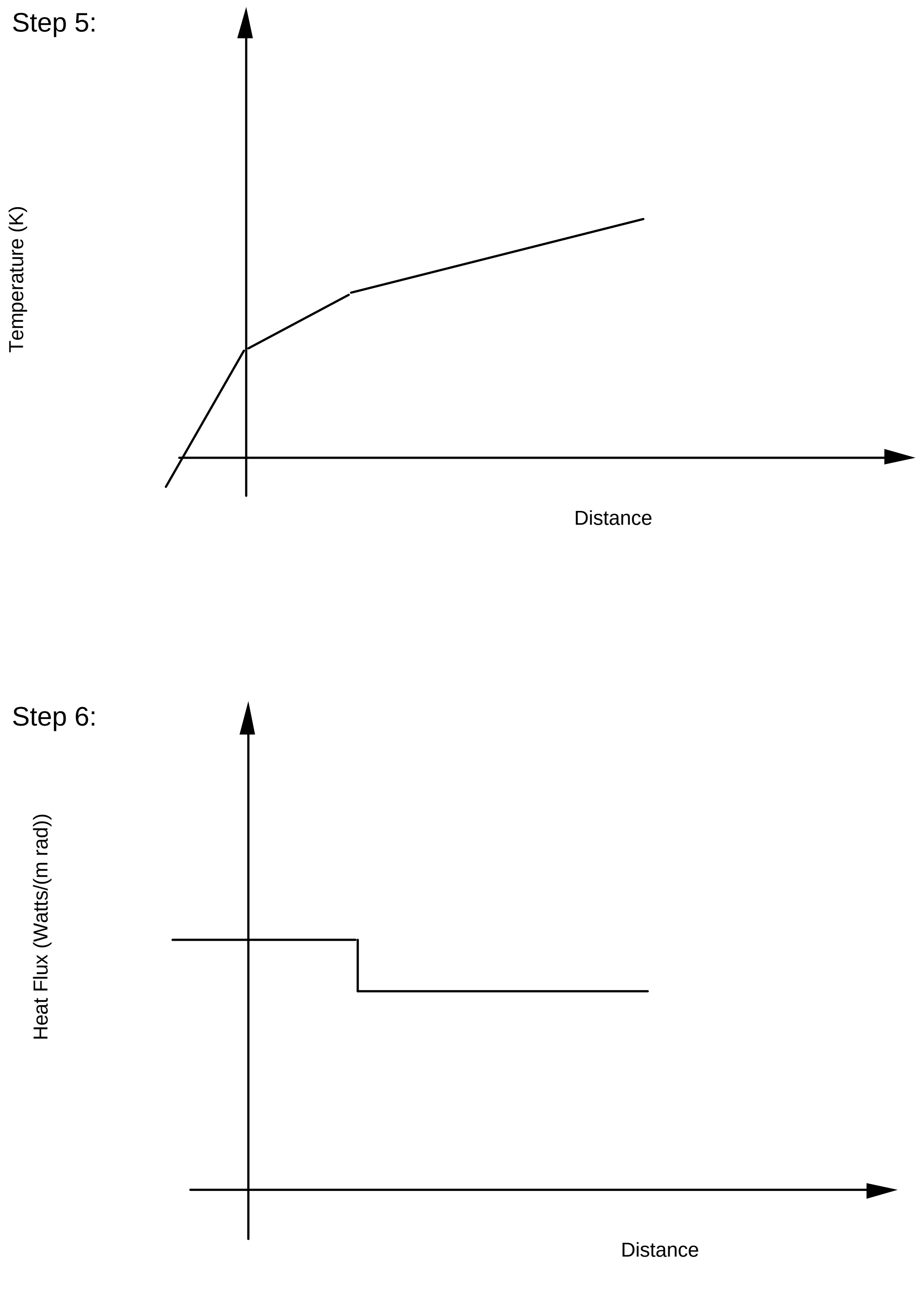

FIGURE 4.13 - Solidification Analysis Algorithm, Part 3

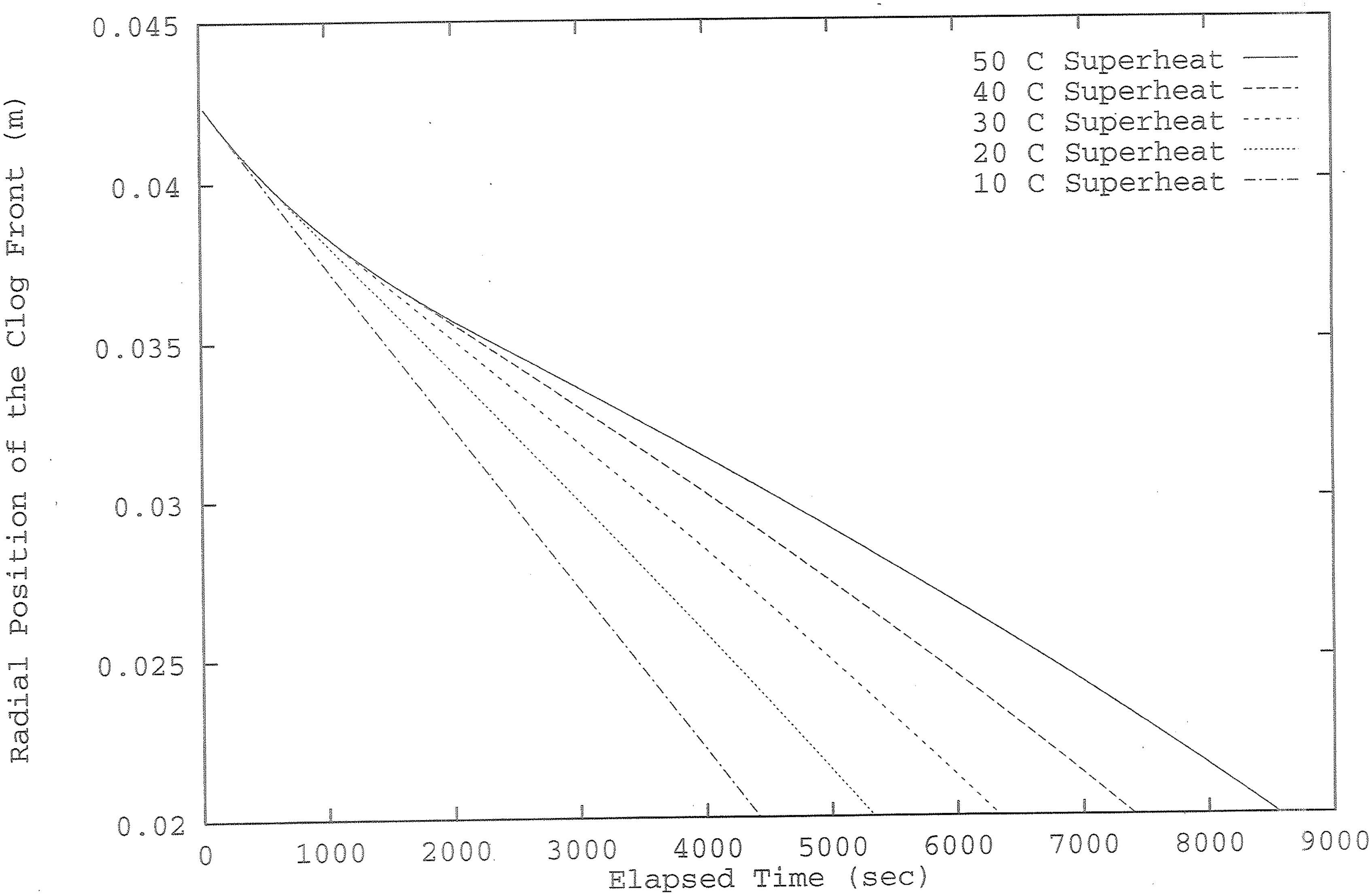

FIGURE 4.14 - Effect of Superheat on Clogging

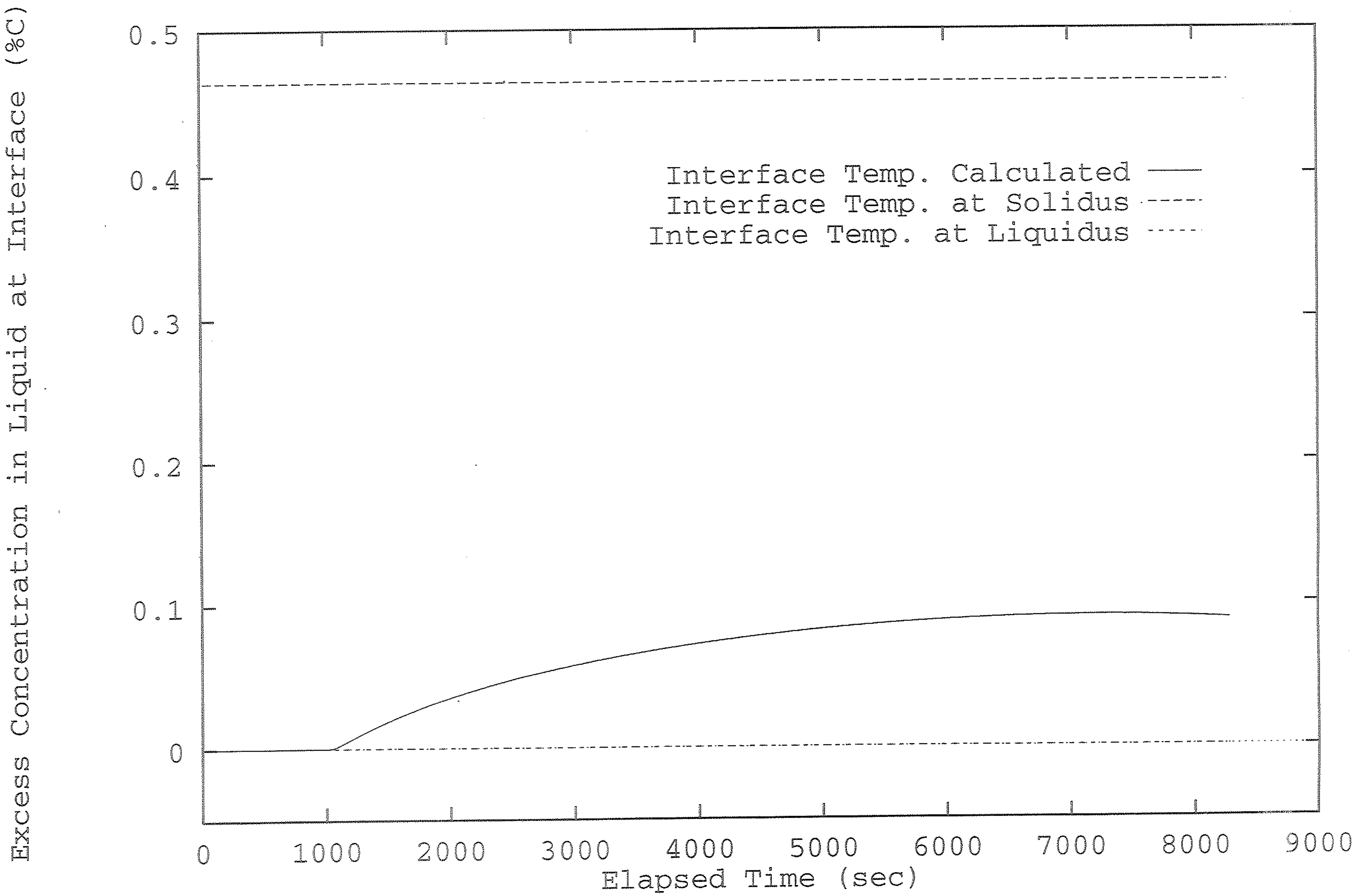

FIGURE 4.15 - Evolution of Excess Solute Concentration

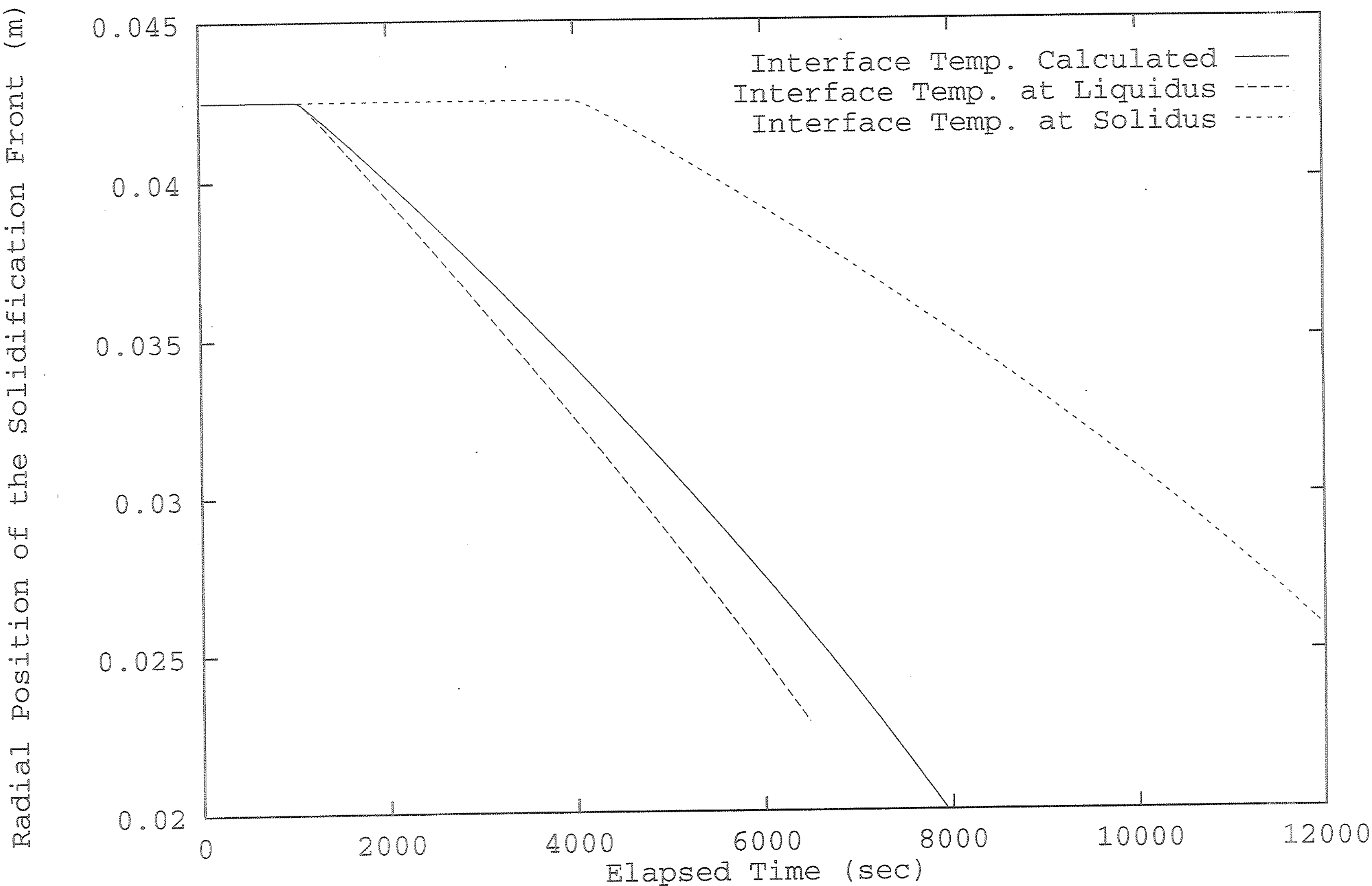

FIGURE 4.16 - Effect of Interface Temperature on Skull Evolution

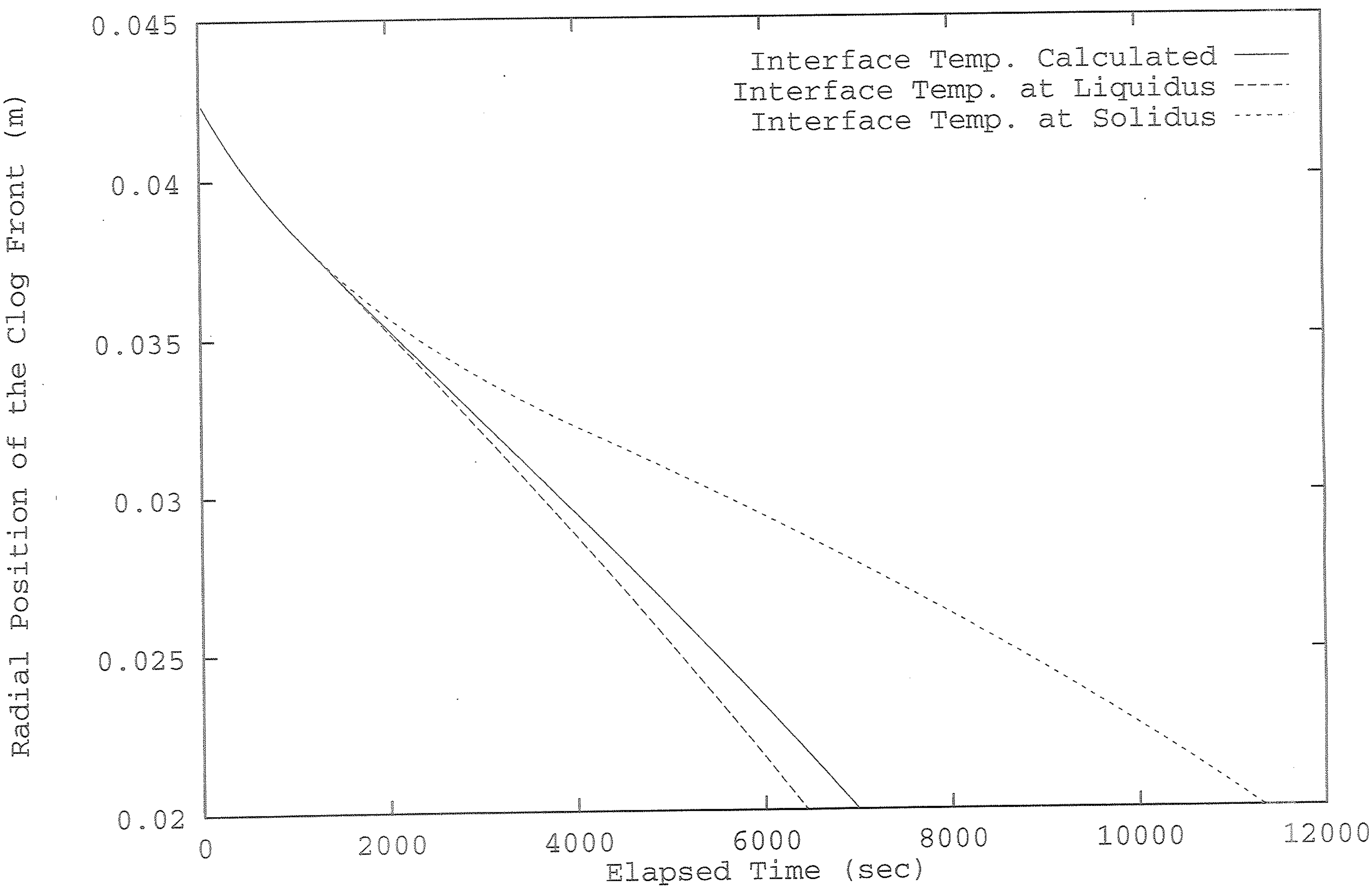

FIGURE 4.17 - Effect of Interface Temperature on Clogging

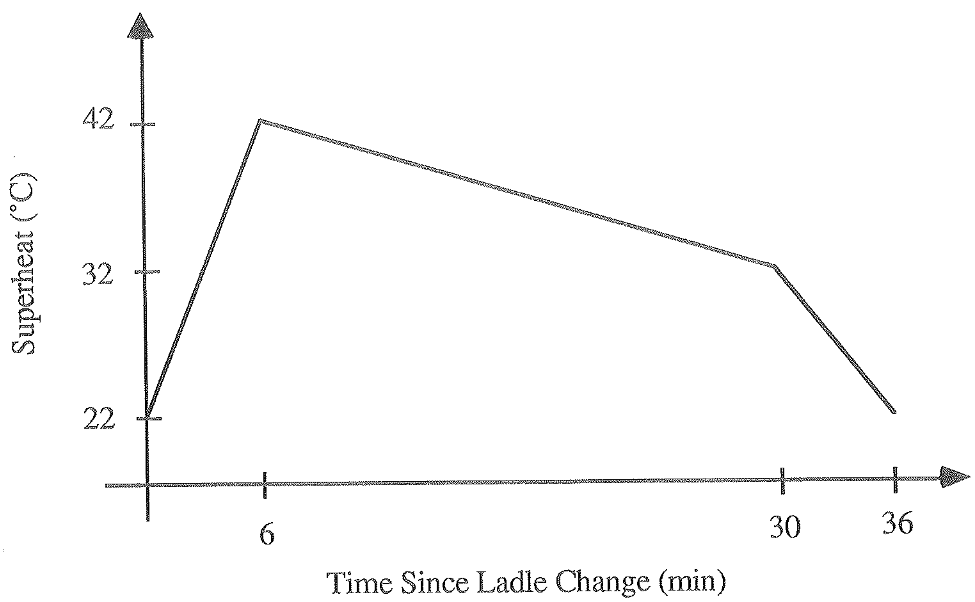

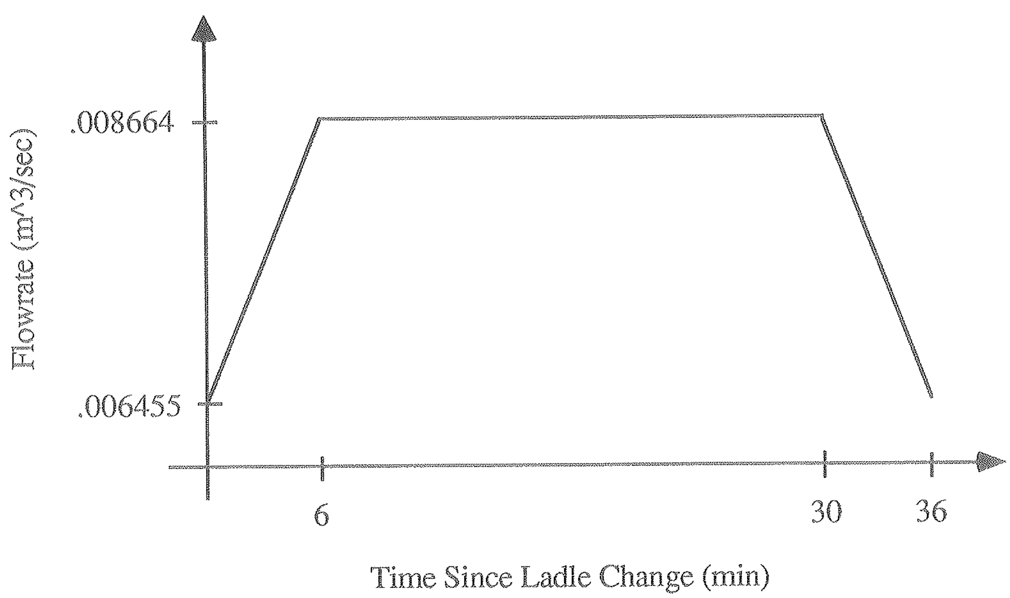

FIGURE 4.18 - Temperature and Flowrate Histories Utilized in Model

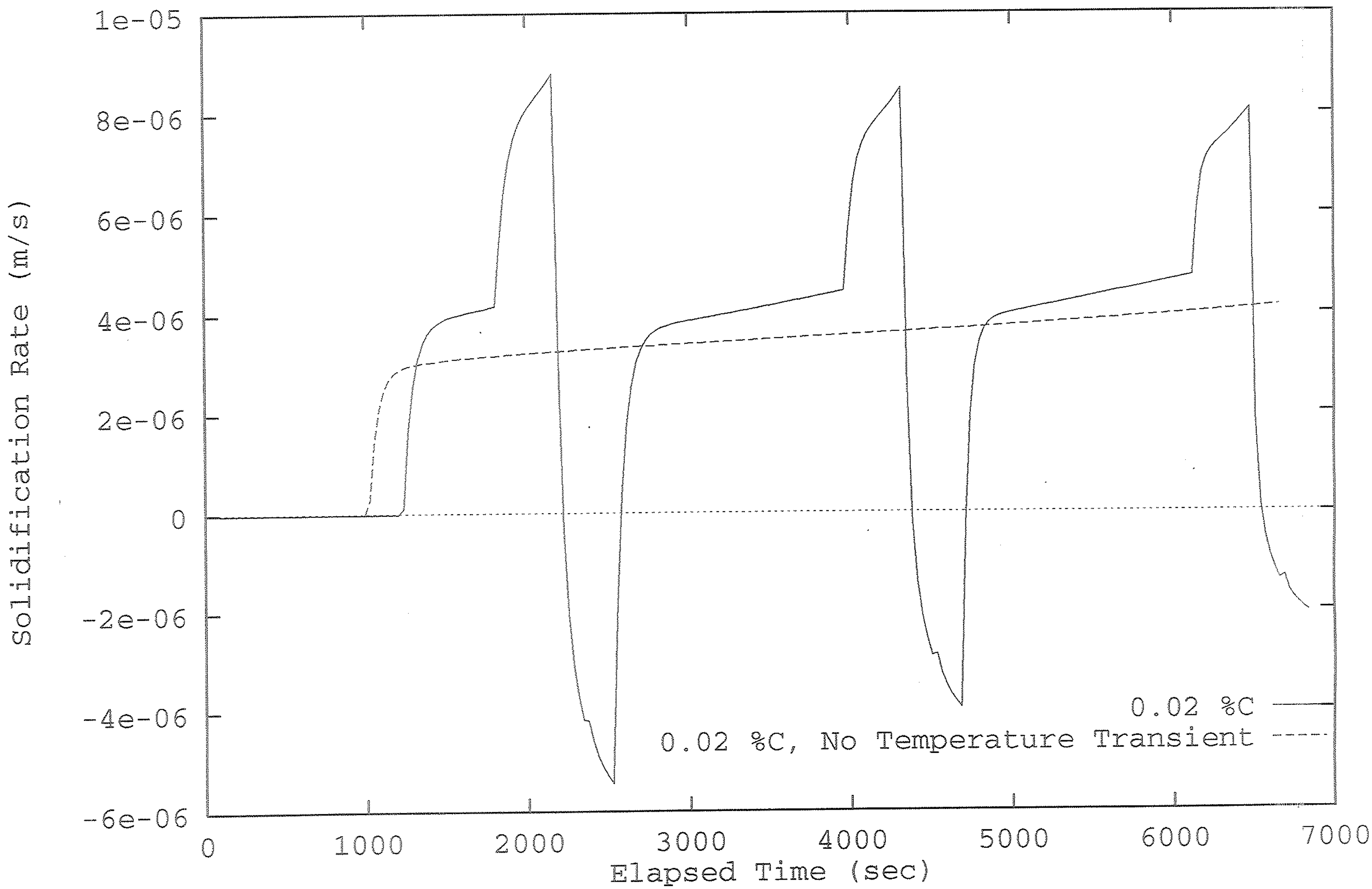

FIGURE 4.19 - Evolution of Solidification Rate

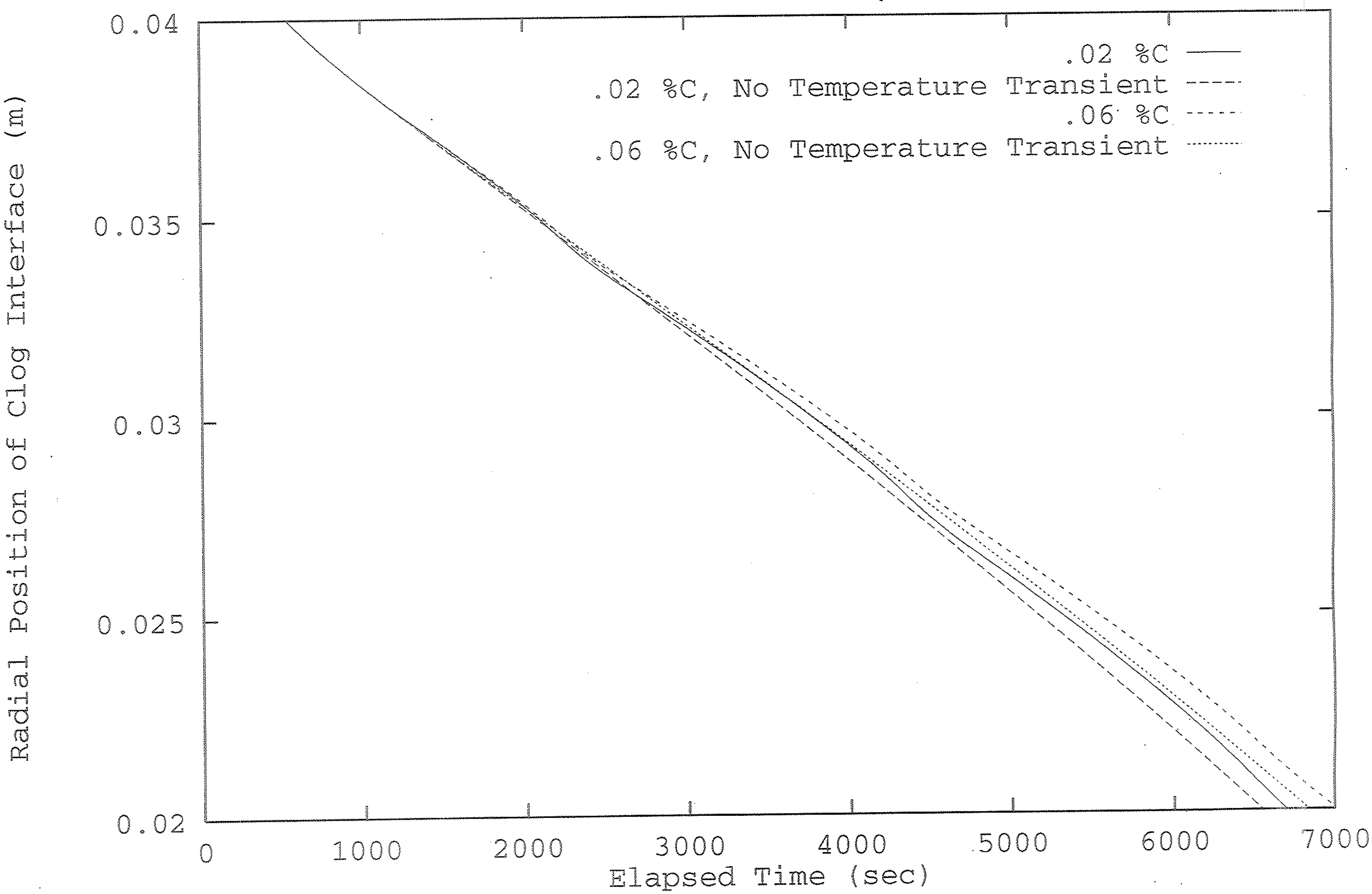

FIGURE 4.20 - Effect of Temperature Transients and Concentration on Clogging

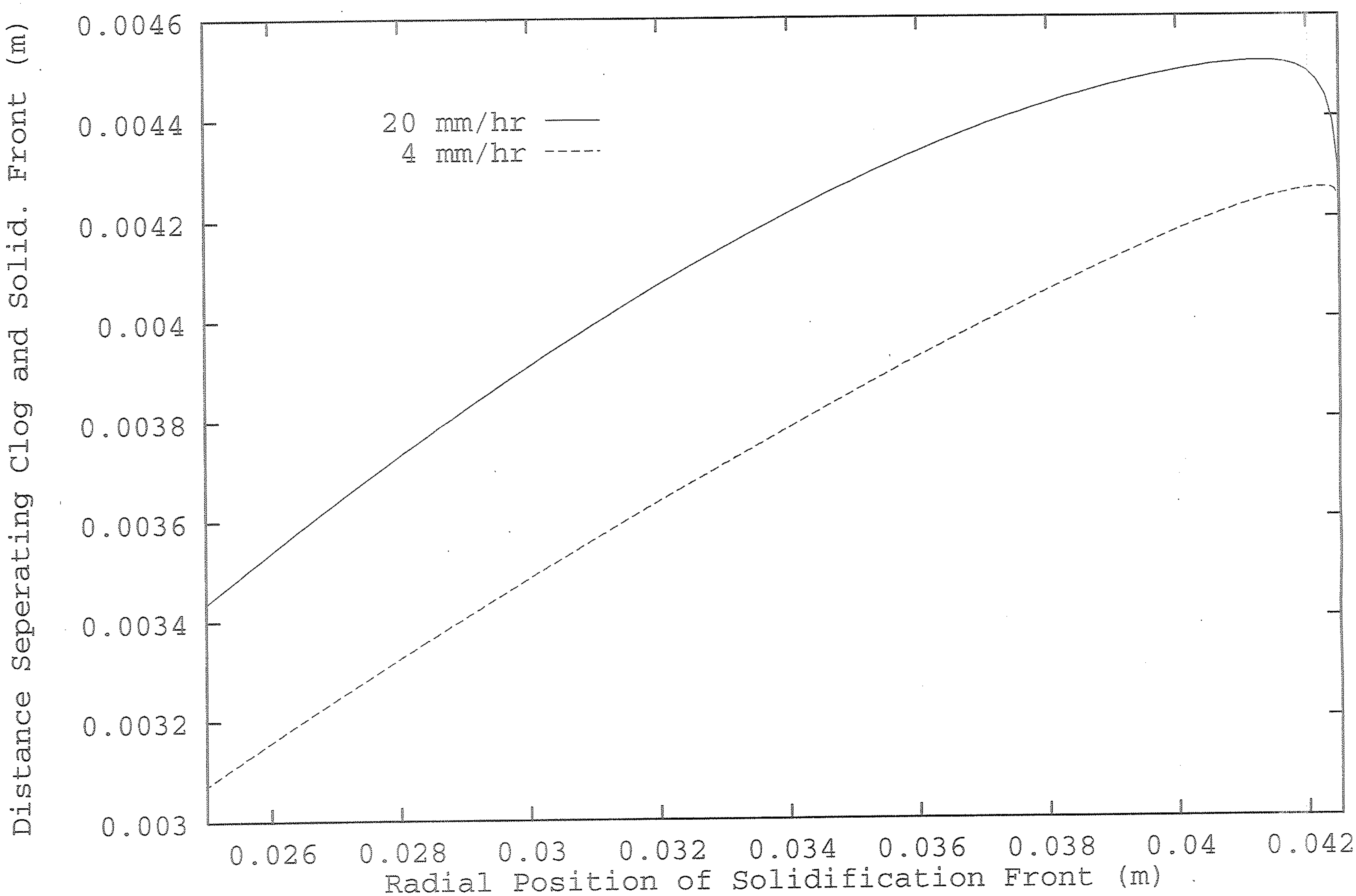

FIGURE 4.21 - Effect of Clogging Rate on Stagnant Layer Thickness

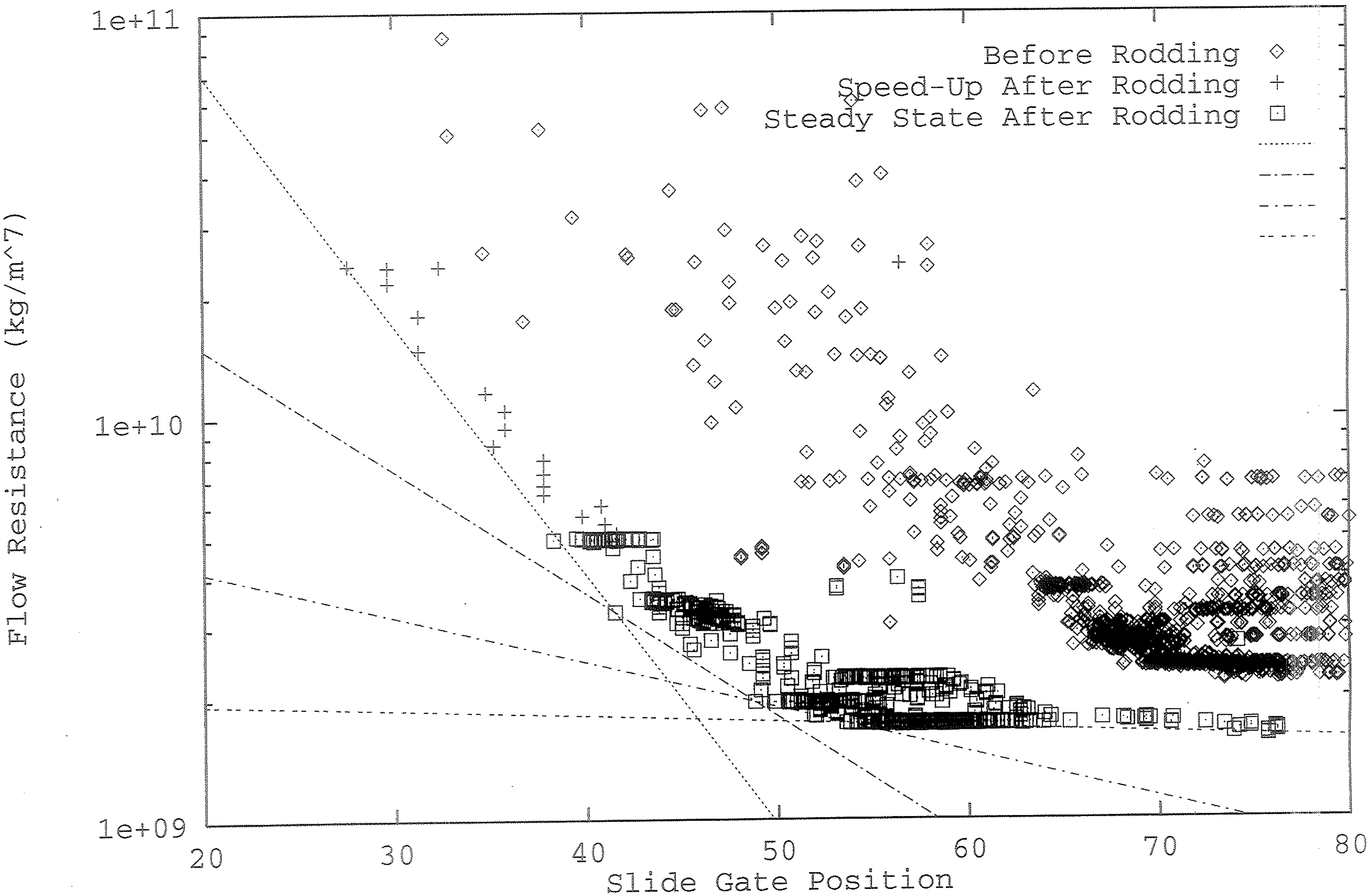

FIGURE 4.22 - Empirical Flow Resistance (Cast 9361, Strand 2)

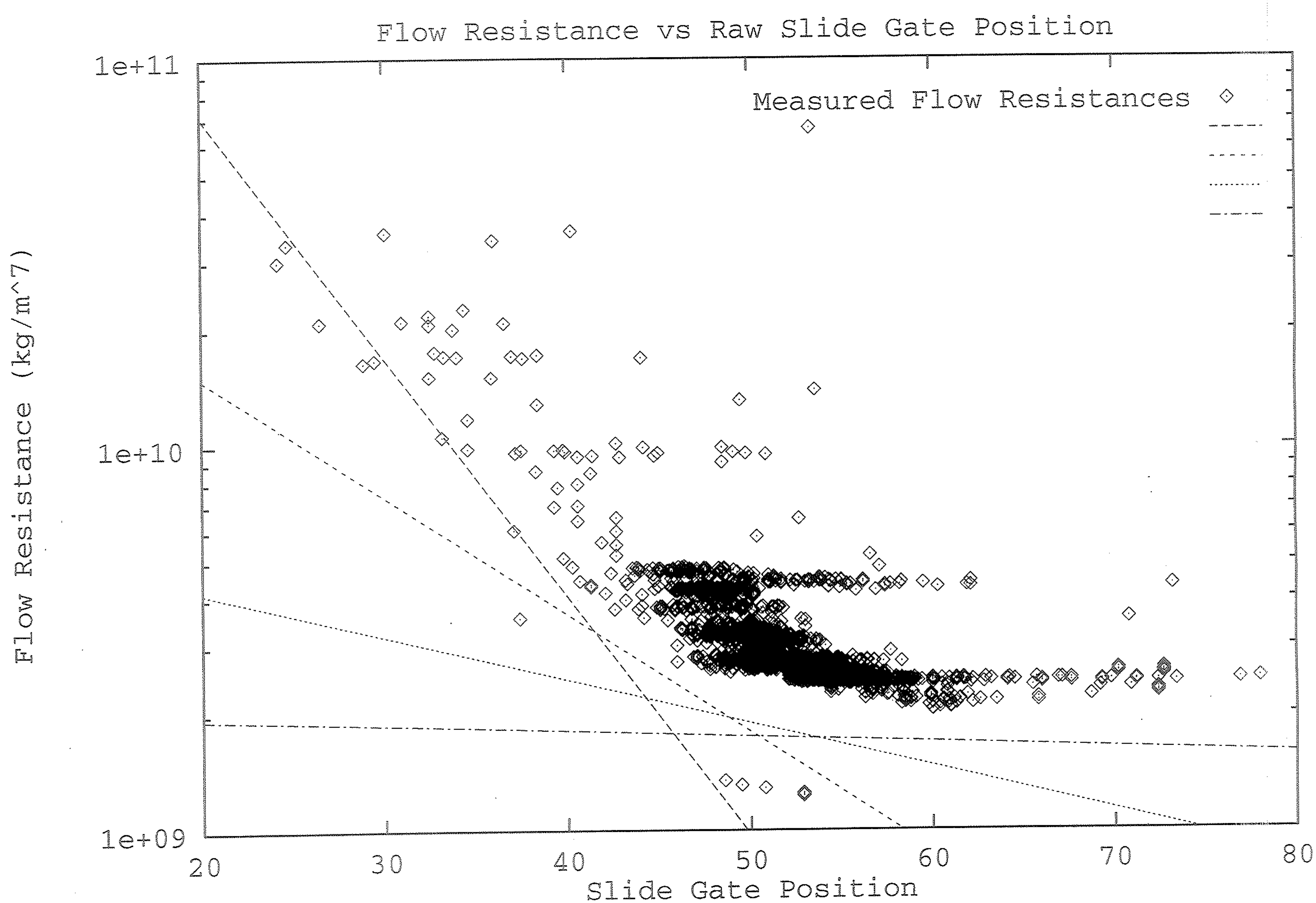

FIGURE 4.23 - Empirical Flow Resistance (Cast 9374, Strand 1)

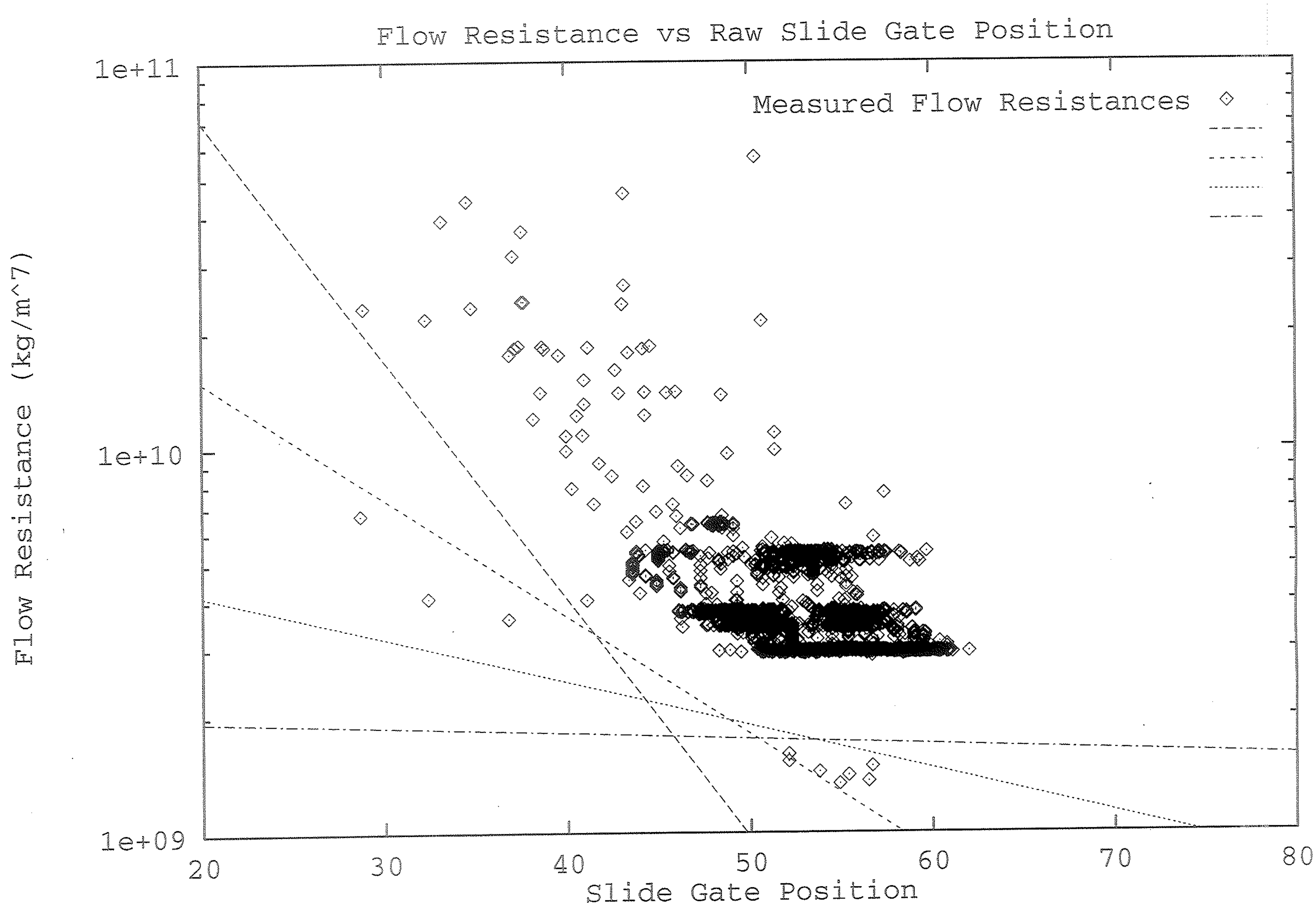

FIGURE 4.24 - Empirical Flow Resistance (Cast 9374, Strand 2)

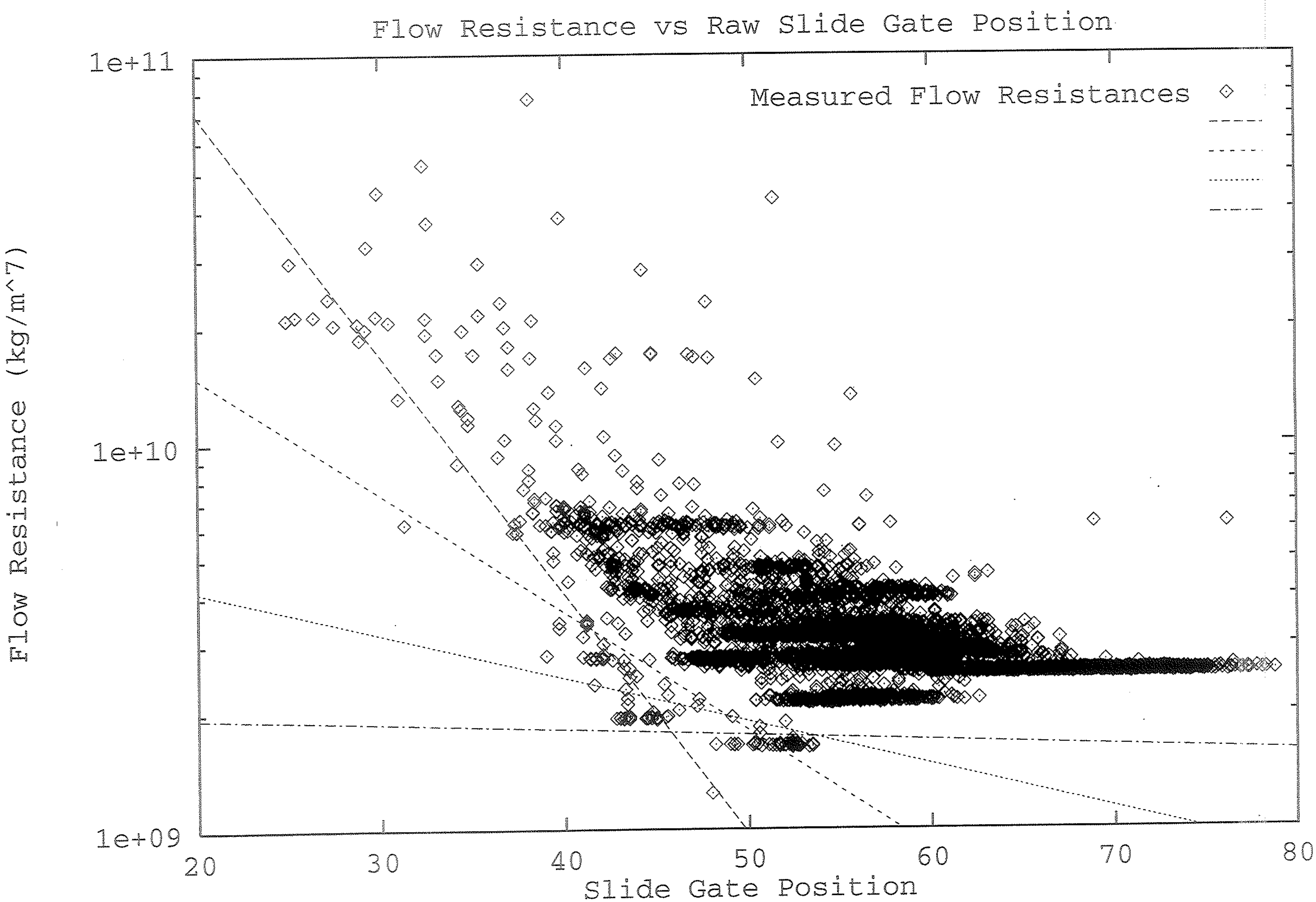

FIGURE 4.25 - Empirical Flow Resistance (Cast 9388, Strand 1)

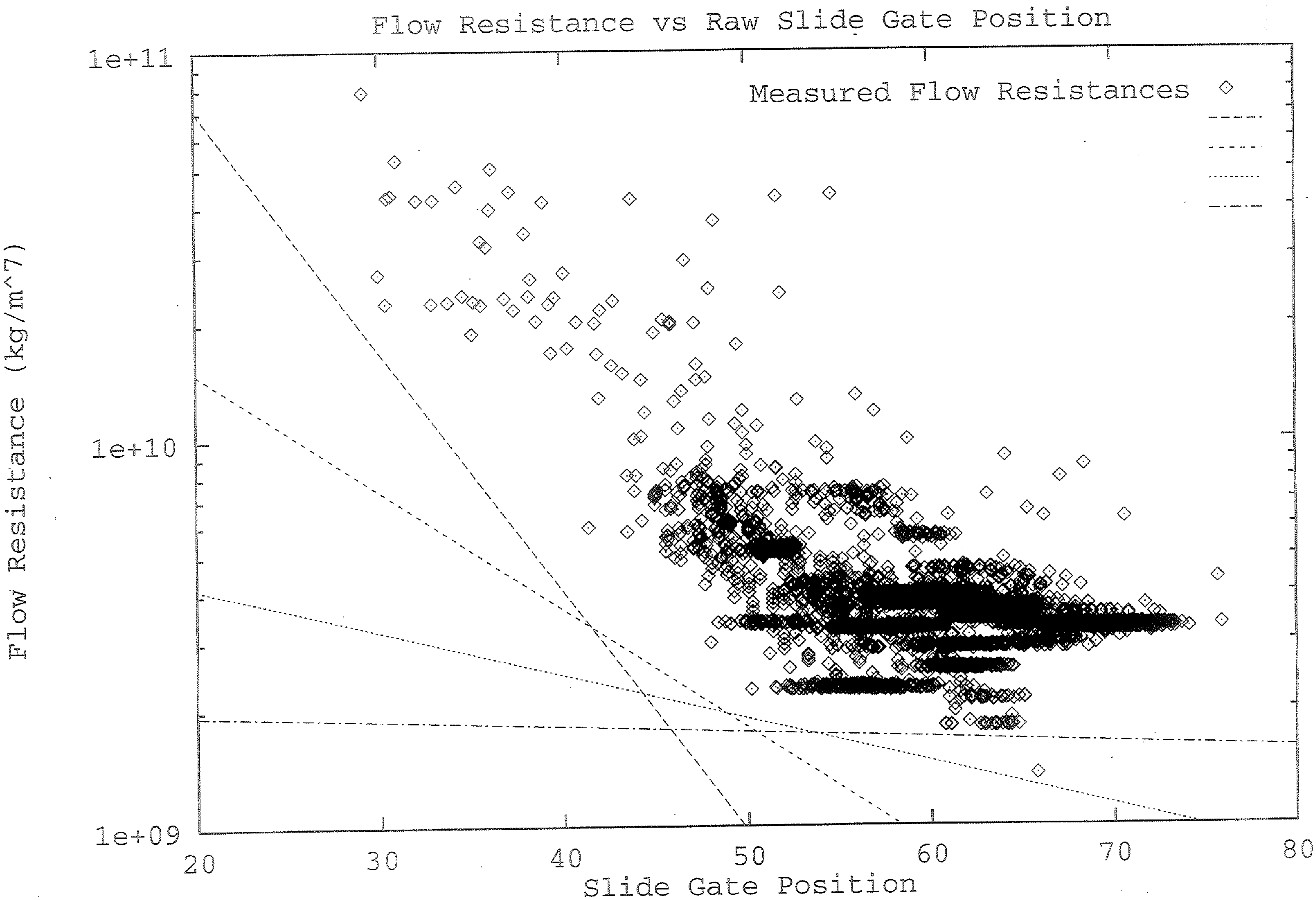

FIGURE 4.26 - Empirical Flow Resistance (Cast 9388, Strand 2)

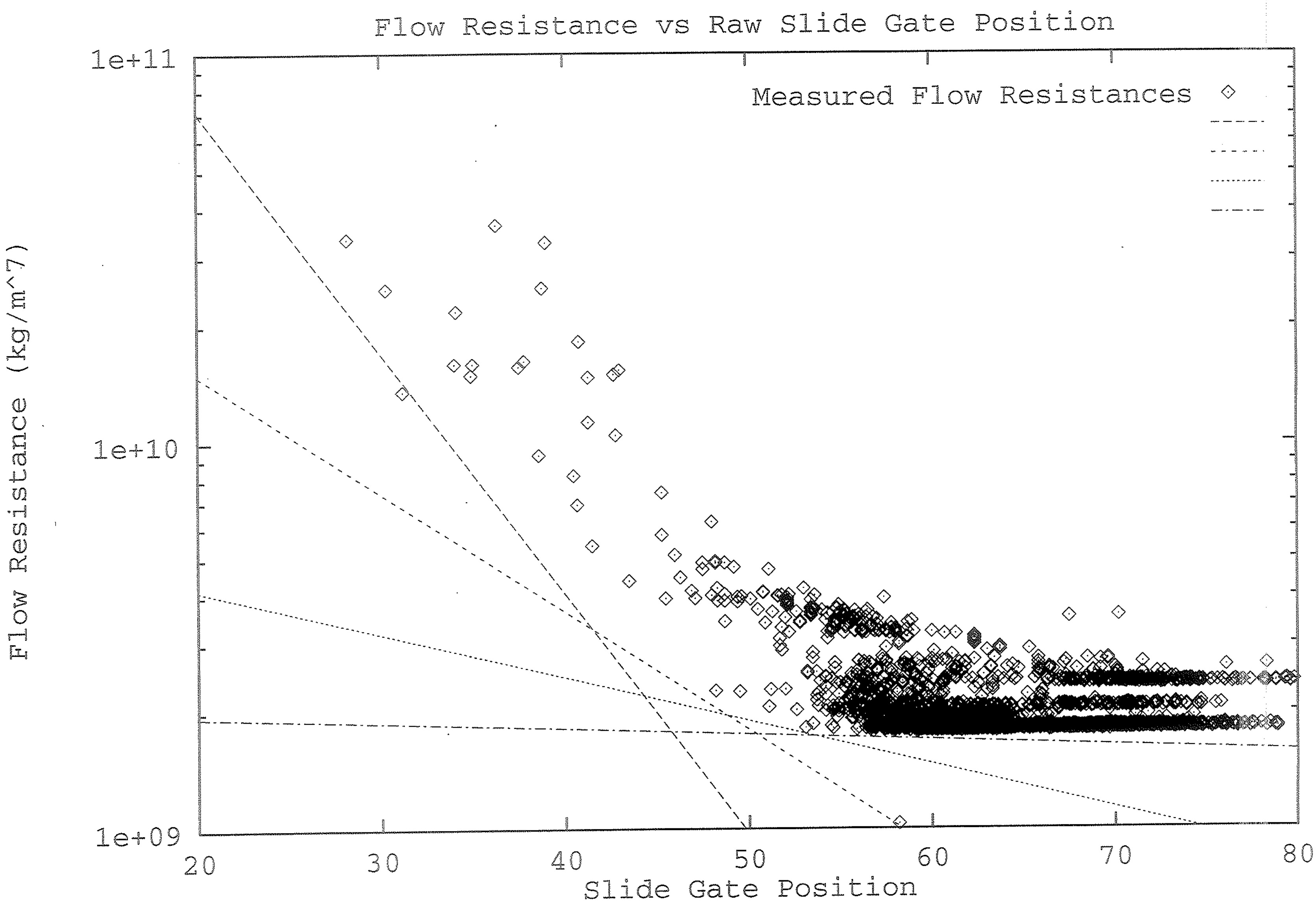

FIGURE 4.27 - Empirical Flow Resistance (Cast 9030, Strand 1)

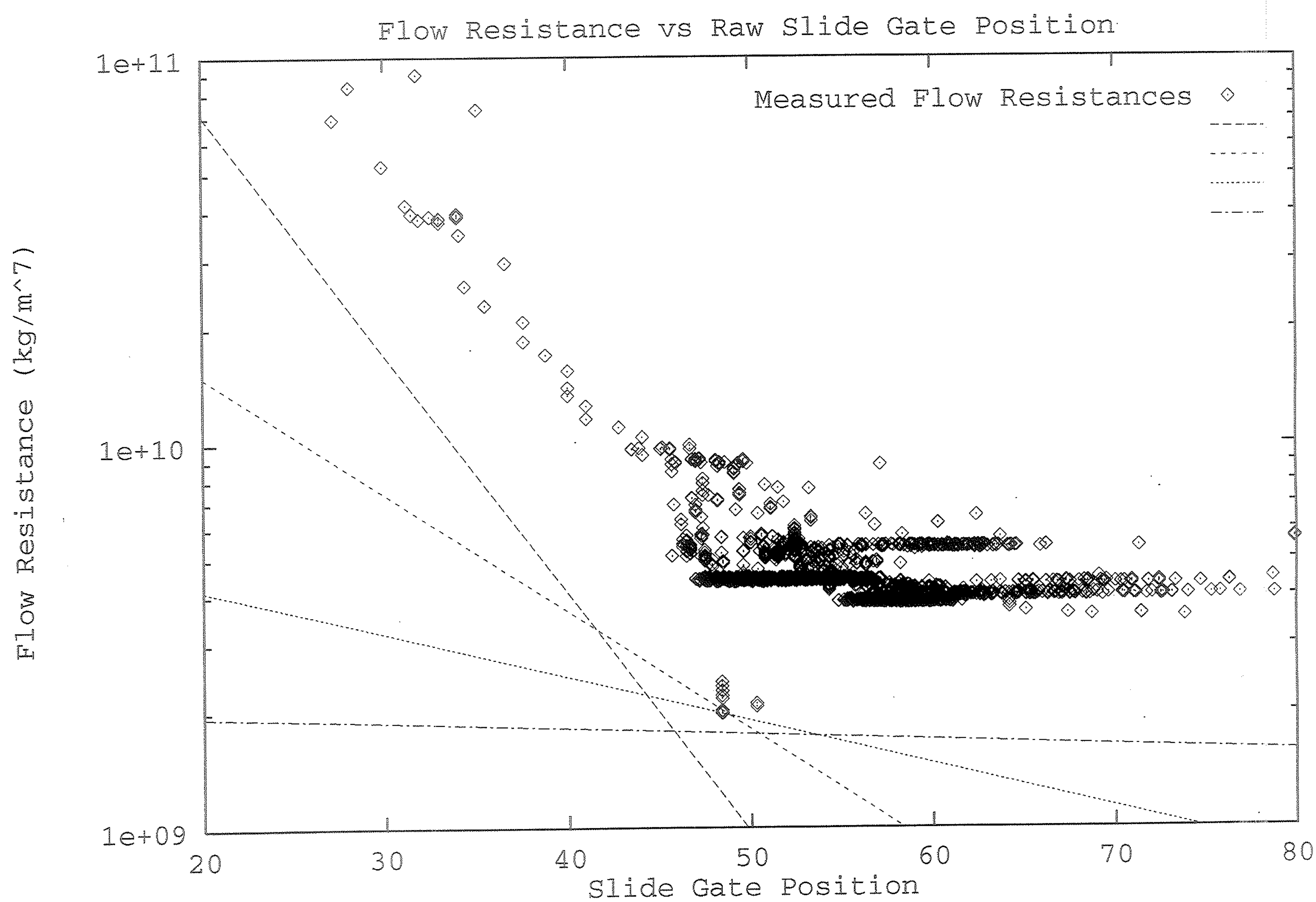

FIGURE 4.28 - Empirical Flow Resistance (Cast 9030, Strand 2)

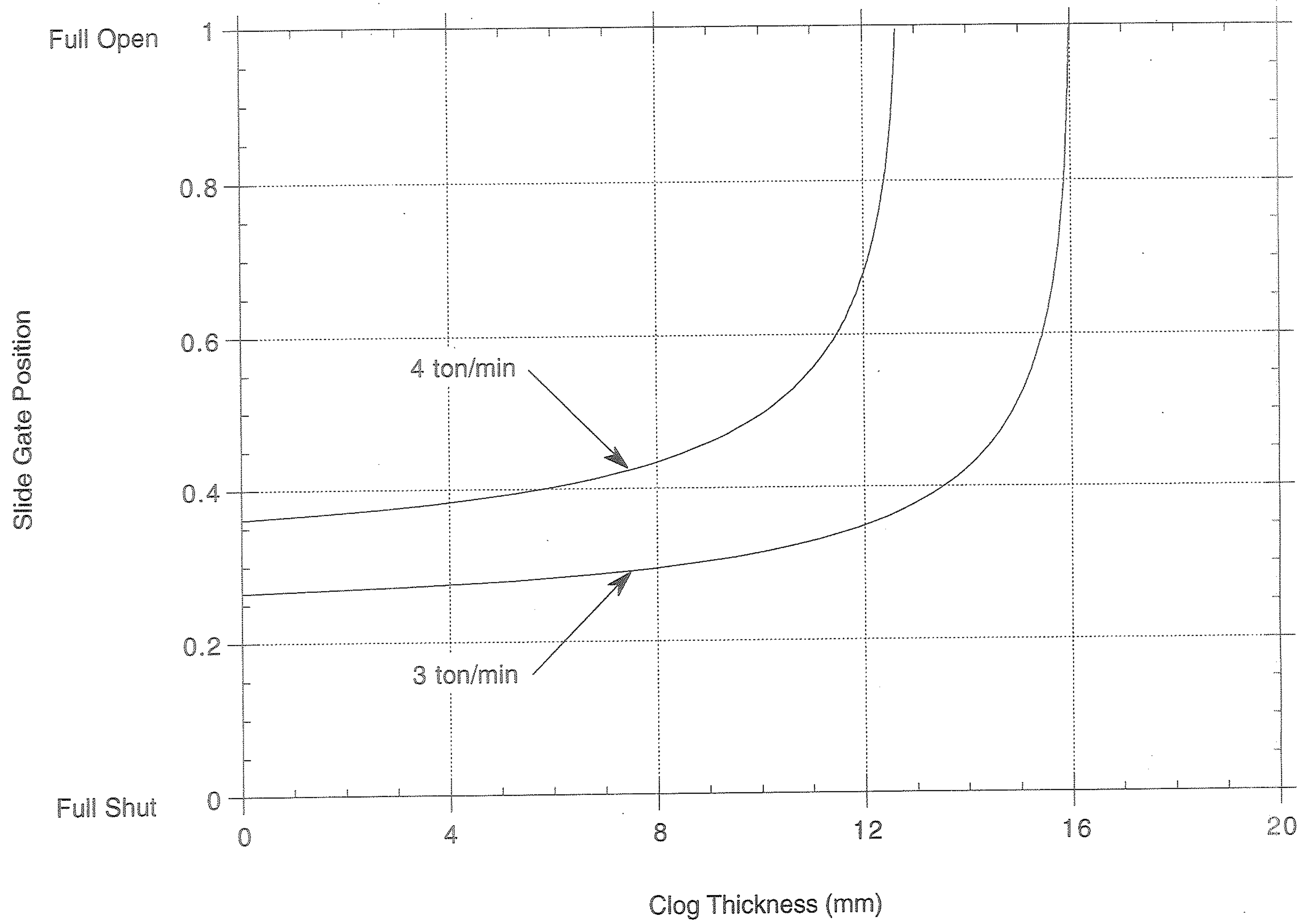

FIGURE 4.29 - Effect of Clog Thickness on Slide Gate Position

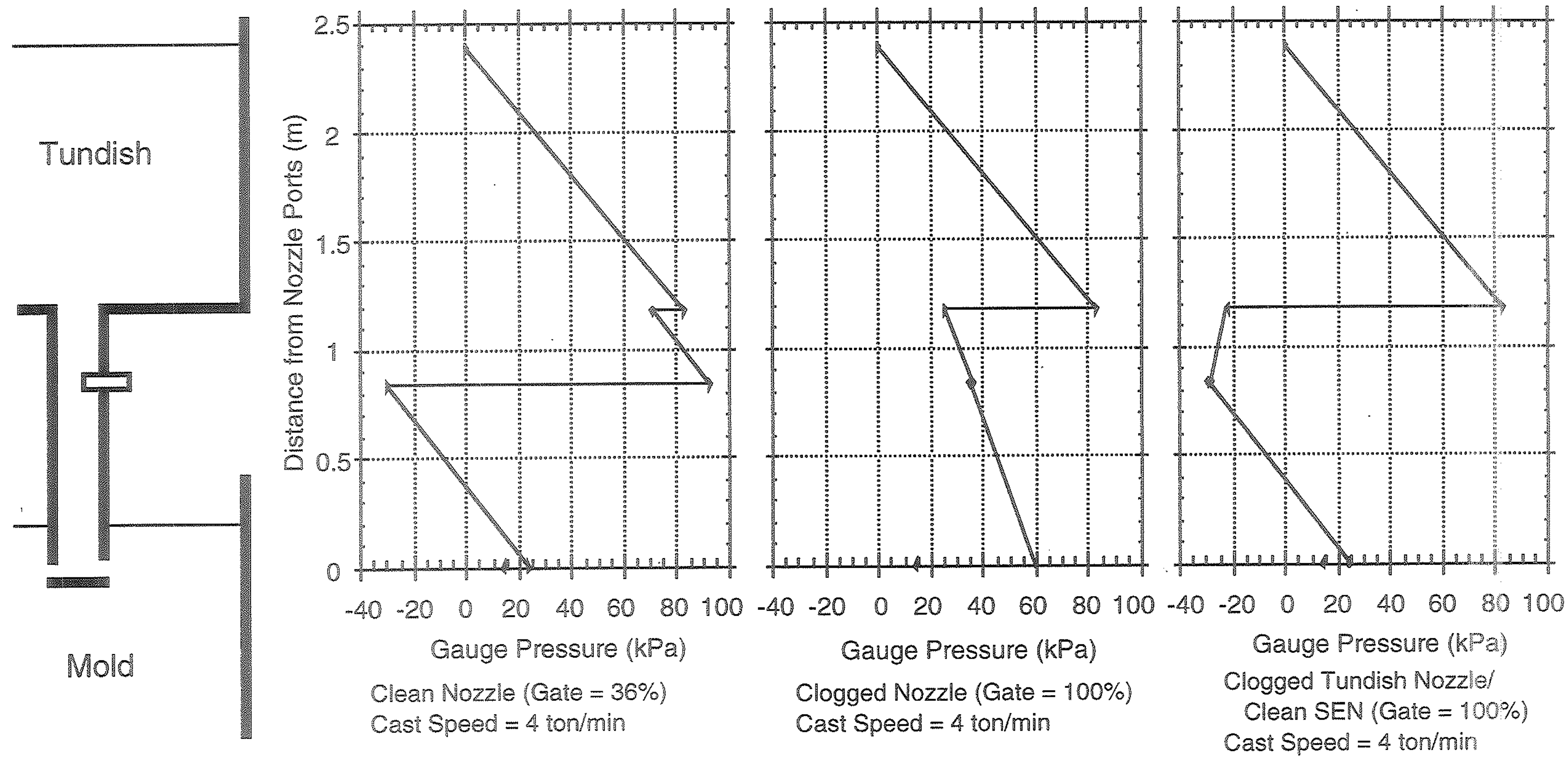

FIGURE 4.30 - Variation of Pressure Within the Nozzles

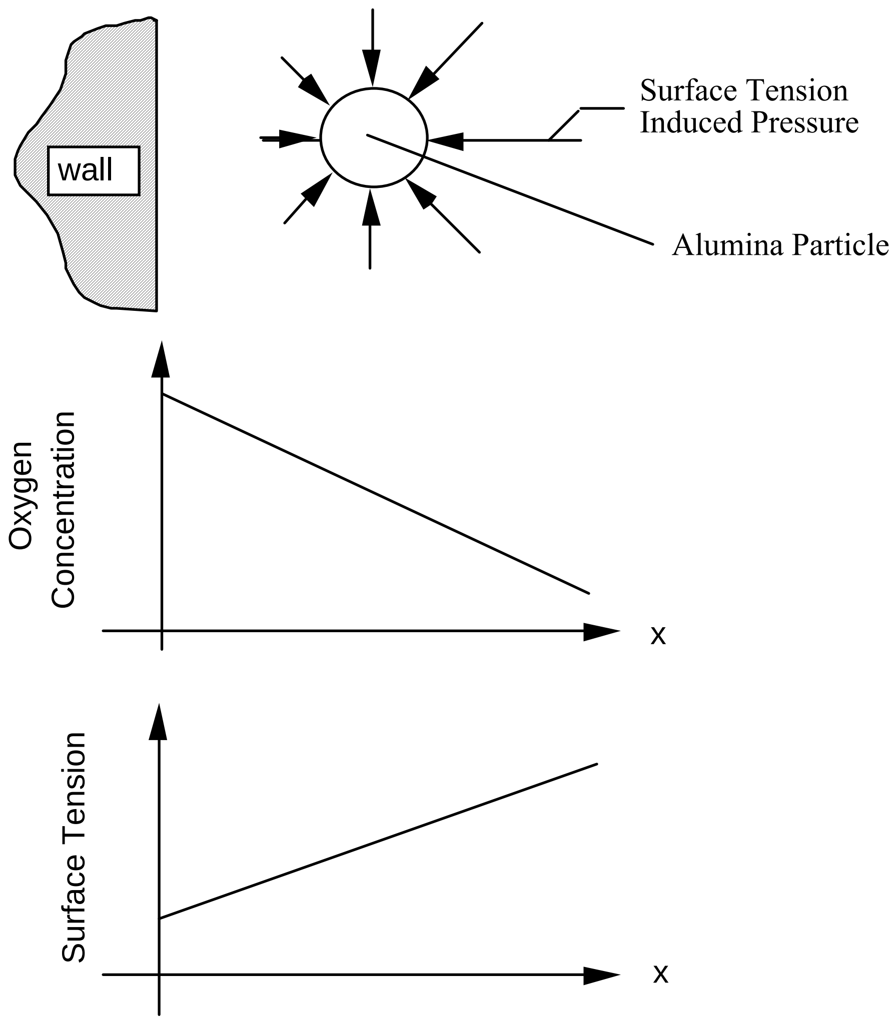

FIGURE 4.31 - Mechanism for Surface Tension Gradient Induced Transport

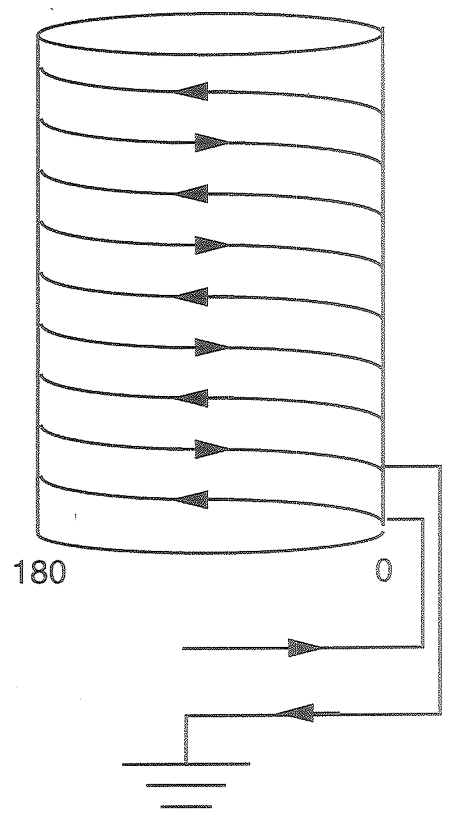

Isometric View of Element
Winding on the Inner Cylinder

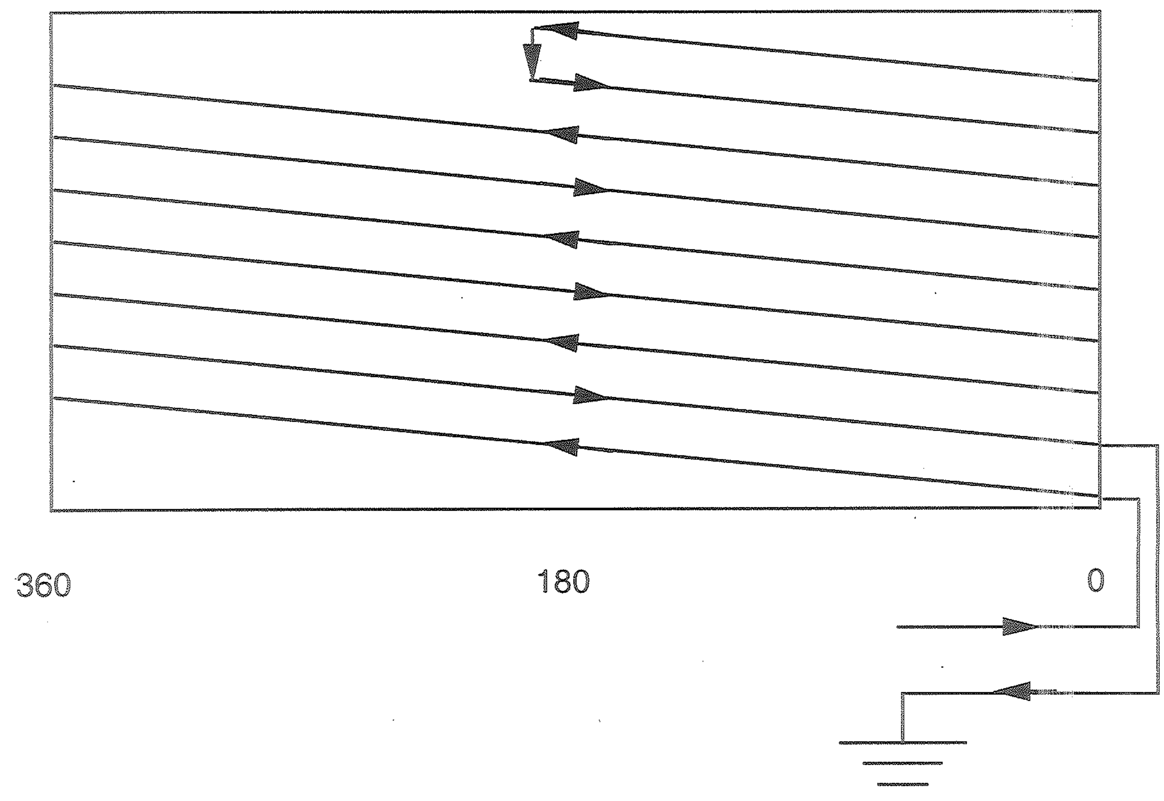

Plan View of Element
Winding on the Inner Cylinder

FIGURE 4.32 - Schematic of Element Winding Concept for Proposed Nozzle

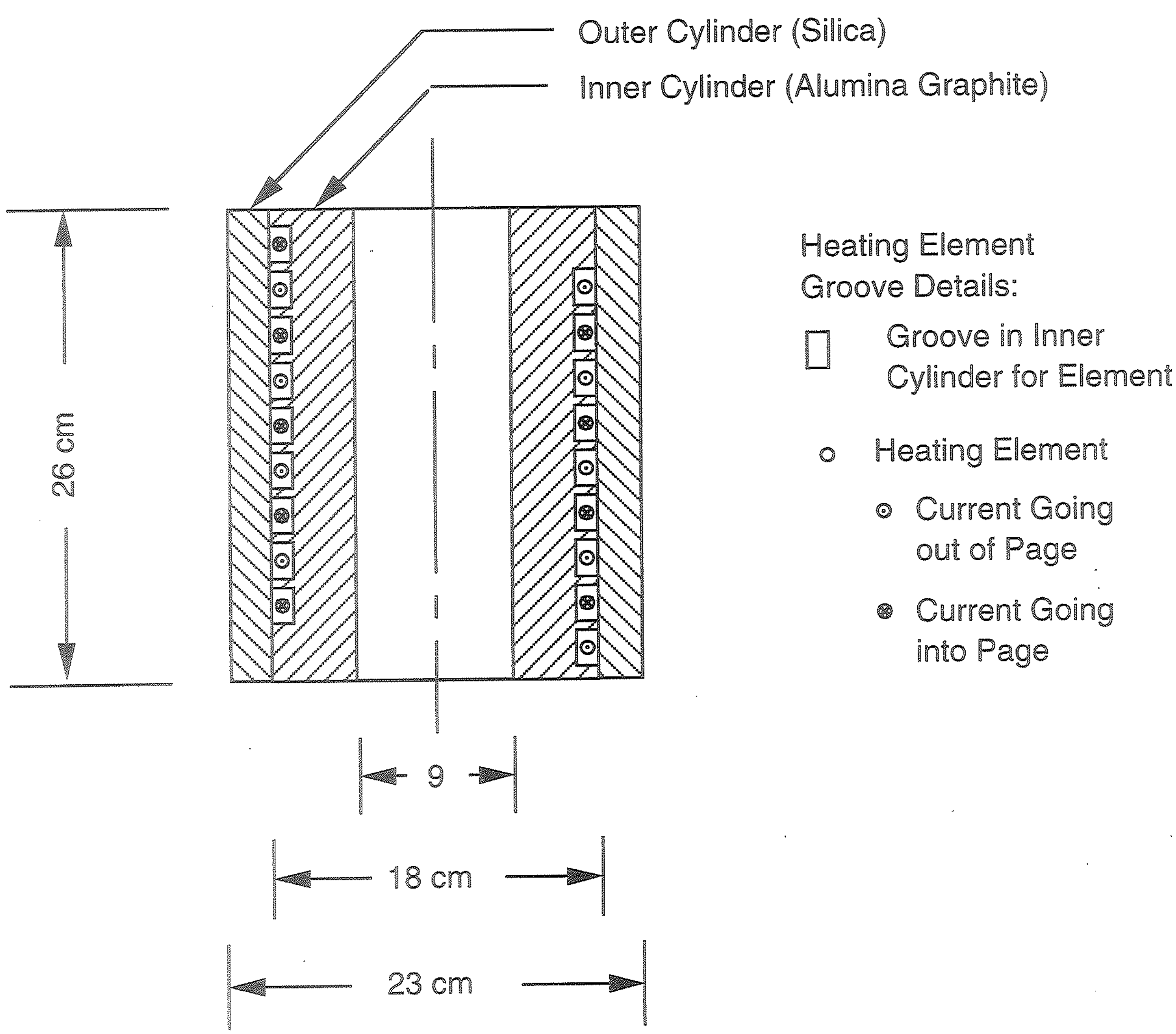

FIGURE 4.33 - Cross-Sectional View of Proposed Nozzle with Element Installed

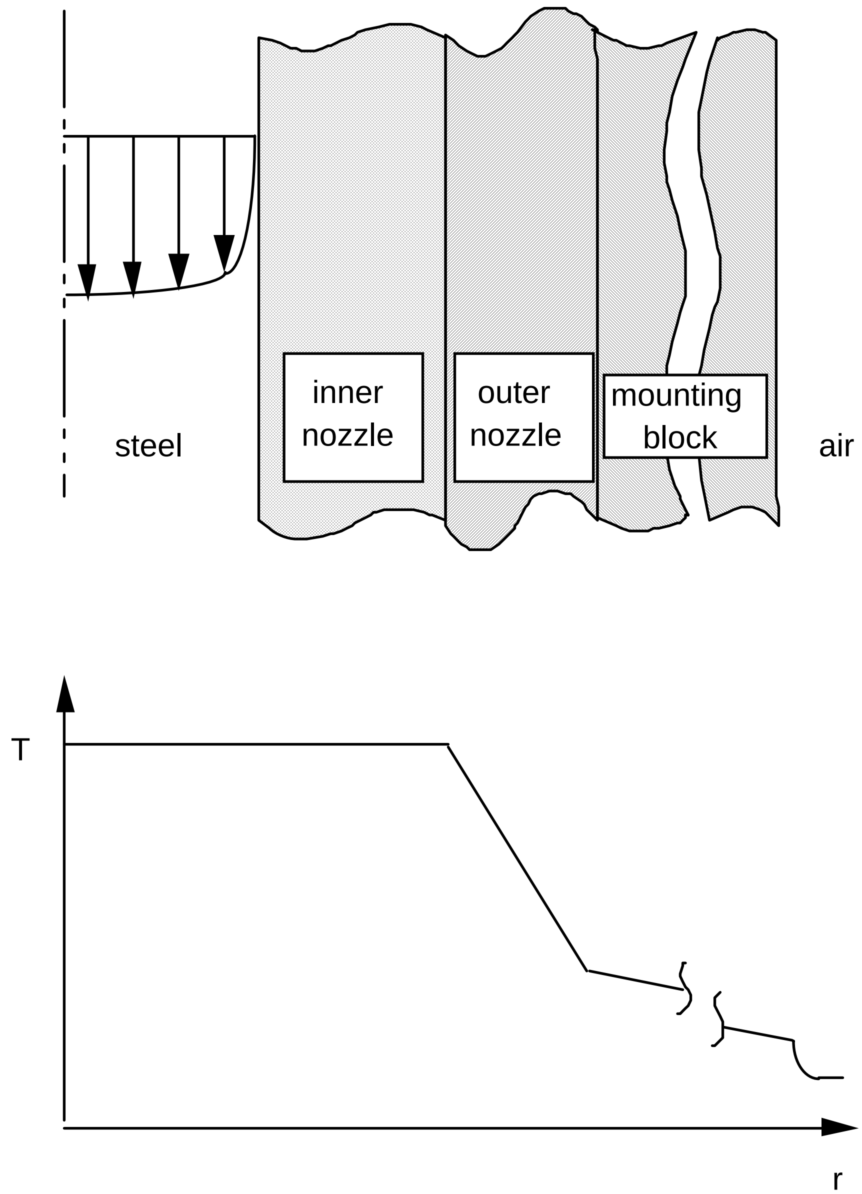

FIGURE 4.34 - Desired Temperature Distribution in the Proposed Nozzle

CHAPTER 5 - CONCLUSIONS

Based on the results of the experimental and mathematical modeling work done to investigate the mechanisms involved in clogging, the following conclusions can be made:

- Steel frozen on the inner diameter of the tundish or submerged entry nozzles will generally melt away if exposed directly to the molten steel stream for most casting conditions.

- Steel will freeze and remain frozen on the nozzle wall if it is located within an inclusion network which extends sufficiently beyond the solid interface.

- The clog buildup contains a significant fraction of steel. The concentration of steel within the clog varied significantly in the samples examined.

- Alumina inclusions must form a network in order reach the extent observed in practice. Since the deposition of deoxidation particles is a random process, a fraction of the buildups will not have a configuration sufficient to withstand the flow forces. The fraction that will continue to grow will increase as the skull more nearly approaches the extent of the buildup.

- Skulling will interfere with the distribution of argon and will thereby hasten clogging of the nozzle.

- The temperature transient in the nozzle wall occurring at the start of cast will cause a small amount of skulling and also may crack the nozzle. Nozzle cracking may cause argon to escape to the ambient instead of flowing into the nozzle.

- An industrial experiment should be performed to clarify the importance of heat transfer in the nozzle clogging process. This may be accomplished by installing a heating element within the nozzle. Ideally, the temperature at the internal diameter of the nozzle should be heated to casting temperature to completely isolate the effect of heat transfer.

- Clogs occurring in practice result from a complex interaction between deoxidation product deposition, skulling, complex oxide formation, and chemical reactions at the nozzle wall. The importance of each of these mechanisms vary between particular casting operations.

- Improved steel cleanliness, argon injection, calcium treatment, and nozzle geometry and material modifications can all be effective means to reduce clogging.

- The size and thermal properties of the mounting block hardware surrounding the tundish nozzle has no significant effect on the initial skulling behavior.

- Clogging behavior of low carbon steel is not significantly affected by short term temperature transients (i.e., corresponding to 20° C temperature drop during ladle changes). For a given nozzle material and design, the skulling, and its consequent effect on clogging, is primarily determined by the average superheat of the steel.

- The temperature of the solidification front is approximately at the liquidus temperature during casting unless superheat variations are present.

- Slide gate position measurements are not sufficiently sensitive to reliably indicate the degree of initial clogging (e.g. clogs $<$ 8 mm thick when casting at 4 ton/min.).

- Air aspiration is not a likely cause of clogging in the regions of the tundish nozzle far from the slide gate because of the high ferrostatic pressure in those regions.

- Air aspiration is possible in the submerged entry nozzle, especially near the slide gate, due to the significant vacuum created. The propensity for aspiration increases as the slide gate is closed. Similarly, the area most prone to aspiration in a stopper rod flow control system is the area just below the stopper rod seating surface.

- The back-pressure in the argon line feeding the tundish nozzle must be greater than the pressure within the nozzle for argon to flow into the nozzle. Rapid clogging was clearly observed for one cast having insufficient back-pressure.

- Improved argon flow uniformity on the nozzle inner surface can be obtained by tailoring the nozzle wall argon flow resistance to account for the ferrostatic pressure variation and/or by simultaneously increasing the overall magnitude of the flow resistance and back pressure.

- A significant fraction of the alumina in the steel is deposited on the nozzle wall when clogging countermeasures are not employed.

- Air aspiration into the nozzle and consequent reoxidation product formation can cause significant clogging.

- Air aspiration can promote deposition of deoxidation products by causing a variation in steel surface tension within the nozzle.

APPENDIX A - MATHEMATICAL FORMULATION OF MODELS

This appendix presents the formulation of mathematical models pertaining to nozzle clogging. These models are written in MATHEMATICA format. The bold text represents the input. The text following the input is the output. Comments will appear in the type being used now. The MATHEMATICA programming environment is documented in the book: "Mathematica: A System for Doing Mathematics by Computer". by Stephen Wolfram, Addison-Wesley Publishing Company, Copyright 1988.

The model formulations are presented as follows. The governing equations are first stated and manipulated. Then numerical data is entered. Finally, the equations are solved and plots are generated.

A.1 STRUCTURAL ANALYSIS OF A CLOG BUILDUP

In this appendix, the strength of the clog buildup is estimated. The buildup is modelled as a rod extending out into a constant mean flow.

Table of variables:

- F - total drag on the rod (N)
- Cd - drag coefficient
- ReD - the Reynolds number based on rod diameter
- stress - outer fiber bending stress (Pa)
- Inertia - moment of inertia of a rod (m^4)
- M - moment on rod at fixed end (N m)
- r - radius of the rod (m)
- L - length of rod (m)
- V - bulk fluid velocity (m/s)
- rho - fluid density (kg/m^3)
- mu - fluid viscosity (kg/(m s))
- m,kg,s,N - SI units

The drag on the rod is:

`F = Cd rho (V^2)/2 (2 r) L`

$$Cd\ L\ r\ rho\ V^2$$

`Cd = (1+10/ReD^(2/3))` (*White pg 183, good to ReD=250,000*)

$$1 + \frac{10}{ReD^{2/3}}$$

```
ReD = rho V (2 r) / mu
```

$$\frac{2\ r\ rho\ V}{mu}$$

```
stress = M r / Inertia
```

$$\frac{M\ r}{Inertia}$$

```
Inertia = 1/4 Pi r^4
```

$$\frac{Pi\ r^4}{4}$$

```
M = F L/2
```

$$\frac{L^2\ r\ rho\ V^2\ (1 + \frac{5\ 2^{1/3}}{(\frac{r\ rho\ V}{mu})^{2/3}})}{2}$$

Data:

```
V=1.6;
rho=7021;
mu=.0056;
```

Find the maximum length for a 10 micron dia. rod:

```
FindRoot[3 10^8 == (stress /. r->5 10^-6) , {L,.02}]

{L -> 0.00052762}
```

Develop a function that will caculate the radius at which failure would occur given the porosity and the length of the rod:

```
fr[x_,y_] := (eqn1 = x 3 10^8 == (stress /. L->y);
                   FindRoot[eqn1,{r,.0001}] [[1]])
```

Consider a 20 mm long rod. Calculate the req'd radius, the number of 10 micron inclusions req'd in a cross section, and the Reynolds number

```
ep=1.;L=.02;
{r 10^3 mm, ep r^2/(5 10^-6)^2, ReD} /. fr[ep,L]
ep=.;L=.

{0.132591 mm, 703.218, 531.956}
```

Consider a 20 mm long rod with 17% volume fraction alumina:

```
ep=.17;L=.02;
{r 10^3 mm, ep r^2/(5 10^-6)^2, ReD} /. fr[ep,L]
ep=.;L=.

{0.312199 mm, 662.784, 1252.54}
```

A.2 EFFECTIVE DENSITY OF A CLOG BUILDUP

In this appendix, the effective density of a clog with no entrapped steel (i.e." pure" alumina) is calculated. Consider the clog as a bunch of rods (radius = r) growing radially inward from the nozzle wall in a close packed configuration with a space of del between them.

Table of variables:

- ep = volume fraction of alumina in the clog
- a0 = cell width (m)
- ratio = r/del
- gamma = surface tension (N/m)
- theta = contact angle for steel on alumina (rad)
- P = ferrostatic pressure (Pa)

By the geometry of a closed packed configuration, we know:

```
a0 = Sqrt[1/2] (r + del + 2 r + del + r)
```

$$\frac{2\ \mathrm{del} + 4\ r}{\mathrm{Sqrt}[2]}$$

Taking the ratio of the cross-sectional area of the rods enclosed within that close packed cell to the cell area gives:

```
ep = Simplify[2 Pi r^2 / a0^2 /. r->del ratio]
```

$$\frac{\mathrm{Pi\ ratio}^2}{(1 + 2\ \mathrm{ratio})^2}$$

Ogbiyashi's formula for the separation distance at which molten steel will be ejected from between alumina particles is:

```
eqn1= -gamma Cos[theta] 4 Pi / (r P Sqrt[3]) ==
                            (4 - 2 Pi/Sqrt[3]) + 4/ratio + 1/ratio^2
```

$$\frac{-4\ \mathrm{gamma\ Pi\ Cos[theta]}}{\mathrm{Sqrt}[3]\ P\ r} == 4 - \frac{2\ \mathrm{Pi}}{\mathrm{Sqrt}[3]} + \mathrm{ratio}^{-2} + \frac{4}{\mathrm{ratio}}$$

Solving this equation for ratio (i.e. the ratio of the particle radius to particle spacing) gives:

```
ratio1 = Solve[eqn1,ratio] [[1,1]]
```

```
ratio -> (-4 Sqrt[3] P r -
      Sqrt[48 P^2 r^2 - 4 Sqrt[3] P r
        (4 Sqrt[3] P r - 2 P Pi r + 4 gamma Pi Cos[theta])])\
      / (2 (4 Sqrt[3] P r - 2 P Pi r + 4 gamma Pi Cos[theta]))
```

Solving this equation for the critical value of ratio (i.e. the ratio of the particle radius to particle spacing at which steel will be ejected) gives:

```
ratio1 = Simplify[Solve[eqn1,ratio] [[1,1]]]

ratio -> (-4 Sqrt[3] P r -
     2 Sqrt[2] Sqrt[Sqrt[3] P Pi r
        (P r - 2 gamma Cos[theta]])]) /
   (2 (4 Sqrt[3] P r - 2 P Pi r + 4 gamma Pi Cos[theta]))
```

Plugging in material properties and a reasonable ferrostatic pressure gives this critical ratio as a function of radius only:

```
ratio2 = Simplify[ratio1 /. {gamma->1600 10^-3,
                             theta->Pi 130/180,
                             P->100 10^3}] //N

ratio ->
   0.5 (-692820. r - 2086.41 Sqrt[r (2.05692 + 100000. r)])
   --------------------------------------------------------
                  -12.924 + 64501.8 r
```

Consider how the volume fraction varies with particle radius:

```
ParametricPlot[{10^6 r,ep /. ratio2},
                                   {r,.1 10^-6,10 10^-6},
                                   AxesLabel->{"r (micron)","ep"}]
```

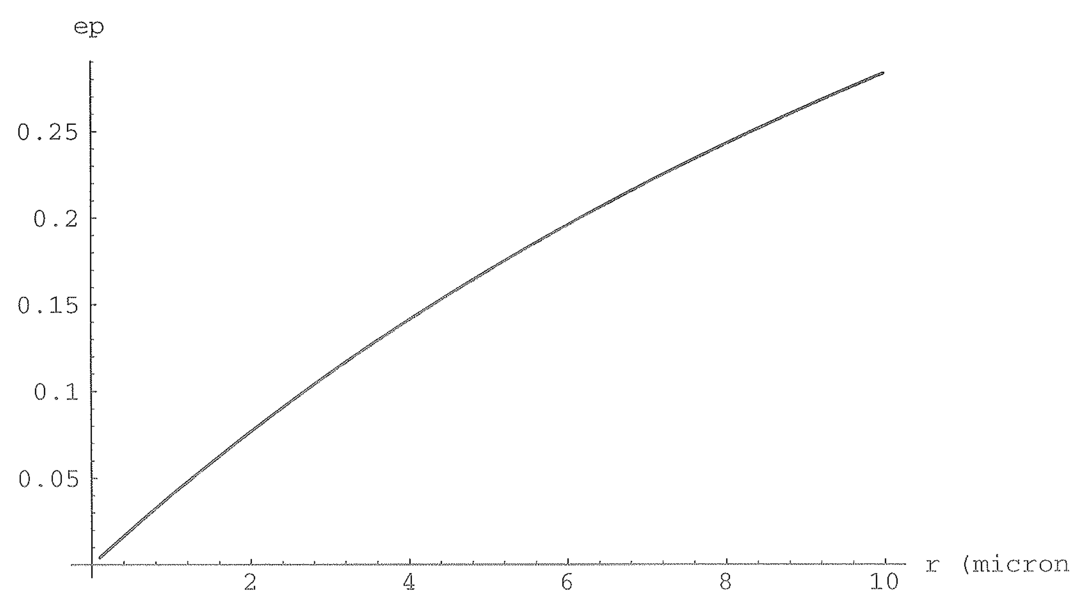


```
-Graphics-
```

For a 10 micron diamater particle, the volume fraction is:

```
(ep /. ratio2) /. r->({2.5,5,10} 10^-6) //N

{0.0938508, 0.169349, 0.2833}
```

Therefore for 5, 10, and 20 micron diamater rods, the volume fractions are 9%, 17%, and 28% respectively.

A.3 SUBMERGED ENTRY NOZZLE HEAT TRANSFER ANALYSIS

In this appendix, the steady state temperature distribution in the submerged entry nozzle and clog buildup is calculated.

Table of variables:

q78 - heat flux from steel stream to clog (W/(m rad))
q67 - heat flux in clog-liquid steel region
q56 - heat flux in clog-solid steel region
q45 - heat flux in nozzle wall
q04 - heat loss to ambient
ksl - conductivity of liquid steel (W/(m K))
kss - conductivity of solid steel
kw - conductivity of nozzle wall
T0- temperature of ambient (K)
T4 - temperatue of nozzle outer diameter
T5 - temperature of nozzle inner diameter
T6 - temperature of solid/liquid interface
T7 - temperature of clog front
T8 - temperature of steel stream
rx - radial position of location x (m)
sig = Stefan-Boltzmann constant (W/(m^2 K^4))
emmis = thermal emmisivity of the mounting block
h78,Nu78 = heat transfer coefficient and Nusselt # between
stream and clog (W/(m^2 K))
a,b = Sleicher and Rouse correlation paramaters
Reynolds = Reynolds # of the steel stream
Prs = Prandtl # of the steel stream
U = bulk stream velocity (m/s)
nus = kinematic viscosity of steel (m^2/s)
flowrate = volume flowrate of stream (m^3/s)

First calculate the heat flux through each region:

Radiation heat loss to ambient:

```
q04 = sig emmis (T4^4 - T0^4) r4
```

$$\text{emmis r4 sig } (-T0^4 + T4^4)$$

Heat transfer by conduction through nozzle wall and clog

```
q45 = kw  (T5 - T4) / Log[r4/r5]
q56 = kss (T6 - T5) / Log[r5/r6[i]]
q67 = ksl (T7 - T6) / Log[r6[i]/r7[i]]
```

$$\frac{\text{kw}\ (-\text{T4} + \text{T5})}{\text{Log}[\frac{\text{r4}}{\text{r5}}]}$$

$$\frac{\text{kss}\ (-\text{T5} + \text{T6})}{\text{Log}[\frac{\text{r5}}{\text{r6[i]}}]}$$

$$\frac{\text{ksl}\ (-\text{T6} + \text{T7})}{\text{Log}[\frac{\text{r6[i]}}{\text{r7[i]}}]}$$

Convective heat transfer from the steel stream

```
q78 = h78 (T8 - T7) r7[i]
```

```
h78 (-T7 + T8) r7[i]
```

Sleicher and Rouse turbulent heat transfer correlation:

```
h78 = Nu78 ksl / (2. r7[i]);
Nu78 = 5. + 0.015 Reynolds^a Prs^b;
a = 0.88 - 0.24/(4+Prs);
b = 1./3. + 0.5 Exp[-0.6 Prs];
Prs = nus/alphas;
Reynolds = U (2. r7[i]) / nus;
U = flowrate / (Pi r7[i]^2);
```

Define a function which takes flowrate in metric tons/min and converts it to m^3/s:

```
ft2m[x_] := (x ton/min)(10^3 kg/ton)(1/(7015 kg))(min/60) //N
```

Numerical Data:

```
sig=5.6697 10^-8;       (* - W/(m^2 K^4)*)
ksl=33.;                (*Kurz, pg 293 - W/(m K)*)
kss=35.;                (*Kurz, pg 293 - W/(m K)*)
gravity=9.8;            (* - m/s^2*)
nus=0.0055/7015.;       (*Smithells, pg 14-7 - m^2/s*)
alphas=6.1 10^-6;       (*Kurz, pg 293 - m^2/s*)
r4=0.135/2.;            (*Vesuvius - m*)
r5=.076/2.;             (*Vesuvius - m*)
T0=300.0;               (* - K*)
T8=1823.;               (* - K*)
```

Define the set of equations to be solved:

```
eqns1 = {q==q04,q==q45,q==q56,q==q67,q==q78};
```

Develop a function to numerically solve the equations given the clog thickness, flowrate, emmisivity, nozzle conductivity, and solid/liq. interface temp:

```
fsen[x1_,x2_,x3_,x4_,x5_] :=
(eqns2 = eqns1 /. {r7[i]->r5-x1,flowrate->x2,emmis->x3,
                   kw->x4,T6->x5};
 FindRoot[eqns2,{T4,T4g},
                   {T5,T5g},{r6[i],r6g},{T7,T7g},{q,qg},
                   MaxIterations->25] )
(*Define the initial guesses:*)
T4g=1360;T5g=1779;r6g=r5-.0001;T7g=1815;qg=6551;
```

Consider five cases:

```
Case 1 - standard
    flowrate - 4 ton/min      (position 2100 for K1 data)
    emmis - .5                (Ozisk, pg 758, 100 micron grain)
    kw - 9.0 W/(m K)          (Shaw, pg 40, carbon bonded
                                             alumina-graphite)
    Ti - 1798 K               (liquidus temp for .16% C
                                             - using Kurz data)
Case 2
    flowrate - 3 ton/min(position 100 for K1 data)
Case 3
    emmis - .96               (oxidized steel coating, pg 108,
                                             USS book)
Case 4
    kw - 1.5 W/(m K)          (high alumina castable, pg 56,
                                             USS book)
Case 5
    Ti - 1766 K               (solidus temp)
```

Consider case 1. A typical result is:

```
fsen[.005,ft2m[4],.5,9,1798]

{T4 -> 1365.89, T5 -> 1790.08, r6[i] -> 0.036448,
  T7 -> 1818.01, q -> 6644.85}
```

Variation of temperatures with clog thickness for case 1:

```
pT = Plot[{T4 /.fsen[ts,ft2m[4],.5,9,1798],
          T5/.fsen[ts,ft2m[4],.5,9,1798],
          T7/.fsen[ts,ft2m[4],.5,9,1798]},{ts,.0002,.02}]
```

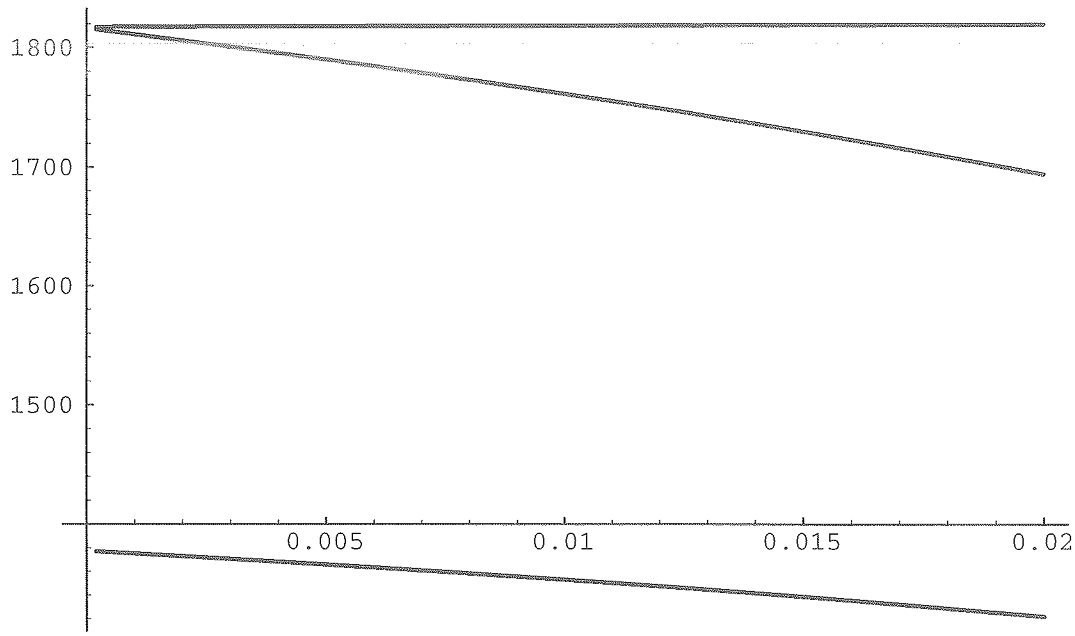

-Graphics-

Enlarge the region around 1800 K in the above plot:

```
Show[pT,PlotLabel->"stagnant zone thickness vs temp"
       ,AxesLabel->{meters,K}
       ,AxesOrigin->{0,1798}
       ,PlotRange->{1750,1825}]
```

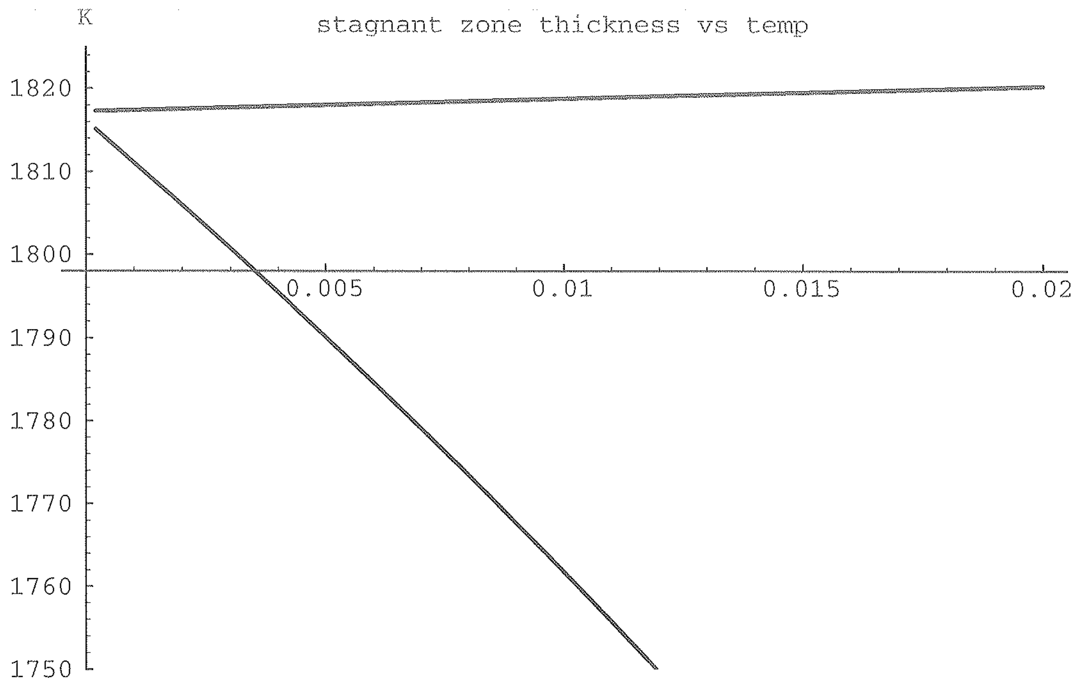

-Graphics-

The remainder of the cases are summarized in Chapter 4.

A.4 TUNDISH NOZZLE HEAT TRANSFER ANALYSIS

In this appendix, the steady state temperature distribution in the tundish nozzle, mounting block, and clog buildup is calculated.

Table of variables:

q78 - heat flux from steel stream to clog (W/(m rad))
q67 - heat flux in clog-liquid steel region
q56 - heat flux in clog-solid steel region
q45 - heat flux in nozzle wall
q24 - heat flux in mounting block
q02 - heat loss to ambient
ksl - conductivity of liquid steel (W/(m K))
kss - conductivity of solid steel
kw - conductivity of nozzle wall
T0- temperature of ambient (K)
T2 - temperature of mounting block outer diameter
T4 - temperatue of nozzle outer diameter
T5 - temperature of nozzle inner diameter
T6 - temperature of solid/liquid interface
T7 - temperature of clog front
T8 - temperature of steel stream
rx - radial position of location x (m)
sig = Stefan-Boltzmann constant (W/(m^2 K^4))
emmis = thermal emmisivity of the mounting block
h78,Nu78 = heat transfer coefficient and Nusselt # between
stream and clog (W/(m^2 K))
a,b = Sleicher and Rouse correlation paramaters
Reynolds = Reynolds # of the steel stream
Prs = Prandtl # of the steel stream
U = bulk stream velocity (m/s)
nus = kinematic viscosity of steel (m^2/s)
flowrate = volume flowrate of stream (m^3/s)

First calculate the heat flux through each region:

Radiation heat loss to ambient:

```
q02 = sig emmis (T2^4 - T0^4) r2;
```

Heat transfer by conduction through mounting block, nozzle wall, and clog

```
q24 = kss (T4 - T2) / Log[r2/r4];
q45 = kw  (T5 - T4) / Log[r4/r5];
q56 = kss (T6 - T5) / Log[r5/r6[i]];
q67 = ksl (T7 - T6) / Log[r6[i]/r7[i]];
```

Convective heat transfer from the steel stream:

```
q78 = h78 (T8 - T7) r7[i];
```

Sleicher and Rouse turbulent heat transfer correlation:

```
h78 = Nu78 ksl / (2. r7[i]);
Nu78 = 5. + 0.015 Reynolds^a Prs^b;
a = 0.88 - 0.24/(4+Prs);
b = 1./3. + 0.5 Exp[-0.6 Prs];
Prs = nus/alphas;
Reynolds = U (2. r7[i]) / nus;
U = flowrate / (Pi r7[i]^2);
```

Define a function which takes flowrate in metric tons/minand converts it to m^3/s:

```
ft2m[x_] := (x ton/min)(10^3 kg/ton)(1/(7015 kg))(min/60) //N
```

Numerical Data:

```
sig=5.6697 10^-8;     (* - W/(m^2 K^4)*)
emmis=0.96;           (*USS, pg 108, oxidized steel*)
ksl=33.;              (*Kurz, pg 293 - W/(m K)*)
kss=35.;              (*Kurz, pg 293 - W/(m K)*)
kw=9;                 (*Shaw, pg 40, carbon-bonded AG *)
gravity=9.8;          (* - m/s^2*)
nus=0.0055/7015.;     (*Smithells, pg 14-7 - m^2/s*)
alphas=6.1 10^-6;     (*Kurz, pg 293 - m^2/s*)
r4=0.193/2.;          (*Vesuvius - m*)
r5=.085/2.;           (*Vesuvius - m*)
flowrate=ft2m[4];     (*K1 data, position 2100 - m^3/s*)
T0=300.0;             (* - K*)
T6=1798;              (* - K*)
T8=1823.;             (* - K*)
```

Define the set of equations to be solved:

```
eqns1 = {q==q02,q==q24,q==q45,q==q56,q==q67,q==q78};
```

Develop a function to numerically solve the equations given the clog thickness and mounting block outer radius.

```
futn[x1_,x2_] :=
(eqns2 = eqns1 /. {r7[i]->r5-x1,r2->x2};
 FindRoot[eqns2,{T2,T2g},{T4,T4g},
                       {T5,T5g},{r6[i],r6g},{T7,T7g},{q,qg},
                       MaxIterations->25] )
(*Define the initial guesses:*)
T2g=900;T4g=1360;T5g=1779;r6g=r5-.0001;T7g=1815;qg=6551;
```

Consider a mounting block of outer radius of 25 cm and a clog thickness of 5 mm

```
futn[.005,.25]

{T2 -> 871.628, T4 -> 1082.24, T5 -> 1787.83,
  r6[i] -> 0.0405908, T7 -> 1816.59, q -> 7743.88}
```

The effect of clog thickness on skull thickness is:

```
putn1 = Plot[r5 - r6[i] /. futn[ts,.25],{ts,.003,.02}
,PlotLabel->"Skull Thickness vs Clog Thickness"
,AxesLabel->{meters,meters}]
```

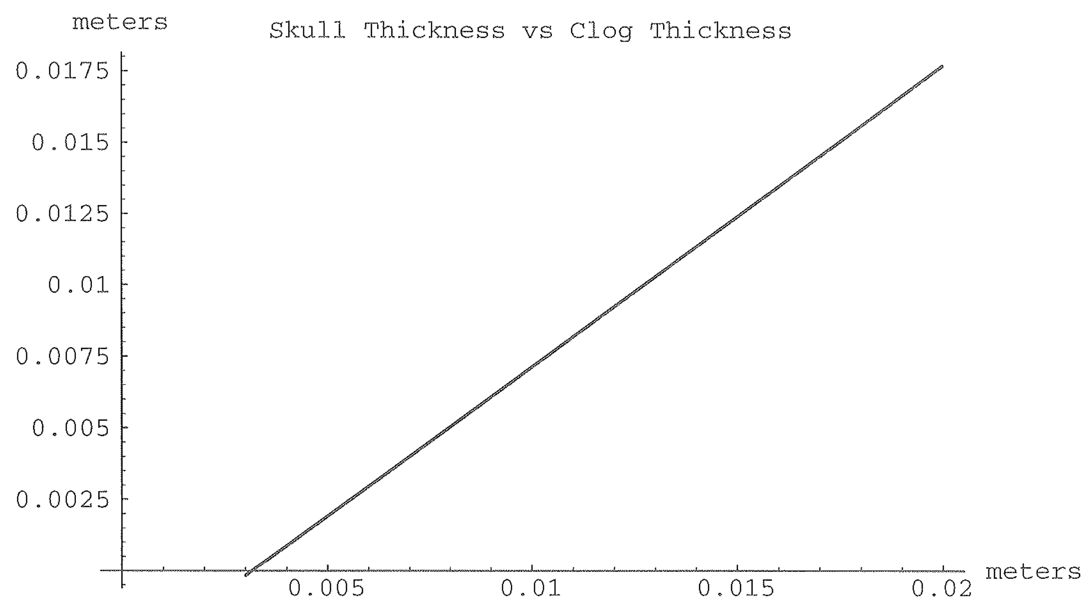


```
-Graphics-
```

As seen above, the addition of the mounting block has littleeffect on the skulling behavior. This results from the mounting block acting as a radiator instead of an insulator. This is shown in the following plot for the case of a 20 mm thick clog:

```
putn2 = Plot[r5 - r6[i] /. futn[.02,rb],{rb,r4+.001,.5}
,PlotLabel->"Skull Thickness vs Mounting Block Radius"
,AxesLabel->{meters,meters}]
```

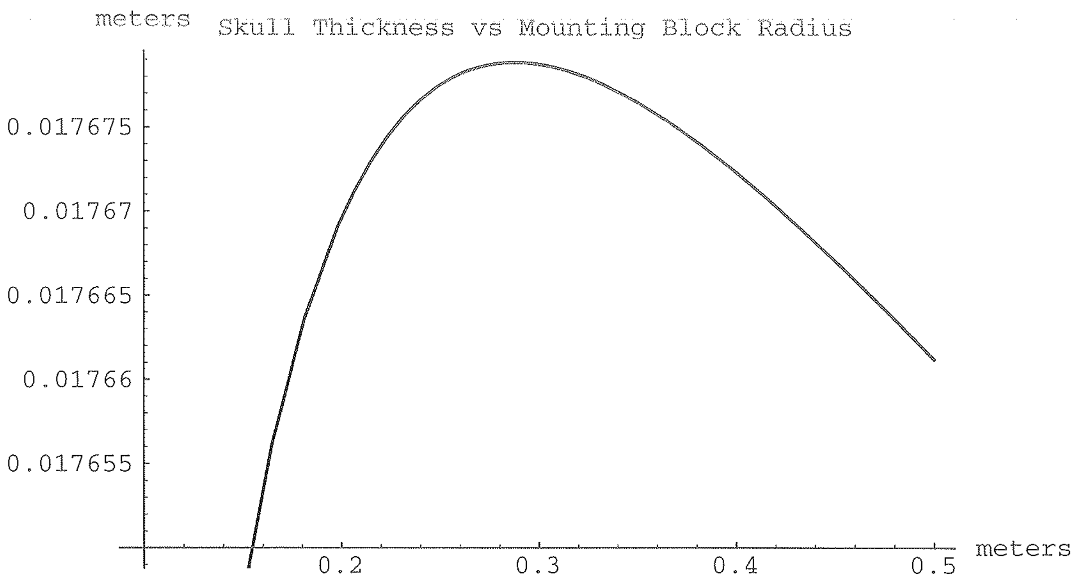

-Graphics-

A.5 SOLIDIFICATION TRANSIENT ANALYSIS

In this appendix, a model will be formulated to predict the time evolution of the clog and skull buildup in a tundish nozzle. The model utilizes one dimensional heat and mass transfer models to account for latent heat and solute rejection at the skull front.

Nomenclature:

qxy = heat flux / (2 Pi length) from position y to x (W/m^2)
sig = Stefan-Boltzmann constant (W/(m^2 K^4))
emmis = thermal emmisivity of the mounting block
Tx = Temperature at position x (K)
Tl = liquidus temperature for free stream concentration (K)
rx = radial position of x (m)
kx = thermal conductivity of region (ss - solid steel, w - nozzle wall, sl - liquid steel) (W/(m K))
h78,Nu78 = heat transfer coefficient and Nusselt # between stream and clog (W/(m^2 K))
a,b = Sleicher and Rouse correlation paramaters
Reynolds = Reynolds # of the steel stream
Prs = Prandtl # of the steel stream
U = bulk stream velocity (m/s)
nus = kinematic viscosity of steel (m^2/s)
flowrate = volume flowrate of stream (m^3/s)
Tf = freezing temperature of pure iron (K)
ml = slope of the liquidus curve (K/(wt% C))
k = equilibrium partition coefficient
Lf = latent heat of fusion (J/m^3)
Csx,Clx = carbon concentration at position x in solid,liquid relative to the free stream concentration (wt% C)
Cl7a = absolute carbon concentration in free stream (wt% C)
mCl = excess mass of carbon in the liquid / (density length) (i.e. additional mass due to solute rejection) (wt% C m^2)
xo = value of variable at prior time step
dt = time step size
J7 = flux of carbon into steel stream / density (wt %C m / s)
Dc = Diffusion constant for carbon in liquid steel (m^2/s)
qout,qin = q56,q67
mV7,bV7 = constants describing relationship between clog front interface velocity and unsupported clog length
c1,c2 = liquid concentration profile constants
V6 = solidification front velocity
Vc = maximum plane front growth velocity

tcst = time required to develop a 20 mm thick pure alumina clog

Heat fluxes through regions:

```
q02 = sig emmis (T2^4 - T0^4) r2;
q24 = kss (T4 - T2) / Log[r2/r4];
q45 = kw  (T5 - T4) / Log[r4/r5];
q56 = kss (T6 - T5) / Log[r5/r6[i]];
q67 = ksl (T7 - T6) / Log[r6[i]/r7[i]];
q78 = h78 (T8 - T7) r7[i];
```

Sleicher and Rouse turbulent heat transfer correlation:

```
h78 = Nu78 ksl / (2. r7[i]);
Nu78 = 5. + 0.015 Reynolds^a Prs^b;
a = 0.88 - 0.24/(4+Prs);
b = 1./3. + 0.5 Exp[-0.6 Prs];
Prs = nus/alphas;
Reynolds = U (2. r7[i]) / nus;
U = flowrate / (Pi r7[i]^2);
```

The relationship between the liquid carbon concentration at the interface and the amount of carbon in the liquid will now be developed. Assuming that the solute profile is approximately at steady state (i.e., assume mass diffusion >> mass accumulation), the concentration of carbon will be:

```
Cl = c1 Exp[-V6[i-1]/Dc (r6[i]-r)] +c2;
```

Given the concentration of carbon at the liquid side of the interface and forcing the concentration to equal the free stream value at the clog front yields a solution for the constants c1 and c2:

```
ans1a = Solve[{(Cl /. r->r6[i]) == Cl6[i],
               (Cl /. r->r7[i]) == 0    },{c1,c2}] [[1]];
```

The total excess carbon concentration in the liquid can be found by integration:

```
mCla = Integrate[Cl 2. Pi r,{r,r7[i],r6[i]}];
```

The time stepping procedure will calculate the carbon concentration at the interface at the next time step by a mass balance which accounts for solute flow between the solid and liquid and between the liquid within the clog and the stream.

```
ans1 = Solve[(mCla/.ans1a) + dmCso + 2. Pi r7[i-1] J7o dt ==
            mCl[i-1],Cl6[i]] [[1,1]];

(*Carbon flux into the stream is given by.*)
J7o = Dc D[(Cl/.ans1a),r] /.  {Cl6[i]->Cl6[i-1],r6[i]->r6[i-1],
                               r->r7[i-1]};

(*Change in the mass of carbon in solid since the last time step.*)
dmCso = V6[i-1] Cs6[i-1] 2. Pi r6[i-1] dt;
```

I have assumed a relationship between the unsupported clog length and the growth rate. This relationship takes into account the decreased clog rentrainment due to reinforcement by skulling. The relationship is of the form:

```
V7o = Vc7 Exp[-(r6[i-1]-r7[i-1]) / rc7] ;

(*Local thermodynamic equilibrium relationship:*)
T6 = Tf + ml (Cl7a + Cl6[i]);

(*Numerical Data:*)
sig=5.6697 10^-8;        (* - W/(m^2 K^4)*)
emmis=0.96;              (*USS, pg 108, oxidized steel*)
ksl=33.;                 (*Kurz, pg 293 - W/(m K)*)
kss=35.;                 (*Kurz, pg 293 - W/(m K)*)
gravity=9.8;             (* - m/s^2*)
nus=0.0055/7015.;        (*Smithells, pg 14-7 - m^2/s*)
alphas=6.1 10^-6;        (*Kurz, pg 293 - m^2/s*)
r2=0.5/2.;               (*Inland - m*)
r4=0.193/2.;             (*Inland - m*)
r5=.085/2.;              (*Inland - m*)
T0=300.0;                (* - K*)
Tf=1811.;                (*Kurz - K*)
Lf=1.93 10^9;            (*Kurz, pg 293 - J/m^3*)
k=.17;                   (*Kurz, pg 295*)
ml=-81.;                 (*Kurz, pg 295 - K/(wt%) *)
Dc=2. 10^-8;             (*Kurz, pg 295 - m^2/s*)
```

Now I will choose the constants for the clog growth rate relationship. I will choose the constants so as to provide a reasonable bound to the growth rates observed in practice (2 heats - 10 heats). It was found in the fluid flow calculations that nozzle replacement was required when the clog reached approximately 20 mm thickness. Noting that a heat lasts approximately 1/2 hr, the upper bound growth rate is 20 mm/hr. This gives Vc7 = 20 mm (i.e., clog and skull fronts are identical).

```
Vc7 = .02/3600.;
```

The characteristic length (rc7) is now chosen to chosen to create clogging in 10 heats (5 hrs) if no skull forms. The time required to form a 20 mm thick clog (tcst) for this condition can be found by integrating the inverse of the velocity equation (i.e. dx/dt = V => dt = dx/V)..

```
tcst = Integrate[1/(V7o /. {(r6[i-1]-r7[i-1])->x}),{x,0,.020}]
```

$$-180000.\ rc7 + 180000.\ E^{0.02/rc7}\ rc7$$

Solving this equation for the value of the rc7 which generates clogging in 5 hrs gives:

```
FindRoot[tcst == 5*3600,{rc7,.01}]

{rc7 -> 0.00751767}
```

Therefore I will choose rc7 = 7.5 mm.

```
rc7 = .0075;
```

To simplify the numerical solution, I will linearize the radiation heat transfer equation:

```
q02a = Normal[Series[q02,{T2,T2o,1}]];
```

I can now solve for the temperature distribution on either side of the interface analytically if given the interface temperature (note that I neglect sensible heat).

```
ans2 = Solve[{qout==q02a,qout==q24,qout==q45,qout==q56},
             {qout,T2,T4,T5}] [[1,4]];

ans3 = Solve[{qin==q67,qin==q78},{qin,T7}] [[1,1]];
```

The mathematical formulas for the transient algorithm can be generated in standard fortran format by using the following statements:

```
(*r6[i]=*) FortranForm[r6[i-1] - V6[i-1] dt]
(*r7[i]=*) FortranForm[r7[i-1] - V7o dt]

r6(-1 + i) - 12.*V6(-1 + i)

(*Cl6[i]=*) FortranForm[Cl6[i] /. ans1]

(*mCl[i]=*) FortranForm[mCla /. ans1a]

(*V6[i]=*) FortranForm[(qout - qin) / (Lf r6[i]) /. {ans2,ans3}]

(*For freezing: Cs6[i]=*) FortranForm[k (Cl7a + Cl6[i]) - Cl7a]
(*For melting: Cs6[i]=see below*)
```

The algorithim will also be defined as a Mathematica function. The algorithm starts with the clog and solidification front velocities from the prior time step. These velocities are used to determine the new position of the interfaces. Then a mass balance which accounts for the movement of the interfaces is done to obtain the concentration of carbon at the interface. Using this concentration, the amount of excess carbon in the liquid is calculated. Also, given the concentration at the interface, the temperature at the interface is known and from this the velocity of the solidfication front can be calculated. The concentration in the solid at the interface is determined by the equilibrium phase diagram if the interface velocity is positive (i.e. freezing) or by the concentration that the solid at that location froze at if the interface velocity is negative (i.e. melting).

```
fstep[i_] := (
    r6[i]= r6[i-1] - V6[i-1] dt;
    r7[i]= r7[i-1] - V7o dt;
    Cl6[i]= Cl6[i] /. ans1 //N;
    mCl[i] = mCla /. ans1a // N;
    V6[i]=(qout - qin) / (Lf r6[i]) /. {ans2,ans3};
    If[V6[i]>0,Cs6[i] = k (Cl7a + Cl6[i]) - Cl7a
             ,If[r6[i]<r5,(j=i-1;
                             While[r6[i]>r6[j],j=j-1];
                             Cs6[i] = Cs6[j])
                            ,(r6[i]=r6[1];Cl6[i]=Cl6[1];
                             mCl[i]=mCl[1];V6[i]=V6[1];
                             Cs6[i]=Cs6[1];)]])
```

This algorithm assumes planar growth. To check the validity of this assumption, I will calculate the maximum plane front growth rate (Vc) and compare it with the actual growth rate after the run.

```
Tl = T6 /. Cl6[i]->0;

ans4 = Solve[q78==(qin/.ans3),T7] [[1,1]];

Vc = ((T7 /. ans4) - T6) / (r6[i]-r7[i]) Dc/(Tl - T6);
```

To illustrate the solution behavior, consider casting a steel with carbon equivalent of .095%. Assume that the casting speed and temperature are at 1835 K and 3.6 ton/min for 24 min and then drop to 1825 K and 2.7 ton/min for 12 min (simulating a ladle change).

```
(*Base Case*)
kw=9.;                  (*Shaw, pg 40, carbon-bonded AG *)
Cl7a=.095;
```

By a time stiep refinement study, I have found that a time step of 3 seconds is adequate.

```
dt=3.;
```

A temperature is needed to linearize the radiation BC around. Find this by solving for the steady state temperature for a nozzle ID at the liquidus temperature.

```
Solve[{q==q02,q==q24,q==q45 /. T5->(T6/.Cl6[i]->0)},
                {T2,T4,q}] [[4]]

{T4 -> 1088.06, q -> 7849.93, T2 -> 874.556}

T2o=875.;
```

Now choose the starting conditions for the run. I will start with no clog or skull, no excess carbon, and zero interface velocity.

```
r6[1] = r5 + 10^-8;
r7[1] = r5 - 10^-8;
V6[1] = -10.^-8;
Cl6[1] = 10.^-8;
mCl[1] = 10.^-8;
Cs6[1] = k (Cl7a + Cl6[1]) - Cl7a;
```

Note that the program goes through one iteration every time fstep is executed. Since the time step is 3 seconds, 480 time steps are required to simulate 24 minutes:

```
T8 = 1835;
flowrate=.008664;
Do[fstep[i],{i,2,480}]
```

Now simulate the ladle change event:

```
T8 = 1825;
flowrate=.006455;
Do[fstep[i],{i,481,720}]
```

Again simulate the steady state casting behavior.

```
T8 = 1835;
flowrate=.008664;
Do[fstep[i],{i,721,1200}]
```

Results:

First check to see if the plane front growth velocity was exceeded. I will check this by taking the ratio of the actual growth rate to the critical growth rate:

```
ListPlot[Table[{i*3/60,V6[i]/Vc},{i,2,1200}]
          ,PlotRange->{0,1}
          ,PlotJoined->True
   ,PlotLabel->"Fraction of Critical Velocity vs Time"
   ,AxesLabel->{min,ratio}]
```

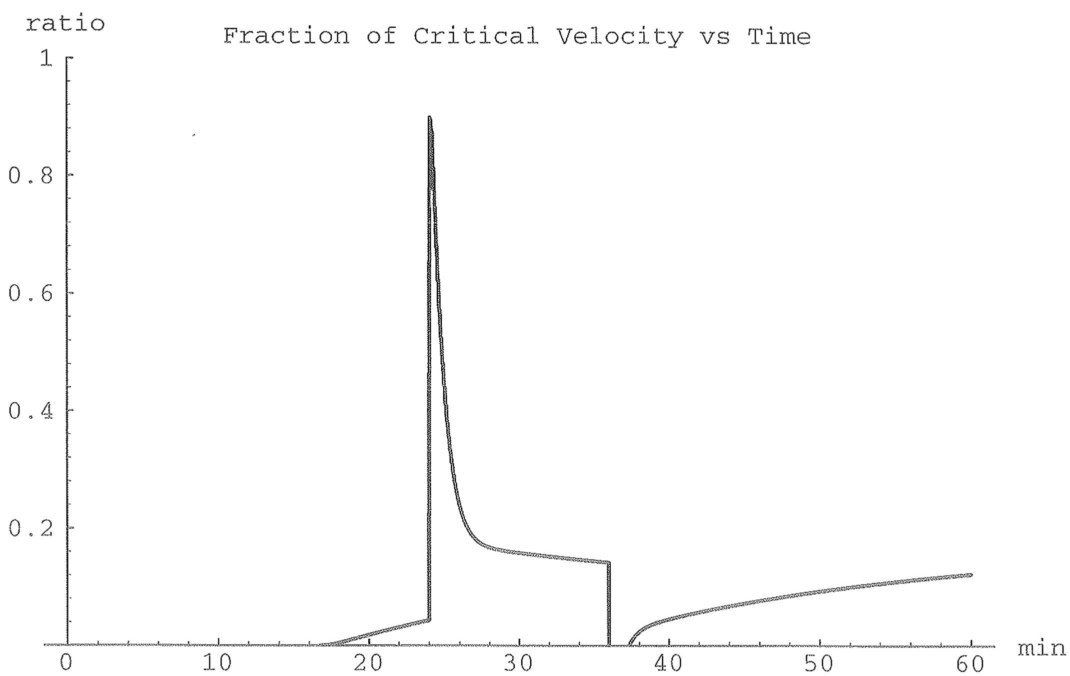

-Graphics-

It is observed that the step change decrease in casting temperature and speed causes the solidification front velocity to closely approach the critical velocity. In practice, the changes will not be so abrupt and so the plane front growth assumption is expected to be valid.

Next consider the variation of excess carbon concentration at the skull front:

```
ListPlot[Table[{i*3/60,C16[i]},{i,2,1200}]
            ,PlotJoined->True
    ,PlotLabel->"Excess Concentration at Interface vs Time"
    ,AxesLabel->{min,"% C"}]
```

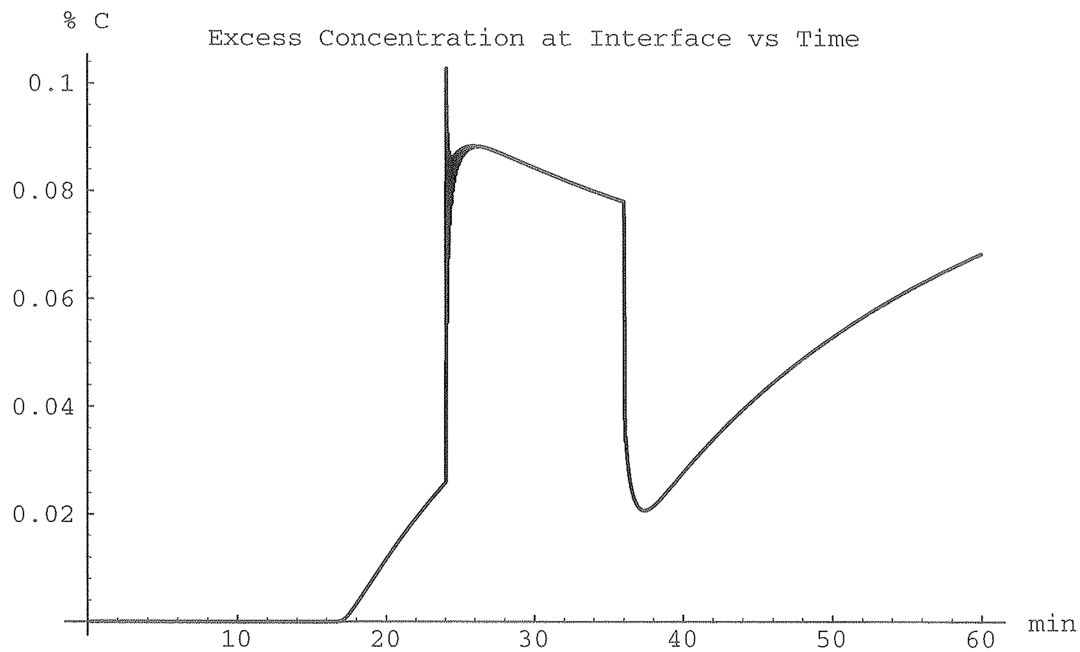

-Graphics-

Here it is seen that the carbon concentration begins to increase at approximately 17 minutes, corresponding to the beginning of skull formation. At 24 minutes, the concentration increases rapidly as the interface velocity increases (notice there is some numerical error at the step change). Upon completion of the ladle change transient, the concentration drops to adjust the interface temperature toward the now higher equilibrium temperature.

The resulting skull interface velocities are considered now:

```
pv6 = ListPlot[Table[{i*3/60,V6[i]*1000*3600},{i,2,1200}]
        ,PlotJoined->True
        ,AxesLabel->{min,"mm/hr"}
        ,PlotLabel->"Skull Front Velocity vs Time"]
```

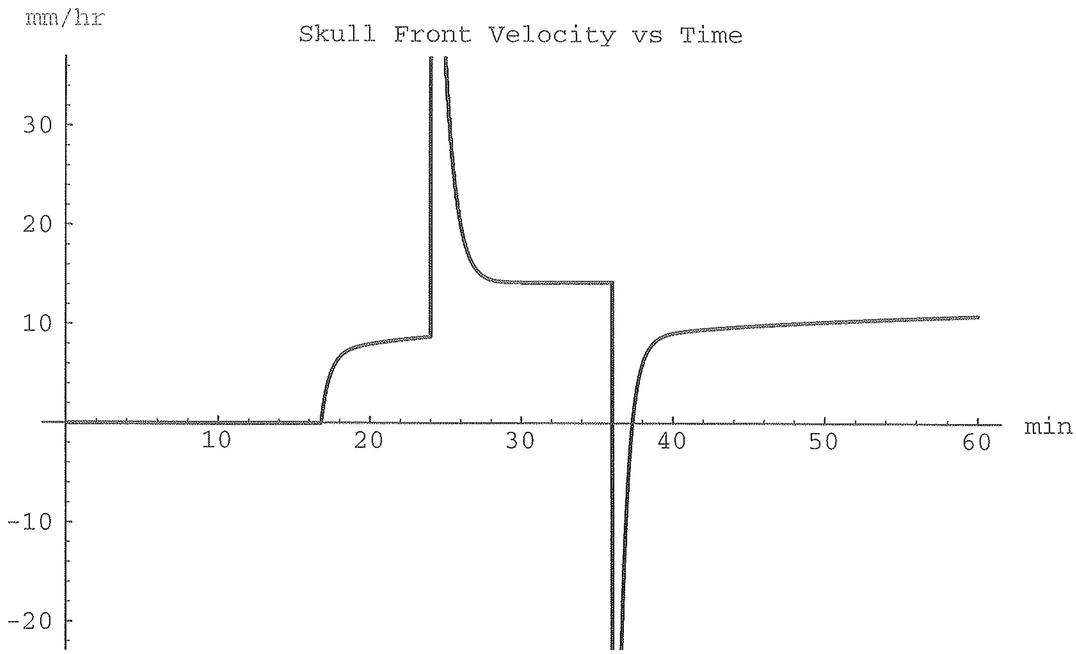

It is observed that the solidification rate increases during the ladle change transient because the distance between the clog and skull fronts is decreased. The skull remelts for approximately two minutes after completion of the ladle change and then freezing commences again.

Now compare the skull velocity with the clog front velocity:

```
pv7 = ListPlot[Table[{i*3/60,V7o*1000*3600},  {i,2,1199}]
            ,PlotJoined->True]
```

```
Show[{pv6,pv7}
	,AxesLabel->{min,"mm/hr"}
	,PlotLabel->"Interface Velocities vs Time"
	,PlotRange->{0,20}]
```

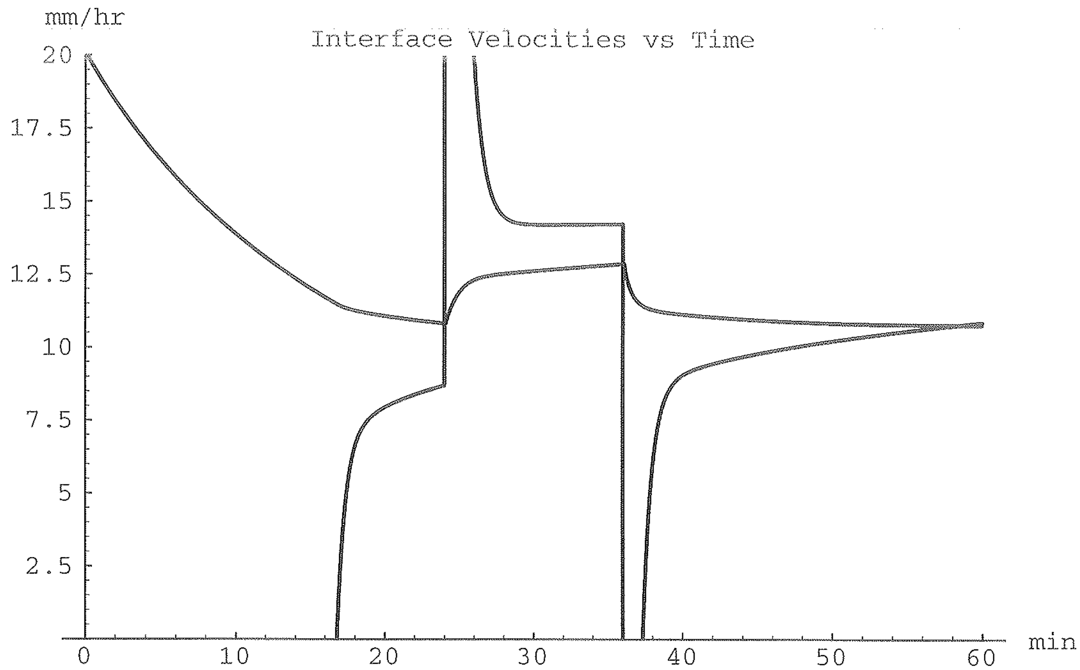

-Graphics-

Finally consider the net result of this transient on the clog thickness:

```
ListPlot[Table[{i*3/60,(r5-r7[i])*1000},{i,2,1200}]
        ,PlotJoined->True
        ,AxesLabel->{min,mm}
        ,PlotLabel->"Clog Thickness vs Time"]
```

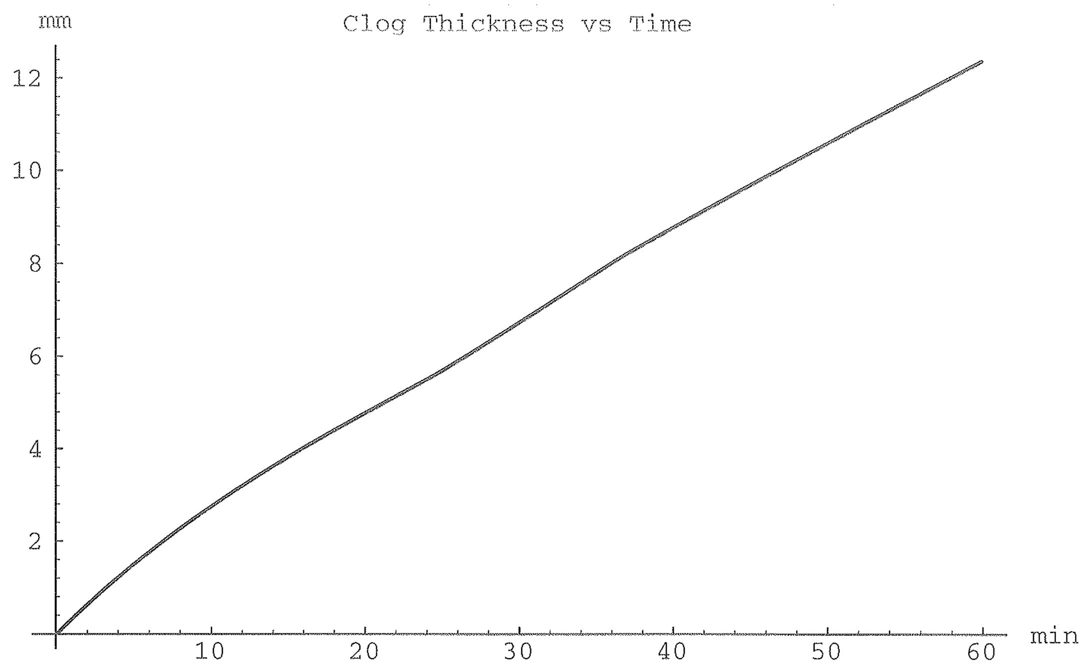

-Graphics-

It is seen that for this case the net effect of the ladle change on clogging is barely perceptible.

A.6 CALCULATION OF THE FLOW THROUGH THE NOZZLES

In this appendix, the flow rate of steel between the tundish and mold will be estimated by modelling the major elements of the system as pipes, tees, and orifices.

Table of Variables:

Q = volume flow rate through nozzle
rho = density
Vx,Ax,rx,Lx,epx,dpx,Rx,Kx = average velocity, cross section area, radius, length, roughness, pressure drop, flow resistance, and loss coefficient of section x
where x = utn - upper tundish nozzle
= sg - slide gate
= sen - submerged entry nozzle
= port - both nozzle ports
ustar = friction velocity for turbulent channel flow
tauw = wall shear stress
Cd = orifice discharge coefficient
beta = ratio of orifice diameter to pipe diameter
sgpos = fraction of channel diameter of slide gate travel
rutn0 = unclogged utn radius
tsg = half width of slide gate perpendicular to direction of slide gate travel
g = gravitational acceleration
Ltun = tundish steel height
Lsub = SEN port submergence depth

Upper Tundish Nozzle and SEN:

Assume: Fully Turbulent (i.e. Re independent)

```
eqn1 = V/ustar == 2.44 Log[2 r / ep] + 3.2;

eqn2 = eqn1 /. ustar-> (tauw / rho)^(1/2);

eqn3 = tauw 2 Pi r L == dp Pi r^2;

eqn4 = Eliminate[{eqn2,eqn3},tauw];

eqn5 = Q == Pi r^2 V;

eqn6 = Eliminate[{eqn4,eqn5},V];

dppx = dp /. Solve[eqn6,dp] [[1,1]];

Rpx = dppx / Q^2;

Rutn = Rpx /. {L->Lutn,r->rutn,ep->eputn};

Rsen = Rpx /. {L->Lsen,r->rsen,ep->epsen};
```

Slide Gate:

Approximate pressure drop through the slide gate as the nonrecoverable pressure drop through an orifice with same flow area. The general relation between the loss coefficient and the pressure loss is:

```
dpfx = K rho V^2/2    /. V->Q/(Pi r^2);

(*Noting that V is the throat velocity for the orifice gives:*)
dpsg = dpfx /. {K->Ksg,r->rsg};

Rsg = dpsg/Q^2;

(*Generate a curve fit for loss coefficient as fcn of beta (Fig 6.38 pg 367 - White '86):*)

Ksg = c1 beta^3 + c2 beta^2 + c3 beta + c4;

Kpts = {2.5,2.0,1.5,1.0};
betapts = {.25,.46,.59,.71};

Ksgeqns = Kpts == Ksg /. beta -> betapts;

cn = Solve[Ksgeqns,{c1,c2,c3,c4}];

beta = rsg/rutn0;
```

Calculation of Slide Gate effective radius. The slide gate opening area will be that area enclosed by two overlapping circles. This area is found below by integration:

```
possqrt = Sqrt[x_^2 y_] -> x Sqrt[y] ;
                (*fcn to take the positive square root*)

tsg = Simplify[Sqrt[rutn0^2-(rutn0 - sgpos rutn0)^2]] /.possqrt;

eqn8 = Asg == 4 Integrate[Sqrt[rutn0^2-x^2]-(rutn0-sgpos rutn0),
        {x,0,tsg}];

negsqrt = Sqrt[(x_+y_)^2] -> -x-y;
                (*fcn to take the negative square root*)

eqn9 = Simplify[(eqn8 /. possqrt) /. negsqrt];

N[eqn9 /. {sgpos->{0,.5,0.9999},rutn0->1}];

eqn11 = eqn9 /. Asg->Pi r2^2;

rsg = r2 /. Solve[eqn11,r2] [[2,1]];

sgpos = 0.8 sgtrue + 0.2;     (*based on emperical fit to data*)
```

Nozzle Ports:

Model the nozzle ports as a tee.

```
dpport = dpfx /. {K->Ktee,r->rsen};

Rport = dpport/Q^2;
```

Nozzle Entrance:

Approximate the pressure drop at the tundish nozzle entrance as the pressure drop resulting from flow acceleration alone.

```
dpin = dpfx /. {K->1,r->rutn};
Rin = dpin/Q^2;
```

Total Pressure Drop:

Since I have assume Reynolds number independent flow through each component, the pressure drop will be proportional to the velocity (or flow rate) squared. I will therefore define a total flow resistance:

```
dptotal = Q^2 Rtotal;
```

I can now solve for the flow resistance by summing the individual pressure drops

Since the flow is gravity driven, I know that the total pressure drop must equal the ferrostatic pressure:

```
eqn16 = dptotal == rho g (Ltun + Lutn + Lsen - Lsub);
```

Given the total flow resistance and ferrostatic pressure, the flow rate is given by:

```
Q1 = Q /. Solve[eqn16,Q][[2,1]];
```

The total flow resistance is equal to the sum of the individual resistances:

```
Rtotal = Rutn + Rsg + Rsen + Rport + Rin;
```

Define a function which takes flowrate in metric tons/min and converts it to m^/s:

```
ft2m[x_] := (x ton/min)(10^3 kg/ton)(1/(7015 kg))(min/60) //N

(*Numerical Data:  (Clean Nozzle)*)
dataflow = {
g->9.8,
cn[[1,1]],cn[[1,2]],cn[[1,3]],cn[[1,4]],
rho->7015,                  (*Smithells*)
Lsen ->(0.65+0.133+0.057),(*Vesuvius Y-005-1061&BW01565&KAO5971*)
Lutn -> 0.343,              (*Clogging Factor (NCF) Algorithim,
                                  compares well with dwg - 0.304 m*)
rutn0-> 0.08/2,             (*Inland #1 Slab Caster*)
Ltun -> 1.066*44/39,        (*Inland K1 tracking block data and
                                  NCF - typical observation*)
Lsub -> 0.203,              (*Hershey Thesis pg 51*)
rsen -> rnoz,
rutn -> rnoz,
epsen-> 0.0005,             (*above predicted max alumina length*)
eputn-> 0.0005,             (*"   "    "    "    "    "    "   *)
Ktee -> 0.8                 (*White-'86, pg 334 - 2 in. dia tee*) };
```

Examine the relationship between the slide gate position and the clog thickness fo a typical high and low flow rate (e.g. 3 and 4 ton/min):

```
eqn17a = Q==Q1 /. dataflow;

fr[x_,y_] := (
     eqn17b = eqn17a /. {Q->ft2m[x],sgtrue->y};
     .04-(rnoz /. FindRoot[eqn17b,{rnoz,.04}]) )

pr1 = Plot[fr[3,sgtrue],{sgtrue,.26,.99}];

pr2 = Plot[fr[4,sgtrue],{sgtrue,.35,.99}];
```

```
Show[{pr1,pr2},PlotRange->{{0,1},{0,.04}},
        AxesLabel->{"SG Pos.","thickness (m)"},
        PlotLabel->"Effect of Clogging on Slide Gate Position"]
```

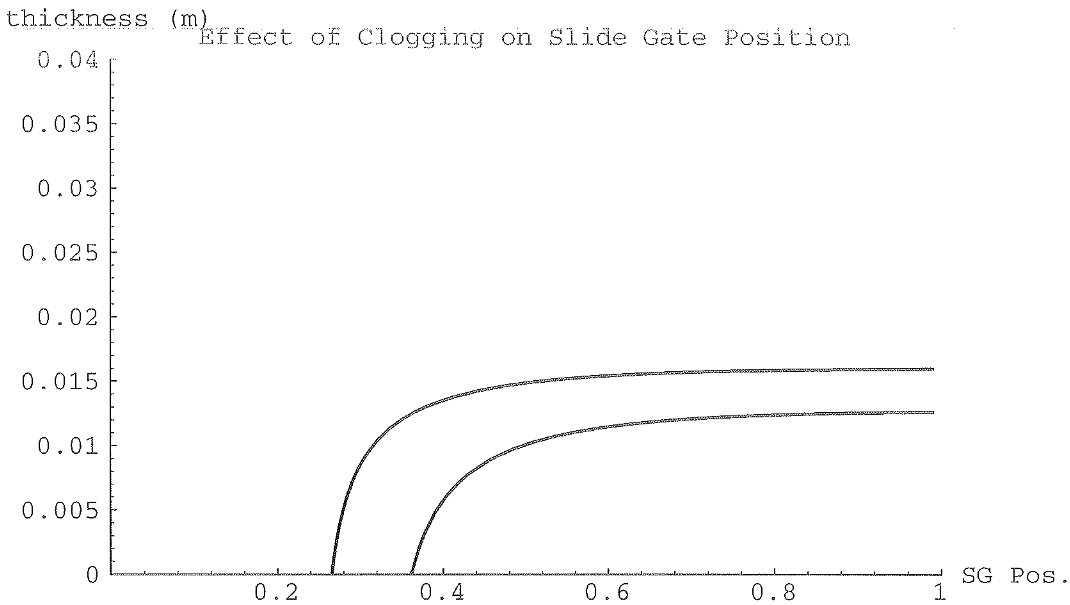


```
-Graphics-
```

Discussion of the emperical adjustment for the slide gate pressure drop.

The detailed Inland data for cast 9361, strand 2 was utilized to backcalculate the actual total flow resistances during casting (i.e., the pressure drop divided by the flow rate squared). It is clear that the actual flow resistance for a clean nozzle must be less than or equal to the flow resistances obtained from this data (because the data includes the effect of clogging). A lower bound curve of the emperical data was generated. It was found that prior to emperical adjustment of the slide gate model, the pressure drop was overestimated as shown below:

```
Rtotalnofudge = Simplify[
    ((Rtotal /. sgtrue -> (sgtrue-.2)/.8)
        /. dataflow)  /. rnoz->.04];

(*Emperical lower bound flow resistance data:*)
y1u=3.28 10^9;y1l=2.4 10^10;x1u=41.5;x1l=27.6;y2u=1.96 10^9;
    y2l=y1u;x2u=48.8;x2l=x1u;y3u=1.73 10^9;y3l=y2u;
    x3u=53.6;x3l=x2u;y4u=1.6 10^9;y4l=y3u;x4u=75.7;x4l=x3u;

(*Emperical resistances:*)
Re1 = y1l*(y1u/y1l)^((x-x1l)/(x1u-x1l)) /. x->76 sgtrue+24;
Re2 = y2l*(y2u/y2l)^((x-x2l)/(x2u-x2l)) /. x->76 sgtrue+24;
Re3 = y3l*(y3u/y3l)^((x-x3l)/(x3u-x3l)) /. x->76 sgtrue+24;
Re4 = y4l*(y4u/y4l)^((x-x4l)/(x4u-x4l)) /. x->76 sgtrue+24;
```

```
pR1 = Plot[Re1,{sgtrue,.05,.23}]
pR2 = Plot[Re2,{sgtrue,.23,.33}]
pR3 = Plot[Re3,{sgtrue,.33,.39}]
pR4 = Plot[Re4,{sgtrue,.39,1}]
pR5 = Plot[Rtotalnofudge,{sgtrue,.1,.99}]
```

```
Show[{pR1,pR2,pR3,pR4,pR5}
     ,PlotRange->{{0,1},{0,3 10^10}}
     ,AxesLabel->{"%", "kg/m^7"}
,PlotLabel->"Predicted and Actual Flow Resistance vs Gate Travel"]
```

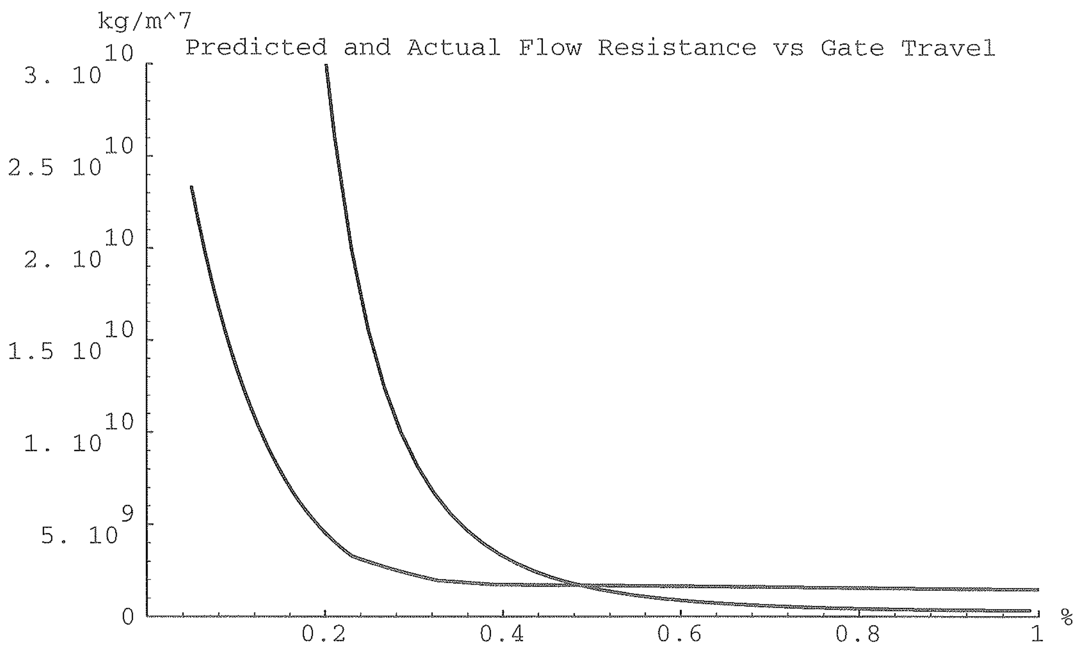


```
-Graphics-
```

On log scale, the results are:

```
pRL1 = Plot[Log[10,Re1],{sgtrue,.05,.23}];
pRL2 = Plot[Log[10,Re2],{sgtrue,.23,.33}];
pRL3 = Plot[Log[10,Re3],{sgtrue,.33,.39}];
pRL4 = Plot[Log[10,Re4],{sgtrue,.39,1}];
pRL5 = Plot[Log[10,Rtotalnofudge],{sgtrue,.1,.99}];
```

```
Show[{pRL1,pRL2,pRL3,pRL4,pRL5},PlotRange->{{0,1},{8,12}}
     ,AxesLabel->{"%", "Log[kg/m^7]"}
,PlotLabel->"Predicted and Actual Flow Resistance vs Gate Travel"]
```

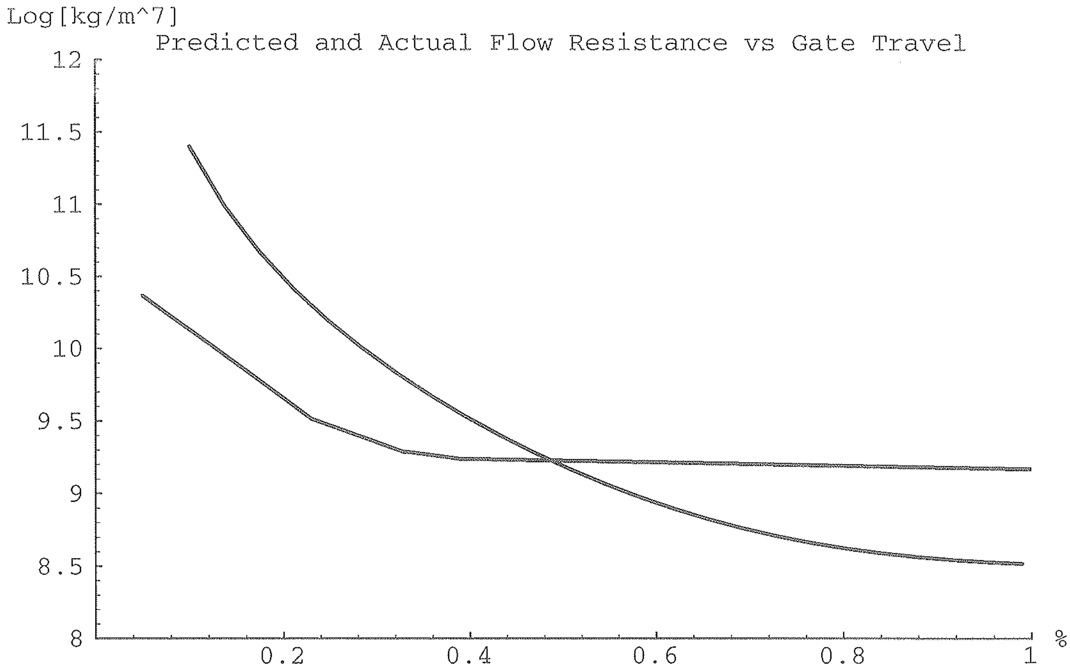


```
-Graphics-
```

It is seen that my predicted flow resistance (before emperical adjustment) is much higher than the actual value for small gate openings. The difference between the curves at large gate openings may not represent an error in the model but rather that the lower bound emperical curve is including the effects of clogging.

It was found that if the slide gate position was emperically adjusted to an opening corresponding to approximately 20% less travel that a fair match between the actual and predicted flow resistance is obtained:

```
Rtotalfudge = (Rtotal/.dataflow)/.rnoz->.04;

pRL6 = Plot[Log[10,Rtotalfudge],{sgtrue,.1,.99}]
```

```
Show[{pRL1,pRL2,pRL3,pRL4,pRL6},PlotRange->{{0,1},{8,12}}
     ,AxesLabel->{"%", "Log[kg/m^7]"}
,PlotLabel->"Predicted and Actual Flow Resistance vs Gate Travel"]
```

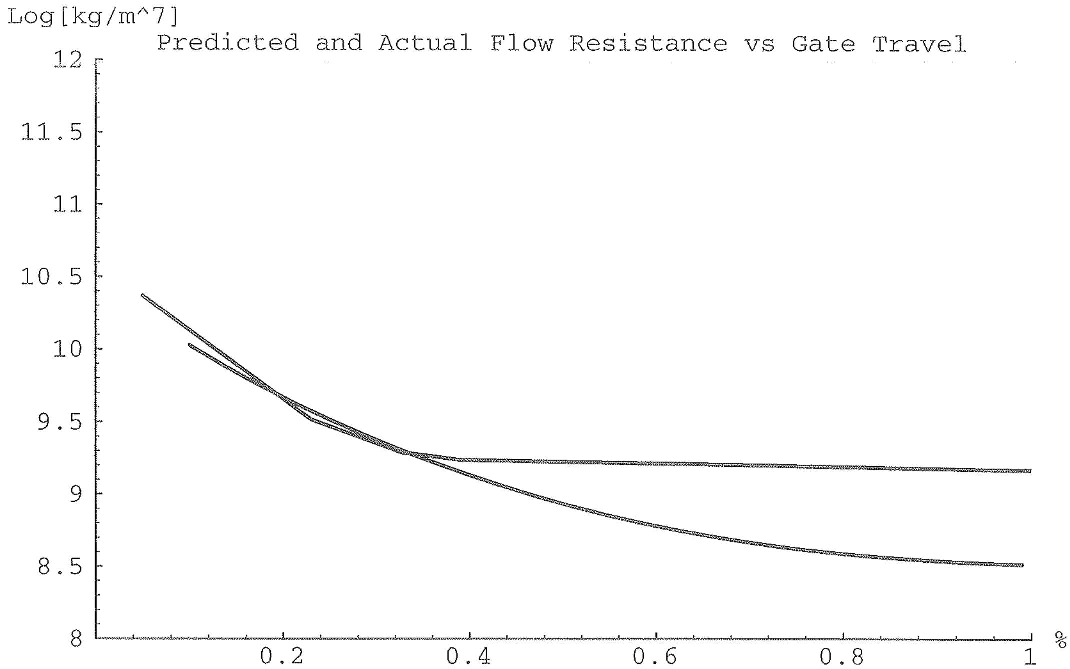

-Graphics-

A.7 OTHER CLOGGING RELATED MODELS

A.7.1 FRACTION OF ALUMINA CAPTURED IN NOZZLE

Cnosider a 40 mm radius x 1 m long nozzle which becomes clogged (20 mm thick, 83% porosity alumina) after casting 2 heats (1-2 per Bou 85 w/o Ca, 2-3 per Ham 85 w/o argon) having 30 ppm of oxygen present as inclusions. A typical ladle size might be:

290 ton - Hae 88
250 ton - Inland
225 ton - Sch 87

The density of pure alumin is taken as 3980 kg/m^3 (Askeland). the alumina passsing though the nozzle is:

```
aluminathru = (2 heat) (250 tonsteel/heat) *
  (30 10^-6 kgoxygen/kgsteel) (1000 kgsteel/tonsteel) *
  ((27 2 + 16 3) kgalumina/(16 3 kgoxygen)) // N

31.875 kgalumina
```

The amount of the alumina in the above clog is:

```
aluminaclog = (Pi (.04^2-.02^2) 1.  mclog^3/nozzle) (2 nozzle) *
     (.17 malumina^3/mclog^3) (3980 kgalumina/malumina^3) // N

5.10144 kgalumina
```

Therefore, the fraction of alumina deposited on the nozzle wall for this case then is:

```
aluminaclog/aluminathru

0.160045
```

A.7.2 REOXIDATION RELATED CLOGGING

Considr a 5 ppm a 5 ppm nitrogen pickup and assume all the associated oxygen forms alumina. In two (250 ton) heats you would get:

```
(5 10^-6 kgN/kgsteel) (kgair/(0.79 kgN)) (0.21 kgO/kgair) *
(250 10^3 kgsteel/heat) (2 heat) *
((27 2 + 16 3) kgalumina/(16 3 kgO))
```

```
1.41218 kgalumina
```

Note that this is a significant fraction of the above calculated clog mass.

A.7.3 SURFACE TENSION INDUCED CLOGGING

Table of Variables:

gamma = surface tension of liquid steel
x = component perpindicular to the wall of the distance from the particle center
dp = pressure exerted by the liquid steel on the particle owing to the curved interface
dA = differential area on surface of particle
Fx = net force on particle due to surface tension gradient
U = terminal velocity of particle (assuming Stokes Drag)
mu = viscosity of steel
R = particle radius
tauw = wall shear stress
ustar = friction velocity
uav = average stream velocity
y = distance from wall (for turbulence calculations)
rho = density of steel
D = pipe diamater

Aspiration of air into the nozzle will generate a variation of oxygen concentration with position which will in turn cause a variation of the surface tension of the liquid steel. This surface tension gradient will force a particle toward the wall. The relationship between surface tension gradient (mgamma) and particle velocity can be found as follows:

```
gamma = mgamma x;
x = R Cos[theta];
dp = gamma/R;
dA = 2 Pi R^2 Sin[theta];
Fx = Integrate[-dp Cos[theta] dA,{theta,0,Pi}]
```

$$\frac{-4 \text{ mgamma Pi } R^2}{3}$$

```
U = Fx / (6 Pi mu R)            (*Stokes Drag*)
```

$$\frac{-2\ mgamma\ R}{9\ mu}$$

The oxygen concentration profile can be estimated by assuming that the oxygen must diffuse across the viscous sublayer and buffer layer (i.e., y+ = 30). The thickness of these layers is found as follows:

```
eqna1 = tauw == 0.0396 rho^(3/4) uav^(7/4) mu^(1/4) / D^(1/4)
                        (*pg 423, White 91*);

eqna2 = eqna1 /. {tauw -> rho ustar^2, uav -> Q/(Pi D^2/4)};

eqna3 = yplus == y ustar/ (mu/rho);

(*Function that convertns ton/min to m^3/s)
ft2m[x_] := (x ton/min)(10^3 kg/ton)(1/(7015 kg))(min/60) //N

dataasp = {
rho->7015,
mu->.0056,
Q->ft2m[4], (*4 ton/min*)
D->.08,      (*nozzle diameter*)
yplus->30};

eqnsa5 = {eqna2,eqna3} /. dataasp;

ansa1 = Solve[eqnsa5,{ustar,y}] [[2]]

{y -> 0.000290747, ustar -> 0.0823695}
```

So the thickness over which the turbulent transport does not dominate is approximately 3 mm.

The flux of oxygen can be found as follows. Consider 0.3 ppm nitrogen pickup (92 Cam), in a 1 m long x 80 mm dia. nozzle. Assume no oxygen reacts (all diffuses). Casting rate = 4 ton/min. Diffusion Coefficient - pg 411 (USS book). The flux of oxygin is:

```
fluxO = (0.3 10^-6 kgN/kgFe) (kgair/(0.79 kgN)) *
        (0.21 kgO/kgair) *
        (7015 kgFe/m^3) (ft2m[4] m^3/s) / (Pi .08 m 1 m) // N
```

$$\frac{0.0000211535\ kgO}{m^2\ s}$$

The concentration gradient need to transport this flux by diffusion is:

```
eqna6 = fluxO == (2.5 10^-5 cm^2/s) (m/(100 cm))^2 *
                    (7015 kgFe/m^3) gradC ;
ansa2 = Solve[eqna6,gradC]
```

$$\{\{gradC \to \frac{1.20619\ kgO}{kgFe\ m}\}\}$$

This oxygen concentration gradient gives rise to a surface tension gradient. The variation of surface tension with oxygen conten is (from pg 413, USS book).

```
dgdO = (1300-1835) 10^-3 N/m  / ((.001-0) atomO/atomFe *
        16 kgO / (AvgNo atomO) * AvgNo atomFe / (56 kgFe))
```

$$\frac{-1872.5\ kgFe\ N}{kgO\ m}$$

This yields a surface tension gradient of:

```
mgamma = gradC dgdO /. ansa2
```

$$\{\frac{-2258.59\ N}{m^2}\}$$

This in turn causes a terminal particle velocity of:

```
(-2*mgamma* (10 10^-6 m))/(9* (0.0056 kg/(m s)) )/. N -> kg m/s^2
```

$$\{\frac{0.896264\ m}{s}\}$$

This analysis indicates that aspiration can generate a relatively high particle velocity toward the nozzle wall.

To check the reasonableness of the predicted oxygen concentration profile, I will use the above results to calculate the oxygen concentration at the nozzle wall.

```
(gradC (0.0003 m) /. ansa2 [[1,1]]) /.  kgO/kgFe -> 10^6 ppmO
```

361.856 ppmO

In terms of atom percent oxygen this is:

```
gradC (0.0003 m) (56 kgFe)/(AvgNo atomFe) *
        (AvgNo atomO)/(16 kgO) /. ansa2
```

$$\{\frac{0.0012665\ atomO}{atomFe}\}$$

Therefore the predicted oxygen concentration at the wall is 0.12 atom %. This concentration is within the range of validity of the oxygen-surface tension relationship used above.

APPENDIX B - FORTRAN CODES

B.1 PROGRAM: "inittran.f"

```
******************************************************************
*        Program: inittran.f
*
*        This program calculates the transient temperature
*        distribution in an upper tundish nozzle and mounting
*        block and the resulting skull thickness.
*        The program uses an explicit finite difference
*        algorithm.
*
*        Variables:
*          T(i,j) - temperature at nodal positions i for the
*                   present (j=1) and future (j=2) time steps (K)
*     |   i=1      i=n1           i=n2
*     |---------|--------|---------------|
*     |  steel      nozzle    block         ambient
*
*          dt = time step size (s)
*          rhocpi = product of density and specific heat for
*                   nozzle wall (i=w) and mounting block (i=b) (W/m^3)
*          ki = conductivity of wall (i=w), block (i=b), and
*                   steel skull (i=s) (W/(m K))
*          ri = radius of OD of mounting block (i=2), OD of nozzle
*                   (i=4), ID of nozzle (i=5), and ID of skull (i=6) (m)
*          dr = grid spacing (m)
*          rj = inner (j=in), outer (j=out), and central (j=i)
*                   radius of finite volume (m)
*          emmis = thermal emmisivity of block OD
*          sig = Stefan-Boltzmann constant (W/(m^2 K^4))
*          Tinf = ambient air temperature (K)
*          Tliq = liquidus temperature of steel (K)
*          Tstrm = bulk temperature of steel stream (K)
*          dr6 = change in skull position during time step (m)
*          tprht = length of preheat time (s)
*          rhoLf = product of density and latent heat of
*                   steel (W/m^3)
*          h = heat transfer coefficient between steel
*                   stream and skull (W/(m^2 K))
*
*          ntmax = max # of time steps
*          npint = # of time steps to skip before printing
*          n2 = total number of nodes
```

```
*          n1 = number of nodes in the nozzle
*          nflag - set = 1 to skip code validation
*          np,i = counters
*
********************************************************************

         real T(100,2),dt,rhocpw,kw,rhocpb,kb,r2,r4,r5,dr,
     -   rin,rout,ri,emmis,sig,Tinf,
     -   Tliq,Tstrm,r6,dr6,tprht,ks,rhoLf,h
         integer ntmax,npint,n2,n1,nflag,np,i

*        Read in the preheat time and temp.
         read (*,*) tprht
         read (*,*) T(1,1)
         read (*,*) npint
         read (*,*) nflag
         write (*,98) ' Results from inittran.f '
         write (*,98) ' Preheat time is: ',tprht
         write (*,98) ' Nozzle ID temp during preheat is: ',T(1,1)
         write (*,97) ' Printing interval is: ',npint
         write (*,97) ' Validation run (1 = no): ',nflag

*        Time and Spatial Discretization:
         ntmax = 100000
         n2 = 100
         dt = 0.2

*        Mat'l prop. and dimensions:
         ks = 35.
         rhoLf = 1.93e9
         rhocpw = 3.08e6
         kw = 9.
         rhocpb = 5.73e6
         kb = 35.
         emmis = 0.96
         sig = 5.6697e-8
         Tinf = 300.
         Tliq = 1803.
         Tstrm = 1828.
         r2 = .25
         r4 = .193/2.
         r5 = .085/2.

*        Calculated grid spacing:
         dr = (r2 - r5)/(n2-1)
         n1 = int((r4-r5)/dr)+1

*        Initial Solid Thickness:
```

```
          r6 = r5-.0001

*         Specify Initial Temps.:
          do i=2,n2
            T(i,1) = 300.
          enddo

*         Validation Data (steady state soln)
          if (nflag.eq.1) goto 20
          tprht = 1000.
          T(1,1) = 1803.
          ntmax = 1000
        ri = r5 - dr
          do i=1,n1
            ri = ri + dr
            T(i,1) = 1803. -
     -      871.909822494297*Log(23.52941176470588*ri)
          enddo
          do i = n1+1, n2
              ri = ri + dr
              T(i,1) =1088. -
     -              224.1789947078628*Log(10.36269430051813*ri)
          enddo
 20     continue

*         Main  Loop:
          write (*,99) 'cast',' ',      'nozzle',  ' ','block',
     -              ' ','heat','skull'
          write (*,99) 'time','ID temp','mid temp','OD temp',
     -              'mid temp','OD temp','flux','thickness'
          write (*,99) ' (s)','(K)',' ',' ',' ',' ',' ','mm'
          do nt = 1,ntmax

        if (nt*dt.lt.tprht) goto 30
            if (r6.gt.r5) stop
*           FortranForm[h78 /. {flowrate->.008664}]//N
            h = 16.5*(5. + 4.252092567779206*
     -              (1/r6)**0.8218679315771)/r6
            dr6 = dt/rhoLf *
     -        (-kw*(T(2,1)-T(1,1))/dr -
     -         h*(Tstrm-Tliq) )
            r6 = r6 - dr6
            T(1,1) = Tliq + r6/dr*kw/ks*(T(2,1)-T(1,1))*Log(r5/r6)

 30       rin = r5 - dr/2.
            rout = r5 + dr/2.

            do i = 2,n1-1
```

```
          rin = rin + dr
          rout = rout + dr
          ri   = (rin + rout) / 2.
          T(i,2) = dt/(rhocpw*dr*ri)*
     -   (-kw*rin* (T(i,1)-T(i-1,1))/dr -
     -     -kw*rout*(T(i+1,1)-T(i,1))/dr  ) + T(i,1)
        enddo

        i=n1
          rin = rin + dr
          rout = rout + dr
          ri   = (rin + rout) / 2.
          T(i,2) = dt/(rhocpw*dr*ri)*
     -   (-kw*rin* (T(i,1)-T(i-1,1))/dr -
     -     -kb*rout*(T(i+1,1)-T(i,1))/dr  ) + T(i,1)

        do i = n1+1, n2-1
          rin = rin + dr
          rout = rout + dr
          ri   = (rin + rout) / 2.
          T(i,2) = dt/(rhocpb*dr*ri)*
     -   (-kb*rin* (T(i,1)-T(i-1,1))/dr -
     -     -kb*rout*(T(i+1,1)-T(i,1))/dr  ) + T(i,1)
        enddo

        i = n2
          rin = rin + dr
          rout = rout + dr
          ri   = (rin + rout) / 2.
          T(i,2) = 2*dt/(rhocpb*dr*ri)*
     -   (-kb*rin*(T(i,1)-T(i-1,1))/dr -
     -     ri*emmis*sig*(T(i,1)**4 - Tinf**4)  ) + T(i,1)

        np = np+1
        if (np.eq.npint) then
          write (*,100) nt*dt-tprht,T(1,1),T(n1/2,2),T(n1,2),
     -      T((n1+n2)/2,2),
     -      T(n2,2),-kw*r5*(T(2,1)-T(1,1))/dr,(r5-r6)*1000.
          np=0
      endif

        do i=2,n2
          T(i,1) = T(i,2)
        enddo

       enddo
 97    format ('#',A40,i6)
 98    format ('#',A40,f8.3)
```

```
99      format ('#',A10,A11,A11,A11,A11,A11
  -         ,A12,A11,A11)
100     format (f8.2,3x,f8.3,3x,f8.3,3x,f8.3,3x,f8.3,3x,f8.3,
  -         3x,f9.2,3x,f8.6,3x,f8.3)

        end
```

B.2 INPUT FILE: "inittran.inp"

3600.	Preheat time (s)
1600.	Preheat temperature at nozzle ID (K)
10	Interval for printing results
1	Validation Run (1 = no)

* Input file for inittran.f

B.3 PROGRAM: "stdsld.f"

```
C*******************************************************************
C
C       Program:  stdsld.f
C
C       This code will calculate the position of the solid/liquid
C       interface within a tundish nozzle as a function of time.
C
C       By:  Keith Rackers
C
C       Formulas generated by 5.ma (mathematica).
C       The input can be either given interactively or as an input file
C       (e.g., a.out < case1 > r.1)
C
C       Variables:  (see 5.ma)
C
C*******************************************************************

        real*8 r6(9000),r7(9000),V6(9000),Cl6(9000),mCl(9000),
     -     Cs6(9000),kw,flowrate,Cl7a,T8,E,Pi,T2o,dt,
     -     sprht(5),flwrt(5),tm(5),tmel,tmelt,
     -     Vc
        common r6,r7,V6,Cl6,mCl,Cs6,kw,flowrate,Cl7a,T8,E,Pi,T2o,dt,
     -        Vc

*       Define constants and initial values.
        E = 2.718281828459045
        Pi = 3.141592653589793
        tmelt = 0.

*       Get casting characteristics, material properties, and
*         linearization temperature for radiation B.C.
*       open (9,file='Inland.inp')
        read (*,*)
        read (*,*)
        do i = 1,5
         read (*,*) sprht(i),flwrt(i),tm(i)
         tmelt = tmelt + tm(i)
        enddo
        read (*,*) dt
        read (*,*) kw
        read (*,*) Cl7a
        read (*,*) T2o
        read (*,*) npint
```

```
*       Define initial conditions.
        r6(1) = .085/2. + 1.e-8
        r7(1) = .085/2. - 1.e-8
        V6(1) = -1.e-8
        Cl6(1) = 1.e-8
        mCl(1) = 1.e-8
        Cs6(1) = -Cl7a + 0.17*(Cl7a + Cl6(1))

*       Main Program
        do i2 = 0,10
         tmel = 0.
         do i3 = 1,4
          tmel = tmel + tm(i3)
          ilo=1 + tmel/dt+i2*tmelt/dt+1
          ihi=tm(i3+1)/dt + tmel/dt+i2*tmelt/dt+1
          do i = ilo, ihi
           T8 = sprht(i3) + (sprht(i3+1)-sprht(i3))*
     -      (i-ilo)/(ihi-ilo) + 1811. - 81.*Cl7a
           flowrate = flwrt(i3) + (flwrt(i3+1)-flwrt(i3))*(i-ilo)/
     -      (ihi-ilo)
           call fstep(i)
           np = np + 1
           if (np.lt.npint) goto 50
            np=0
            write (*,100) i*dt,r6(i),r7(i),Cl6(i),mCl(i),V6(i),Cs6(i),
     -                 V6(i)/Vc
 50        continue
          enddo

          if (r7(ihi).lt. .02) stop
         enddo
        enddo

 100    format (f6,3x,e9.4,3x,e9.4,3x,e9.3,3x,e9.3,3x,e9.3,3x,e9.3,
     -        3x,e9.3)

        stop

        end

*       Subroutine:

        subroutine fstep(i)
        real*8 r6(9000),r7(9000),V6(9000),Cl6(9000),mCl(9000),
     -     Cs6(9000),kw,flowrate,Cl7a,T8,E,Pi,T2o,dt,
     -     Vc
        common r6,r7,V6,Cl6,mCl,Cs6,kw,flowrate,Cl7a,T8,E,Pi,T2o,dt,
     -     Vc
```

```
      r6(i) = r6(i-1) - dt*V6(i-1)
      r7(i) = -5.555555555555556e-6*dt/
-   E**(133.3333333333333*(r6(-1 + i) - r7(-1 + i))) +
-  r7(-1 + i)

      Cl6(i) =  - 1.*2.718281828459045**
-       (5.e7*(r6(i) - r7(i))*V6(i-1))*
-      (-1. + 2.718281828459045**
-         (5.e7*(r6(i) - r7(i))*V6(i-1)))*
-      V6(i-1)**2*
-      (-1.*mCl(i-1) +
-        2.*dt*Pi*Cs6(i-1)*r6(i-1)*V6(i-1) +
-        6.283185307179587*dt*
-          (Cl6(i-1) +
-            Cl6(i-1)/
-             (-1 +
-               E**(5.e7*(r6(i-1) - r7(i))*V6(i-1))
-               ))*r7(i-1)*V6(i-1)/
-         E**(5.e7*(r6(i-1) - r7(i-1))*V6(i-1)))
-      /(2.513274122871834e-15*
-        2.718281828459045**
-         (5.e7*(r6(i) - r7(i))*V6(i-1)) -
-       2.513274122871834e-15*
-        2.718281828459045**
-         (1.e8*(r6(i) - r7(i))*V6(i-1)) +
-       1.256637061435917e-7*
-        2.718281828459045**
-         (1.e8*(r6(i) - r7(i))*V6(i-1))*r6(i)*
-        V6(i-1) -
-       1.256637061435917e-7*
-        2.718281828459045**
-         (5.e7*(r6(i) - r7(i))*V6(i-1))*r7(i)*
-        V6(i-1) -
-       3.141592653589793*
-        2.718281828459045**
-         (5.e7*(r6(i) - r7(i))*V6(i-1))*r6(i)**2*
-        V6(i-1)**2 +
-       3.141592653589793*
-        2.718281828459045**
-         (5.e7*(r6(i) - r7(i))*V6(i-1))*r7(i)**2*
-        V6(i-1)**2)


      mCl(i) = -1.*Pi*Cl6(i)*r6(i)**2/
-   (-1 + E**(5.e7*(r6(i) - r7(i))*V6(i-1))) +
-  1.*Pi*Cl6(i)*r7(i)**2/
-   (-1 + E**(5.e7*(r6(i) - r7(i))*V6(i-1))) -
```

```
     -  8.000000000000001e-16*Pi*
     -    (Cl6(i) + Cl6(i)/
     -       (-1 + E**(5.e7*(r6(i) - r7(i))*V6(i-1))))/
     -   V6(i-1)**2 + 4.e-8*Pi*
     -    (Cl6(i) + Cl6(i)/
     -       (-1 + E**(5.e7*(r6(i) - r7(i))*V6(i-1))))*r6(i)
     -    /V6(i-1) - 2.*
     -    E**(5.e7*(-r6(i) + r7(i))*V6(i-1))*
     -    (-4.000000000000001e-16*Pi*
     -       (Cl6(i) + Cl6(i)/
     -          (-1 + E**(5.e7*(r6(i) - r7(i))*V6(i-1)))) +
     -      2.e-8*Pi*(Cl6(i) +
     -         Cl6(i)/
     -          (-1 + E**(5.e7*(r6(i) - r7(i))*V6(i-1))))*
     -       r7(i)*V6(i-1))/V6(i-1)**2

      V6(i) = 5.181347150259067e-10*(-1.*
     -       (-1569.286068817784*kw*
     -          (110.218968 + 4.082183999999999e-8*T2o**4) -
     -         2.440424564400326e-6*kw*T2o**3*
     -          (-63384.99999999999 + 2835.*Cl7a +
     -            2835.*Cl6(i)))/
     -     (35.*(-2.001243154429133e-6*T2o**3 +
     -           1.219454297194821*kw*
     -            (-36.7678763578969 - 5.442912e-8*T2o**3)) -
     -        2.440424564400326e-6*kw*T2o**3*Log(0.0425/r6(i)))
     -       + 1.*(59763. - 2673.*Cl7a - 2673.*Cl6(i))/
     -     Log(r6(i)/r7(i)) +
     -    33.*(-59763. + 2673.*Cl7a + 2673.*Cl6(i) -
     -         8904.33046155188*T8*Log(r6(i)/r7(i))*
     -          (0.00926515478690147 +
     -            0.3903089072542588*
     -             (flowrate/r7(i))**0.8218679315771))/
     -     (Log(r6(i)/r7(i))*
     -       (33. + Log(r6(i)/r7(i))*
     -          (82.5 + 3475.439492279123*
     -             (flowrate/r7(i))**0.8218679315771))))/r6(i)


      if (V6(i).gt.0.) then
        Cs6(i) = -Cl7a + 0.17*(Cl7a + Cl6(i))
      else
        if (r6(i).lt.r6(1)) then
          j = i
20        j = j-1
          if (r6(i).gt.r6(j)) goto 20
          Cs6(i) = Cs6(j)
        else
```

```
           r6(i)=r6(1)
           Cl6(i)=Cl6(1)
           mCl(i)=mCl(1)
           V6(i)=V6(1)
           Cs6(i)=Cs6(1)
          endif
        endif

        Vc = 2.e-8*(-1811. + 81.*(Cl7a + Cl6(i)) +
-      0.0001123049065078967*
-        (3.552713678800501e-15*Cl7a +
-          3.552713678800501e-15*Cl6(i) +
-          1418.654392042576*Log(r6(i)/r7(i)) -
-          63.45168733045206*Cl7a*Log(r6(i)/r7(i)) -
-          63.45168733045206*Cl6(i)*Log(r6(i)/r7(i)) +
-          1.958385411433706*T8*Log(r6(i)/r7(i))**2 +
-          59763.*Log(r6(i)/r7(i))*
-           (flowrate/r7(i))**0.8218679315771 -
-          2673.*Cl7a*Log(r6(i)/r7(i))*
-           (flowrate/r7(i))**0.8218679315771 +
-          0.*T8*Log(r6(i)/r7(i))*
-           (flowrate/r7(i))**0.8218679315771 -
-          2673.*Cl6(i)*Log(r6(i)/r7(i))*
-           (flowrate/r7(i))**0.8218679315771 +
-          165.*T8*Log(r6(i)/r7(i))**2*
-           (flowrate/r7(i))**0.8218679315771 +
-          3475.439492279123*T8*Log(r6(i)/r7(i))**2*
-           (flowrate/r7(i))**1.6437358631542)/
-       (Log(r6(i)/r7(i))*
-         (0.00926515478690147 +
-           0.3903089072542588*
-            (flowrate/r7(i))**0.8218679315771)*
-         (0.00949520199483009 +
-           0.02373800498707522*Log(r6(i)/r7(i)) +
-           1.*Log(r6(i)/r7(i))*
-            (flowrate/r7(i))**0.8218679315771)))/
-  ((0. - 81.*Cl7a + 81.*(Cl7a + Cl6(i)))*
-    (r6(i) - r7(i)))

        end
```

B.4 INPUT FILE: “stdsld.inp”

```
*       Input file for Inland.f
*       Superheat     Flowrate      Time
        22.           .006455              0.
        32.           .007560              180.
        42            .008664              180.
        32.           .008664              1440.
        22.           .006455              360.
3.      Time step
9.      Refractory Conductivity
.02     Carbon Equivalent Concentration in Free Stream
875.    Approx. Temp of T2 (for series expansion)
10      Printing Interval
```